The Interactions of Optoelectronically Active Molecules and Complexes with (Bio) macromolecules for Applications in Biosensors and Directed Assembly

Ammar Al-azzawi

A thesis submitted for the Degree of Doctor of Philosophy

School of Chemistry

Cardiff University

December 2017

DECLARATION

This work has not been submitted in substance for any other degree or award at this or any other degree or other award.

Signed…….. (candidate) Date ...……..…

STATEMENT 1

This thesis is being submitted in partial fulfilment of the requirements for the degree of Doctor of philosophy.

Signed…… (candidate) Date ...……..…

STATEMENT 2

This thesis is the result of my own independent work/investigation, except where otherwise stated, and the thesis has not been edited by a third party beyond what is permitted by Cardiff University's Policy on the Use of Third Party Editors by Research Degree Students. Other sources are acknowledged by explicit references.

The views expressed are my own.

Signed……... (candidate) Date ...……..…

STATEMENT 3

I hereby give consent for my thesis, if accepted, to be available online in the University's Open Access repository and for inter-library loan, and for the title and summary to be made available to outside organisations.

Signed……... (candidate) Date ...……..…

STATEMENT 4: PREVIOUSLY APPROVED BAR ON ACCESS

I hereby give consent for my thesis, if accepted, to be available online in the University's Open Access repository and for inter-library loans after expiry of a bar on access previously approved by the Academic Standards & Quality Committee.

Signed……... (candidate) Date...……..…

Acknowledgements

I take this opportunity to thank Almighty Allah for helping me to undertake and complete this research.

Now, I express my sincere gratitude to everyone who helped me and supported me during this thesis. First and foremost, I am immensely indebted to my Supervisor, and I would like to express my sincere appreciation to my supervisor Dr Niek Buurma for all the support and encouragement, for his patience and immense knowledge he gave me during my PhD study. Without his guidance and constant feedback, this PhD would not have been accomplishable. It has been pleasuring to be part of his Research Group.

I am also very thankful to my supervisor Dr Simon Pope and Dr James Redman for their continual support and help, for providing most of the ligands during my research. Many thanks also go to our collaborators (Emily Langdon-Jones, Nick Fletcher, Alaa El-Betany, Richard Wheelhouse, Lara), who provided me with a variety of compounds. I am also very grateful to Prof Angela Casini and Prof. Thomas Wirth for acting as my mentor and internal examiner for all events and progress examinations.

I would like to acknowledge and thank the essential financial support from the ministry of higher education and scientific research in Iraq and the Iraqi cultural attaché in London for being my sponsor.

Special thanks also go to the best friends who help me a lot: Hiwa Ahmad, Ibrahim Qadur, for all the help they kindly offered to me in the Laboratory during my study. I thank my fellow lab mates in the POC, for the help and for all the fun we have had during my research. I greatly appreciate the support and help received throughout my study from Dr. Mohammed ALsharbini, Dan, Hider, Abbas, Mohammed, and Raid from Cardiff. Out of the lab, and for making my time in Cardiff enjoyable, I would like to thank: Ivan Karomi, Ali Al-zughabi, who deserve special mention for their attempts to keep me sane, Warren for our good-humoured arguments.

I am truly holy and grateful to my loving parents especially my mother for her emotional support and prayers for me in the hard times, and to all of my brothers, sisters and members of my wider family for their encouragement throughout my PhD studies. Especial and Huge thanks go to my adopted Welsh family, Carol and Bryn Kesiny for their love, prayers, calls, advice,

and being there whenever I needed. also, I would like to thank Sandra and John for their kindness and engagement.

Finally, and more importantly I offer my deepest, heartfelt thanks to my beloved wife Baydaa

For the love and care
For the value, you have taught
For the support, you have always given

And my wonderful kids: Mohammed, Zainab, Almustafa and my adorable baby Anwar, for their patience and immeasurable love, which encouraged me to finish this thesis.

List of abbreviations

°C	Degree Celsius
A	Absorbance
a.u.	Arbitrary unit
AA	Alginic acid
BBC	Berberine chloride
Bp	Base pairs
BSA	Bovine serum albumin
CD	Circular Dichroism
CTAB	Cetyltrimethylammonium bromide
DMSO	Dimethyl sulfoxide
DNA	Deoxyribonucleic acid
DNA	Fish sperm deoxyribonucleic acid
ds DNA	double-stranded deoxyribonucleic acid
HA	Hyaluronic acid
ITC	isothermal titration calorimetry
Kcal	Kilocalorie
MB	Methylene blue
Ml	Millilitre
MOPS	3-(*N*-morpholino) propane sulfonic acid
N.P.	Natural polymer
NaCl	Sodium Chloride
PAA	Polyacrylic acid
POSA	Polystyrene sulfonic acid
RNA	Ribonucleic Acid
S.P.	Synthetic polymer
SA	Serum albumin
SDS	Sodium dodecyl sulphate
ss DNA	single-stranded deoxyribonucleic acid
TF	Transferrin

Summary

This thesis explores the effect of biopolymers (serum albumin, transferrin, hyaluronic acid and alginic acid), synthetic polymers (sodium polystyrenesulfonic acid and polyacrylic acid), and surfactants (CTAB, SDS, Tween-20) on DNA binding, in support of the development of biosensors using optoelectronically active DNA binders as sensitisers. Such biosensors have become essential in the field of biochemistry and medicine.

Chapter one introduces the central dogma, nucleic acids, proteins and properties of selected proteins serum albumin and transferrin. This chapter presents DNA biosensors and the modes of interactions of molecules with DNA. It introduces self-assembled nanostructured materials.

Chapter two shows that **2.1-2.15**, except negatively charged **2.9** bind to DNA.

Chapter three reports that **3.1, 3.2, 3.3, 3.7**, and **3.9** bind to serum albumin while **3.1, 3.2, 3.8** and **3.10** bind to transferrin. Ligands **3.1, 3.5, 3.7, 3.8, 3.10** and **3.11** do not show a change in affinity for DNA in the presence of SA, but the affinity of **3.2, 3.4, 3.6** and **3.12** for DNA decreases. The apparent affinity of **3.3** for DNA increases in the presence of SA. TF had no effect on DNA binding of **3.1**, but **3.2** increase in affinity for DNA in the presence of TF.

Chapter four shows that **4.1** and **4.2** bind to HA and AA but **4.7** and **4.8** interact only with HA. Ligands **4.4, 4.5, 4.6, 4.10, 4.11** and **4.12** do not show any change in affinity for DNA, but **4.2, 4.7** and **4.8** do. An increase in affinity of **4.1** for DNA was observed.

Chapter five describes that **5.1, 5.2, 5.7** and **5.8** bind to PAA and POSA, while **5.4, 5.5, 5.10** and **5.12** bind to POSA only. Ligands **5.1** and **5.7** bind to DNA in the presence of PAA and POSA. Moreover, **5.2** interacts with DNA in the presence of PAA with precipitation and **5.8** binds to DNA with precipitation in the presence of POSA. All compounds decreased in affinity for DNA in the presence of POSA. Compounds **5.4, 5.10, 5.11** and **5.12** do not change affinity for DNA in the presence of PAA. An increased apparent affinity of **5.1** for DNA in the presence of PAA was attributed to sensitisers binding to PAA instead of the DNA backbone, increasing the apparent K_{binding}.

Chapter six reveals that cationic **6.1, 6.2, 6.4, 6.5, 6.7, 6.8** and **6.12** bind to SDS. Anionic **6.4, 6.9** and **6.14** bind to CTAB. In the presence of Tween 20, **6.12** and **6.15** decrease in affinity for DNA while **6.13** shows no change in affinity.

Chapter seven outlines the conclusion from previous chapters and finishes with suggestions for future work.

Table of contents

Chapter one

Introduction

Abstract

Since the discovery of DNA as the template for protein synthesis, great effort has been made by researchers to develop DNA as a target for drugs and biosensors. For biosensors small molecules DNA-binder are required that change chemical and physical properties (such as absorbance spectra, redox properties) on binding.

Proteins and enzymes are still a predominant target for disease therapy. However, DNA can also be a target for medicine.[1] In fact,small molecules which bind to DNA function as drugs or as sensitisers in biosensors. This chapter gives a general overview of the DNA structure. Chapter one starts by introducing some important concepts of development of biosensors. The chapter discusses DNA functions and the mode of interaction of small molecules with double-stranded DNA as well as the types of binding, such as electrostatic, intercalation and groove interactions. Moreover, the chapter briefly describes supramolecular and self-assembled nanostructured materials based on natural and synthetic polymers. The chapter finishes with the biophysical techniques which can be used to quantify the interaction between molecules and duplex DNA, such as UV-visible spectroscopy, circular dichroism (CD) and isothermal titration calorimetry (ITC).

1.1 General introduction to the thesis

These days, there is great interest in molecules that bind to nucleic acids.[2] Some ligands bind to proteins and DNA with high selectivity, affinity, stability and great resistance to enzymatic degradation.[3,2] Information about the binding mode and affinity between DNA, proteins and ligands can help us understand the functions of nucleic acid, design effective medicines and understand the effects of the presence of various biomacromolecules on DNA biosensor readings.[4] The determination of ligand-binding sites on DNA and proteins is also necessary for docking studies in drug design.[4,5] Compounds binding to plasma proteins are an interesting study area in several fields such as medicinal chemistry, biochemistry, pharmacy, clinical medicine, life science, etc.[6-8] The interaction between the small molecules and DNA is vital for developing effective therapeutic agents. [9-10]

DNA has been studied widely in order to understand the cause of diseases and to develop specific molecular drug targets. Within biological systems, DNA is known to function through interacting with ligands that activate or block the function of specific genes. Compounds that interact with DNA are classed as DNA-binding molecules in this study. One of the most interesting examples of noncovalent interactions of compounds are those that give rise to systems with different optoelectronic properties.

This thesis focusses on developing biosensors by using small molecules that target DNA[11-12] and that act as sensitisers. Understanding the interactions of sensitisers with other components, for instance, selected proteins, polymers and surfactant are crucial in the development of biosensors.[13] For example, whole blood contains serum albumin, transferrin, etc. If the sensitiser binds to these other components of serum[14], then biosensors may be affected by stopping target binding or causing a false positive signal. It is also important to know how sensitisers in genosensors interact with (for example) natural biomacromolecules (HA and AA) and synthetic polymers (PAA and POSA) because this affects assay design. Therefore, it is imperative to study the interactions of biomolecules with optoelectronically active molecules.

1.2 Central Dogma

DNA is the principle component of the cell which stores the hereditary information in a living organism. DNA serves as the instructions for protein generation. This is molecular biology's central dogma, which explains the essential processes of information transfer between macromolecules: DNA is transcribed to RNA, RNA is translated to protein[15-17] (Figure 1.1).

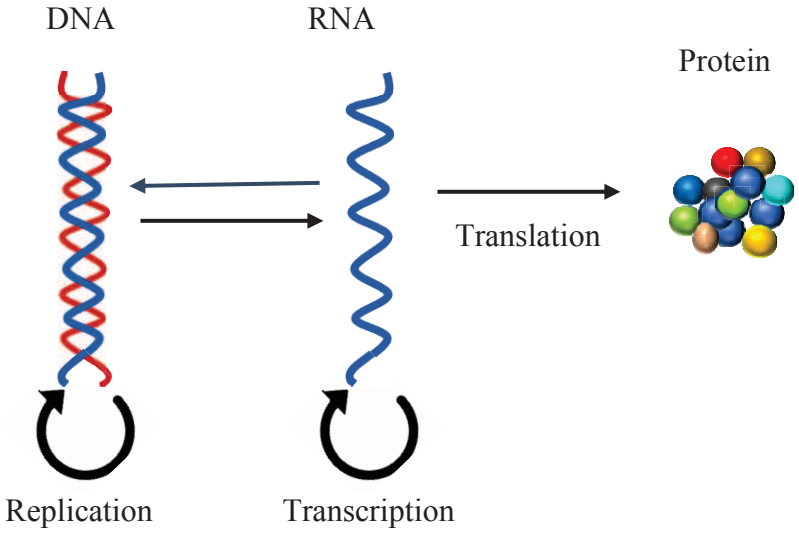

Figure 1.1: Central dogma of molecular biology.[15]

Every amino acid in the protein is encoded on the DNA by three consecutive bases, a so-called codon.

1.3 Structure and Function of Nucleic Acids

DNA (Deoxyribose Nucleic Acid) is a long double-stranded, right-handed, helical structure according to Watson and Crick's model DNA[18]. It is composed of two antiparallel complementary strands that are joined together by hydrogen bonding.[19]

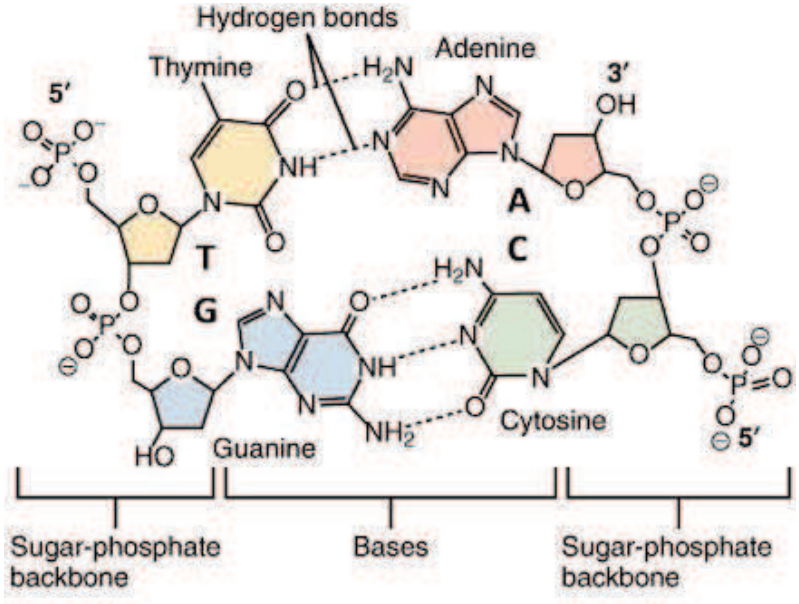

Figure 1.2*:* Schematic structure of a polymer double helix DNA.[18, 20]

DNA strands are polymers of nucleotides. The nucleotide consists of a phosphate group, a pentose sugar and a nitrogenous heterocyclic base, which is either a purine or a pyrimidine**.** A nucleoside consists of a purine or pyrimidine base bonded to sugar, the N-9 of a purine or the N-1 of a pyrimidine is attached to the C-1 of the sugar as shown in Figure 1.3.[19, 21]

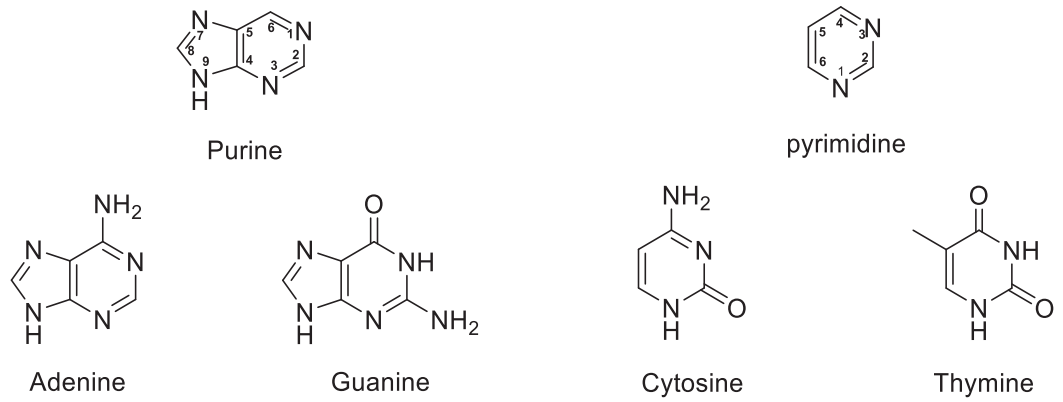

Figure 1.3: purine and pyrimidine to DNA base pairs

The chains of nucleotides are joined by phosphodiester bonds crossing from the 5' position of one nucleoside to the 3' position of the adjacent nucleoside. The nitrogenous bases are the purines adenine (A), and guanine (G) and the pyrimidines thymine(T) and Cytosine (C) (Figure 1.4). The sugar in a deoxyribonucleic acid is deoxyribose.[22-23]

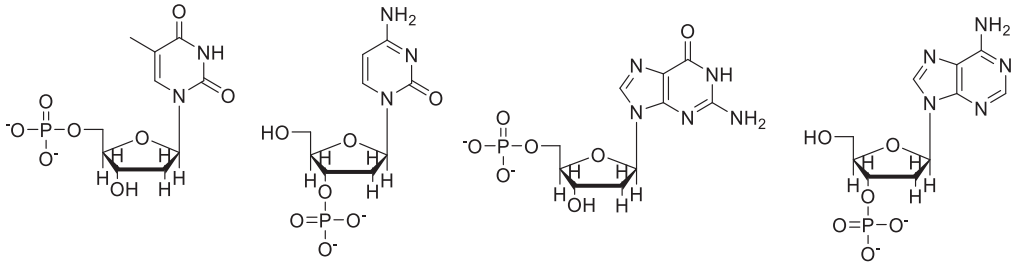

Figure 1.4: The structures of the four nucleosides, deoxythymidine, deoxycytidine, deoxyguanosine and deoxyadenosine from (left to right).

DNA typically forms a double helix, although other structures can also form. Double helix dsDNA can exist in three different conformations viz.the right-handed helical A-form, the Watson & Crick B-form and the left-handed helical Z-form.[24] Two grooves, viz. minor and major, are present in the double-stranded DNA in both A and B-form[25]. The Z-form is a left-handed structure without major and minor grooves.[26]

Figure 1.5: The main double helix DNA conformations (from left to right): (a) A-DNA (NDB ID: AD0003), (b) B-DNA (NDB ID: BD0003) and (c) Z-DNA (NDB ID: ZD0008).

1.4 Proteins

1.4.1 General structure of proteins

Proteins are built from the 20 amino acids. In proteins, amino acids are covalently linked together by amide links known as peptide bonds formed as result of dehydration reaction between carboxyl group (C-terminus) of one amino acid which reacts with the amino group (N-terminus) of another amino acid as shown in (Figure 1.6).

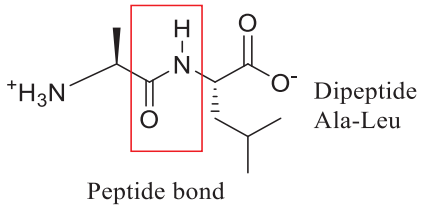

Figure 1.6: Peptide bond demonstrated as dipeptide Ala-Leu

Proteins have many functions in the cell, such as signalling, regulation, transportation, catalysis, structure and movement. There are many types of proteins, such as structural proteins like keratin, which is found in hair and nails, or globular proteins such as haemoglobin, which transports oxygen in the bloodstream. Another group of globular proteins are enzymes, which catalyse chemical processes by reducing the activation energy.[27,28] Proteins may be source of

the damage of the cells which may cause a diseases or death of the organism.[16] The main drug targets for new therapeutical agents are proteins.[29] Interactions involving globular proteins are critical in many biological processes. The interactions between proteins and ligands occur in a so-called ligand-binding site.[30-31]

1.4.2 Properties of selected proteins

Serum albumin (SA) is one of the most abundant proteins in blood plasma with a normal concentration of 50 g / L, *i.e.* around 0.6 mM. SA functions as a transporting agent for numerous endogenous and exogenous substances like hormones, amino acids, drugs and so on. SA also plays a major role in regulating the osmotic pressure of blood.[32] SA is also responsible for the pH maintenance in blood by acting as buffer due to the presence of -COOH and$-NH_2$ residues. Therefore, understanding the functions and properties of serum albumins is important in knowing their interactions with molecules. Examples of albumins are human serum albumin (HSA) and bovine serum albumin (BSA), which perform similar biological functions but in different organisms.[33,34] The most interesting property of serum albums is the high affinity for various kinds of ligands which are located in different binding regions in serum albumins[35]. Albumin binding to molecule has been reserached more than half decade, serum albumin has higher affinity for small negativily charged of hydrophobic molecules.

A single chain of BSA consists of 583 amino acids, 17 disulphide bonds, with no carbohydrates.[36] BSA contains three homologous domains (I, II and III) connected by peptide chain which forms a heart-shaped molecule.

Every domain contains two subdomains which are referred to as (IA, IB), (IIA, II B) & (IIIA, IIIB). The hydrophobic pockets in subdomain IIA and IIIA are the main binding sites for ligands to serum albumin[37] as shown in (Figure 1.7). Under physiological conditions. SA typically binds with two moles of ligand, viz in the bidning sites in domain IIA and IIIA, whereas it could bind up to six moles of ligand under certain disease states.[38]

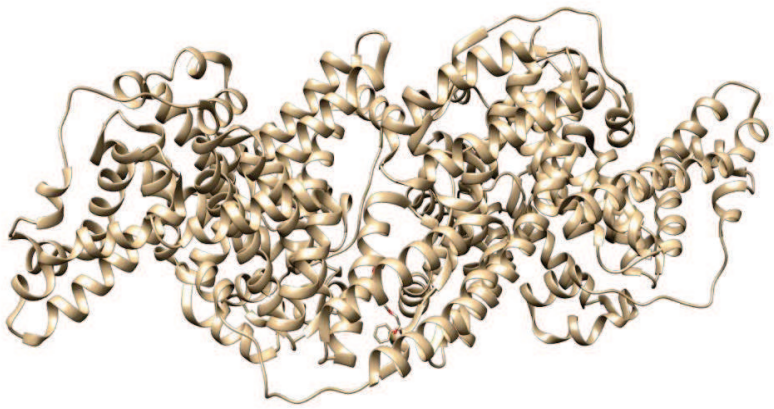

Figure 1.7: Crystal structure of bovine serum albumin (PDB: 4F5S)

Transferrin TF is a glycoprotein that binds strongly and reversibly to iron, TF consists of a polypeptide chain containing 679 amino acids and 19 intrachain disulphides, with two homologous N-terminal (residues 1-336) and C-terminal (residues 337-678). It has a molecular weight of 80 KD. The binding of iron to the TF depends on carbonate anions, viz. two Tyr, a His, and Asp (Figure 1.8).[39-40] Transferrin is a crucial biomacromolecule for normal cell growth and maintenance.[41] The crystal structure of TF has two binding sites in the N lobe and one in the C lobe of hTF.[42]

Figure 1.8: Apo-human serum transferrin non-glycosylated (PDB:2HAU)

1.5 Other biopolymers.

A lot of research has been done on synthetic polymers as well as on natural polymers, which are also called biopolymers**.** Natural polymers are produced by organisms, and include proteins and nucleic acids as mentioned above, but also polysaccharides. An example of a biopolymer is cellulose (Figure 1.9).

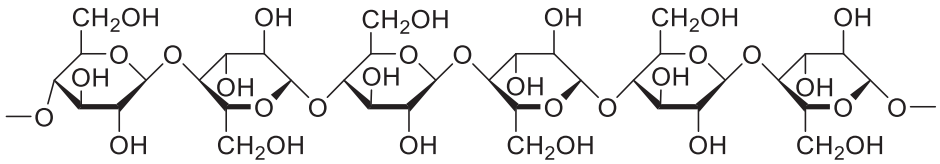

(1-4)-beta-D-glucopyranan

Figure 1.9: Natural polymer cellulose.[43]

1.6 Synthetic polymers.

Synthetic polymers include nylon, polyacrylic acid and polystyrene sulfonic acid .[44]

Sodium Poly styrene sulfonate

Poly acrylic acid

Figure 1.10: The structures of synthetic polymers POSA and PAA

A polymer is a high molecular weight macromolecule made up of multiple repeating units of chemical units (monomer). A homopolymer is made of only one kind of monomer, for example, polyacrylic acid (PAA).If a homopolymer (A) is linked to another homopolymer (B), we obtain a block copolymer for example if polyacrylic acid (PAA) and polystyrene sulfonic acid (POSA) are joined through covalent bonds to form single macromolecules[45] (Figure 1.11).

Homopolymer (A): PAA-PAA-PAA-PAA-PAA

Block copolymer (AB): PAA-PAA-PAA-PAA-PAA-POSA-POSA-POSA-POSA-POSA

Figure 1.11: Schematic representation of various types of synthetic polymer structures

Homopolymer (A) involves monomers of acrylic acid A while block copolymer AB involves both acrylic acid and styrene sulfonate.

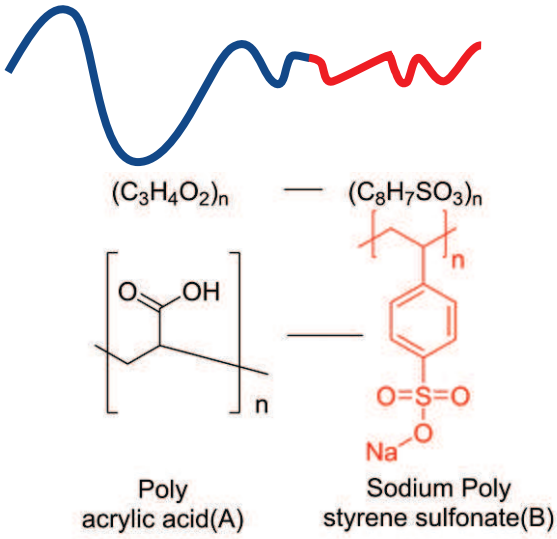

Figure 1.12: Linear AB diblock copolymer consist of the A (black) and B (red) blocks

Block copolymers can be assembled in aqueous media[46-47] In fact, many structures can be formed by manipulating different factors such as block length, temperature, concentration and preparation method of the sample.[48-49] For example, incompatible blocks can be used to drive the self-assembly behaviour of block copolymers. For example , the structural specificity of these molecules permits the hydrophobic aggregation of fragments in a particular polar solvent, while the hydrophilic groups have high affinity for polar (aqueous) media.[50]

1.6.1 Conjugated Polymers and Oligomers

Polymers consist of a high but finite number of repeated monomer units linked by covalent bonds, while oligomers contain low numbers of repeated monomer units.[51] In 2000, the chemistry Noble Prize was awarded to Alan Heeger, Alan G. MacDiarmid and Hideki Shirakawa for their discovery and development of conductive polymers.[52]

The delocalized π-system and low band gap give polyacetylenes semi-conducting properties.[53] The electronic structure of conducting polymers needs to be manipulated by doping the polymers by oxidation or reduction to increase the conductivity.[54] Conjugated polymers can be used in a wide range of applications, such as fuel cells and biosensors.[55] Many conjugated oligomeric and polymeric systems can bind to DNA and give a high response because of high sensitivity to the changing environment due to alteration in the chain as a consequence of the interaction between π-conjugated oligomeric and polymers and DNA.[56-57] Optical and electronic properties can be optimised by adding different functional groups to the backbone of the polymers.[56, 58] Some structures of conjugated polymers are shown in Figure 1.13.

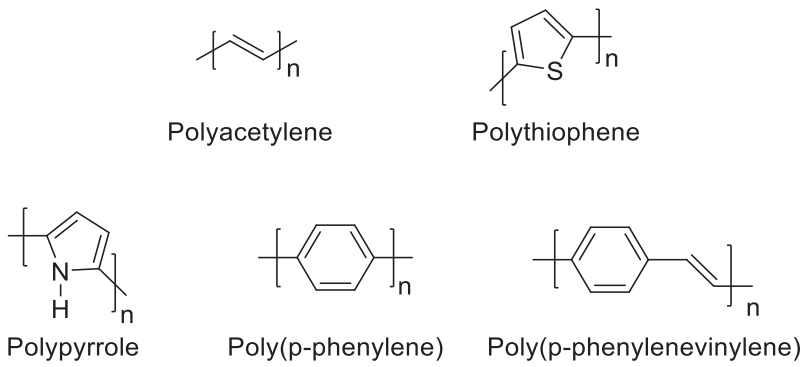

Figure 1.13: The structures of some conjugated polymers polyacetylene, polythiophene, polypyrrole, poly (p-phenylene) and poly (p-phenylene vinylene).

π-conjugated molecules are often rigid molecules, and interchain forces occur that typically lead to conjugated polymers being insoluble in many organic solvents and in an aqueous medium. As a result, positive or negative charges are often introduced on the backbone of the polymers to increase their solubility.[53, 59] When cationic functional groups are added to in some of these π-conjugated oligomer systems an increased driving force for these compounds to bind to DNA has been shown.[60] It is crucial to understand the specificity of the binding of these compounds to DNA to design useful biosensors. By understanding the mechanism of specific interaction with DNA, it is possible to check whether or not the compound behaves in a specific manner.[61]

1.7 Biosensors

Biosensors are systems that are able to detect biochemical species such as nucleic acid and protein. Biosensor applications range from health care, medicine, biotechnology and environmental science.[62] A biosensor contains a biotransducer that is attached to the bioreceptor element. The bioreceptor is the sensing element that recognises target analyte which links to a physical element that transduces the recognition event into a measurable physical change.[63]

In a biosensor, the bioreceptor may be a polysaccharide, nucleic acid (RNA, DNA), antibody, enzyme and living cell which interfaces with the analyte, and the biotransducer converts this binding into an electronic signal.[64] Biosensors that use nucleic acid (DNA or RNA) binding are also called genosensors.[65-66] The procedure depends on base pairing adenine−thymine (A-T) and cytosine−guanine (C-G) in DNA. Single-stranded DNA probe based bioreceptors are immobilised on the surface of the sensors to capture single−strand target DNA by a hybridization reactions.[67] As a result of the interaction, a transducer response is generated as shown in Figure1.14.[63, 67]

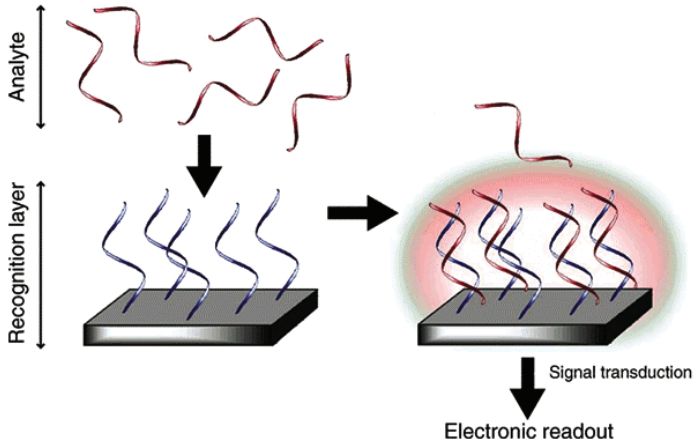

Figure 1.14: General DNA biosensor design.[63]

DNA biosensors (genosensors) open the door for faster, cheaper, sensitive and simpler nucleic acid detection in mixtures.[68,69] Professor Leland C. Clark[70] was the first researcher that developed the biosensor in 1956; an enzyme electrode to measure glucose.[71] After that, many modifications were made to promote sensor sensitivity, selectivity, and specificity.[72]

Kongsuphol, Ng *et al*[73] introduced a new method to develop the biosensors which deal with the serum background, which is an essential issue for biosensor development because components of serum may interfere with the determination of the analyte interest and could give rise to the false positive signal. The process involves detecting tumour necrosis factor (TNF) or TNF-α from human serum in three steps. Firstly, Abundant protein backgrounds are depleted from serum using albumin combined with magnetic beads and IgG antibodies. Secondly, following background depletion, TNF-α is captured using a magnetic bead-coupled TNF-α antibody. Finally, the captured TNF, is eluted from the magnetic beads and detected utilize the EIS method which is used to improve the sensitivity of detection. They found that the depletion of serum background decreases the effect of background interference.[73]

The challenges in our thesis are to develop and improve biosensors detecting DNA in mixtures, for example in serum from whole blood, without further work, and also to increase the sensitivity with reduced nonspecific interactions that may lead to false positive or negative signal. We introduce a new method that it is easy to use, involves cheap compounds and is fast.

The Figure 1.16 explains how the bioreceptor binds to an interesting analyte and how the sensitisers interact in both specific and nonspecific interaction. In addition, nonspecific binding to 6-mercapto-1-hexanol (6.M.1.H) might lead to negative or positive false.

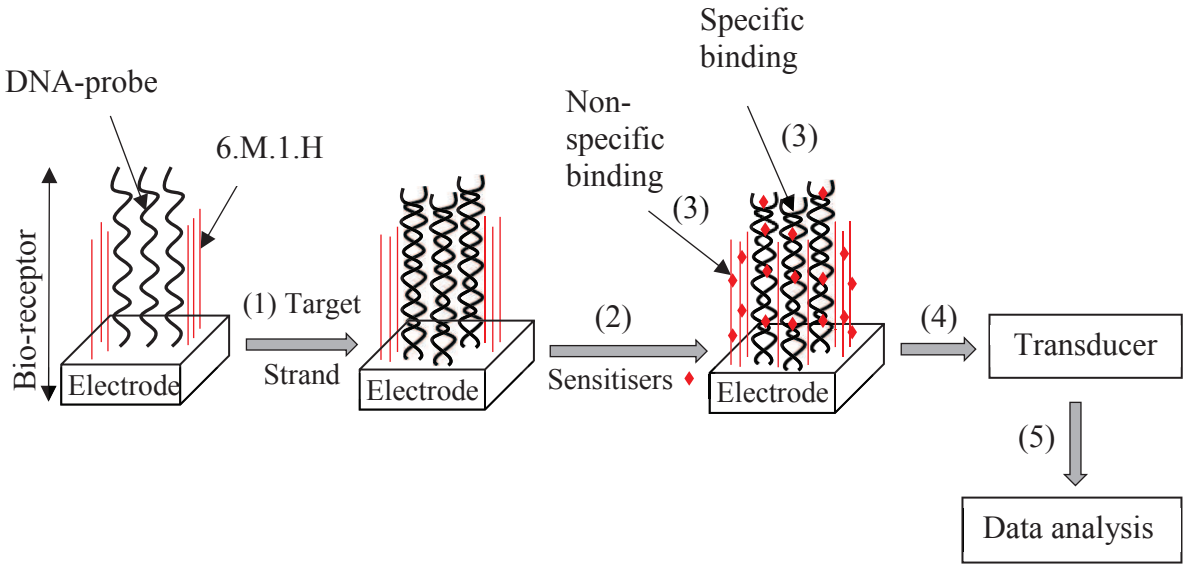

Figure 1.15: General design of the biosensors proposed

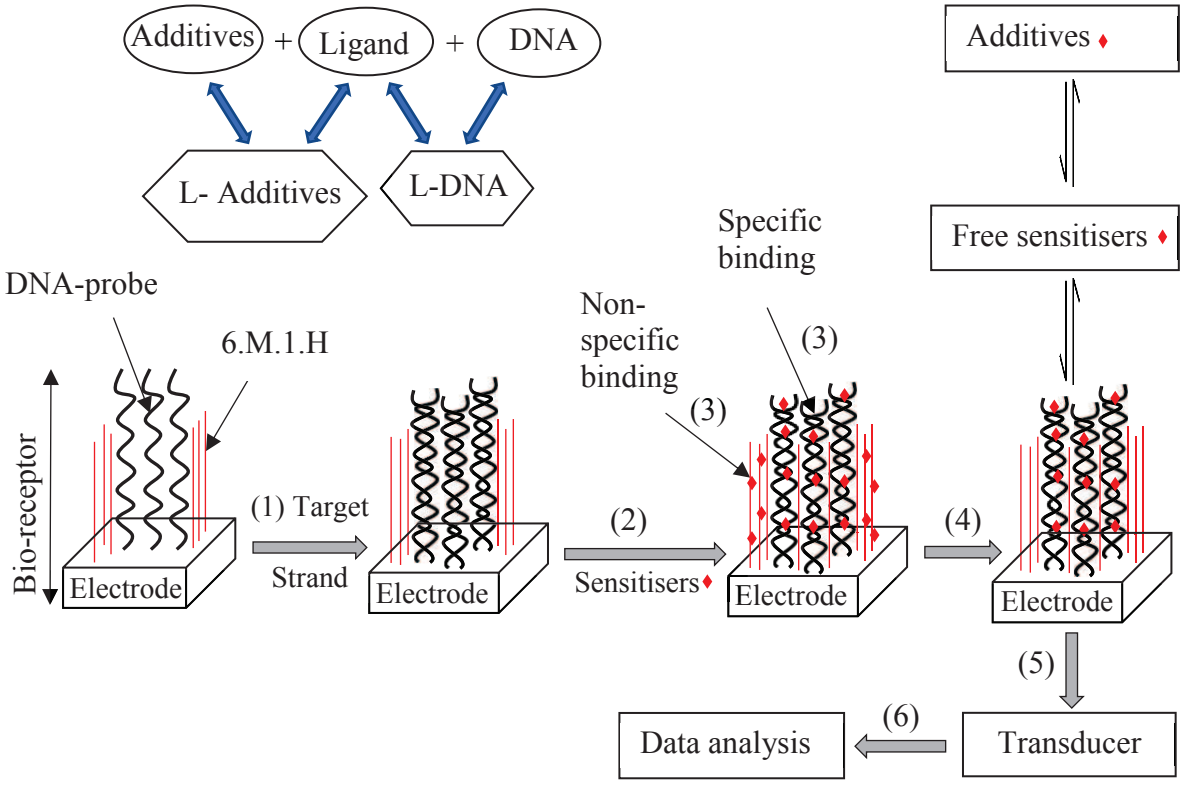

Figure 1.16: Overview of the interactions leading to false positives and false negatives as affected by the additives such as selected proteins SA and TF, biopolymers HA and AA, synthetic polymers POSA and PAA and surfactant Tween -20. The interaction between target strand and probe DNA forms duplex DNA (1). Binding occurs between double−stranded DNA and sensitisers (2). Specific and non-specific interaction may occur (3). The potential sensitisers stay in equilibrium between binding with DNA or binding with additives (4). The transducer detects the biological event (5). The data analysis generates a measurable output (6).

Figure 1.16 shows how nonspecific binding to the (6.M.1.H) can lead to high baseline signal (e.g. current) and / or a false positive. We need the sensitisers to bind just to DNA and minimise any nonspecific binding between ligands and electrode surface which lead to the false positive signal. This also minimises the baseline.

1.8 Detection Methods for genosensors.

1.8.1 Optical detection of DNA

The optical detection in biosensors involves an optical transducer and a bioreceptor. The biorecognition event is registered in a non-destructive manner by the optical transduction method. In addition, high selectivity is possible in optical detection in biosensors by wavelengths selection. Optical detection in biosensors uses absorbance, fluorescence and / or phosphorescence.[74]

It is vital in biological samples to detect and quantify small amounts of DNA.[62, 75] Leclerc and co-workers reported how cationic polythiophenes can be used to study DNA-hybridisation,[56, 76] some structures used for the detection of DNA are shown in Scheme 1.1.

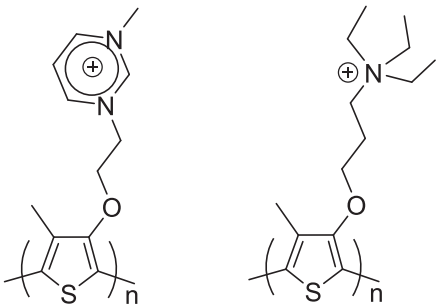

Polymer 1 Polymer 2

Scheme 1.1

Detection of ssDNA using a capture strand together with cationic polythiophenes is very flexible due to several points. First, a maximum absorption around 397 nm associated with yellow colour was observed for water-soluble cationic polythiophene in aqueous solution in the absence of DNA. Second, it is possible to produce a strong red-shift, which has been attributed to an increase in effective conjugation length resulting from an increase in the planarity of polythiophenes, upon addition a single−stranded DNA. Third, upon addition of a complementary single-stranded DNA, a complex of double-stranded DNA with cationic polythiophene will be formed which causes the UV-visible spectrum to shift to the blue region

relative to the single strand of DNA–polythiophene complex. The final absorption is still red-shifted in comparison with the absorption of free cationic polythiophene. The colour changes can be seen by naked eye. After adding of the single strand of DNA, the colour of the cationic polythiophene moves from yellow to red, and then back to yellow upon adding the complementary single strand of DNA[76-77] (Figure 1.17 and Figure 1.18).

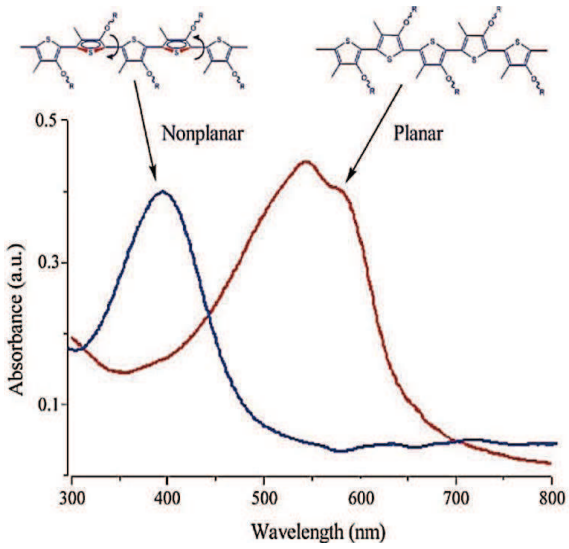

Figure 1.17: Conformations and corresponding UV-visible absorption spectra of polythiophene.[77]

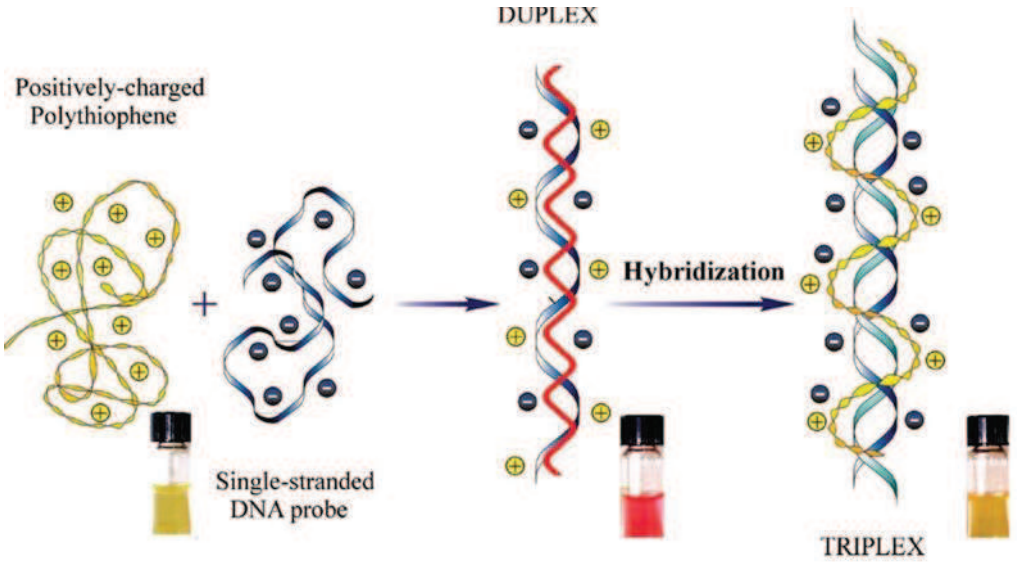

Figure 1.18 Optical detection of double-stranded DNA using polythiophenes taken from reference.[56, 76]

1.8.2 Electrochemical detection DNA technique.

The binding of a biological molecule, *i.e.* a target analyte of interest, with the bioreceptor is translated into an electrical signal by an electrochemical process which can be observed and converted into a signal by the transducer system.[78]

Electrochemical detection of DNA has been studied intensively by many researchers, and these methods are easy-to-use, fast, inexpensive, have high sensitivity, and allow miniaturisation of sensors.[79-82] The first introduced work in this field was by Garnier and co-workers to detect DNA hybridization electrochemically.[61] In their design, a polypyrrole backbone was covalently connected to a single-stranded of DNA (ssDNA) probe. Upon hybridization with a target strand, a decline in the current and a move to more positive redox potential could be detected in the electronic system.[83] These electronic changes were attributed to the modification of the structure of polypyrrole that occurs upon interacting of the polymer-ssDNA probe with the target strand leading to formation of DNA duplex.[84]

Moreover, functionalized polythiophenes were also used to determine DNA hybridization electrochemically according to the method suggested by Garnier and Co-Workers.[85] For example, a terthiophene that has a carboxyl group COOH may be electropolymerized on a glass carbon electrode as described by Lee et al Lee,*et al*..[86]

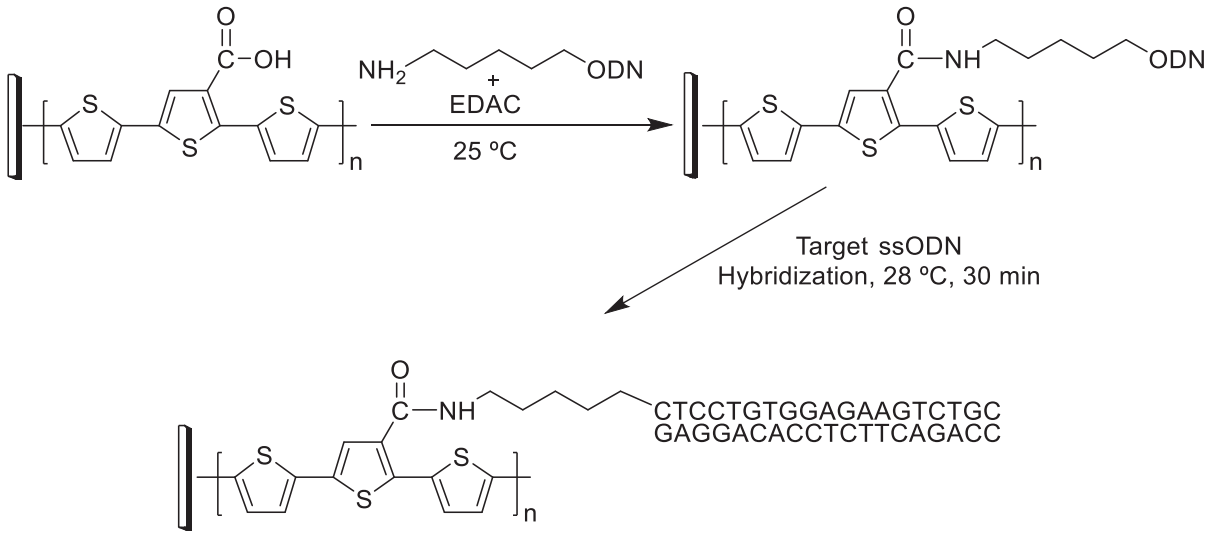

Scheme 1.2[85]

The hybridization of the complementary analyte target oligonucleotide with the probe immobilized on the sensing surface causes a reduction in values of resistance because the double-stranded DNA has higher impedance than single-stranded DNA. The hybridization

process can, therefore, be easily confirmed based on the variation of the resistance values before and after hybridization.

In addition, Lee, *et al.* studied the response of the polythiophene-oligonucleotide probe to mismatched oligonucleotides, such as one-base mismatch and two-base mismatch. They found a limited difference in impedance before and after hybridization.

The polythiophene-oligonucleotide probe formed in this study therefore especially distinguishes matched and mismatched oligonucleotide sequences.[85]

An electrochemical biosensor normally comprises of an electrode surface which is attached to a bioreceptor sensing element. An electrical change in either current transfer (amperometric), voltage (potentiometric and field effect devices), impedance (impedimetric) or conductivity (conductometric) across the electrode can be quantified upon binding of an analyte with probe bioreceptor.[87-88]

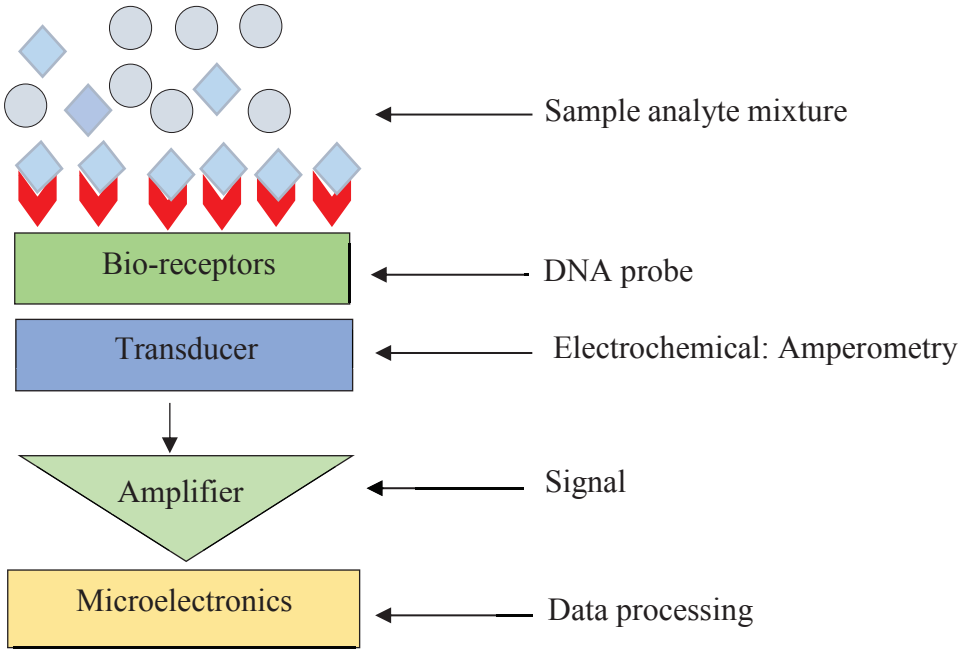

Figure 1.19: Biosensor Scheme.[88]

Figure 1.19 shows an electrochemical biosensing system. A suitable bio-recognition layer that exploits a physical or chemical process is used to modify the electrode surface.[89] Research usually concentrates on finding the most appropriate recognition element and optimising the interaction to support the binding efficiency besides the signal produced.[90]

1.9 Reversible interactions of small molecules with DNA

There are three categories of non-covalent interaction modes of small molecules with DNA: electrostatic interaction, intercalation and groove binding.[91]

1.9.1 Electrostatic interactions

DNA exists as a polyanionic species which attracts positively charged groups of compounds by electrostatic interactions.[92-93] The interactions can occur between cations (Na^+ , Ca^{2+} and NH_4^+) and the polyanionic backbone of DNA[94]. Changing salt concentration (ionic strength), changing the amount of water present, and binding between DNA and molecules can lead to a change of conformation of DNA.[95-96] Electrostatic interactions may be modulated by both size and charge of ligand, as well as the hydrophobicity of ligand.[97-99] The stability of the DNA conformation normally depends upon this interaction. In aqueous solutions, small inorganic cations, for example, Na^+ or Ca^{2+}, bind with DNA which results in partial neutralisation of the phosphate backbone's charge. Hence, the binding of small molecules with DNA is influenced by the ionic strength of the solution.[94]

1.9.2 Intercalation and Intercalators

Intercalation simply means the insertion of a rigid planar aromatic ring system between DNA base pairs. Intercalation is typically enthalpically driven and leads to considerable changes in nucleic acid structure.[100] We can find many examples of intercalators, such as 9-amino acridine, ellipticine, and chlorpheniramine (Scheme 1.3). Intercalators are often flat aromatic and rigid.

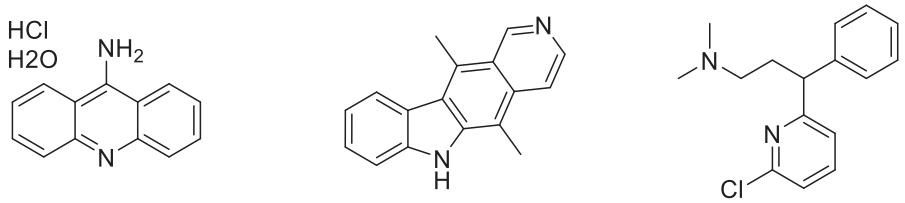

9-Aminoacridine Elipticine Chloropheniramine

Scheme 1.3

In fact, the major binding force in intercalation are π-π stacking interactions as well as Van der Waals interactions between the aromatic DNA binder and the base pairs of DNA.[101-102]

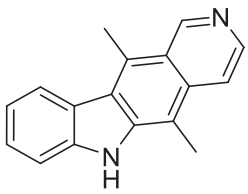

Elipticine

Figure 1.20: Binding of ellipticine intercalator in complex with a 6-base pair of DNA (**NDB D**: DD0070).

For intercalators, the neighbour exclusion principle means a binding site typically distorts and blocks the neighbouring binding site.[103] Therefore, accommodation of the second intercalator between base pairs adjacent to bound intercalator is blocked.[98] Increasing positive charge on an intercalator leads to an increase in the affinity.[104]

1.9.3 Groove binding (Major and Minor)

The DNA structure has two grooves due to the double-helical structure and the geometry of the base pairs. In fact, in B−DNA there are two unequal size grooves in the helix, a major groove which is wide and shallow (12 Å) and minor groove which is narrower and deeper (6 Å).[105]

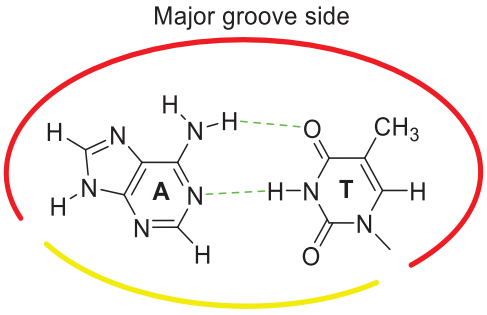

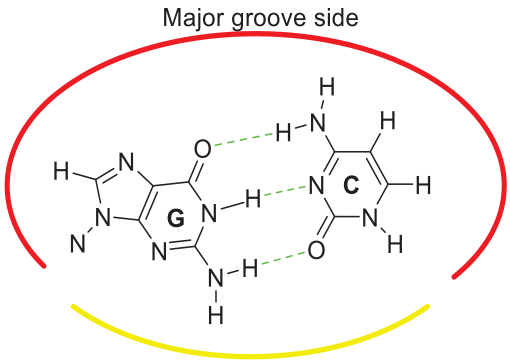

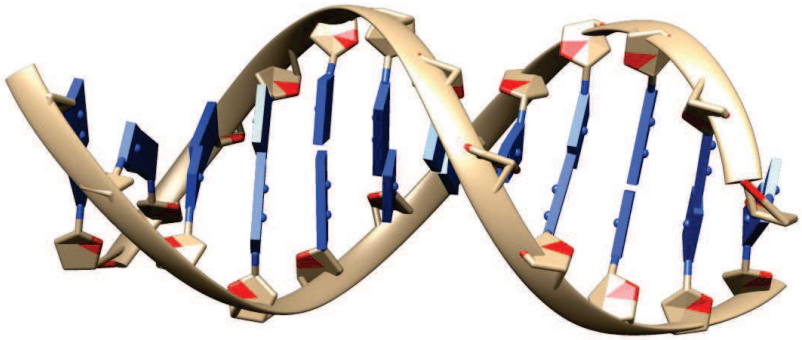

Figure 1.21: DNA base pairs showing the exposed functional groups in the major and minor grooves showing possible H bond donor and acceptors[106] (top). Major and minor grooves of DNA (NBD ID: BD003) (bottom).

Ligands can bind in the major and minor grooves of DNA helix.[106] Common groove binders are usually long crescent-shaped cationic molecules (Scheme 1.4). Like intercalators, groove binders can be used for clinical treatment of cancer and bacterial infection.[107]

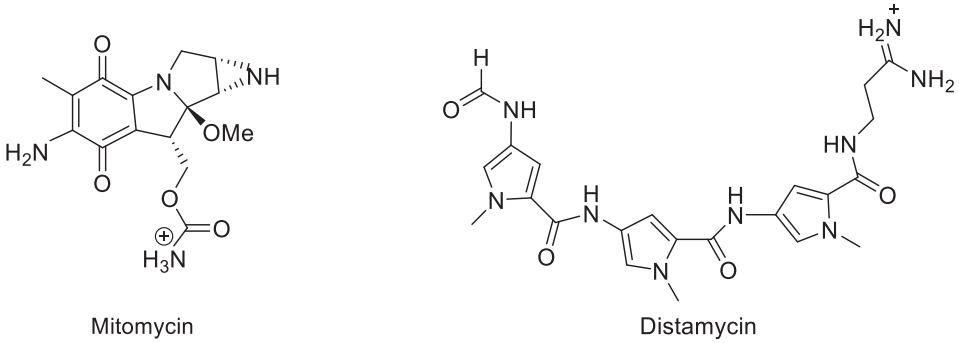

Scheme 1.4

Groove binding is not like intercalation which causes significant changes to the structure of the DNA molecule. Groove binding can be described more as a lock-and-key model where a biomacromolecule and a ligand match together.[108-109] Groove binding, both in the minor and major groove, is driven by electrostatic interaction and hydrogen bond formation between the complex and DNA base pair. DNA-ligand complex is further stabilised by hydrophobic and Van der Waals forces in the grooves.

1.10 Supramolecular and self-assembled nanostructured materials.

One of the most active areas of research in recent years is supramolecular chemistry. Weak non-covalent interactions between molecules, such as electrostatic, Van der Waals, hydrogen bonding, charge transfer and π-stacking, play a major role in driving assembly processes. Self-assembly is an automatic process that arranges the components into ordered aggregates or structures without external force.[110-112] Nature also uses these weak non-covalent interactions in forming large and ordered complex supramolecular biomolecules.[113-114]

1.11 Techniques used for quantification affinity of small molecules for macromolecules

The interactions between biomacromolecules and oligoheteroaromatics can be measured via several techniques such as UV-visible, circular dichroism spectroscopy and isothermal titration calorimetry (ITC). A brief discussion of these methods is presented below.

1.11.1 UV-visible Spectroscopy (UV-vis)

In UV−visible spectroscopy, light is employed to elevate electrons in molecules from the ground state to an excited state. When the light absorbed is measured as a function of its wavelength λ (or frequency ν) a spectrum is obtained. Light is usually absorbed in the visible region (400-800 nm) or the near–uv region (150-400 nm) by molecules that have a delocalised aromatic system that needs less energy to enhance electrons to an excited state (Equation 1.1).

$$\Delta E = E_1 - E_2 = \nu = \frac{hc}{\lambda} \qquad \text{..... (1.1)}$$

Here the energy gap ΔE is between ground state and excited state, ν is the frequency of light, h is the Planck constant, c is the speed of light, λ represents the wavelength of radiation. This technique is instrumental in analysing conjugated organic compounds and biologically macromolecules, such as nucleic acids and proteins, whose concentration in aqueous buffer can be accurately measured by absorbance quantities through the Beer Lambert law.

The delocalized π-system in the studied DNA binders can absorb light in UV-visible region. As a result, UV-vis spectroscopy is an appropriete tool for binding studies. The absorption intensity depends on the substance concentration, the chemical nature, and the molecular chromophore environment. The absorbance analysis is based on the Beer-Lambert law, which shows that the concentration of an ideal solution is linearly related to its absorption.[115-116] Changes to a

spectrum may correspond to increase (hyperchromic) or decrease (hypochromic) in absorption coefficient or a shift of the wavelength of maximum absorption to higher wavelength (red shift or bathochromic shift) or lower wavelength (blue shift or hypsochromic shift).[116]

Non-covalent interactions of a chromophore with macromolecules can be studied through these spectroscopic responses. These spectroscopic responses can be due to environmental change experienced by the ligands or to a confirmation change. The change from aqueous solution to a more hydrophobic environment is an example of an environmental change. When plotting several spectra for one titration in one graph an isosbestic point may be observed, an isosbestic point is a point where two species have the same extinction coefficient. The presence of an isosbestic point is typically interpreted as presenting two species viz. free and bound ligand in equilibrium.[117-118]

A titration curve can be obtained from the UV-visible spectroscopy data when all spectra have been recorded. By analysing spectroscopic data for a binding process, the binding constant $K_{binding}$ and stoichiometry n can be obtained. The formation of a complex (C) can be defined as the binding of the ligand (L) with the binding site of DNA (*bs*), and the concentrations of the ligands and DNA are related through $K_{binding}$ (equation 1.4). Any binding process covers a ligand-specific number of bases, the binding site size n. The concentration of binding sites is defined as the concentration of DNA base pairs over N (equation 1.5). The equilibrium between three compounds (free DNA, free ligand and the ligand bound (complex) is called the binding constant $K_{binding}$ (equation 1.3). As the concentration of free ligand $[L]_f$ and the complex concentration [C] are related via the total ligand concentration $[L]_{tot}$, it is possible to establish an equation describing the equilibrium (1.8).

$$\boldsymbol{L_f + bs_f \leftrightarrow L_b} \quad \textbf{..... (1.2)}$$

$$\boldsymbol{K_{bind} = {[L]_b}/{[L]_f \cdot [bs]_f}} \quad \textbf{..... (1.3)}$$

$$\boldsymbol{[C] = K_{bind} \cdot [bs]_f \cdot [L]_f} \quad \textbf{..... (1.4)}$$

$$\boldsymbol{[bs] = {[DNA]}/{N}} \quad \textbf{..... (1.5)}$$

$$\boldsymbol{[L]_{tot} = [C] + [L]_F \leftrightarrow [L]_f = [L]_{tot} - [C]} \quad \textbf{..... (1.6)}$$

$$\boldsymbol{[bs]_{tot} = [C] + [bs]_f \leftrightarrow [bs]_f = [bs]_{tot} - [C]} \quad \textbf{..... (1.7)}$$

$$\boldsymbol{[C] = K_{bind} \cdot ([bs]_{tot} - [C]) \cdot ([L]_{tot} - [C])} \quad \textbf{..... (1.8)}$$

$$[C] = K_{bind}.[bs]_{tot}.[L]_{tot} - K_{bind}.[C].[bs]_{tot} - K_{bind}.[C][L]_{tot} - K_{bind}.[C]^2 \quad \text{..... (1.9)}$$

It is possible to rearrange equation (1.9) to give a quadratic equation:

$$K_{bind}[C]^2 - (1 + K_{bind}.[bs]_{tot} + K_{bind}.[L]_{tot.}[C]) + K_{bind.}[bs]_{tot.}L_{tot} = 0 \quad \text{... (1.10)}$$

Using the classic solution, the quadratic equation can be treated to obtain the concentration of complex $[C] = \frac{-b \pm \sqrt{b^2-4ac}}{2a}$ as a function of total ligand and DNA concentrations.

$$[C] = \frac{1 + K[bs]_{tot}K[L]_{tot} \pm \sqrt{(1 + K[bs]_{tot} + K[L]_{tot})^2 - 4K^2[bs]_{tot}K[L]_{tot}}}{2K} \quad \text{... (1.11)}$$

Combining equation 1.11 with the Beer-Lambert Law ($A = \varepsilon.L.[C]$) modified for background absorbance, the absorbance is expressed by Equation 1.12. This equation can be fitted to a relation between absorption and total DNA concentration to determine the best approximations for K_{bind} and the binding site size.

$$Signal_{obsd} = background + Sig_{f.m.}L_f + \Delta_{bind}.Sig_m \frac{1+K.\frac{DNA}{N}+K.[L]_{tot}-\sqrt{\left(1+K.\frac{DNA}{N}+K.[L]_{tot}\right)^2 - 4K^2.\frac{DNA}{N}.[L]_{tot}}}{2K}$$

(Equation 1.12)

In equation 1.12, $\text{Signal}_{\text{obsd}}$ is the observed absorbance; background is the buffer absorbance; $\text{Signal}_{\text{free,m}}$ is the product of cuvette path length and the extinction coefficient; $\Delta_{\text{binding}}.\text{signal}_{\text{m}}$ is the product of cuvette path length and change in extinction coefficient upon binding; K is the binding constant; X is the concentration of DNA or protein; N is the binding site size in base pair and $[L]_{tot}$ is the ligand concentration.

1.11.2 Isothermal Titration Calorimetry (ITC)

Isothermal titration calorimetry (ITC) is a powerful method used to measure the heat absorbed or generated as result of interactions. All the thermodynamic parameters (K, N, ΔH and ΔS) of a macromolecule–ligand interaction can be obtained at the same time by using this technique.[119] By getting the binding affinity, it is possible to determine the standard molar Gibbs free energy ($\Delta G^{\ominus}$)[66] which together with the enthalpy changes ΔH also provides the standard molar entropy changes ($\Delta S^{\ominus}$)[120-121] (equation 1.14).

$$\Delta G^{\Theta}_{binding} = \Delta G^{\Theta}_{H-bond} + \Delta G^{\Theta}_{vdw} + \Delta G^{\Theta}_{HI} + \Delta G^{\Theta}_{electrostatic} \quad \text{..... (1.13)}$$

$$\Delta G^{\Theta} = -R.T.\ln K = \Delta H^{\Theta} - T\Delta S^{\Theta} \quad \text{..... (1.14)}$$

$$K = e^{\frac{-\Delta G^{\Theta}}{RT}} \quad \text{..... (1.15)}$$

Here *R* is the gas constant (8.314 J / mole), *T* is a temperature in Kelvin. One disadvantage of ITC is the need of high concentrations of ligand and biomacromolecule. This means due consideration must be taken into account to the potential for self-aggregation of the molecule.

Isothermal titration calorimetry includes two cells, the reference cell usually includes water or MOPS buffer. The other cell is a sample cell which contains a solution of biomacromolecules.

The syringe contains a solution of the ligand. The process involves injection of the solution of the ligand into the host cell.[122]

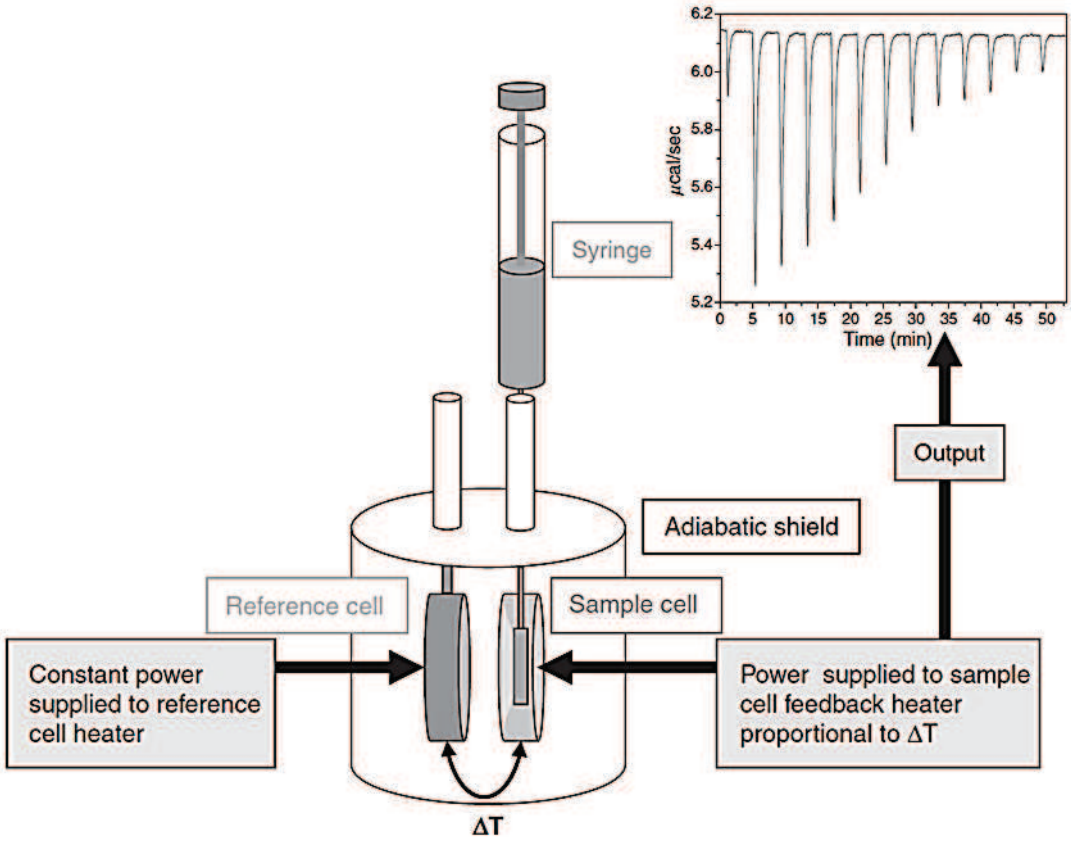

Figure 1.22: Schematic representation of the ITC instrument.[123]

When constant power is provided to both cells, they should stay at the same temperature. Two things may be observed when an interaction between the ligand and the macromolecule happens:

1- In an exothermic reaction, adding ligand to the macromolecule causes an increase in the temperature of the sample cell. For this reason, the feedback power to the sample cell is decreased in order to maintain an equal temperature between the two cells.

2- In an endothermic reaction, the opposite occurs, the temperature in the sample cell goes down, so a feedback power needs to increase in order to maintain a constant temperature.[122, 124] In a typical experiment, the raw data are plotted as a heat flow per unit time needed to maintain the sample cell at the same temperature of the reference cell as a function of time. After that, the raw data is divided by the amount of material injected which gives the molar heat effects. These heat effects can be analysed in terms of a binding model.[123]

1.11.3 Circular Dichroism (CD)

Circular dichroism is an essential absorption technique to determine biomacromolecule binding. An induced CD signal is beneficial in studying the binding between ligands and DNA when small ligands, chiral or non-chiral, bind to the chiral DNA polymer. The transition dipole moments of the binder will interact with the nucleobase transition dipole moments in such a way that they will display a new CD signal, the induced CD. An induced CD signal only appears when the ligand interacts with DNA.[125-126]

Circular dichroism measures the differential absorption of the left and the right circularly polarized light which will be absorbed by the active chiral molecules (equation 1.16).

$$\boldsymbol{CD = \Delta A = A_l - A_{r=}\, \Delta\varepsilon . C . L} \qquad \textbf{…… (1.16)}$$

Where, ΔA is the difference between absorbance of the left and right circularly polarized light; A_l is the absorbance of left-handed circularly polarized light and A_r is the absorbance of right-handed circularly polarized light. Δε is the difference between two different extinction coefficients of right and left polarized light.

The molecule that has a chiral chromophore will absorb one of these circularly polarised lights more than the other. The difference in absorption of the right and left-handed is measured using CD technique.[127-128]

The binding between a chiral biomolecule and achiral compound leads to induced circular dichroism (ICD) of the achiral counterpart. The binding mode can be interpreted from the induced CD spectra for DNA binding,[129] due to molecules interacting with DNA, the interaction between the transition dipole moments of the ligand and the DNA bases substantially affects the ICD signal of the binder.[127]

1.12 Selected nucleic binders

The oligoheteroaromatic molecules used in this study all have a π-conjugated chromophore and auxochromes. These molecules, therefore, have absorption and fluorescence spectra in the UV-visible region of the spectrum, and consequently, they could be used as DNA−binding sensitisers in biosensors. Moreover, these π-conjugated molecules have flat, rigid, structures and some of them have interesting redox properties. The charges can help to increase the electrostatic interactions and solubility in water.

Three poly(amidoamines) (PAMAM) compounds **1.1, 1.2** and **1.14** (Scheme 1.5) were provided by a collaborator.[130] The structure of these compounds has an important effect on their chemical properties and binding with DNA.[131-132] The ligands contain a highly fluorescent flat core that is connected to different small poly(amidoamine) side-groups to increase solubility in aqueous medium. Based on this structure, we anticipate the molecules of this dendrimeric family to bind to duplex DNA[133-134] via intercalation and the optical and electronic properties may change upon binding with DNA. Compounds **1.1** and **1.2** are highly fluorescent, and they could be used as components in DNA biosensors based on the fluorometric detection.

Compounds **1.3, 1.4, 1.5** and **1.6** (Scheme 1.5) were provided by Simon Pope group. These compounds are comprised of a rigid flat, and fluorescent aromatic framework (1,8-naphthalimide)[135] with different side-groups joined to increase the solubility in MOPS buffer. These compounds interact with DNA.[136-137] These compounds are water-soluble oligoheteroaromatics which have a strong interaction with dsDNA according to studies by our groups[138]. Changes in the spectroscopic response and electronic properties of molecules will occur upon binding with DNA, leading to a decrease in its molar absorptivity. This family may be used as a signal enhancer during detection of DNA.

Hoechst 33258 **1.7**, Methylene blue **1.8**, Fluorescein **1.9**, Thioflavin “yellow basic” **1.10** and Berberine chloride **1.11** are commercially available. Hoechst dye H33258 is used as a fluorescent stain[139] with excellent DNA binding characteristics (*i.e.* it has a crescent shape,

long, possesses a π- conjugated oligo heteroaromatic framework and flexible). The presence of single bonds, which connect the aromatic rings, permits enough rotational flexibility to fit into the minor groove.[140-141] The chromophore can be excited at approximately 352 nm to produce an emission around 455 nm in the case of binding between DNA and Hoechst.[142-143]

Hoechst 33258 is formed from two central benzimidazoles bound to a phenol ring on one side and a N-methyl piperazine on the other side. The configuration of the molecule produces a crescent shape which fits into the minor groove[144] of DNA helix without distorting the DNA.[145,146] H33258 also interacts with bovine serum albumin BSA.[147] Previous studies have found[148] a $K_{binding}$ 1.1×10^{6} M^{-1} Finally, it can be used as an antitumour agent.[149,150]

Methylene blue MB is water soluble phenothiazine family fluorescent dye that binds noncovalently with DNA.[151] It is a polyaromatic positively charged compound that is mainly used for staining of DNA and RNA. The main type of binding with DNA is as an intercalator, and the binding mode is strongly dependent on the electrostatic interaction of DNA.[151,152] The intercalator has known reversible electrochemical properties. Absorption spectra titrations have shown that one MB binds to three to four base pairs (n / b p). Moreover, **1.8** has a relatively high binding constant $K_{binding}$ with DNA[153] of approximately 10^{6} $M.^{-1}$

Fluorescein dye has a high extinction coefficient ε at 488 nm.[154] The fluorescein structure can be covalently attached to biomacromolecules, for example to DNA, to protein as well as to amino acids.[155-156] Fluorescein in aqueous solution occurs in four types namely: cationic, neutral, anionic and di-anionic. The absorption and fluorescence properties strongly depend on pH.[157-158] Fluorescein is usually used for labelling and tracking cells in microscopy applications.[159] Furthermore, fluorescein can be attached to biologically active molecules like antibodies, that allows biologists to target the fluorophore to specific proteins or structures within cells.[160]

Thioflavin "yellow basic" is a cationic benzothiazole dye which is water−soluble and shows enhanced fluorescence upon binding to DNA. DNA binding is further accompanied by red-shift in UV-visible absorption.[161] The structure of Thioflavin includes a hydrophobic end with a dimethylamino group linked with phenyl group to the positive charge on the benzothiazole group including N and S[162]

Berberine chloride is a quaternary isoquinoline alkaloid. It is classified as naturally occurring medicine.[163] The main use of berberine chloride is as a treatment against cancer[164] and

Alzheimer's disease.[165] It can be utilised for the binding to the DNA, and it offers biological activities by blocking transcription or replication.[166-167]

Oligothiophene **1.12** displays strong interactions with duplex DNA. As result, these cationic conjugated oligo hetero-aromatics can be used to detect double-stranded DNA.[168,169,170] In addition, π –conjugated oligothiophene has been used in previous work by the Buurma group and has a suitable size and shape to bind to DNA. Thiophene rings link together to produce flat, rigid and hydrophobic structure with two cationic charges and as a result, have a high affinity for DNA.Compounds **1.13** and **1.15** were prepared and used by Buurma group.

1.13 Project aims

The project aims to develop optoelectronically active compounds for use as sensitisers in sensors. Many molecules bind reversibly to biomacromolecules such as nucleic acids, selected proteins (serum albumin SA, transferrin TF), polymers (natural HA, AA and synthetic POSA, PAA) and surfactant (SDS, CTAB). When sensitisers bind to biomacromolecules, their spectroscopic and electronic properties may change due to the interaction, which leads to different applications such as in biosensors and self-assembled nanostructures

The use of optoelectronically active compounds in biosensors means that we need to understand how these compounds interact with DNA and what the effect of the presence of selected proteins and polymers (natural and synthetic) could have on genosensors. Understanding the interactions of sensitisers with other components of serum[14] and biopolymers is crucial for the development of biosensors[171] because such interactions may interfere with detection of target molecules which can lead to the false positive signal.[13] The interaction of these compounds with nucleic acids is studied in parallel projects in the group, but it is also important to know how sensitisers in genosensors interact with (for example) selected proteins of whole blood and polymers because this affects assay design. Also, we studied the binding with different types of surfactant which may be used to clean the biosensors after use.

We needed to know whether the presence of biomolecules and biopolymers affect DNA binding of ligands by offering a competing binding site.

We investigate the effect of selected proteins (SA and TF) on DNA-binding properties of potential sensitisers. The procedure includes competition between biomolecules and DNA for the same molecule. We measure the binding constant to see the effect of selected proteins on DNA-binding properties.

We can use SA, TF, natural polymers, synthetic polymers and surfactant to suppress non−specific binding through competition. Furthermore, we used negative polymers for the same purpose. In addition, we used anionic and cationic surfactant to remove the molecules which stick on the surface of the biosensor. From this work, we are looking forward to developing a new technique for developing DNA biosensors that can eventually improve clinical diagnosis of inherited genetic diseases and infections by pathogens.

The interactions can be studied using UV-visible spectroscopy, circular dichroism (CD) and isothermal titration calorimetry (ITC). UV-visible & CD spectroscopy will be used for studying the interactions in this research.

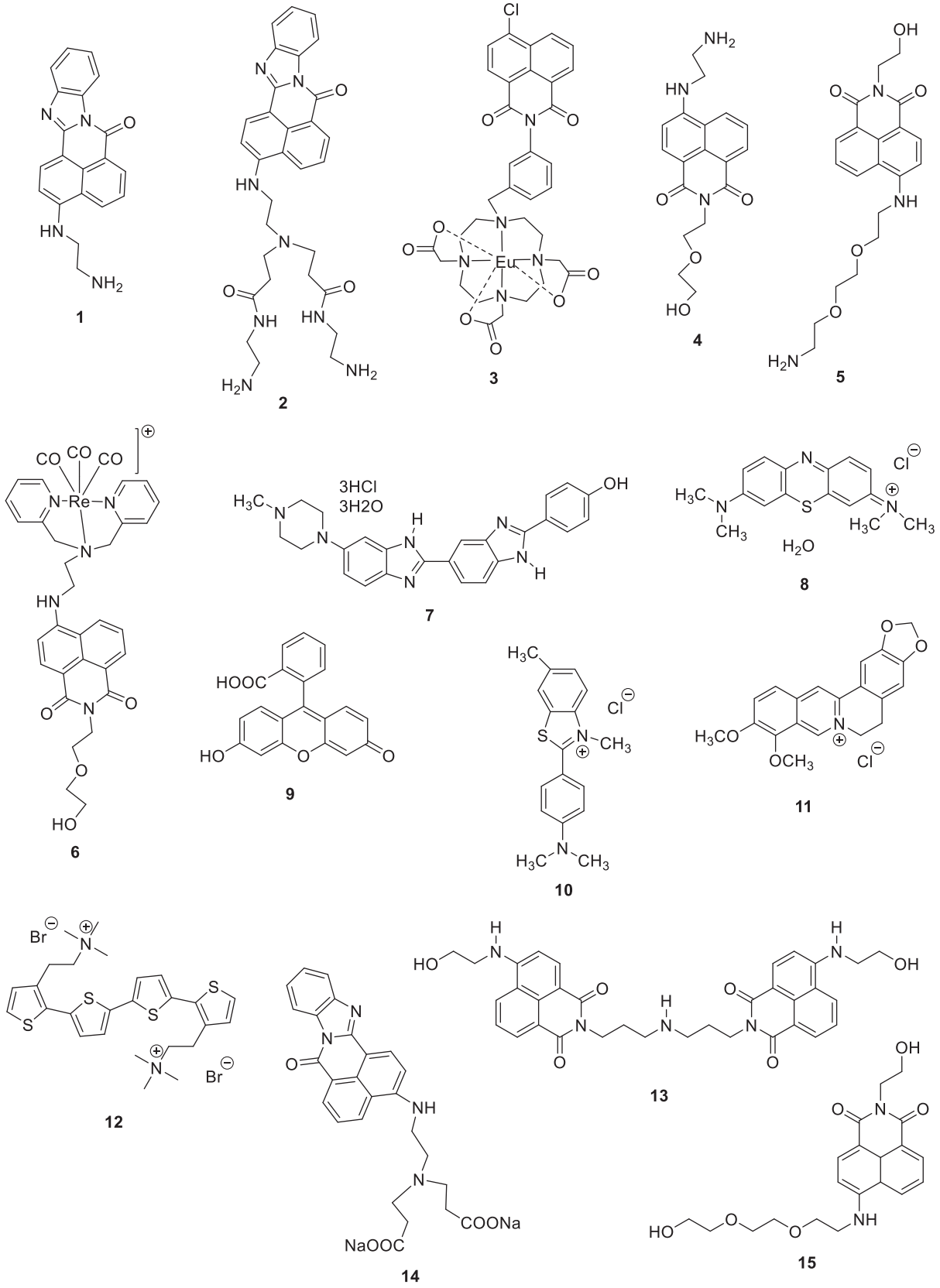

Scheme 1.5

Chapter two

DNA binding properties of π-conjugated ligands

Abstract

Chapter two presents the results of studies of the binding between π-conjugated molecules as shown in (Scheme 1.5) and double-stranded DNA.

1,8-Naphthalamide derivatives, like the previously studied **2.3, 2.4, 2.5,** have moderate affinity for DNA with binding constants of ~ 10^4 M^{-1}. The highest affinity for DNA of all naphthalamide studied here is for **2.6** which has a binding constant around 10^5 M^{-1}.

UV-visible spectroscopy was also used to investigate the binding of ligands **2.7, 2.8, 2.10, 2.11** and **2.13** to DNA. The studies confirmed that ligands **2.7, 2.8,** and **2.12** have strong affinity for DNA of ~10^5 M^{-1} under the experimental conditions explored. Moreover, we found the lowest affinity for DNA for the ligands **2.10, 2.11, 2.13** and **2.15**.

Compound **2.9** does not show any affinity for duplex-DNA. We attribute this to the negative charge of the carboxylate COO^- group on the ligand, leading to electrostatic repulsion between ligand and DNA.

2.1 Introduction

As described in chapter one, optoelectronically active DNA binders can be used as sensitisers in biosensors for DNA.

2.2 Aim

Our aims in this Chapter are to measure the binding constants and binding site sizes for π-conjugated molecules (Scheme 1.5) interacting with DNA. We will use the results as a reference for studies in later chapters to see the effect of the addition of different (bio)macromolecules on binding parameters. Ligands that have previously been studied by our group are **2.1, 2.2, 2.3, 2.4** and **2.6**.[172] Here; we want to complement this data with binding constants for **2.7, 2.8, 2.10** and **2.11**. We want to measure the affinity and binding site sizes in the same buffer (MOPS) and under identical conditions in all Chapters in this thesis.

2.3 Results and discussion

The binding of π-conjugated compounds to duplex DNA was studied using UV-visible spectroscopy. Binding studies for **2.1, 2.2, 2.3, 2.4** and **2.6** were not carried out because these compounds had already been studied[172] and were found to show good affinity for duplex DNA.

2.3.1 Compound 2.4 binding with DNA

To confirm results from previous studies[172] the binding of **2.4** to DNA was studied. The changes in absorption of **2.4** upon addition of DNA were measured in buffer (25 mM MOPS, pH 7.0, 50 mM NaCl) at 25 °C (Figure 2.1).

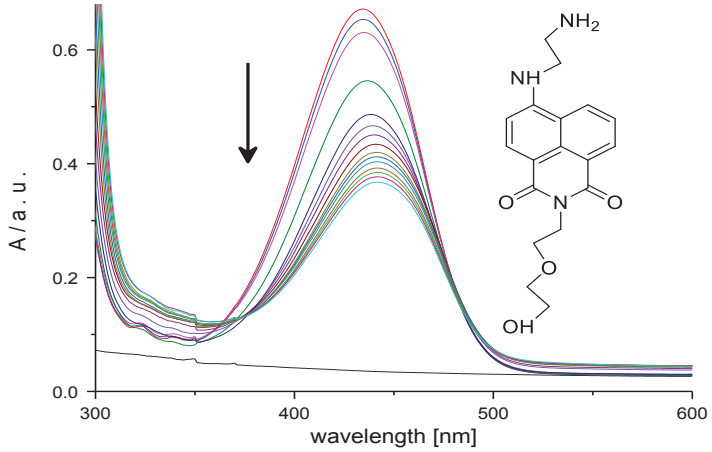

Figure 2.1: UV-visible spectra for 0.058 mM **2.4** upon addition of 0 – 3.1 mM DNA, at 25 °C in buffer (25 mM MOPS, pH 7.0, 50 mM NaCl).

Figure 2.1 shows a hypochromic shift in absorbance upon addition of DNA, with a maximum change in absorbance at 434 nm. This decrease in UV-visible absorption may have occurred as a result of geometrical distortion of **2.4** when it interacts with DNA, but it may also be as a result of a local medium effect. The binding of **2.4** with DNA is also accompanied by a slight redshift, which may be attributed to **2.4** becoming slightly more planar when binding to DNA, leading to an increase in the effective conjugation length. However, considering that **2.4** is already significantly planar when free in solution, this will be a very small effect at most.

To quantify the affinity of **2.4** for DNA, the absorbances at 434 nm were plotted as a function of the concentration of DNA (Figure 2.2, for data in tabular format, see Appendix, Tables A55.1 & A55.2).

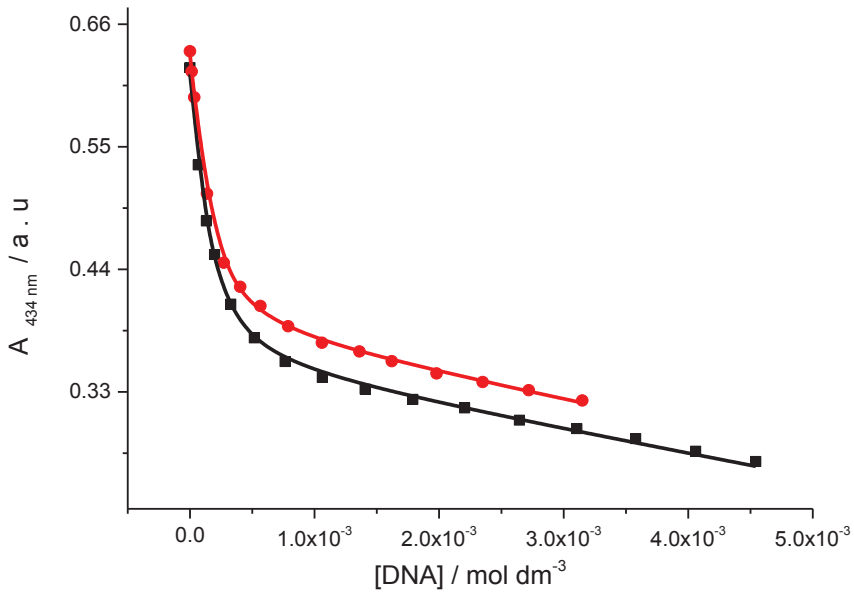

Figure 2.2: Absorbance at 434 nm for solution of 0.057 mM **2.4** (■) and 0.058 mM **2.4** (●) as a function of DNA concentration, at 25 °-C in buffer (25 mM MOPS, pH 7.0, 50 mM NaCl). The solid lines represent a global fit of the multiple independent binding sites model to the data.

Figure 2.2 shows a clear decrease in the absorbance for **2.4** upon the addition of DNA. The binding affinity $K_{binding}$ and binding site size n were determined by fitting a multiple independent binding sites model, which also takes ligand dilution into account, to the data. The fit gives an equilibrium constant $K_{binding}$ of (3.4 ± 0.6) $\times 10^4$ M^{-1} for a binding site size of (2.3 ± 0.2) base pairs. Previous studies[172] have found $K_{binding}$ of (3.3 ± 0.4) $\times 10^4$ M^{-1} for a binding site size restricted to 3 base pair. The obtained binding parameters from data analysis were reasonable in term of stoichiometry and affinity and correspond well with previous work.[172]

2.3.2 Compound 2.5 binding with DNA

For comparison with 1,8-naphthalamides **2.3, 2.4** and **2.6**, we wanted to determine the affinity of **2.5** for DNA as well. The binding of **2.5** to DNA was studied using UV-visible spectroscopy. The changes in absorption of **2.5** upon addition of DNA were measured in buffer (25 mM MOPS, pH 7.0, 50 mM NaCl) at 25 °C (Figure 2.3).

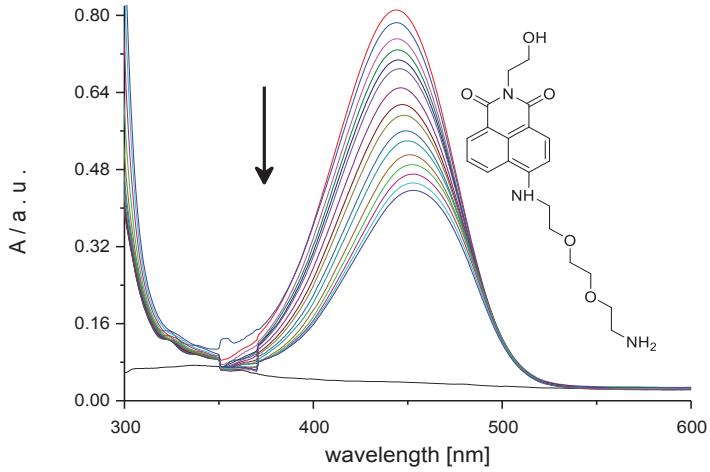

Figure 2.3: UV-visible spectra for 0.075 mM **2.5** upon addition of 0 – 2.5 mM DNA, at 25 °C in buffer (25 mM MOPS, pH 7.0, 50 mM NaCl).

Figure 2.3 shows a hypochromic shift in absorbance upon addition of DNA, with a maximum change in absorbance at 444 nm. This decrease in UV-visible absorption may have occurred as a result of geometrical distortion of **2.5** when it interacts with DNA, but it may also be as a result of a local medium effect. A slight red shift suggests a small increase in effective conjugation length, which may be attributed to an increase in planarity of **2.5** upon addition DNA.

To quantify the affinity of **2.5** for DNA, the absorbances at 444 nm were plotted as a function of the concentration of DNA (Figure 2.4, see appendix, Tables A55.3).

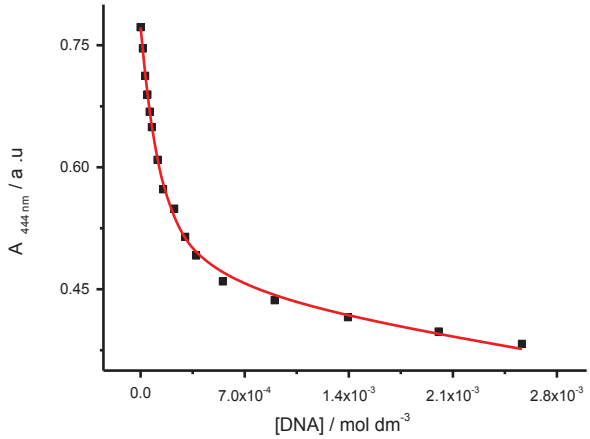

Figure 2.4: Absorbance at 444 nm for 0.075 mM **2.5** upon addition of 0 – 2.5 mM DNA concentration, at 25 °C in buffer (25 mM MOPS, pH 7.0, 50 mM NaCl). The solid line represents the best fit to the data in terms of a multiple independent binding sites model.

Figure 2.4 shows a clear decrease in the absorbance for **2.5** on the addition of DNA. The binding affinity $K_{binding}$ and binding site size n were determined by fitting a multiple independent

binding sites model, which also takes ligand dilution into account to, the data, giving an equilibrium constant $K_{binding}$ of (1.6 ± 0.7) $\times 10^4$ M^{-1} for a binding site size of (1.2 ± 0.3) base pairs. The obtained binding parameters were reasonable. Nevertheless, for comparison the data were reanalyzed with the stoichiometry restricted to a binding site size of 3.0 base pairs, giving a binding constant $K_{binding}$ of (8.9 ± 2.3) $\times 10^4$ M^{-1}.

2.3.3 Compound 2.7 binding with DNA.

For comparison with commercial compound **2.8**, **2.9**, **2.10** and **2.11**, we wanted to determine the affinity of **2.7** for DNA in our buffer as well. The binding of **2.7** to DNA was studied using UV−visible spectroscopy, the changes in absorption of **2.7** upon addition of DNA were measured in buffer (25 mM MOPS, pH 7.0, 50 mM NaCl and 10 vol.% DMSO) at 25 °C (Figure 2.5).

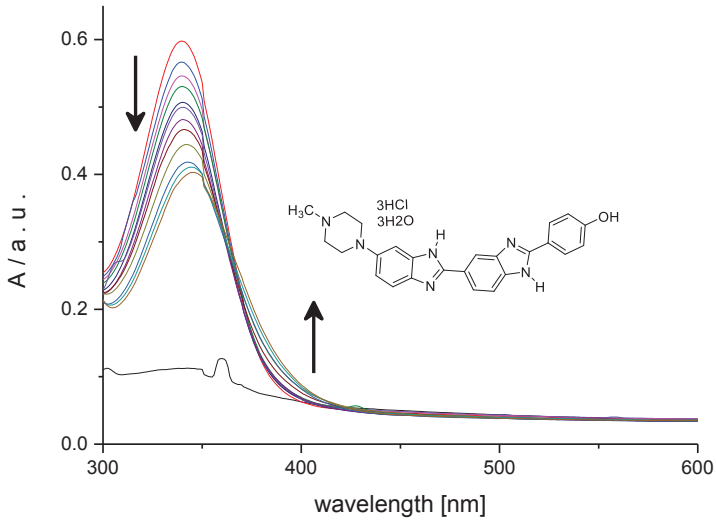

Figure 2.5: UV-visible spectra for 0.00143 mM **2.7** upon addition of 0 – 0.0797 mM DNA, at 25 °C in buffer (25 mM MOPS, pH 7.0, 50 mM NaCl and 10 vol-% DMSO).

Figure 2.5 shows that **2.7** exhibits a red shift in absorbance. The red shifts suggest an increase in effective conjugation length, which is attributed to an increase in the planarity of **2.7** upon interaction with DNA.

To quantify the affinity of **2.7** for DNA, the absorbances at 339 and 385 nm were plotted as a function of the concentration of DNA (Figure 2.6, for data in tabular format, see Appendix, Tables A55.4).

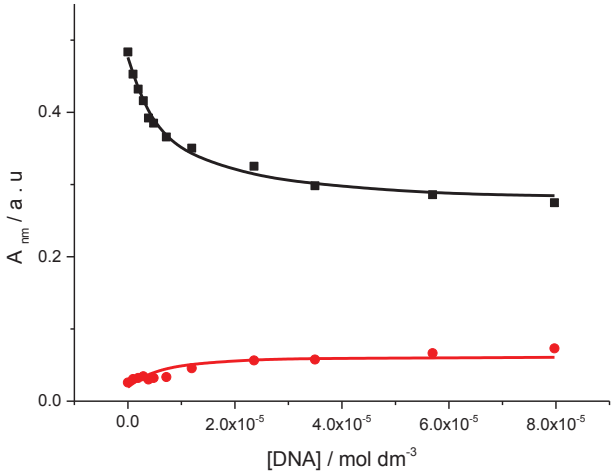

Figure 2.6: Absorbance at 339 and at 385 nm for 0.00143 mM **2.7** as a function of DNA concentration, at 25 °C in buffer (25 mM MOPS, pH 7, 50 mM NaCl and 10 vol-%. DMSO). The solid lines represent a global fit of a multiple independent sites model to the data.

The binding affinity $K_{binding}$ and binding site size *n* were determined by fitting a multiple independent binding sites model, which also takes ligand dilution into account, to the data. The fit produces an equilibrium constant $K_{binding}$ of $(5\times10^{-3}\pm1.4)\times10^{6}\ M^{-1}$ for a binding site size of $(3\times10^{-2}\pm 8.8)$ base pairs. The obtained binding parameters from data analysis were not reasonable for affinity and binding site size. Therefore, the data were reanalyzed with the stoichiometry restricted to a binding site size of 3.0 base pairs, giving a binding constant $K_{binding}$ of $(7.7\pm1.5)\times10^{5}\ M.^{-1}$. Previous studies[173] have found a $K_{binding}$ of $(5\times10^{5})\ M^{-1}$.

2.3.4 Compound 2.8 binding with DNA.

We wanted to know whether **2.8** binds with DNA. The changes in absorption of **2.8** upon addition of DNA were measured in buffer (25 mM MOPS, pH 7.0, 50 mM NaCl) at 25 °C. Figure 2.7)

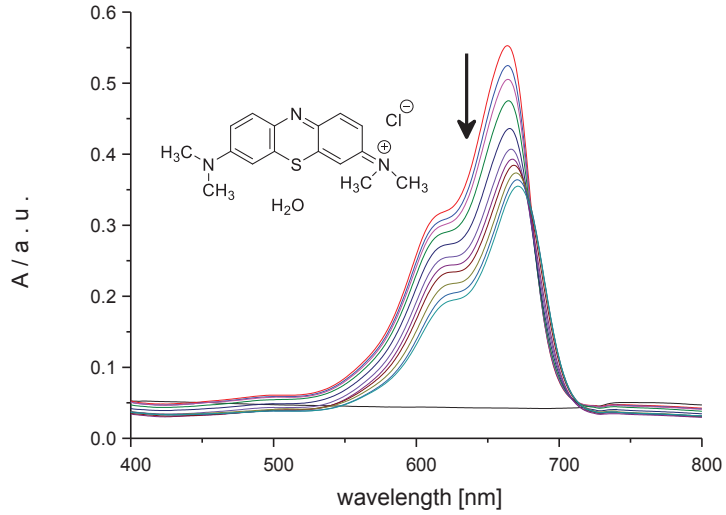

Figure 2.7: UV-visible spectra for 0.00759 mM **2.8** upon addition of 0 - 0.303 mM DNA, at 25 °C in buffer (25 mM MOPS, pH 7.0, 50 mM NaCl).

Figure 2.7 shows that **2.8** exhibits a hypochromic shift in absorbance. The small red shift suggests a minor increase in effective conjugation length, which is attributed to an increase in the planarity of **2.8** upon interaction with DNA. The decrease in UV-visible absorption may have occurred as a result of geometrical distortion of methylene blue when it interacted with DNA or as a result of local medium effect.

To quantify the affinity of **2.8** for DNA, the absorbances at 664 nm were plotted as a function of the concentration of DNA (Figure 2.8, for data in tabular format, see appendix, Tables A55.5).

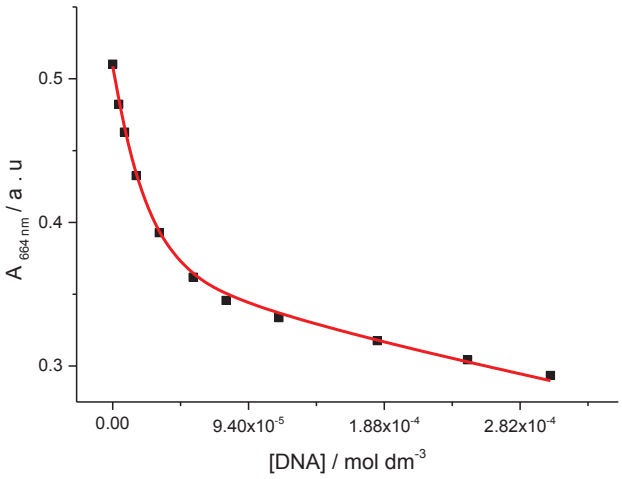

Figure 2.8: Absorbance at 664 nm for 0.00759 mM **2.8** upon addition of 0 - 0.303 mM DNA concentration, at 25 °C in buffer (25 mM MOPS, pH 7.0, 50 mM NaCl). The solid line represents the best fit to the data in terms of a multiple independent binding sites model.

Figure 2.8 shows a clear decrease in the absorbance for **2.8** upon addition of DNA. The binding affinity $K_{binding}$ and binding site size n were determined by fitting a multiple independent binding sites model, which also takes ligand dilution into account, to the data. The fit gives an equilibrium constant $K_{binding}$ of (4.5 ± 1.8) $\times 10^5$ M^{-1} for a binding site size of (3.07 ± 0.5) base pairs. The obtained binding parameters from data analysis were reasonable for affinity and binding site size. Nevertheless, for comparison the data were also reanalysed with the stoichiometry restricted to a binding site size of 3.0 base pairs, giving a binding constant $K_{binding}$ of (4.4 ± 0.5) $\times 10^5$ M^{-1}.

2.3.5 Compound 2.9 with DNA

We wanted to know whether **2.9** and DNA interact. The changes in absorption of **2.9** upon addition of DNA were measured in buffer (25 mM MOPS, pH 7.0, 50 mM NaCl) at 25 °C (Figure 2.9).

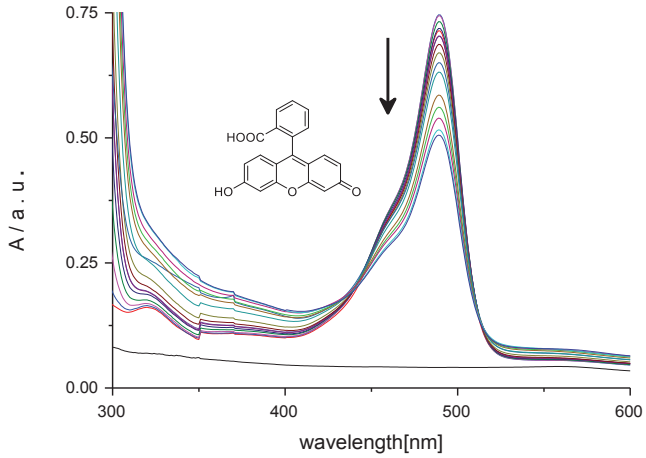

Figure 2.9: UV-visible spectra for 0.012 mM **2.9** upon addition of 0 – 6.7 mM DNA, at 25 °C in buffer (25 mM MOPS, pH 7.0, 50 mM NaCl).

Figure 2.9 shows that **2.9** displays a decrease in absorbance with a maximum change in absorbance at 489 nm upon addition of DNA. This decrease in UV-visible absorption may have occurred as a result of geometrical distortion of **2.9** when it interacts with DNA, it may also be as a result of a local medium effect, but it could also merely be the result of ligand dilution.

To quantify the affinity of **2.9** for DNA, the absorbances at 489 nm were plotted as a function of the concentration of DNA (Figure 2.10, for data in tabular format, see appendix, Tables A55.6).

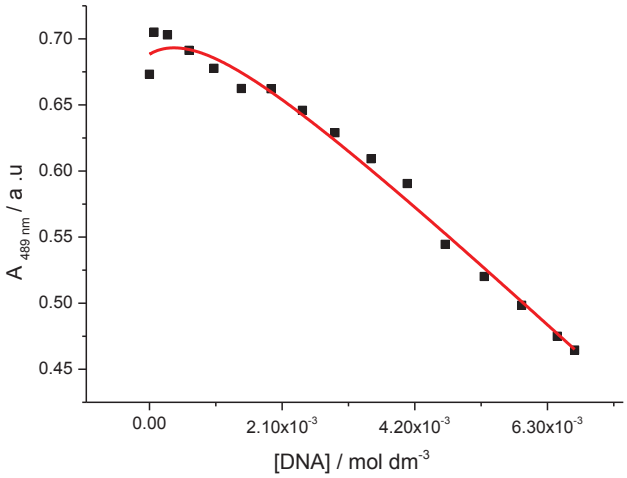

Figure 2.10: Absorbance at 489 nm for 0.012 mM **2.9** as a function of DNA concentration, at 25 °C in buffer (25 mM MOPS, pH 7.0, 50 mM NaCl). The solid line represents the best fit to the data in terms of a multiple independent binding sites model.

Figure 2.10 shows how the binding affinity $K_{binding}$ and binding site size n were determined by fitting a multiple independent binding sites model, which also takes ligand dilution into account to the data. The fit indicates a small equilibrium constant $K_{binding}$ of $(4\times10^{-3} \pm 2.2) \times10^{5}\ M^{-1}$ for a binding site size of (0.4 ± 264) base pairs. The fit suggests that **2.9** does not interact with DNA and the decrease in absorbance is the result of simple dilution only. The absence of interaction is reasonable considering **2.9** is negatively charged.

2.3.6 Compound 2.10 binding with DNA.

We wanted to study the binding of **2.10** to DNA; the changes in absorption of **2.10** upon addition of DNA were measured in buffer (25 mM MOPS, 50 mM NaCl) at 25 °C (Figure 2.11).

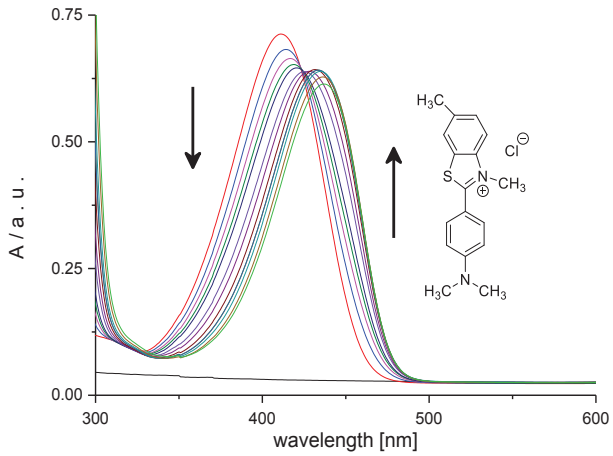

Figure 2.11: UV-visible spectra for 0.0262 mM **2.10** upon addition of 0 - 3.09 mM DNA, at 25 °C in buffer (25 mM MOPS, pH 7.0, 50 mM NaCl).

Figure 2.11 shows a redshift upon addition of DNA. This red shift in UV-visible absorption occurs as a result of the interaction of **2.10** with DNA.This change in UV-visible absorption probably occurs because of geometrical distortion of **2.10** when it interacts with DNA, but a local medium effect may also contribute.

To quantify the affinity of **2.10** for DNA, the absorbances at 411 and 432 nm were plotted as a function of the concentration of DNA. (Figure 2.12 see Appendix, Tables A55.7).

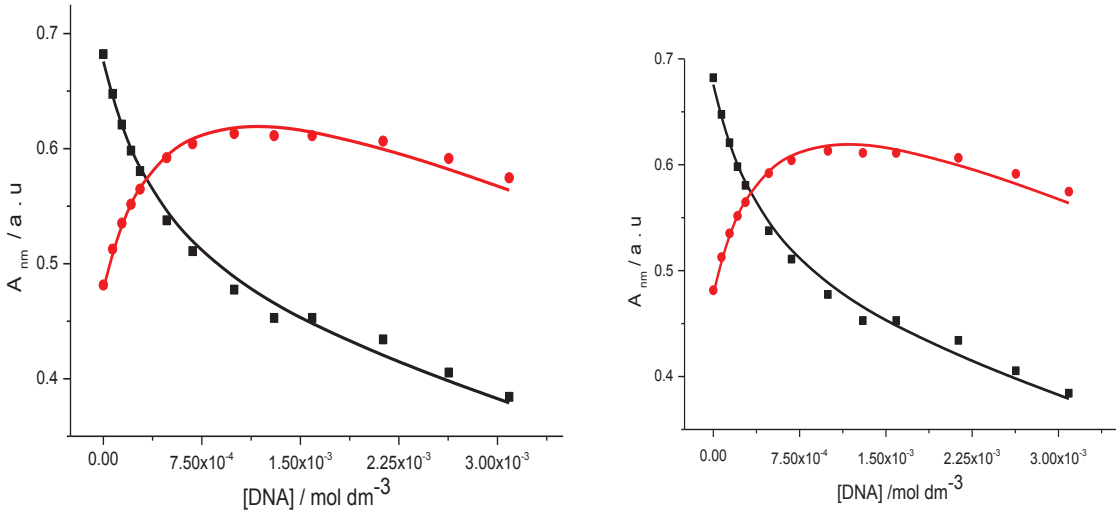

Figure 2.12: Absorbance at 411 nm and at 432 for 0.0262 mM **2.10** upon addition of 0 - 3.09 mM DNA concentration, at 25 °C in buffer (25 mM MOPS, pH 7.0, 50 mM NaCl). The solid lines represent a global fit of a multiple independent sites model to the data.

Figure 2.12 shows the decrease in absorbance at 411 nm and the increase in absorbance at 432 nm. The peak at 411 nm corresponds predominantly to free ligand, and the peak at 432 nm represents the DNA-ligand complex. By adding more DNA, the amount of free ligand will decrease as the ligand binds to DNA while the DNA complex peak increases. The bathochromic shift corresponds to an increase in conjugation length and hence in planarity of **2.10** upon binding to DNA. The binding affinity $K_{binding}$ and binding site size n were determined by fitting a multiple independent binding sites model, which also takes ligand dilution into account, to the data. The fit gives an equilibrium constant $K_{binding}$ of $(0.39 \pm 1.4) \times 10^4$ M^{-1} for a binding site size of (1.3 ± 4.4) base pairs. The obtained stoichiometry and affinity were unreasonably small without restricting the parameters (Figure 2.12, left panel). Therefore, the data were reanalysed with the stoichiometry restricted to 3.0 base pairs, giving an equilibrium constant $K_{binding}$ of $(6.9 \pm 0.7) \times 10^3$ M^{-1} (Figure 2.12, righ panel). Previously reported binding affinities for **2.10**[174-175] were in the order of 10^4 M^{-1}.

2.3.7 Compound 2.11 binding with DNA

We wanted to know whether **2.11** binds to DNA. The changes in absorption of **2.11** upon addition of DNA were measured in buffer (25 mM MOPS, pH 7.0, 50 mM NaCl) at 25 °C (Figure 2.13).

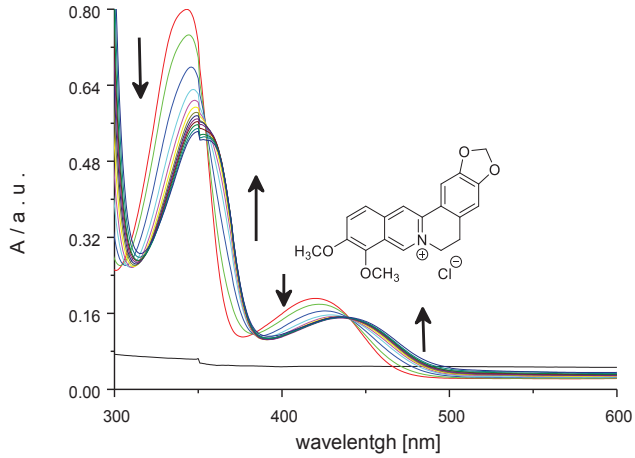

Figure 2.13: UV-visible spectra for 0.0253 mM **2.11** upon addition of 0 – 3.3 mM DNA, at 25 °C in buffer (25 mM MOPS, pH 7.0, 50 mM NaCl).

In the studies, **2.11** showed a red shift in absorbance with a maximum decrease in absorbance at 343 nm and an increase at 375 nm upon addition of DNA. The data show good isosbestic point, suggesting that only two species are involved in the titration, viz. free and bound ligand. Because of the region in which the spectroscopic changes take place in combination with the extent of the shift in λ_{max} this redshift in UV-visible absorption has probably occurred as a result of geometrical distortion of **2.11** when it interacts with DNA, but it may also be as a result of a local medium effect.

To quantify the affinity of **2.11** for DNA, the absorbances at 343 and 375 nm were plotted as a function of the concentration of DNA (Figure 2.14, for data in tabular format, see Appendix, Tables A55.8).

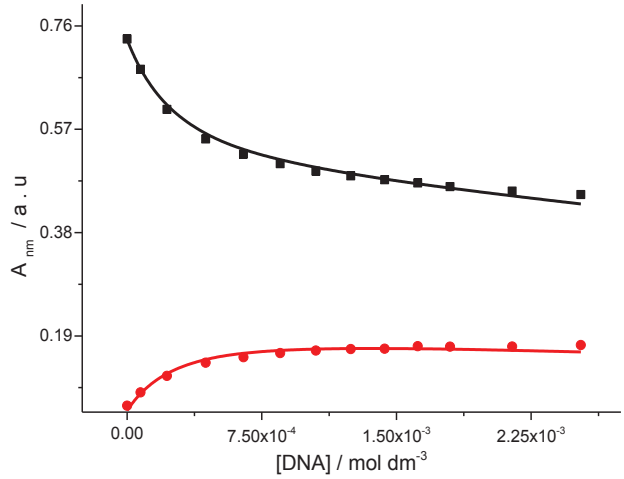

Figure 2.14: Absorbance at 343 and at 375 nm for 0.0253 mM **2.11** as a function of DNA concentration, at 25 °C in buffer (25 mM MOPS, pH 7, 50 mM NaCl). The solid lines represent a global fit of a multiple independent sites model to the data.

Figure 2.14 shows the maximum decrease in absorbance at 343 nm and the highest increase in absorbance at 375 nm. The peak at 343 nm corresponds to free ligand, and the peak at 375 nm represents DNA-ligand complex. The shift to a longer wavelength is known as a bathochromic shift. The bathochromic shift is interpreted as an increase in effective conjugation and planarity of 2.11 upon binding to DNA. The binding affinity $K_{binding}$ and binding sites size n were determined by fitting a multiple independent binding sites model, which also takes ligand dilution into account, to the data. The fit gives an equilibrium constant $K_{binding}$ of (6.5 ± 4.7) $\times 10^4$ M^{-1} for a binding site size of (8.03 ± 3.2) base pairs. The obtained binding parameters were reasonably for both stoichiometry and binding constant. For comparison the data were reanalysed with the stoichiometry restricted to 3.0 base pairs, giving an apparent equilibrium constant $K_{binding}$ of (1.6 ± 0.2) $\times 10^4$ M^{-1}. Previous studies have found[176] a $K_{binding}$ of (3.54×10^4) M^{-1}.

2.3.8 Compound 2.12 binding with DNA

We wanted to know whether the binding of **2.12** to DNA. The changes in absorption of **2.12** upon addition of DNA were measured in buffer (25 mM MOPS, pH 7.0, 50 mM NaCl) at 25 °C. (Figure 2.15).

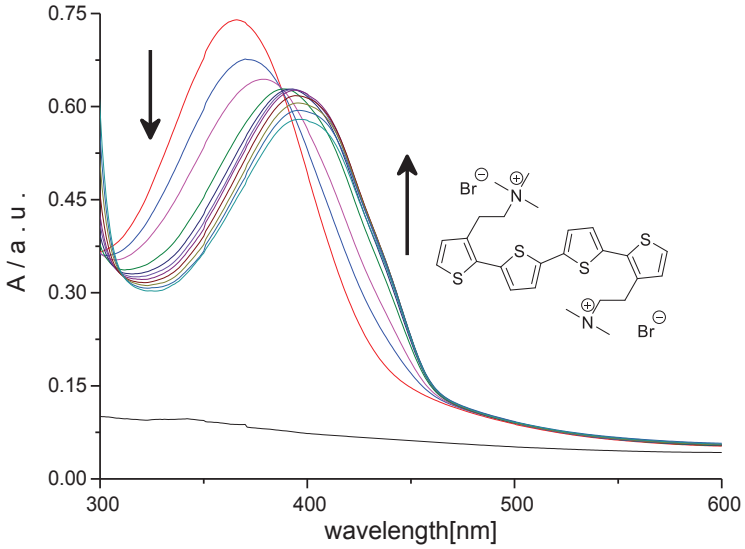

Figure 2.15: UV-visible spectra for 0.024 mM **2.12** upon addition of 0 – 0.833 mM DNA, at 25 °C in buffer (25 mM MOPS, pH 7.0, 50 mM NaCl).

Figure 2.15 shows a clear red−shift in absorbance. This red shift in UV-visible absorption occurs as a result of the interaction of **2.12** molecules with DNA, which forces **2.12** to become planar.

To quantify the affinity of **2.12** for DNA, the absorbances at 367 and 430 nm were plotted as a function of the concentration of DNA (Figure 2.16, for data in tabular format, see appendix, Tables A55.9).

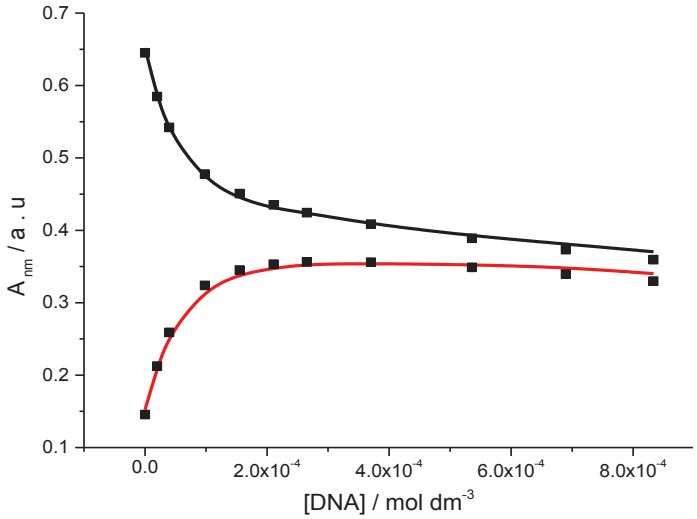

Figure 2.16: Absorbance at 367 and at 430 nm for 0.024 mM **2.12** as a function of DNA concentration, at 25 °C in buffer (25 mM MOPS, pH 7, 50 mM NaCl). The solid lines represent a global fit of a multiple independent binding sites model to the data.

The titration curves in figure 2.16 were analysed globally by the fitting of a multiple independent binding sites model, which also takes ligand dilution into account, to the data. The fit indicates an equilibrium constant $K_{binding}$ of (5.2 ± 2.8) $\times 10^4$ M^{-1} and a binding site size of (1.5 ± 0.5) base pairs. The obtained value of affinity and binding site size were reasonable. The data of the titration curves were reanalysed for comparison purposes giving an equilibrium constant $K_{binding}$ of (1.8 ± 0.38) $\times 10^5 M^{-1}$ for a binding site size restricted to 3 base pairs.

2.3.9 Compound 2.13 binding with DNA

We wanted to study the binding of **2.13** to DNA. The changes in absorption of **2.13** upon addition of DNA were measured in buffer (25 mM MOPS, pH 7.0, 50 mM NaCl) at 25 °C (Figure 2.17).

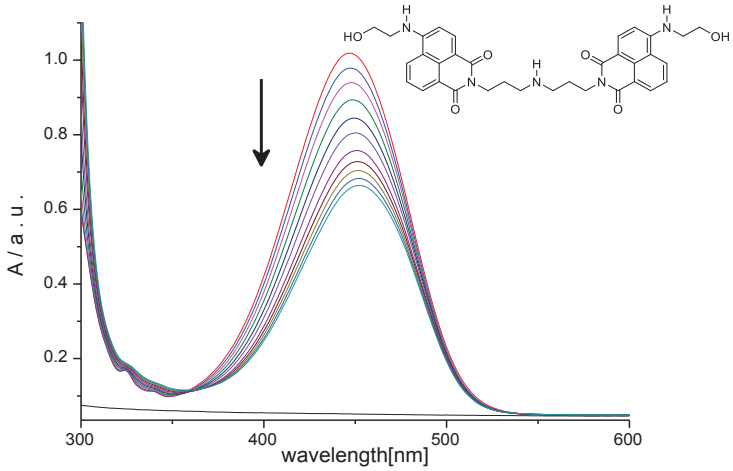

Figure 2.17: UV-visible spectra for 0.044 mM **2.13** upon addition of 0 – 2.2 mM DNA, at 25 °C in buffer (25 mM MOPS, pH 7.0, 50 mM NaCl).

Figure 2.17 shows that **2.13** revels a hypochromic shift in absorbance. The small redshifts suggest some increase in effective conjugation length, which is attributed to an increase in the planarity of **2.13** upon interaction with DNA. The decrease in UV-visible absorption may have occurred as a result of geometrical distortion of **2.13** when it interacted with DNA or as a result of local medium effect.

To quantify the affinity of **2.13** for DNA, the absorbances at 446 nm were plotted as a function of the concentration of DNA (Figure 2.18, for data in tabular format, see Appendix, Tables A55.10).

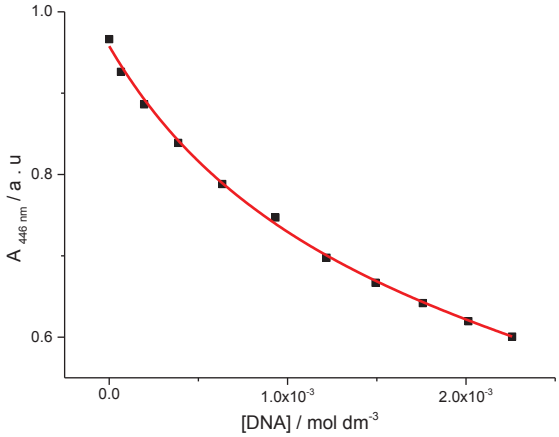

Figure 2.18: Absorbance at 446 nm for a solution of 0.044 mM **2.13** as a function of DNA concentration, at 25 °C in buffer (25 mM MOPS, pH 7.0, 50 mM NaCl). The solid line represents the best fit to the data in terms of a multiple independent binding sites model.

Figure 2.18 shows a clear decrease in the absorbance for **2.13** upon the addition of DNA. The binding affinity $K_{binding}$ and binding site size *n* were determined by fitting a multiple independent binding sites model, which also takes ligand dilution into account, to the data. The fit reproduces the data well and gives an equilibrium constant $K_{binding}$ of (2.9 ± 0.3) $\times 10^3$ M^{-1} for a binding site size restricted to 3 base pairs. The binding parameters obtained from data analysis were reasonable, and the fit suggests that **2.13** interacts with DNA, albeit weakly, and thus that DNA binding sites are accessible to **2.13**.

2.3.9 Compound 2.15 binding with DNA

The binding of **2.15** to DNA was studied using UV−visible spectroscopy. The changes in absorption of **2.15** upon addition of DNA were measured in buffer (25 mM MOPS, pH 7.0, 50 mM NaCl) at 25 °C (Figure 2.19).

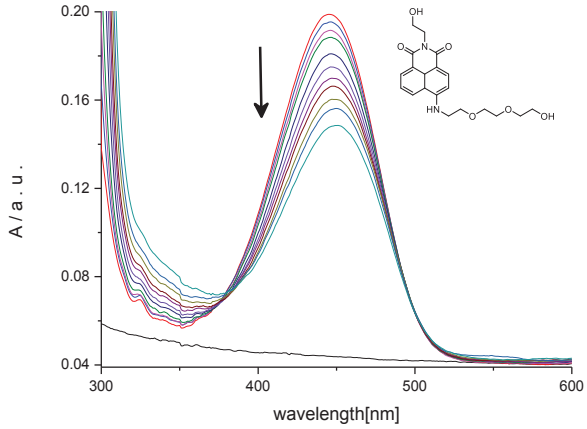

Figure 2.19: UV-visible spectra for 0.014 mM **2.15** upon addition of 0 – 2.5 mM DNA, at 25 °C in buffer (25 mM MOPS, pH 7.0, 50 mM NaCl).

Figure 2.19 shows a hypochromic shift in absorbance. The decrease in UV-visible absorption may have occurred as a result of geometrical distortion of methylene blue when it interacted with DNA or as a result of local medium effect.

To quantify the affinity of **2.15** for DNA, we plotted the absorbances at 446 nm as a function of the concentration of DNA (Figure 2.20, see appendix, Tables A55.11).

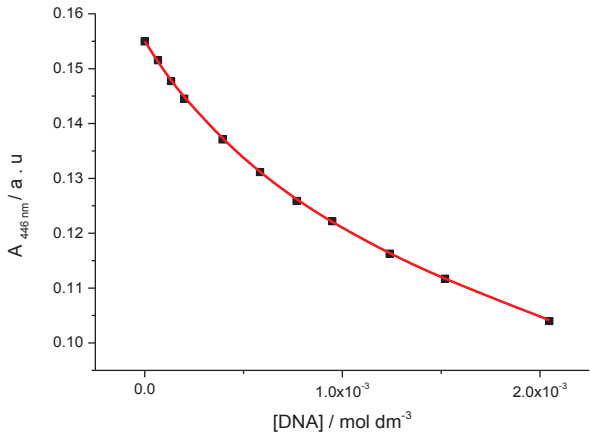

Figure 2.20: Absorbance at 446 nm for a solution of 0.014 mM **2.15** as a function of DNA concentration, at 25 °C in buffer (25 mM MOPS, pH 7.0, 50 mM NaCl). The solid line represents the best fit to the data in terms of a multiple independent binding sites model.

Figure 2.20 shows a clear decrease in the absorbance for **2.15** upon the addition of DNA. The binding affinity $K_{binding}$ and binding site size n were determined by fitting a multiple independent binding sites model, which also takes ligand dilution into account, to the data. The fit reproduces the data well and gives an equilibrium constant $K_{binding}$ of $(2.9 \pm 0.09) \times 10^3\ M^{-1}$ for a binding site size restricted to 3 base pairs. The binding parameters obtained from data analysis were reasonable, and the fit suggests that **2.15** interacts with DNA and thus that DNA has binding sites size accessible to **2.15**.

Summary

The UV-visible titrations for our π-conjugated compounds with duplex DNA show that these ligands **2.1-2.15** bind to DNA as summarised in Table 2.1.

Table 2.1 Binding affinities and binding site sizes for binding of 2.1-2.15 to DNA in buffer (25 mM MOPS, pH 7.0, 50 mM NaCl) at 25 °C.

Ligands	*Binding constant / DNA* K / M^{-1}	*Binding site size* n
2.1 [c] **($C_{20}H_{16}N_4O$)**	$(1.5 \pm 0.1) \times 10^4$	n =3* a
2.2 [c] **($C_{31}H_{37}N_7O_3$)**	$(6.4 \pm 1.6) \times 10^4$	n =3* a
2.3 [c] **($C_{41}H_{57}ClEuN_5O_8$)**	$(1.7 \pm 0.4) \times 10^4$	n =3*
2.4 [c] **($C_{18}H_{21}N_3O_4$)**	$(3.4 \pm 0.2) \times 10^4$	n =3*
2.5 ($C_{20}H_{25}N_3O_5$)	$(8.9 \pm 2.3) \times 10^4$	n =3*
2.6[c] **($C_{35}H_{35}N_5O_7Re$)**	$(11.3 \pm 2.7) \times 10^4$	n =1*
2.7 ($C_{25}H_{37}Cl_3N_6O_6$)	$(7.7 \pm 1.5) \times 10^5$	n =3*
2.8 ($C_{16}H_{20}ClN_3OS$)	$(4.4 \pm 0.5) \times 10^5$	n =3*
2.9 ($C_{20}H_{18}NO_4$)	No binding	
2.10 ($C_{17}H_{19}ClN_2S$)	$(6.9 \pm 0.7) \times 10^3$	n =3*
2.11 ($C_{20}H_{18}ClNO_4$)	$(2.0 \pm 0.2) \times 10^4$	n =3*
2.12 ($C_{26}H_{33}N_2S_4^{2+}$)	$(1.8 \pm 0.38) \times 10^5$	n =3*
2.13 ($C_{34}H_{35}N_5O_5$)	$(2.9 \pm 0.3) \times 10^3$	n =3*
2.15 ($C_{20}H_{24}N_2O_6$)	$(2.9 \pm 0.09) \times 10^3$	n =3*

a) apparent binding constant for the event following initial precipitation.
b) *restricted.
c) Data from[172]

Table 2.1 shows the interactions that occurred between π-conjugated aromatic molecules and DNA. The interactions of the 1,8-naphthalimide family show that the rhenium complex **2.6** has the highest affinity with α binding constant of around $10^5\ M^{-1}$. We attribute this high affinity to the presence of more aromatic rings which leads to an increase in hydrophobic interactions between ligand and DNA as well as the presence of a positive change. Compounds **2.4, 2.5** and **2.6** have moderate affinities of $\sim 10^4\ M^{-1}$ for DNA. Compound **2.9** does not show any affinity for duplex DNA. We may attribute this to the negative charge of the carboxylate group on the ligand, leading to an increase electrostatic repulsion between ligand and DNA.

We found that ligands **2.7, 2.8, 2.10, 2.11** and **2.12** have moderate affinity for DNA. The highest affinity is for **2.7, 2.8** and **2.12**. We attribute the higher affinities to the presence of more than one positive charge and multiple aromatics rings. The weakest binders are **2.10, 2.13** and **2.15**. The low affinities may be because the structure of thioflavin and double naphthalimides demonstrate a hydrophobic end with a dimethylamino group linked with phenyl group to the positive charge on the benzothiazole group.

2.4 Conclusion

According to the results presented in this chapter, positivily charged molecules **2.4, 2.5, 2.7, 2.8**, **2.10, 2.11, 2.12, 2.13** and **2.15** bind with DNA by electrostatic and hydrophobic interaction. The binding constants found vary between $10^3 - 10^6\ M^{-1}$ for binding site sizes of 3. The anionic ligand **2.9** doesn't show any binding with DNA as a result of the presence of a negative charge.

2.5 Materials and Methods

π-conjugated compounds **2.1, 2.2** and **2.14** were provided by our collaborators Prof McKeown and Dr ElBetany.[130] Ligands **2.7, 2.8, 2.9, 2.10** and **2.11** were acquired from known commercial sources at the highest available purity and used as received from Sigma-Alderich and Acros Organic company. Compounds **2.3, 2.4, 2.5** and **2.6** (Scheme 1.5) were provided by Prof Simon Pope group. Cationic oligothiophene **2.12,** and naphthalimide derivatives **2.13** and **2.15** have been used in previous work by the Buurma group. For purification, **2.12** was dissolved in distilled water, filtered and freeze-dried. The solid was redissolved in a small amount of ethanol and left in a sealed round bottom flask in the oven for two days at 60 °C. The solid was redissolved in a small amount of ethanol and precipitated from ethanol on the wall of the flask. The precipitate was then cooled again to -20 °C. DNA was procured from Acros and Sigma-Aldrich as a lyophilised solid sodium salt. The buffer components were purchased from Melford Laboratories Ltd and Sigma-Aldrich.

2.5.1 Equipment

A Jasco V-630 Bio spectrophotometer equipped with a Peltier temperature controller was used to record the UV-visible spectra. pH of buffers was determined using a Hanna Instruments pH 210 pH meter equipped with a VWR 662−1759 glass electrode. Water was purified using an ELGA option-R 7BP water purifier.

2.6 Solutions preparation

2.6.1 MOPS buffer solution

MOPS (3-(*N*-morpholino) propane sulfonic acid (10.46 g, 50 mmoles), NaCl (5.84 g, 100 mmoles) were transferred to a beaker and ~ 1000 ml of deionised water was added. The solution was stirred until all MOPS and salt had completely dissolved. A concentrated NaOH (aq) solution was prepared, and this was added dropwise to the solution until the pH was 7.0.

This solution was placed in a 2.0 liter volumetric flask and made up to 2 liter with deionised water.

2.6.2 DNA preparation

The stock solution of DNA was prepared by dissolving around 0.12 g of DNA in MOPS, sonicating the solution of DNA around 15 minutes. The solution of DNA was dialysed against 2.0 litre of MOPS buffer by using a 3.5 kDa MWCO dialysis membrane for one day. The concentration of DNA was determined using UV-visible spectroscopy using an extinction coefficient $\varepsilon_{260\ nm}$ of 12800 M^{-1} cm^{-1} at 260 nm. [177]

$$\boldsymbol{A = \varepsilon \times C \times L} \qquad \textbf{…… 2.1}$$

where, A= absorbance, l= path length, C= concentration, ε= extinction coefficient

$$\boldsymbol{\varepsilon = \frac{A}{C \times L}} \qquad \textbf{……. 2.2}$$

$$\boldsymbol{\varepsilon = M^{-1}\, cm^{-1}} \qquad \textbf{…….. 2.3}$$

2.7 Spectroscopic studies

2.0 ml of MOPS buffer was placed in a 1.0 cm path length cuvette. The required volumes of the stock solutions of all molecules in MOPS buffer, sometimes involving 10 vol. % DMSO, were added to the cuvette. All UV-visible titrations were carried out by adding aliquots of the DNA stock solutions into the 1.0 cm path length cuvette recording the absorption in the range of 200 – 800 nm after each addition. Absorptions were kept in the range of 0.0 − 1.0. The absorptions at selected wavelengths were plotted against DNA concentrations, and a multiple independent binding sites model was used to analyse the UV-visible spectra using the Origin 9.0 software.

Chapter three

The effect of selected blood plasma proteins on DNA-binding properties of π-conjugated ligands

Abstract

This Chapter explores the binding between π-conjugated ligands and SA and TF and the result of binding to these proteins on DNA-binding. The studies found that ligands **3.1, 3.2, 3.3, 3.7** and **3.9** bind to SA with strong affinity in the order of $\sim 10^4\ M^{-1}$ while binding of ligands **3.1, 3.2, 3.8** and **3.10** to transferrin confirmed that the ligands have a strong affinity of $\sim 10^4\ M^{-1}$ for TF under the experimental conditions. We further compared the affinity of ligands for DNA in absence and presence of SA and TF. We found that ligands **3.1, 3.5, 3.7, 3.8, 3.10, 3.11** and **3.12** do not show a change in the affinity for DNA when SA is present. Our work demonstrated a decrease in affinity of ligands **3.2, 3.4** and **3.6** for DNA in the presence of SA, suggesting that binding of these potential sensitisers to serum albumin leads to decreased $K_{binding}$. This could be a source of false negative results. An increase in the apparent affinity of **3.3** for DNA was also observed in the presence of SA. We attribute this to sensitisers binding to serum albumin instead of binding non-specifically to DNA and increasing the apparent $K_{binding}$.. This increase could cause false positives. Furthermore, we investigated the effect of TF on DNA binding. Binding of **3.1** was not affected by TF. However, **3.2** showed a decrease in affinity for DNA in the presence of TF.

3.1 Introduction

3.1.1 The effect of proteins on biosensors

Whole blood is a complex mixture that contains many components, including significant amounts of serum albumin and transferrin. We need to know whether the presence of the main components of blood affects the affinity of sensitisers for DNA. The presence of serum albumin and other elements in a sample may cause a false negative because binding of ligands with DNA in the presence of proteins may be hard and not as easy as when a ligand is free in solution.

The challenge in this thesis is to improve biosensors involving sensitisers which detect DNA in a sample containing proteins, such as serum. Protein in the sample may increase the selectivity and sensitivity as a result of reduced non-specific binding as we have shown in Figure 1.16. However, the protein may also bind too strongly to the sensitiser, decreasing DNA binding of the sensitiser. This effect may, therefore, lead to false positive or false negative signals.

In general, a bioreceptor requires binding with high selectivity, sensitivity, affinity and minimal non-specific interaction toward their targets. We introduce a method that it is easy to use, exploits cheaper compounds, is fast and which involves competition between biomolecules and DNA for the same sensitiser molecule to minimise non-specific interactions that cause a false positive signal (Figure 1.16).

The interaction between selected proteins, such as SA and TF, and sensitisers and the effect of these species on DNA binding of sensitisers can be studied using several techniques such as UV-visible spectroscopy, and other methods that exploit the thermodynamic characteristics of these compounds such as isothermal titration calorimetry.

3.1.2 Aim

Our goals in this chapter are to measure the binding affinity $K_{\text{binding,}}$ and binding sites size n of sensitisers binding to serum albumin and transferrin. Moreover, we will investigate the effect of the presence of serum albumin SA and transferrin TF on the DNA binding parameters of potential sensitisers.

3.2 Results and Discussion

The findings of the studies of the interactions of compounds **3.1-3.12** with proteins SA and TF, and the effect of SA and TF on the interactions of these compounds with DNA, will be discussed for each compound.

Part A: Serum albumin binding studies

3.2.1 Compounds 3.1 and 3.2 binding to SA

We wanted to know whether compounds **3.1** and **3.2** bind with SA. The changes in absorption of **3.1** upon addition of SA were measured in buffer (25 mM MOPS, pH 7.0, 50 mM NaCl) at 25 °C (Figure 3.1). For the analogous data for **3.2** see appendix A1 (see appendix, Tables A55.15 & A55.16).

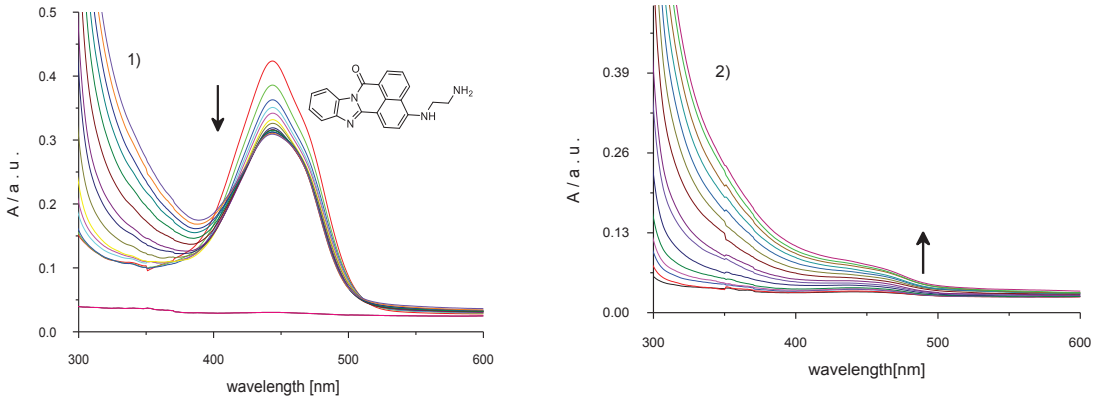

Figure 3.1: UV-visible spectra for 0.0246 mM **3.1** upon addition of 0 - 0.28 mM SA at 25 °C, in buffer (25 mM MOPS, pH 7.0, 50 mM NaCl) (*left*). UV-visible spectra for 0.0023 - 0.27 mM SA in absence of the ligand **3.1** (*right*).

Figure 3.1 shows that compound **3.1** displays a hypochromic shift in absorbance upon addition of SA, with a maximum change in absorbance at 443 nm. This decrease in UV-visible absorption may have occurred as a result of geometrical distortion of **3.1** when it interacts with SA, but it may also be as a consequence of a local medium effect. The binding of **3.1** to SA is also accompanied by a small red-shift in the UV-visible absorption. The red shift suggests an increase in effective conjugation, *i.e.,* an increase in the planarity of **3.1** upon interaction with SA. On the other hand, Figure 3.1 (right) also shows an increase in absorbance in the range of 300-500 nm upon the additions of SA to the buffer solution in the absence of ligand **3.1**. This observation suggests absorbance and scattering of light by SA in the solution. As result, we need to remove any effect caused by SA from the UV-visible spectra. Otherwise, there could be an effect on the binding constant parameters.

To quantify the affinity of **3.1** for SA, the absorbances at 443 nm were corrected for the absorbances and scattering caused by SA alone. A stock solution of 1.0 mM SA in buffer (25 mM MOPS, pH 7.0, 50 mM NaCl) was prepared. From this stock solution, a series of

solutions was prepared and UV-visible spectra were recorded for these solutions in a 1.0 cm pathlength cuvette (Figure 3.2, for data in tabular format, see appendix, Tables A55.14).

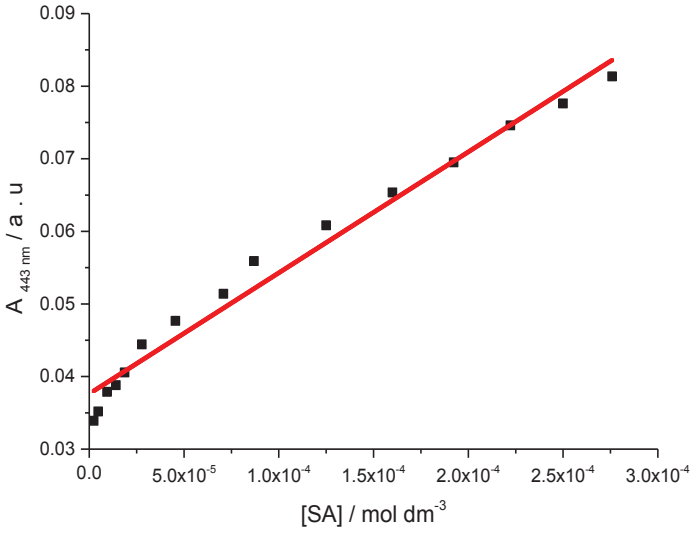

Figure 3.2: Absorbance at 443 nm for SA as a function of SA concentration, at 25 °C in buffer (25 mM MOPS, pH 7, 50 mM NaCl). The solid line represents the best fit to the data of a multiple independent binding sites model.

Figure 3.2 shows an increase in the absorbance at 443 nm upon addition of SA to buffer. Because this increase occurs above 300 nm, this increase in UV-visible absorption has probably occurred as a result of scattering by SA in the solution. We need to remove any effect of scattering and/or absorbance by SA by subtracting the absorbance as result of scattering from the titration data. We therefore determined the extinction coefficient for SA at the wavelength of interest.

To quantify the extinction coefficient SA, the absorbances at 443 nm were plotted as a function of the concentration of SA (Figure 3.2, for data in tabular format see appendix, Tables A55.13). A linear fit (red line) was applied to obtain the extinction coefficient for SA of (167 ± 6.5) dm^{-3} $mol^{-1}cm^{-1}$ at 443 nm. The extinction coefficient was used to calculate a predicted absorbance for SA alone for every point of the titration. These predicted absorbances were subtracted from the observed absorbances in the titration to give corrected absorbances $\Delta A_{443\ nm}$ corrected. The corrected absorbances at 443 nm were plotted as a function of the concentration of SA (Figure 3.3, for data in tabular format, see appendix, Tables A55.12 & A55.13).

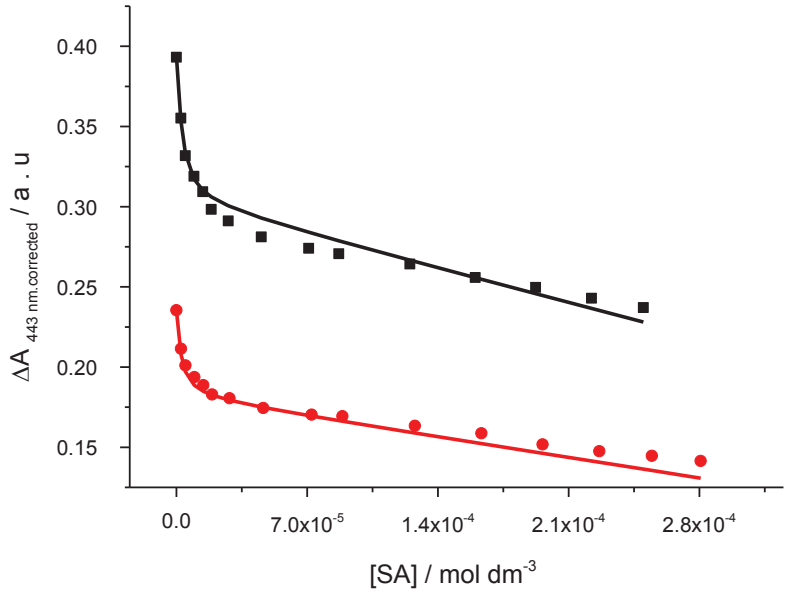

Figure 3.3: Corrected absorbance at 443 nm for 0.024 mM of **3.1** (■) and for 0.014 mM **3.1** (●) as a function of SA concentration, at 25 °C in buffer (25 mM MOPS, pH 7, 50 mM NaCl). The solid lines represent a global fit of a multiple independent sites model to the data.

Figure 3.3 shows a decrease in the absorbance at 443 nm for **3.1** upon addition of SA. The binding affinity $K_{binding}$ and the number of binding sites per protein $1/n$ were determined by fitting a multiple independent binding site model, which also takes ligand dilution into account, to the data. The fit suggests an equilibrium constant $K_{binding}$ of $(1.5 \pm 1.2) \times 10^5$ M^{-1} for a binding sites size of (0.18 ± 0.06) moles of SA per mole of ligand, that means ~ 6.0 molecules of **3.1** bind to one molecules of SA, probably distributed overthe subdomains IIA and IIIA. The obtained value of the binding site was reasonable, and the fit suggests that **3.1** interacts with SA and thus that SA has binding sites accessible to **3.1**.

3.2.2 Compounds 3.3 - 3.6 binding to SA

We wanted to know whether **3.3** -**3.6** interact with SA. UV-visible spectroscopy was similarly used to determine the affinity and stoichiometry of compounds **3.3-3.6** interacting with SA. The changes in absorption of **3.3** upon addition of SA were measured in buffer (25 mM MOPS, pH 7.0, 50 mM NaCl) at 25° C (Figure 3.4).

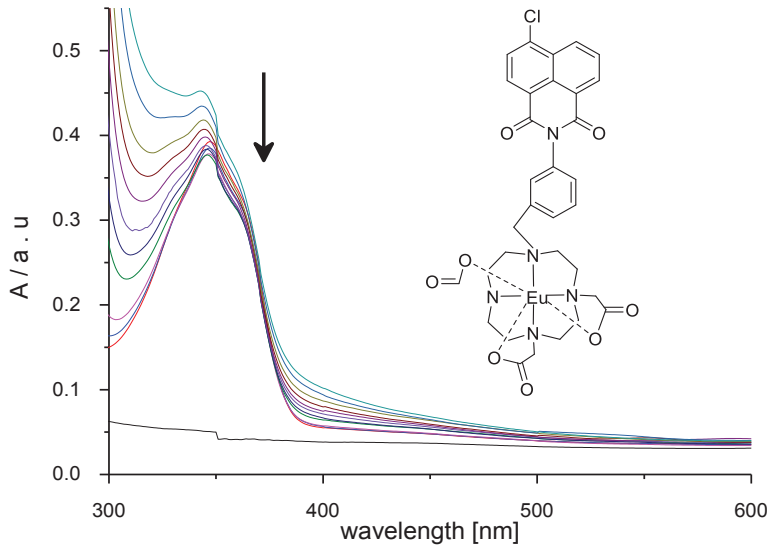

Figure 3.4: UV-visible spectra for 0.033 mM **3.3** upon addition of 0 - 0.21 mM SA, at 25 °C in buffer (25 mM MOPS, pH 7.0, 50 mM NaCl).

Figure 3.4 shows a hypochromic shift in absorbance with maximum change in absorbance at 347 nm. This decrease and increase in UV-visible absorption may have occurred as a result of geometrical distortion of **3.3** when it interacts with SA, but it may also be as a consequence of a local medium effect. The binding of **3.3** to SA is also accompanied by a small red−shift in the UV-visible absorption. The red shift suggests an increase in effective conjugation, *i.e.,* an increase in the planarity of the **3.3** upon interaction with SA. On the other hand, Figure 3.2(right) also shows an increase in the range of 300-500 nm in absorbance upon the first additions of SA to buffer solution in the absence of ligand **3.3**. As result of that, we need to remove any effect caused by SA from the UV-visible spectra and we did this in the same way as for compound **3.1**.

To quantify the affinity of **3.3** for SA, the corrected absorbances at 347 nm were plotted as a function of the concentration of SA (Figure 3.5, for data in tabular format see appendix, Tables A55.17).

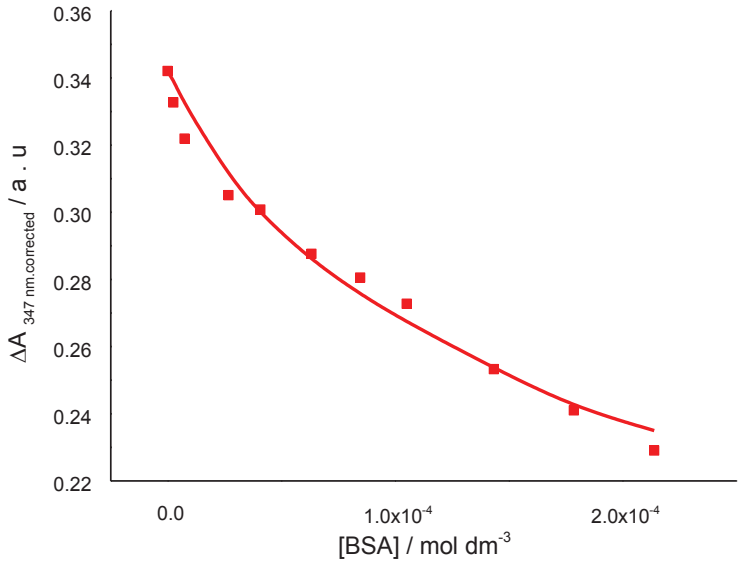

Figure 3.5: Corrected absorbance at 347 nm for 0.033 mM **3.3** as a function of SA concentration, at 25 °C in buffer (25 mM MOPS, pH 7.0, 50 mM NaCl). The solid line represents the best fit to the data of a multiple independent binding sites model.

Figure 3.5 shows a decrease in the absorbances at 347 nm upon addition of SA. The binding affinity $K_{binding}$ and binding sites $1/n$ were determined by fitting a multiple independent binding sites model, which also takes ligand dilution into account, to the data. The fit gives an equilibrium constant $K_{binding}$ of $(1.3\times10^{-3} \pm 5.9) \times10^{4}$ M^{-1} for a binding site of $(6\times10^{-3} \pm 2.7)$. The obtained value of affinity and binding site was too small to be unreasonable. Therefore, the data of the titration curves were reanalysed for a binding site size restricted to 0.5 mole of SA per mole of **3.3** (i.e. two molecules of **3.3** per molecule of SA) giving an equilibrium constant $K_{binding}$ of $(1.16 \pm 0.6) \times10^{4}$ M^{-1}. This means each of the two binding site (one in subdomaine IIA and one in IIIA of SA) binds with one molecule of **3.3**. The fit suggests that **3.3** interacts and that SA has a binding site reachable to **3.3**.

3.2.4 Compound 3.4 binding with SA

We also wanted to know whether **3.4** binds to SA. The changes in absorption of **3.4** upon addition of SA were measured in buffer (25 mM MOPS, pH 7.0 and 50 mM NaCl) at 25 °C (Figure 3.6).

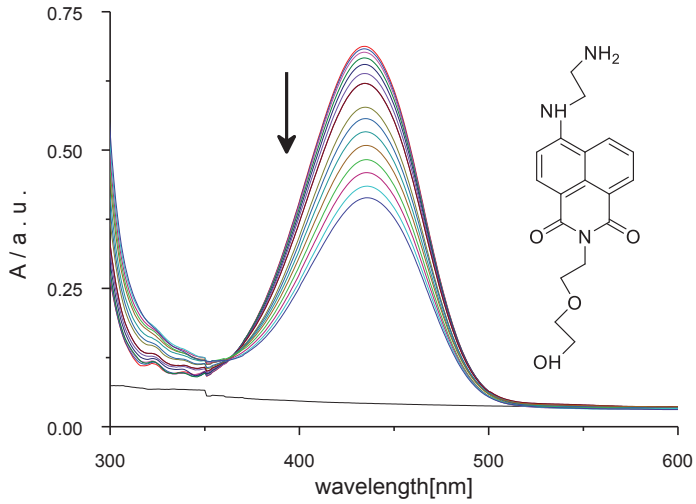

Figure 3.6: UV-visible spectra for 0.06 mM **3.4** upon addition of 0 − 0.054 mM SA, at 25 °C in buffer (25 mM MOPS, pH 7.0, 50 mM NaCl).

Addition of SA to **3.4** was found to result in a decrease in absorbance at 434 nm. The increase in absorbance around 330 nm is the result of scattering resulting from the added SA.

To quantify the affinity of **3.4** for SA, the absorbances at 434 nm were plotted as a function of the concentration of SA (Figure 3.7, for data in tabular format see appendix, Tables A55.18).

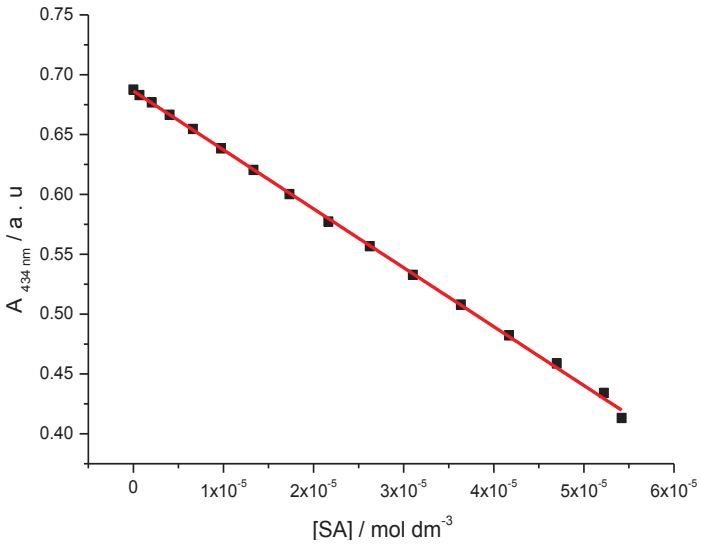

Figure 3.7: Absorbance at 434 nm for 0.06 mM **3.4** as a function of SA concentration, at 25 °C in buffer (25 mM MOPS, pH 7.0, 50 mM NaCl). The solid line represents the best fit to the data in terms of a multiple independent binding sites model.

The binding affinity K_{binding} and binding site size $1/n$ were determined by fitting a multiple independent binding sites model which also takes ligand dilution into account to the data. The

fit suggests that **3.4** does not interact with SA and the decrease in corrected absorbance is the result of simple dilution only. Similarly, molecules **3.5** and **3.6** do not show any affinity for SA either. We may attribute this to the shape of the ligands which does not fit with the binding sites on SA. See appendix A2 for compound **3.5** with SA (see appendix, Tables A55.19); and see appendix A3 for compound **3.6** with SA (see appendix, Table A55.20).

3.2.5 Compound 3.7 interacting with SA

We need to know whether **3.7** binds with SA. The changes in absorption of **3.7** upon addition of SA were measured in buffer (25 mM MOPS, pH 7.0, 50 mM NaCl) at 25 °C (Figure 3.8).

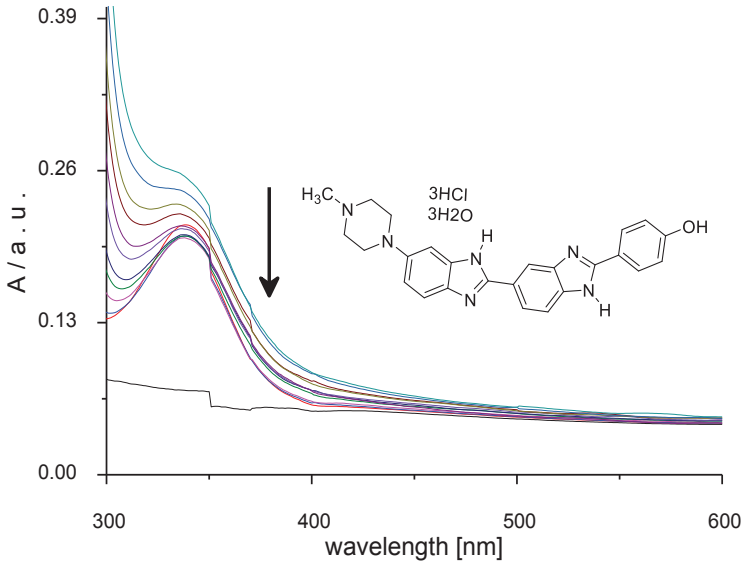

Figure 3.8: UV-visible spectra for 0.0042 mM **3.7** upon addition of 0 - 0.1 mM SA, at 25 °C in buffer (25 mM MOPS, pH 7.0, 50 mM NaCl).

Figure 3.8 illustrates that **3.7** exhibits a hypochromic shift in absorbance upon addition of SA with a maximum change in absorbance at 339 nm. This decrease and increase in UV-visible absorption may have occurred because of geometrical distortion of **3.7** when it interacts with SA, but it may also be as a result of a local medium effect. As a result of high scattering, we need to remove any effect caused by SA from the UV-visible spectra. Otherwise, there could be effect on the binding constant parameters

To quantify the affinity of **3.7** for SA, the corrected absorbances at 339 nm were plotted as a function of the concentration of SA (Figure 3.9, see appendix, Tables A55.21).

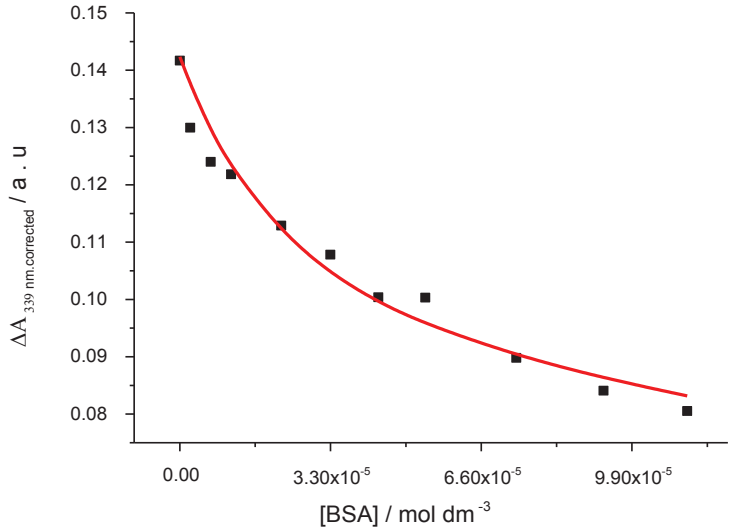

Figure 3.9: Corrected absorbance at 339 nm for 0.0042 mM **3.7** as a function of SA concentration, at 25 °C in buffer (25 mM MOPS, pH 7.0, 50 mM NaCl). The solid line represents the best fit to the data regarding a multiple independent binding sites model.

Figure 3.10 reveals a decrease in the corrected absorbance at 339 nm upon addition SA. The binding affinity $K_{binding}$ and the binding sites per SA $1/n$ were determined by fitting a multiple independent binding sites model, which also takes dilution into account, to the data. This fit produces an equilibrium constant $K_{binding}$ of $(1.4\times10^{-3} \pm 5.6) \times 10^5\ M^{-1}$ for a binding site of $(6\times10^{-2} \pm 33.2)$. The obtained binding site size is too small. We reanalyse of the data for a binding site n restricted to 0.5 moles of SA per mole of ligand. The fit gives an equilibrium constant $K_{binding}$ of $(2.2 \pm 0.5) \times 10^4\ M^{-1}$. That means 2.0 molecules of **3.7** bind to one molecule of SA.

3.2.6 Compound 3.9 binding with SA

The binding of **3.9** to SA was investigated using UV-visible spectroscopy. The changes in absorption of **3.9** upon addition of SA were measured in buffer (25 mM MOPS, pH 7.0 and 50 mM NaCl) at 25 °C (Figure 3.10).

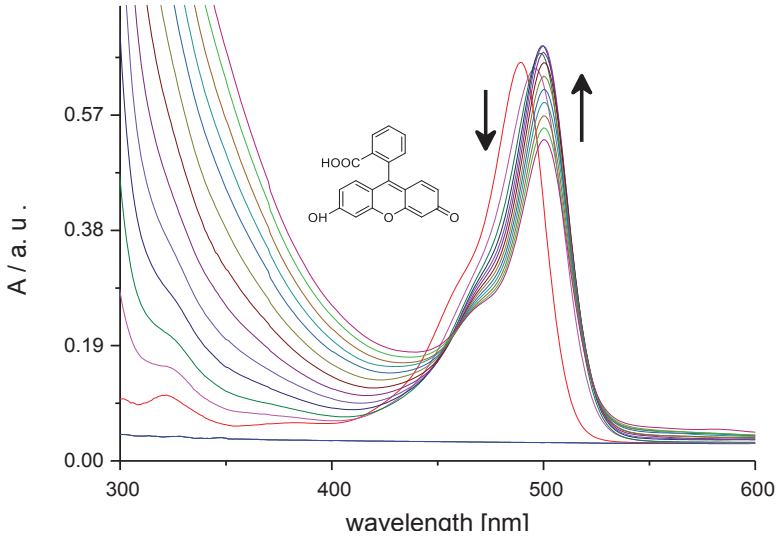

Figure 3.10: UV-visible spectra for 0.012 mM **3.9** upon addition of 0 – 0.29 mM SA, at 25 °C in buffer (25 mM MOPS, pH 7.0, 50 mM NaCl).

Figure 3.10 shows that **3.9** exhibits a hypochromic and hyperchromic shift in absorbance upon addition of SA. Similar redshifts were observed from 489-500 nm. The red shifts suggest an increase in effective conjugation length, which is attributed to an increase in the planarity of **3.9** upon interaction with SA. The decrease and increase in UV-visible absorption may have occurred as a result of geometrical distortion of **3.9** when it interacted with SA or as a result of a local medium effect. Figure 3.11 also shows an increase in absorbance attributed to scattering upon addition SA to the buffer solution. As before we removed any effect caused by SA from the UV-visible spectra.

To quantify the affinity of **3.9** for SA, the corrected absorbances at 489 nm and 500 nm were plotted as a function of the concentration of SA (Figure 3.11 for data in tabular format see appendix, Tables A55.23).

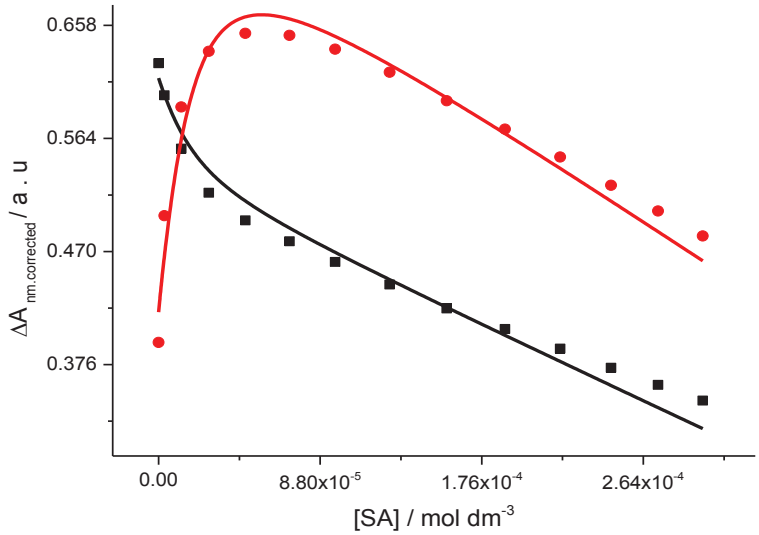

Figure 3.11: Corrected absorbance at 489 nm (■) and at 500 nm (●) for 0.012 mM **3.9** as a function of SA concentration, at 25° C in buffer (25 mM MOPS, pH 7.0, 50 mM NaCl). The solid lines represent a global fit of a multiple independent binding sites model to the data.

Figure 3.12 shows a decrease in the corrected absorbance of **3.9** at 489 nm (■) upon addition of SA. The red line shows a clear increase in the corrected absorbance of **3.9** at 500 nm (●) upon addition of SA. The solid lines represent a global fit in terms of a multiple independent sites model. The fit gives an equilibrium constant $K_{binding}$ of $(4.4\times10^{-2} \pm 5.4) \times10^{4}$ M^{-1} for a binding site of $(4.9\times10^{-2} \pm 6)$. The obtained value of the binding site size was not reasonable. Therefore, the data of the titration curves were reanalysed with n restricted to 0.5 giving an equilibrium constant $K_{binding}$ $(5.4 \pm 0.98) \times10^{4}$ M^{-1}. The fit suggests two molecules of **3.9** interacts with one SA, in agreement with the hypothesis that SA has twobinding sites reachable to **3.9**. Similar experiments for compounds **3.8, 3.10, 3.11** and **3.12** don't give binding with SA, just decreases in absorbance as a result of simple dilution (See appendixes A4-A7).

Summary

The results of UV-visible titrations for ligands **3.1, 3.2, 3.3 3.4, 3.5, 3.6, 3.7, 3.8, 3.9, 3.10, 3.11** and **3.12** with SA are summarised in Table 3.1.

Table 3.1 Binding constants and binding site sizes for interaction of 3.1, 3.2, 3.3 3.4, 3.5, 3.6, 3.7, 3.8, 3.9, 3.10, 3.11 and 3.12 to SA in buffer (25 mM MOPS, pH 7.0, 50 mM NaCl) at 25 °C.

Ligands	*Binding constant for SA* K / M^{-1}	*Binding site size n*	*Binding stoichiometry 1/n*
3.1	$(1.5 \pm 1.2) \times 10^5$	(0.18 ± 0.06)	5.5 ± 3.4
3.2	$(1.7 \pm 0.7) \times 10^5$	0.5^*	2
3.3	$(1.16 \pm 0.6) \times 10^4$	0.5^*	2
3.4	No binding		
3.5	No binding		
3.6	No binding		
3.7	$(2.2 \pm 0.5) \times 10^4$	0.5^*	2
3.8	No binding		
3.9	$(5.4 \pm 0.98) \times 10^4$	0.5^*	2
3.10	No binding		
3.11	No binding		
3.12	No binding		

***** restricted**.**

Table 3.1 shows that **3.1, 3.2, 3.3, 3.7** and **3.9** bind to SA reversibly with binding constants around ~ 10^4 M^{-1}. We note the presence of positive charges on the ammonium NH_3^+ groups of **3.1, 3.2, 3.3, 3.7** and negative group (COO^-) on **3.9**. This suggest that electrostatics does not play a deciding role in the affinity. The presence of aromatic rings leads to increase in hydrophobic interactions between molecules and the hydrophobic cavities located in SA. Compounds **3.4, 3.5, 3.6, 3.8, 3.10, 3.11** and **3.12** do not show any affinity for SA which we attribute to mismatches in the shape of these molecules and SA.

Part B: Transferrin binding studies

3.2.7 Compounds 3.1 and 3.2 binding to TF

We studied the interactions of **3.1** and **3.2** with transferrin (TF). The changes in absorption of **3.1** upon addition of TF were measured in buffer (25 mM MOPS, pH 7.0, 50 mM NaCl) at 25 °C (Figure 3.12). For the analogous data for **3.2** see appendix A8 (see appendix, Tables A55.29).

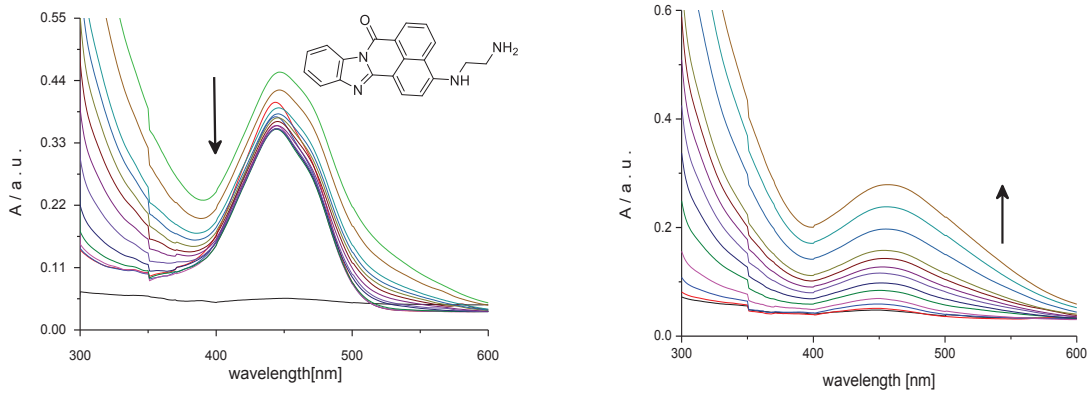

Figure 3.12: UV-visible spectra for 0.0215 mM **3.1** upon addition of 0 − 0.0740 mM TF in buffer (25 mM MOPS, pH 7.0, 50 mM NaCl, at 25 °C) (*left*). UV-visible spectra for 0.00049 - 0.074 mM TF in absence of ligand **3.1** (*right*).

Figure 3.12 shows that **3.1** exhibits a hypochromic and hyperchromic shift in absorbance upon addition of TF with a maximum change in absorbance at 444 nm. This change in UV-visible absorption may have occurred because of geometrical distortion of **3.1** when it interacts with TF, but it may also be as a result of a local medium effect. Figure 3.13 (right) also shows an increase in absorbance in the range of 300-600 nm upon addition of TF to the buffer solution in the absence of ligand **3.1**. This observation suggests absorbance and scattering of light by TF in the solution. As result, we need to remove any effect caused by TF from the UV-visible spectra, similar to the treatment of the data for SA.

To quantify the affinity of **3.1** for TF, the absorbances at 444 nm needed to be corrected for the absorbances and scattering caused by TF alone. A stock solution of 1.0 mM TF in buffer (25 mM MOPS, pH 7.0, 50 mM NaCl) was prepared and a series of dilutions was prepared from the stock solution. UV-visible spectra were recorded for these solutions in a 1.0 cm pathlength cuvette (Figure 3.13 (right) panel 2, see appendix, Tables A55.28 for corrected TF alone). The absorbances were corrected and the corrected absorbances at 444 nm were plotted

as a function of the concentration of TF (Figure 3.13 left) for data in tabular format see appendix, Tables A55.27.

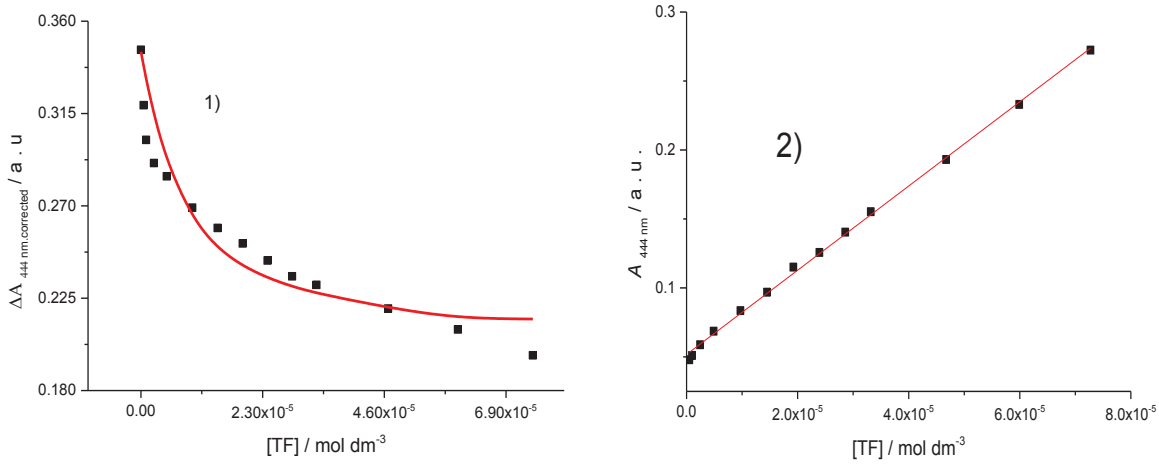

Figure 3.13: Corrected absorbance at 444 nm for 0.0215 mM **3.1** as a function of TF concentration, at 25 °C in buffer (25 mM MOPS, pH 7, 50 mM NaCl). The solid line represents the best fit to the data in terms of a multiple independent binding sites model *(left 1)*. The solid line (*right 2)* represents the extinction coefficient of TF at 444 nm.

Figure 3.13 shows a hypochromic shif at 444 nm for **3.1**. The binding affinity $K_{binding}$ and the number of the binding sites per TF were determined by fitting a multiple independent binding sites model, which also takes ligand dilution into account, to the data. This fit provides an equilibrium constant $K_{binding}$ of $(2\times10^{-3} \pm 1.02) \times10^{5}$ M^{-1} for a binding site of $(3\times10^{-3} \pm 1.1)$. Because the value of $1/n$ was unreasonable, the data were reanalysed for a binding site size n restricted to 0.33 TF. The fit gave an equilibrium constant $K_{binding}$ of $(9.4 \pm 5.9) \times10^{4}$ M^{-1}. The fitting indicates that a binding model involving one molecule of TF interacting with three molecules of **3.1** is reasonable. This is in line with the hypothesis that TF has three binding sites accessible to **3.1**, presumably in subdomains N and C as reported in the literature[42]. For the analogous data for **3.2** see appendix A8 (see appendix, Tables A55.29).

3.2.8 Compound 3.8 binding to TF

We wanted to study the binding of **3.8** and TF. The changes in absorption of **3.8** upon addition of TF were measured in buffer (25 mM MOPS, pH 7.0, 50 mM NaCl) at 25 °C (Figure 3.14).

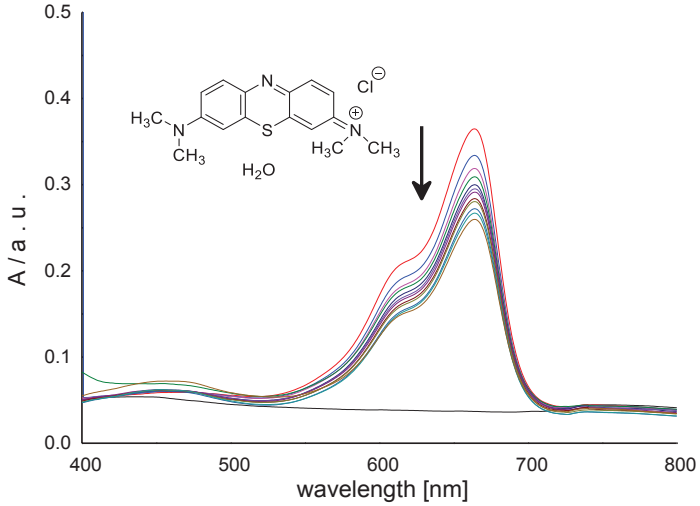

Figure 3.14: UV-visible spectra for 0.004 mM **3.8** at 664 nm upon addition of 0 – 0.045 mM TF, at 25 °C in buffer (25 mM MOPS, pH 7.0, 50 mM NaCl).

Figure 3.14 shows that **3.8** displays a hypochromic shift in the absorbance upon addition of TF with a maximum change in absorbance at 664 nm. This decrease in UV-visible absorption may have occurred as a result of geometrical distortion of **3.8** when it interacts with TF, but it may also be as a consequence of a local medium effect. The increase in absorbance is caused by the increased scattering of TF.

To quantify the affinity of **3.8** for TF, the corrected absorbances at 664 nm were plotted as a function of the concentration of TF (Figure 3.15, see appendix, Tables A55.34).

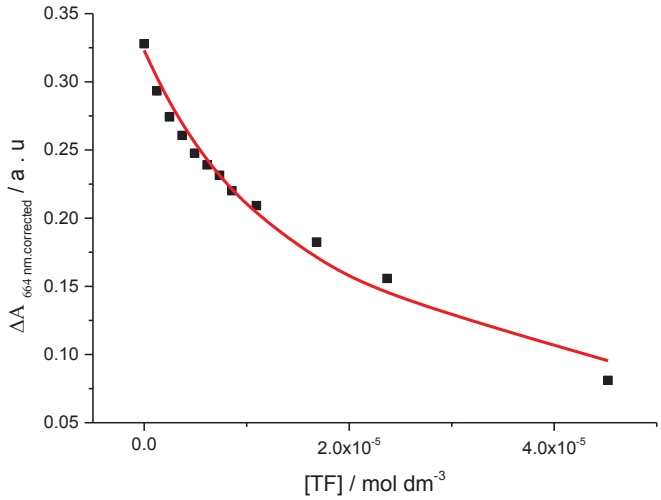

Figure 3.15: Corrected absorbance at 664 nm for 0.004 mM **3.8** upon addition of 0 – 0.04 mM TF, at 25 °C in buffer (25 mM MOPS, pH 7.0, 50 mM NaCl). The solid lines represent the best fit to the data in terms of a multiple independent binding sites model.

Figure 3.15 illustrates the decrease in the absorbance at 664 nm for **3.8** upon addition of TF. The binding constant $K_{binding}$ and the number of binding sites *n* per protein were determined by fitting a multiple independent binding sites model, which also takes ligand dilution into account, to the data. This fit gives an equilibrium constant $K_{binding}$ of $8.5\times10^{-3} \pm 2.1) \times10^{5}$ M^{-1} for an unrealistically small binding site size of $(2.7\times10^{-2} \pm 5.0)$. We then reanalysed the data for a binding site size *n* restricted to 0.33 TF. The fit gave an equilibrium constant $K_{binding}$ of $(2.0 \pm 0.33) \times10^{4}$ M^{-1}. The fit indicates that three molecules of compound **3.8** interact with one molecule of TF.

3.2.9 Compound 3.10 interacting with TF

UV-visible spectroscopy has been used to determine the affinity and stoichiometry for **3.10** binding with TF. The changes in absorption of **3.10** upon addition of TF were measured in buffer (25 mM MOPS, pH 7.0, 50 mM NaCl) at 25 °C (Figure 3.16).

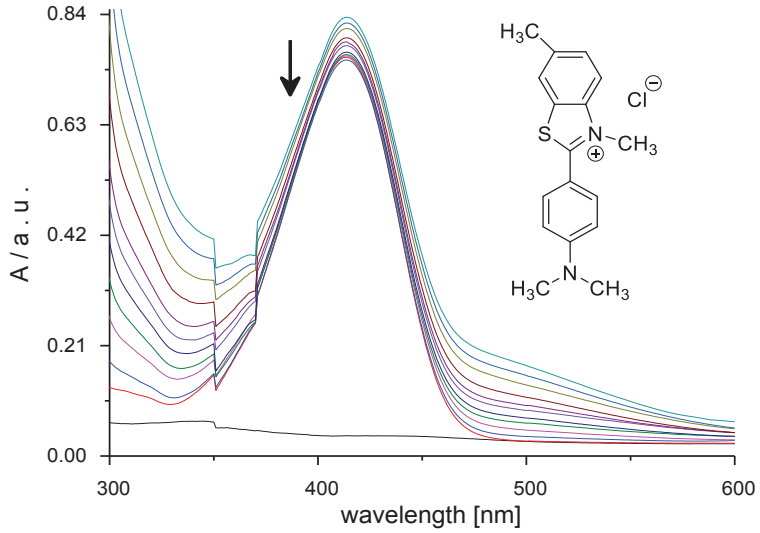

Figure 3.16: UV-visible spectra for 0.0279 mM **3.10** upon addition of 0 – 0.032 mM TF in buffer (25 mM MOPS, pH 7.0, 50 mM NaCl) at 25 °C.

Figure 3.16 demonstrates a hypochromic shift in the absorbance upon addition of TF with a maximum change in absorbance at 413 nm. This change in UV-visible absorption may have occurred because of geometrical distortion of **3.10** when it interacts with TF, but it may also be as a result of a local medium effect. The increase in baseline upon addition of TF is attributed to scattering of light by TF in solution. We therefore measure scattering and remove it from absorbances as before.

To quantify the affinity of **3.10** for TF, the corrected absorbances at 413 nm were plotted as a function of the concentration of TF (Figure 3.17, see appendix, Tables A55.35).

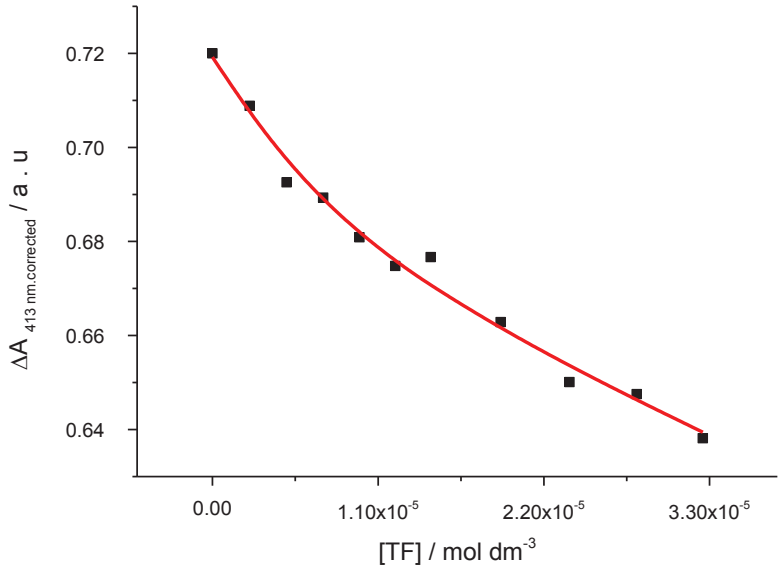

Figure 3.17: Corrected absorbance at 413 nm for 0.027 mM **3.10** upon addition of 0 – 0.032 mM TF concentration, at 25 °C in buffer (25 mM MOPS, pH 7.0, 50 mM NaCl). The solid line represents the best fit to the data in terms of a multiple independent binding sites model.

The titration curve in Figure 3.17 was analysed by fitting a multiple independent binding sites model, which also takes ligand dilution into account, to the data, giving an equilibrium constant $K_{binding}$ of $(3\times10^{-3} \pm 2.1) \times10^{6}$ M^{-1} for a binding site size of $(2\times10^{-3} \pm 18)$. The obtained value of the stoichiometry was too small and therefore unreasonable. Therefore, the data were reanalysed, with a binding site size restricted to 0.33, giving an equilibrium constant $K_{binding}$ of $(1.0 \pm 0.73) \times10^{5}$ M^{-1}. The fit suggests that three molecules of **3.10** interact with each molecule of TF. Similar experiments for compounds **3.3, 3.4, 3.7, 3.9, 3.11** and **3.12** (See appendix) showed no interactions with TF.

Summary

The findings of UV-visible titrations for oligoheteroaromatic compounds **3.1, 3.2, 3.3 3.4, 3.5, 3.6, 3.7, 3.8, 3.9, 3.10, 3.11** and **3.12** with TF are summarised in Table 3.2.

Table 3.2 Binding affinities and binding site sizes for binding of 3.1, 3.2, 3.3 3.4, 3.5, 3.6, 3.7, 3.8, 3.9, 3.10, 3.11 and 3.12 to TF in buffer (25 mM MOPS, pH 7.0, 50 mM NaCl) at 25 °C.

Ligands	*Binding constant for TF* K / M^{-1}	*Binding site n*	*Binding stoichiometry 1/n*
3.1	$(7.4 \pm 5.9) \times 10^4$	0.33*	3
3.2	$(1.4 \pm 1.1) \times 10^5$	0.33*	3
3.3	No binding		
3.4	No binding		
3.5	No binding		
3.6	No binding		
3.7	No binding		
3.8	$(2.0 \pm 0.3) \times 10^4$	0.33*	3
3.9	No binding		
2.10	$(1.00 \pm 0.73) \times 10^5$	0.33*	3
3.11	No binding		
3.12	No binding		
* restricted			

Ligands **3.1, 3.2, 3.8** and **3.10** in Table 3.2 interact with transferrin, and the interaction is accompanied by a change in optoelectronic properties. The other molecules did not show any binding with TF. The absence of interaction might be because of a mismatch in fit between the compound and transferrin.

Part C: Effect of serum albumin on DNA-binding properties.

3.2.10 Compounds 3.1 and 3.2 interacting with DNA in the presence of 0.1 mM SA

To evaluate the binding of **3.1** and **3.2** with DNA in the presence of 0.1 mM SA, UV−visible spectroscopy has been used. The changes in absorption of **3.1** upon addition of DNA were measured in buffer (25 mM MOPS, pH 7.0, 50 mM NaCl) at 25° C in the presence of 0.1 mM SA (Figure 3.18). Similar results were found for **3.2** interacting with DNA in the presence of SA. (See appendix A15, Table A55.39).

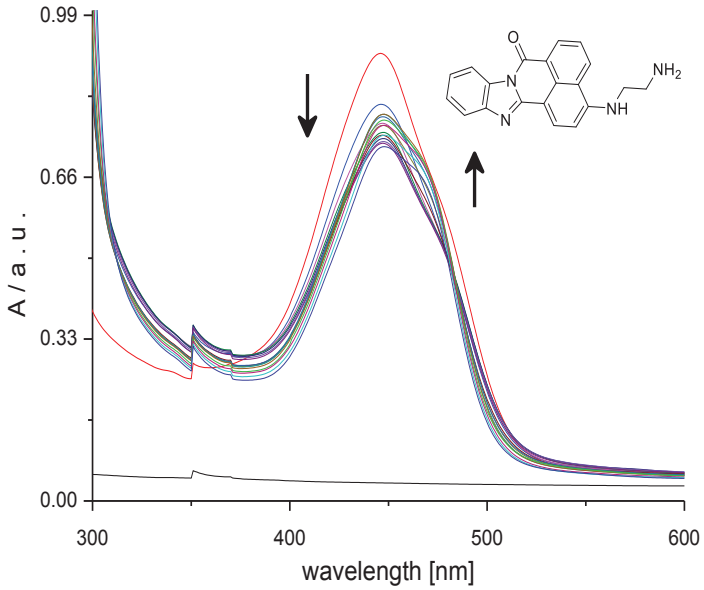

Figure 3.19: UV-visible spectra for 0.054 mM **3.1 (**red line**)** in buffer (25 mM MOPS, pH 7.0, 50 mM NaCl) in the absence of SA and subsequent spectra for **3.1** in the presence of 0.1 mM SA upon addition of 0 – 2.49 mM DNA, at 25 °C.

Figure 3.19 shows a hypochromic shift in absorbance at 446 nm followed by a hyperchromic shift at 446 nm upon addition of DNA in the presence of 0.1 mM SA. The observation suggests precipitation and subsequent dissolution of a DNA ligand complex in the presence of SA, similar to the situation in the absence of SA.

To quantify the affinity of **3.1** for DNA in the presence of SA, the absorbances at 446 nm were plotted as a function of the concentration of DNA (Figure 3.19, see appendix, Tables A55.38).

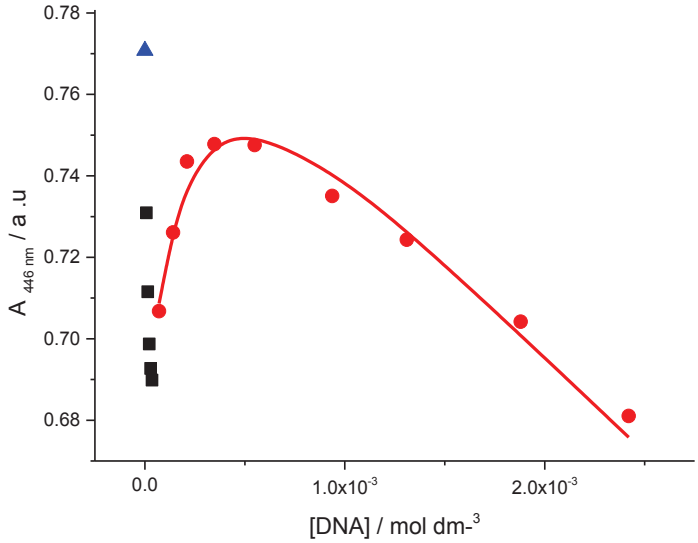

Figure 3.19: Absorbance at 446 nm for a solution of 0.0545 mM **3.1** as a function of DNA concentration of 0 – 0.036 mM (■) and of 0.070 – 2.4 mM (●) in the presence of 0.1 mM SA (▲), at 25 °C in buffer (25 mM MOPS, pH 7, 50 mM NaCl). The solid line represents a global fit of a multiple independent sites model to the data in the 0.070 – 2.4 mM range.

Figure 3.19 shows two events upon addition of DNA to **3.1** in the presence of SA. The first event involves a large decrease in the absorbance at 446 nm up to a concentration of 0.036 mM DNA. We attribute this decline in absorbance to strong binding of **3.1** to the sugar-phosphate backbone of DNA at low concentration of DNA in combination with a high concentration of ligand *i.e.* a high ligand / DNA ratio. These conditions lead to precipitation as a result of charge neutralisation of the **3.1** - DNA complex as also observed previously in the absence of SA.[172] The second event shows a clear increase in the absorbance of **3.1** upon addition of 0.070 – 2.4 mM of DNA in the presence of 0.1 mM of SA. The ligand strongly interacts with DNA, and the titration data in figure 3.18 (with the first event not included) were analysed in terms of a multiple independent binding sites models, which also takes ligand dilution into account. An apparent equilibrium constant $K_{binding}$ of (0.12 ± 24) M^{-1} for a binding site size of (1.6×10^{-5} ± 3.4×10^{-3}) base pairs was found. A $K_{binding}$ of (1.5 ± 0.1) × 10^4 M^{-1} for the binding site size restricted to 3.0 base pairs was observed for **3.1** to DNA in the absence of SA. Therefore, the data were reanalysed with the stoichiometry restricted to 3.0 base pairs to allow comparison, giving an apparent equilibrium constant $K_{binding}$ of (2.6 ± 0.8) × 10^4 M^{-1}. From the similarity in the apparent binding constant in the absence of SA[172] and in the presence of SA, it appears that SA does not significantly compete with DNA for **3.1.** Unfortunately, SA therefore does not help to avoid precipitation. On the other hand, the absence of this competition is beneficial if

compound **3.1** were to be used in a biosensor because it can be used to provide signals to detect DNA hybridization information without being affected by precipitation.

3.2.11 Compound 3.3 interacting with DNA in the presence of 0.2 mM SA

The binding of **3.3** to DNA in the presence of 0.2 mM SA was studied using UV-visible spectroscopy; the changes in absorption of **3.3** upon addition of DNA in the presence of SA were measured in buffer (25 mM MOPS, pH 7.0 and 50 mM NaCl) at 25 °C (Figure 3.20).

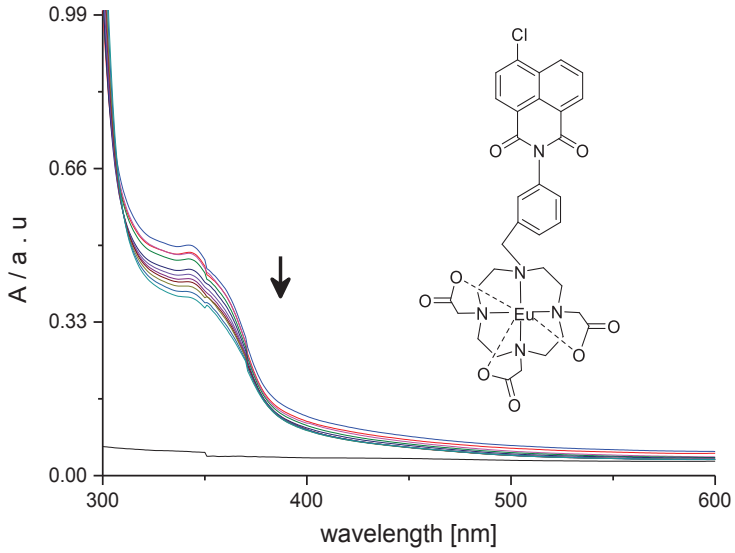

Figure 3.20: UV-visible spectra for 0.041 mM **3.3** upon addition of 0 – 1.9 mM DNA in the presence of 0.2 mM SA, at 25 °C in buffer (25 mM MOPS, pH 7.0, 50 mM NaCl)

Figure 3.20 shows a hypochromic shift in absorbance (at the λ max of 348 nm). The change in UV-visible absorption may occur as a result of geometrical distortion of **3.3** when it interacts with DNA in the presence of SA, but it may also be a local medium effect.

To quantify the affinity of **3.3** for DNA in the presence of SA, the absorbances at 348 nm were plotted as a function of the concentration of DNA in the presence of SA (Figure 3.21, see appendix, Tables A55.40).

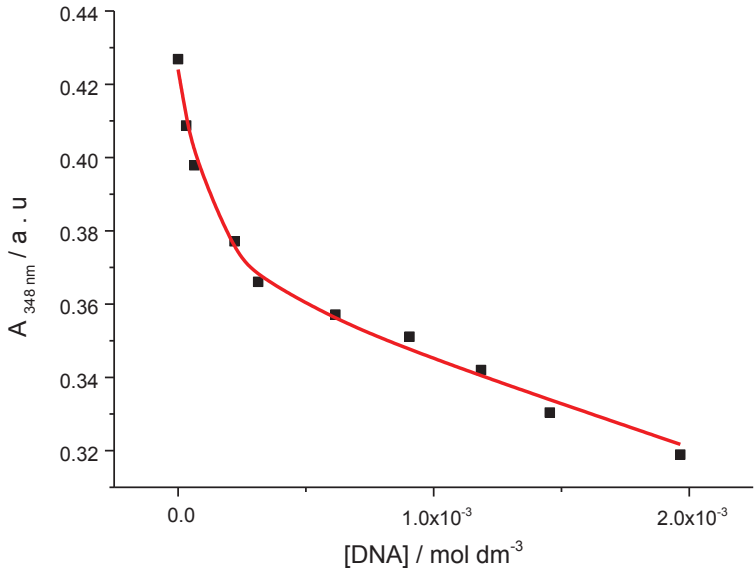

Figure 3.21: Absorbance at 348 nm of a solution of 0.041 mM **3.3** as a function of DNA concentration in the presence of 0.2 mM SA, at 25 °C in buffer (25 mM MOPS, pH 7, 50 mM NaCl). The solid line represents the best fit to the data in terms of a multiple independent binding sites model.

Figure 3.21 shows a hypochromic shift in absorbance upon addition of DNA as also observed previously in the absence of 0.2 mM SA.[172] We attribute this decline in absorbance to binding of **3.3** to DNA in the presence of 0.2 mM SA. The binding affinity $K_{binding}$ and binding sites size n were determined by fitting a multiple independent binding sites model, which also takes ligand dilution into account, to the data. The fit produces an apparent equilibrium constant $K_{binding}$ of $(2\times10^{-3} \pm 3.8) \times10^{5}\ M^{-1}$ for a binding site size of $(2.4 \times10^{-2} \pm 32.4)$ base pairs. A $K_{binding}$ of $(1.7 \pm 0.4) \times10^{4}\ M^{-1}$ for the binding site size restricted to 3.0 base pairs was observed for **3.3** binding to DNA in the absence of SA.[172] Therefore, the data were reanalysed with the stoichiometry restricted to 3.0 base pairs to allow comparison, giving an apparent equilibrium constant $K_{binding}$ of $(6.7 \pm 2.3) \times10^{4}\ M^{-1}$. From the difference in the apparent binding constant in the absence of SA[172] and in the presence of SA, it appears that SA significantly competes with DNA for **3.3**. The presence of this competition is beneficial if the compound **3.3** were to be used in a biosensor because SA can be used to decrease nonspecific binding avoiding false positive signals when detecting DNA hybridization information or it could reduce sensitivity.

3.2.12 Compound 3.4 binding to DNA in the presence of 0.1 mM SA

We wanted to study the binding of **3.4** to DNA in the presence of 0.1 mM SA. The changes in absorption of **3.4** upon addition of DNA in the presence of 0.1 mM SA were measured in buffer (25 mM MOPS, pH 7.0, 50 mM NaCl) at 25 °C (Figure 3.22).

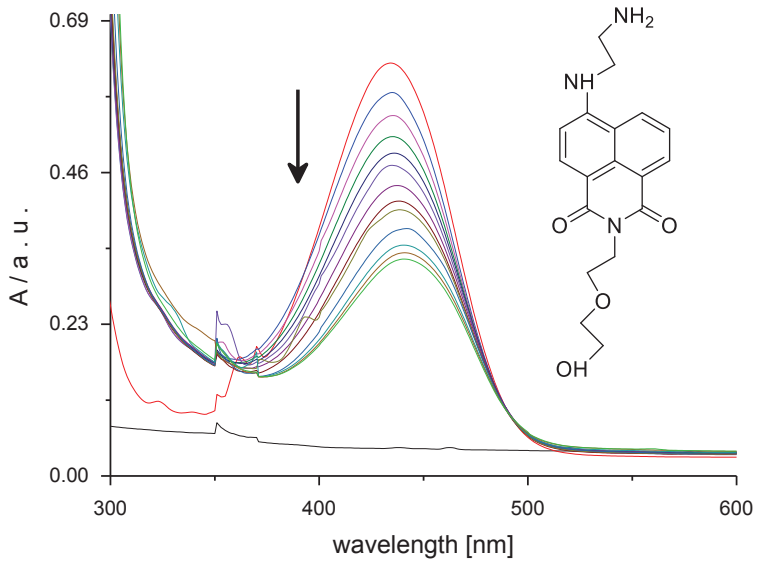

Figure 3.22: UV-visible spectra for 0.053 mM **3.4** upon addition of 0 – 2.3 mM DNA in the presence of 0.1 mM SA, at 25 °C in buffer (25 mM MOPS, pH 7.0, 50 mM NaCl).

In the studies, **3.4** showed a hypochromic shift in absorbance with a maximum change in absorbance at 434 nm upon addition of DNA in the presence of 0.1 mM SA. This decrease in UV-visible absorption may have occurred as a result of geometrical distortion of **3.4** when it interacts with DNA in the presence of SA, but it may also be as a consequence of a local medium effect.

To quantify the affinity of **3.4** for DNA, the absorbances at 434 nm were plotted as a function of the concentration of DNA (Figure 3.23, see appendix, Tables A55.41).

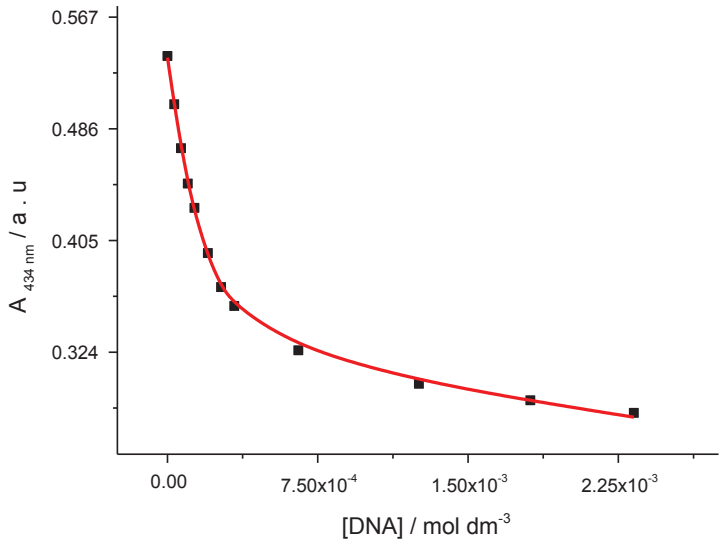

Figure 3.23: Absorbance at 434 nm for 0.053 mM **3.4** as a function of DNA concentration in the presence of 0.1 mM SA, at 25 °C in buffer (25 mM MOPS, pH 7, 50 mM NaCl). The solid line represents the best fit to the data in terms of multiple independent binding sites model.

Figure 3.23 shows a decrease in the absorbance at 434 nm upon addition of DNA in the presence of SA. The binding affinity $K_{binding}$ and the binding sites size n were determined by fitting a multiple independent binding sites model, which also takes simple dilution into account, to the data. The fit gives an equilibrium constant $K_{binding}$ of (6.4 ± 1.1) $\times 10^4$ M^{-1} for a binding site size (3.7 ± 0.3) base pairs. A $K_{binding}$ of (3.5 ± 0.6) $\times 10^4$ M^{-1} for a binding site size of (2.3 ± 0.24) base pairs was observed for **3.4** interacting with DNA in the absence of SA. Although the obtained binding parameters were reasonable for both stoichiometry and binding constant, the data were reanalysed with the stoichiometry restricted to 3.0 base pairs to allow comparison, giving an equilibrium constant $K_{binding}$ of (4.2 ± 0.2) $\times 10^4$ M^{-1}. A $K_{binding}$ of (5.4 ± 0.3) $\times 10^4$ M^{-1} for the binding site size restricted to 3.0 base pairs was observed for **3.4** binding to DNA in the absence of SA. From the small difference in binding constants in the presence and absence of SA, it appears that SA does significantly compete with DNA for **3.4**.

3.2.13 Compound 3.5 binding to DNA in the presence of 0.1 mM SA

We need to know whether of **3.5** interacts with DNA in the presence of 0.1 mM SA. The changes in absorption of **3.5** in the presence of 0.1 mM SA upon addition of DNA were measured in buffer (25 mM MOPS, pH 7.0, 50 mM NaCl) at 25 °C (Figure 3.24).

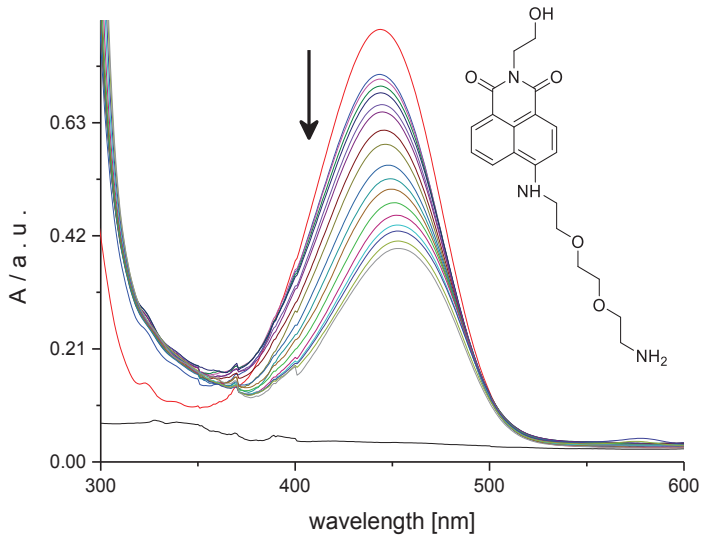

Figure 3.24: UV-visible spectra for 0.0744 mM **3.5** upon addition of 0 – 2.80 mM DNA in the presence of 0.1 mM SA, at 25 °C in buffer (25 mM MOPS, pH 7.0, 50 mM NaCl).

In the studies, **3.5** showed a hypochromic shift in absorbance upon addition of DNA in the presence of 0.1 mM SA with a maximum change in absorbance at 444 nm. The decrease in UV-visible absorption may have occurred as a result of geometrical distortion of **3.5** when it interacts with DNA in the presence of SA, but it may also be as a result of a local medium effect.

To quantify the affinity of **3.5** for DNA in the presence of SA we plotted the absorbances at 444 nm as a function of the concentration of DNA (Figure 3.25, see appendix, Tables A55.42).

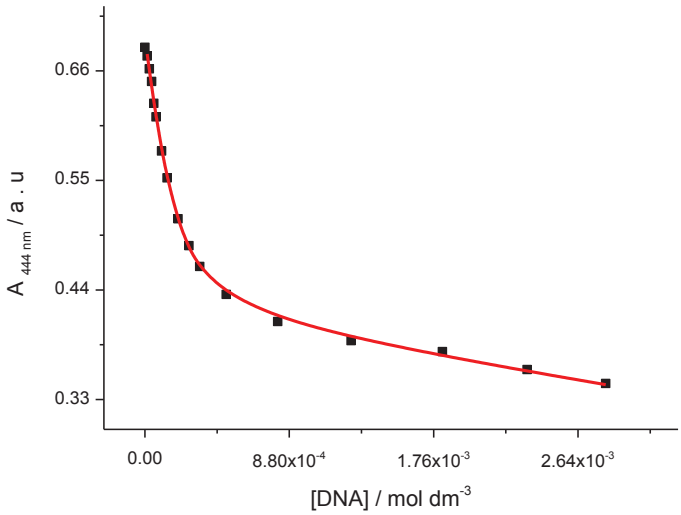

Figure 3.25: Absorbance at 444 nm for 0.0744 mM **3.5** as a function of DNA concentration in the presence of 0.1 mM SA, at 25 °C in buffer (25 mM MOPS, pH 7, 50 mM NaCl). The solid line represents the best fit to the data in terms of a multiple independent binding sites model.

Figure 3.25 shows a clear decrease in the absorbance for **3.5** upon addition of DNA in the presence of 0.1 mM SA. The binding affinity $K_{binding}$ and binding sites size *n* were determined by fitting a multiple independent binding sites model, which also takes ligand dilution into account, to the data. The fit gives an equilibrium constant $K_{binding}$ of (4.9 ± 0.8) $\times 10^4$ M^{-1} for a binding site size of (2.6 ± 0.2) base pairs. A $K_{binding}$ of (1.6 ± 0.5) $\times 10^4$ M^{-1} for the binding site size of (1.2 ± 0.2) base pairs was observed for **3.5** binding to DNA in the absence of SA. The obtained binding parameters were reasonable for both stoichiometry and binding constant. Nevertheless, the data were reanalysed with the stoichiometry restricted to 3.0 base pairs to allow comparison, giving an apparent equilibrium constant $K_{binding}$ of (6.5 ± 0.4) $\times 10^4$ M^{-1}. A $K_{binding}$ of (8.9 ± 2.3) $\times 10^4$ M^{-1} for the binding site size restricted to 3.0 base pairs was observed for compound **3.5** binding to DNA in the absence of SA. From the small difference in binding constant in the presence and absence of SA, it appears that SA does not significantly compete with DNA for **3.5**.

3.2.14 Compound 3.6 binding to DNA in the presence of 0.5 mM SA

We studied the binding of **3.6** with DNA in the presence of 0.5 mM SA. The changes in absorption of **3.6** upon addition of DNA in the presence of 0.5 mM SA were measured in buffer (25 mM MOPS, pH 7.0, 50 mM NaCl) at 25 °C (Figure 3.26).

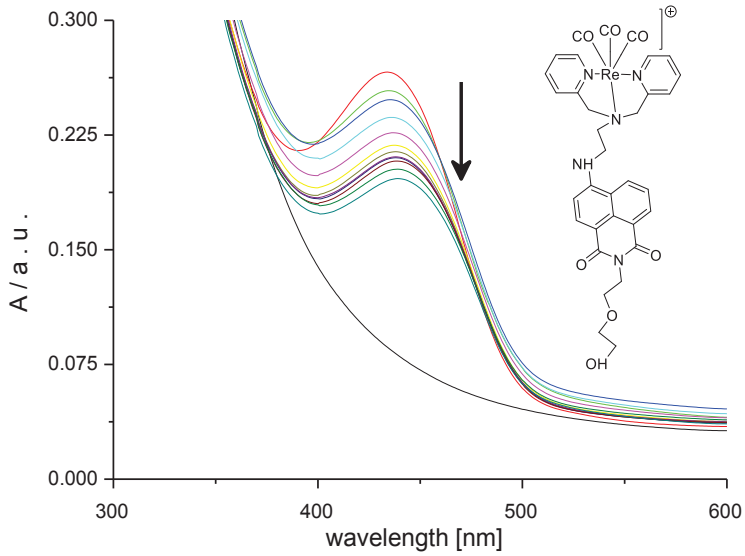

Figure 3.26: UV-visible spectra for 0.011 mM **3.6** upon addition of 0 - 0.203 mM DNA in the presence of 0.5 mM SA, at 25 °C in buffer (25 mM MOPS, pH 7.0, 50 mM NaCl).

Figure 3.26 shows a hypochromic shift upon addition of DNA in the presence of 0.5 mM SA, with a maximum change at 440 nm. This decrease in UV-visible absorption may occur because of geometrical distortion of **3.6** when it interacts with DNA in the presence of SA, or as a result of the different local medium affected by the binding sites.

The absorbance at 440 nm was plotted as a function of the concentration of DNA in the presence of SA (Figure 3.27, see appendix, Tables A55.43).

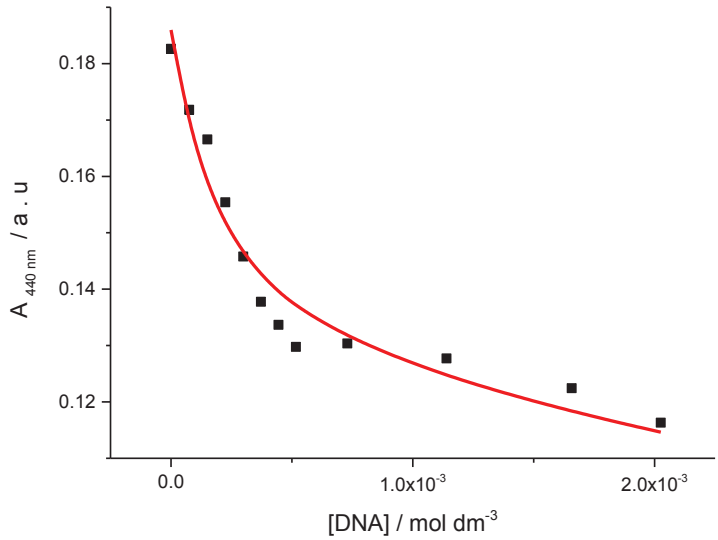

Figure 3.27: Absorbance at 440 nm for a solution of 0.011 mM **3.6** as a function of DNA concentration in the presence of 0.5 mM SA, at 25 °C in buffer (25 mM MOPS, pH 7.0, 50 mM NaCl). The solid line represents the best fit to the data in terms of a multiple independent binding sites model.

Figure 3.27 presents a noticeable decrease in the absorbance of **3.6** on the addition of DNA in the presence of 0.5 mM SA. The binding affinity $K_{binding}$ and binding sites size n were determined by fitting a multiple independent binding sites model, which also takes ligand dilution into account, to the data. The fit gives an equilibrium constant $K_{binding}$ of (1.1 ± 1.4) $\times 10^7$ M^{-1} for a binding site size of (38 ± 2.1) base pairs. A $K_{binding}$ of (11.6 ± 2.7) $\times 10^4$ M^{-1} for the binding site size restricted to 1.0 base pairs was observed for **3.6** binding to DNA in the absence of SA[172]. Therefore, the data were reanalysed with the stoichiometry restricted to 1.0 base pairs to allow comparison, giving an apparent equilibrium constant $K_{binding}$ of (4.6 ± 1.4) $\times 10^3$ M^{-1}. From the difference in binding constants in the absence and presence of SA[172] it appears that SA does significantly compete with DNA for **3.6.** The presence of competition is beneficial because it could reduce nonspecific binding and the presence of SA in a sample could therefore avoid nonspecific interactions or it could cause a drop in sensitivity to the target.

3.2.15 The interaction of compound 3.7 with DNA in the presence of 0.1 mM SA

We wanted to evaluate the binding of **3.7** to DNA in the presence of SA. The changes in absorption of **3.7** upon addition of DNA in the presence of 0.1 mM SA were measured in buffer (25 mM MOPS, pH 7.0, 50 mM NaCl) at 25 °C (Figure 3.28).

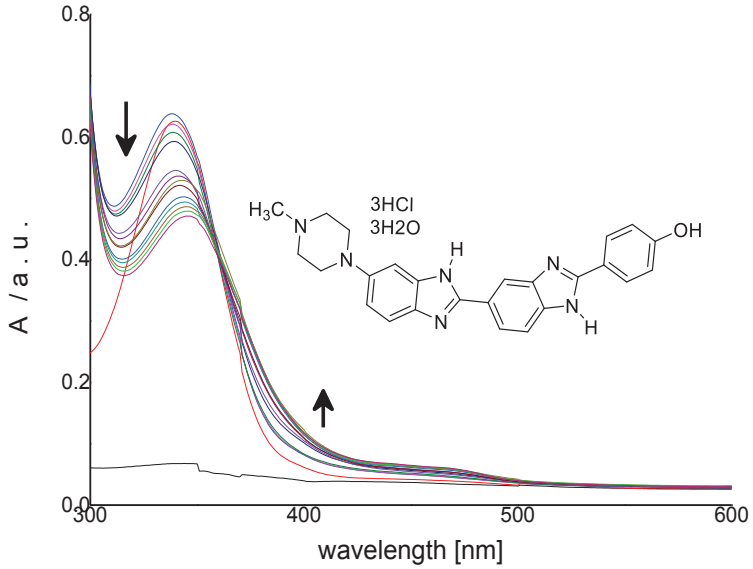

Figure 3.28: UV-visible spectra for 0.014 mM **3.7** upon addition of 0 – 0.15 mM DNA in the presence of 0.1 mM SA, at 25 °C in buffer (25 mM MOPS, pH 7.0, 50 mM NaCl).

Figure 3.28 shows hypochromic and hyperchromic shifts in absorbance at 340 nm and 385 nm upon addition of DNA in the presence of 0.1 mM SA. This change in UV visible absorption may occur as a result of geometrical distortion of **3.7** when it interacts with DNA in the presence of SA, but it may also be a result of a local medium effect.

To quantify the affinity of **3.7** for DNA in the presence of 0.1 mM SA, the absorbances at 340 and 385 nm were plotted as a function of the concentration of DNA (Figure 3.29, see appendix, Tables A55.44).

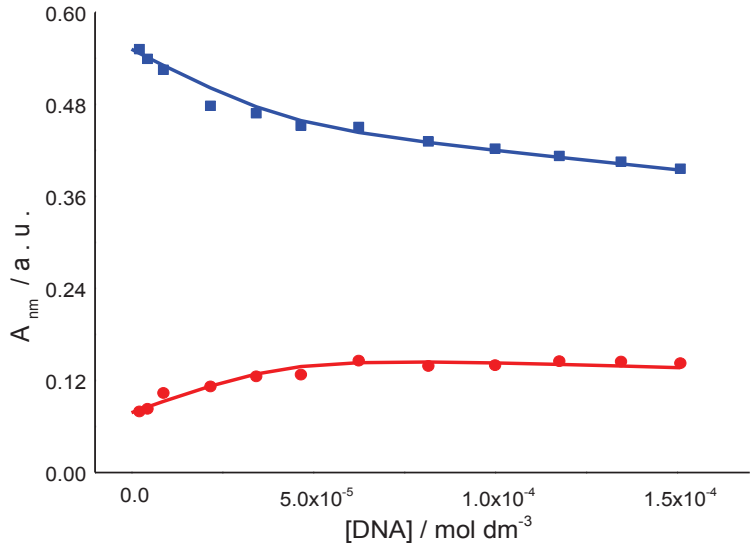

Figure 3.29: Absorbance at 340 nm (■) and at 385 nm (●) for 0.014 mM **3.7** as a function of DNA concentration in the presence of 0.1 mM SA, at 25 °C in buffer (25 mM MOPS, pH 7.0, 50 mM NaCl). The solid lines represent a global fit of a multiple independent binding sites model to the data.

Figure 3.29 shows a clear decrease at 340 nm and increase at 385 nm in the absorbance for **3.7** upon addition of DNA in the presence of 0.1 mM SA. The binding affinity $K_{binding}$ and binding sites size *n* were determined by fitting a multiple independent binding sites model, which also takes ligand dilution into account, to the data. The fit gives an apparent equilibrium constant $K_{binding}$ of $(1.7 \pm 6.2) \times 10^4\ M^{-1}$ for a binding site size of (0.2 ± 0.9) base pairs. A $K_{binding}$ of $(7.7 \pm 1.5) \times 10^5\ M^{-1}$ for the binding site size restricted to 3.0 base pairs was observed for **3.7** binding to DNA in the absence of SA. Therefore, the data were reanalysed with the stoichiometry restricted to 3.0 base pairs to allow comparison, giving an apparent equilibrium constant $K_{binding}$ of $(7.9 \pm 6.2) \times 10^5\ M^{-1}$. From the similarity in the apparent binding constant in the absence of SA and in the presence of SA, it appears that SA does not significantly compete with DNA for **3.7**.

3.2.16 Compound 3.8 interacting with DNA in the presence of 0.1 mM SA

We wanted to study the binding of **3.8** with DNA in the presence of 0.1 mM SA. The changes in absorption of **3.8** upon addition of DNA were measured in buffer (25 mM MOPS, pH 7.0, 50 mM NaCl) at 25 °C (Figure 3.30).

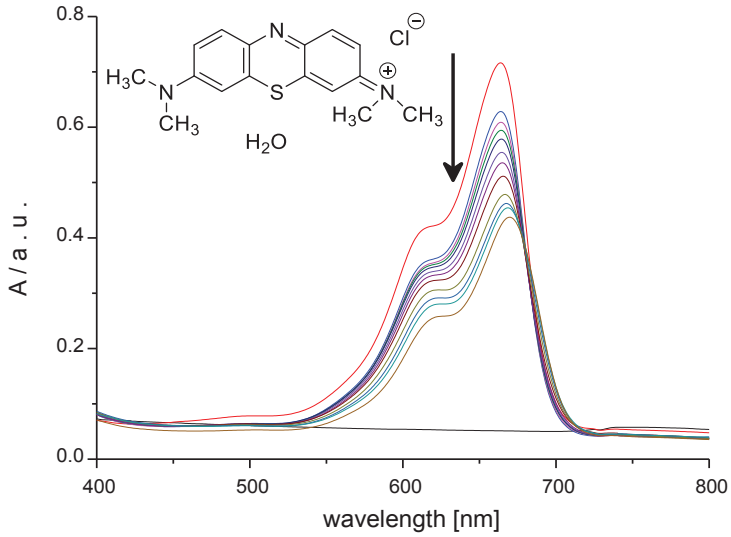

Figure 3.30: UV-visible spectra for 0.00992 mM **3.8** upon addition of 0 - 0.194 mM DNA in the presence of 0.1 mM SA, at 25 °C in buffer (25 mM MOPS pH 7.0, 50 mM NaCl).

Figure 3.30 shows a hypochromic shift at 664 nm upon addition of DNA in the presence of 0.1 mM SA. This decrease in UV-visible absorption may occur as a result of geometrical distortion of **3.8** when it interacts with DNA, or as a result of the different local medium presented by the binding sites on the DNA.

To quantify the affinity of **3.8** for DNA, the absorbances at 664 nm were plotted as a function of the concentration of DNA (Figure 3.31, see appendix, Tables A55.45).

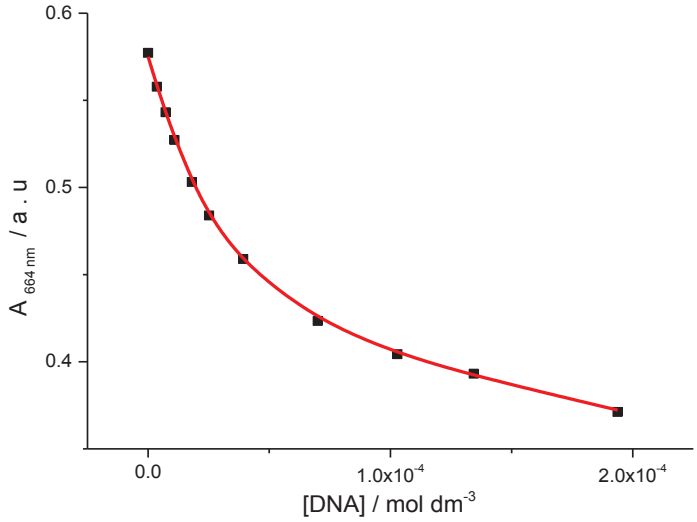

Figure 3.31: Absorbance at 664 nm for 0.0099 mM **3.8** as a function of DNA concentration in the presence of 0.1 mM SA, at 25° C in buffer (25 mM MOPS, pH 7, 50 mM NaCl). The solid line represents the best fit to the data in terms of a multiple independent binding sites model.

Figure 3.31 shows a decrease in absorbance of **3.8** upon addition of the DNA, as also observed previously in the absence of SA. We attribute this decline in absorbance to strong binding of **3.8** to DNA in the presence of 0.1 mM SA. The binding affinity $K_{binding}$ and a binding site size *n* were determined by fitting a multiple independent binding sites model, which also takes ligand dilution into account, to the data. The ligand strongly interacts with DNA giving an equilibrium constant $K_{binding}$ of (1.5 ± 0.34) $\times 10^5$ M^{-1} for a binding site size of (2.2 ± 0.2) base pairs. A $K_{binding}$ of (4.5± 1.8) $\times 10^5$ M^{-1} for the binding site size of (3.07 ± 0.5) base pairs was observed for **3.8** binding to DNA in the absence of SA. The obtained binding parameters were reasonable for both stoichiometry and binding constant. The data were reanalysed with the stoichiometry restricted to 3.0 base pairs to allow comparison, giving an apparent equilibrium constant $K_{binding}$ of (2.5 ± 1.6) $\times 10^5$ M^{-1}. A $K_{binding}$ of (4.4 ± 0.5) $\times 10^5$ M^{-1} for the binding site size restricted to 3.0 base pairs was observed for **3.8** binding to DNA in the absence of SA. From the similarity in binding constants in the presence and absence of SA, it appears that SA does not significantly compete with DNA for **3.8**.

3.2.17 Compound 3.10 binding with DNA in the presence of 0.1 mM SA

We wanted to know the binding of **3.10** to DNA in the presence of SA was studied; the changes in absorption of **3.10** upon addition of DNA were measured in buffer (25 mM MOPS, pH 7.0, 50 mM NaCl) at 25 °C (Figure 3.32).

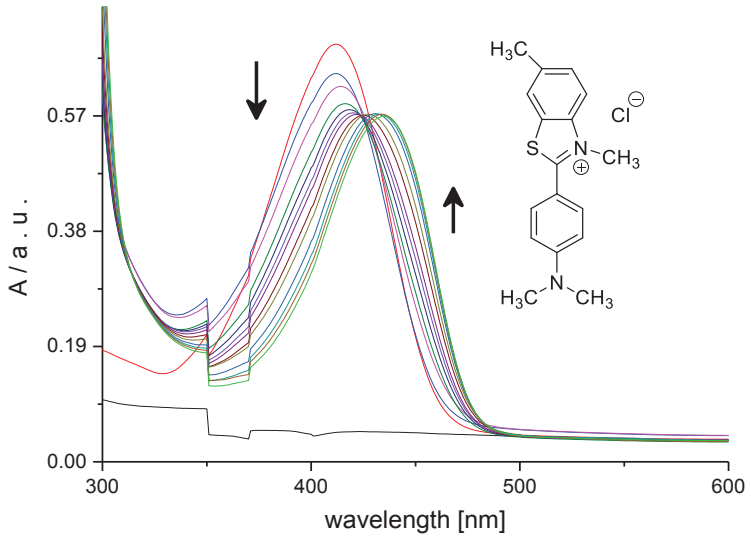

Figure 3.32: UV-visible spectra for 0.019 mM **3.10** upon addition of 0 – 1.84 mM DNA in the presence of 0.1 mM SA, at 25 °C in buffer (25 mM MOPS, pH 7.0, 50 mM NaCl).

Figure 3.32 shows a redshift in absorbance of **3.10** upon addition of DNA in the presence of 0.1 mM SA. This change in UV-visible absorption probably occurs because of geometrical distortion of **3.10** when it interacts with DNA, but it may also be a local medium effect.

To quantify the affinity of **3.10** for DNA in the presence of 0.1 mM SA, the absorbances at 412 and 432 nm were plotted as a function of the concentration of DNA (Figure 3.33, see appendix, Tables A55.46).

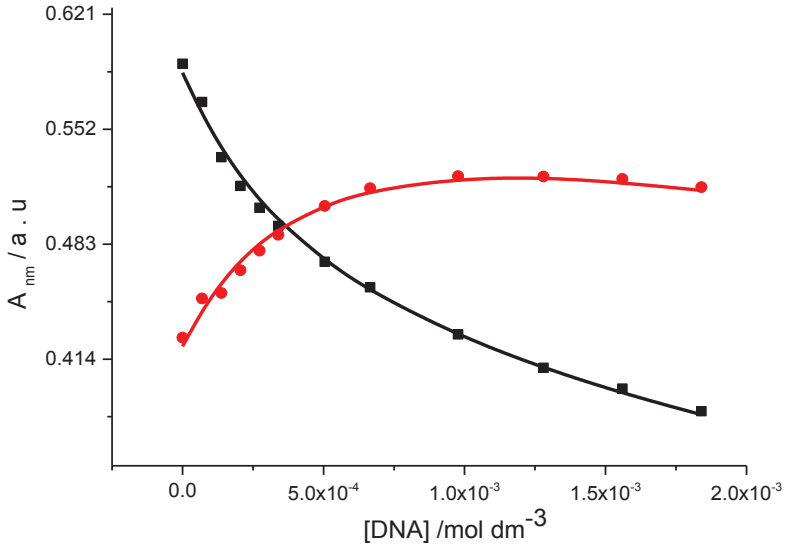

Figure 3.33: Absorbance at 412 nm (■) and at 432 nm (●) for a solution of 0.0236 mM **3.10** as a function of DNA concentration in the presence of 0.1 mM SA, in buffer (25 mM MOPS, pH 7.0, 50 mM NaCl) at 25 °C. The solid lines represent a global fit of a multiple independent sites model to the data.

Figure 3.33 shows the absorbances at 412 nm and at 432 nm. The data at 412 nm predominantly represent free ligand, and the data at 432 nm represent the DNA-ligand complex. Therefore, by adding more DNA the amount of free ligand decreases as the ligand binds to DNA. The bathochromic shift is explained as increased conjugation resulting from increased planarity upon binding to DNA. The binding affinity $K_{binding}$ and binding sites size n were determined by fitting a multiple independent binding sites model, which also takes ligand dilution into account, to the data. The fit gives an equilibrium constant $K_{binding}$ of $(2.1\times10^{-2} \pm 1.6) \times10^{4}$ M^{-1} for a binding site size of $(1\times10^{-1} \pm 8.7)$ base pairs. A $K_{binding}$ of $(3.9\times10^{-1} \pm 1.4) \times10^{4}$ M^{-1} for a binding site size of (1.3 ± 4.4) base pairs was observed for **3.10** to DNA in the absence of SA. The obtained stoichiometry was unreasonably small. Therefore, the data were reanalysed with the stoichiometry restricted to 3.0 base pairs to allow comparison, giving an apparent equilibrium constant $K_{binding}$ of $(6.0 \pm 0.5) \times10^{3}$ M^{-1}. A $K_{binding}$ of $(6.9 \pm 0.7) \times10^{3}$ M^{-1} for the

binding site size restricted to 3.0 base pairs was observed for **3.10** to DNA in the absence of SA. From the similarity in the binding constant, it appears that SA does not significantly compete with DNA for **3.10**. The absence of this competition is beneficial if **3.10** were to be used in a biosensor.

3.2.18 Compound 3.11 binding to DNA in the presence of 0.1 mM SA

The binding of **3.11** to DNA in the presence of 0.1 mM SA was studied using UV−visible spectroscopy. The changes in absorption of **3.11** upon addition of DNA in the presence of SA were measured in buffer (25 mM MOPS pH 7.0, 50 mM NaCl) at 25 °C (Figure 3.34).

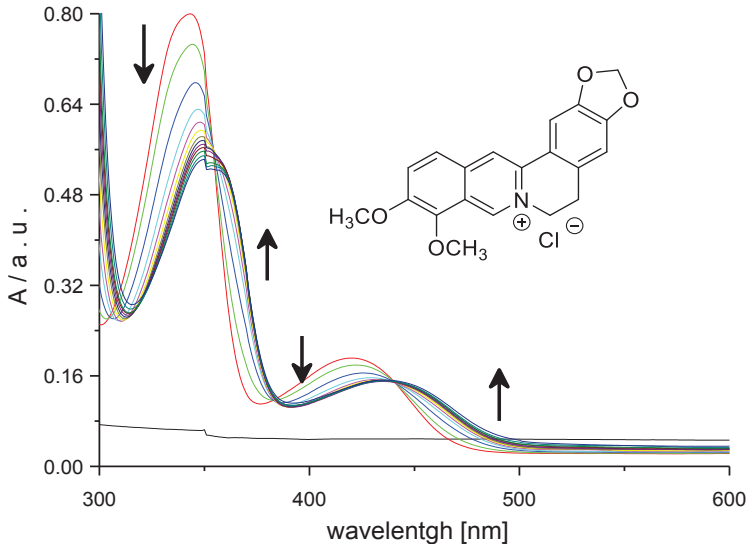

Figure 3.34: UV-visible spectra for 0.024 mM **3.11** upon addition of 0 – 3.3 mM DNA in the presence of 0.1 mM SA, at 25 °C in buffer (25 mM MOPS, pH 7.0, 50 mM NaCl).

In the studies, **3.11** showed a red shift in absorbance upon addition of DNA with maximum changes in absorbance at 343 and 375 nm in the presence of 0.1 mM SA. We recognised isosbestic points suggesting that only two forms of the DNA binder are involved in the titration, viz. the free ligand and DNA−bound ligand. The change in UV-visible absorption may occur as a result of geometrical distortion of **3.11** when it interacts with DNA in the presence of SA, but it may also be a local medium effect.

To quantify the affinity of **3.11** for DNA in the presence of SA, the absorbances at 343 and 375 nm were plotted as a function of the concentration of DNA in the presence of SA (Figure 3.35, see appendix, Tables A55.47).

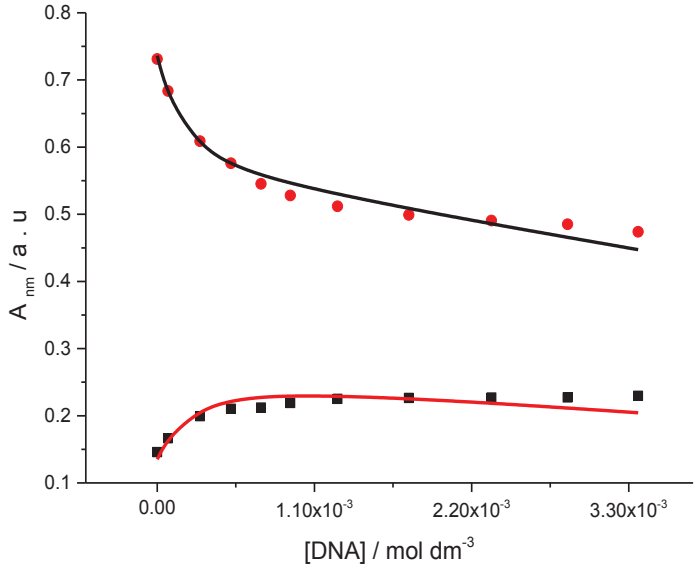

Figure 3.35: Absorbance at 343 and 375 nm for the solution of 0.024 mM **3.11** as a function of DNA in the presence of 0.1 mM SA, at 25 °C in buffer (25 mM MOPS, pH 7, 50 mM NaCl). The solid lines represent a global fit of a multiple independent sites model to the data.

Figure 3.35 shows a clear decrease at 343 nm and an increase at 375 nm in absorbance for **3.11** upon addition of DNA in the presence of 0.1 mM SA. The binding affinity $K_{binding}$ and binding sites size *n* were determined by fitting a multiple independent binding sites model, which also takes simple dilution into account, to the data. The ligand strongly interacts with DNA giving an equilibrium constant $K_{binding}$ of (1.3 ± 2.4) $\times 10^5$ M^{-1} for a binding site size of (12.5 ± 11.0) base pairs. A $K_{binding}$ of (6.5± 0.47) $\times 10^4$ M^{-1} for a binding site size of (8.0 ± 3.2) base pairs was observed for **3.11** binding to DNA in the absence of SA. The data were reanalysed, with the stoichiometry restricted to 3.0 base pairs, to allow comparison, giving an apparent equilibrium constant $K_{binding}$ of (1.6 ± 0.6) $\times 10^4$ M^{-1}. A $K_{binding}$ of (1.6 ± 0.2) $\times 10^4$ M^{-1} for the binding site size restricted to 3.0 base pairs was observed for **3.11** binding to DNA in the absence of SA. From the similarity in the binding constants, it appears that SA does not significantly compete with DNA for **3.11**.

3.2.19 Compound 3.12 binding to DNA in the presence of 0.1 mM SA

The binding of **3.12** to DNA in the presence of 0.1 mM SA was studied using UV−visible spectroscopy. The changes in absorption of **3.12** upon addition of DNA in the presence of SA were measured in buffer (25 mM MOPS pH 7.0, 50 mM NaCl) at 25 °C (Figure 3.36).

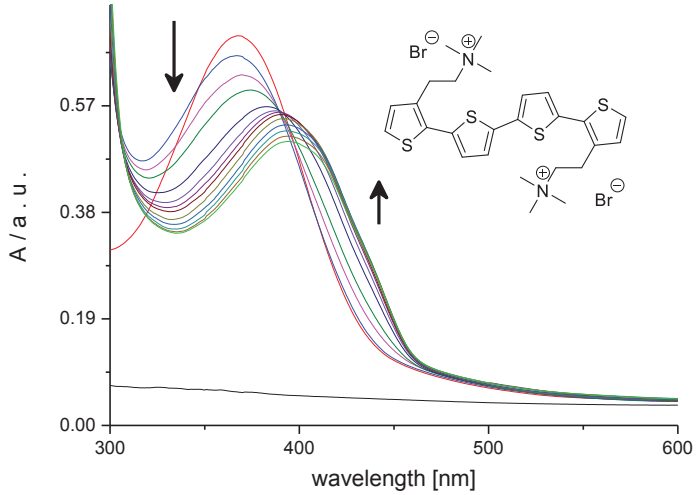

Figure 3.36: UV-visible spectra for 0.023 mM **3.12** upon addition of 0 - 1.03 mM DNA in the presence of 0.1 mM SA, at 25 °C in buffer (25 mM MOPS, pH 7.0, 50 mM NaCl).

Figure 3.36 shows a red shift in absorbance of **3.12** upon addition of DNA in the presence of 0.1 mM SA. The change in UV-visible absorption most likely occur as a result of geometrical distortion of **3.12** when it interacts with DNA in the presence of SA, but a local medium effect may also contribute.

To quantify the affinity of **3.12** for DNA in the presence of 0.1 mM SA, the absorbances at 367 and 420 nm were plotted as a function of the concentration of DNA (Figure 3.37, see appendix, Tables A55.48).

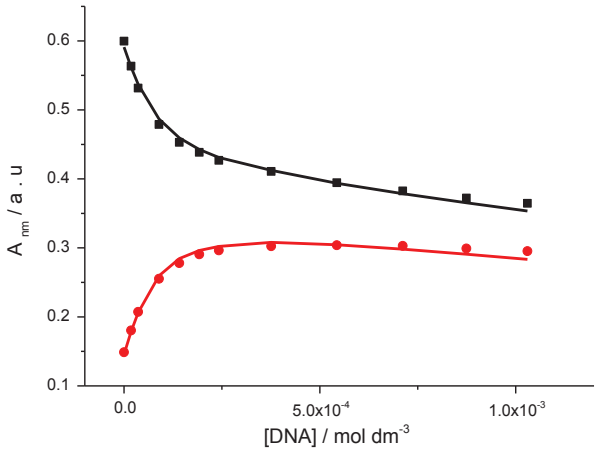

Figure 3.37: Absorbance at 367 nm (■) and at 430 nm (●) for 0.0236 mM **3.12** as a function of DNA concentration, in the presence of 0.1 mM SA, at 25 °C in buffer (25 mM MOPS, pH 7.0, 50 mM NaCl). The solid lines represent a global fit of a multiple independent binding sites model to the data.

Figure 3.37 shows the maximum decrease in absorbance at 367 nm and the highest increase in absorbance at 430 nm. The absorbance at 367 nm corresponds to the free ligand, and the absorbance 430 nm represents the DNA-ligand complex. The binding affinity and binding sites size were determined by fitting a multiple independent binding sites model, which also takes ligand dilution into account, to the data. The two lines give an equilibrium constant $K_{binding}$ of $(7.5 \pm 1.0) \times 10^4$ M^{-1} for a binding site size restricted at 3 base pairs. A $K_{binding}$ of $(1.8 \pm 0.38) \times 10^5$ M^{-1} for a binding site size restricted at 3 base pairs was observed for **3.12** binding to DNA in the absence of SA. From the diffrences in binding constant in the presence of SA, it appears that SA does significantly compete with DNA for **3.12**.

Part D: Effect of transferrin on DNA- binding properties.

3.2.20 Compounds 3.1 and 3.2 interacting with DNA in the presence of 0.1 mM TF

We also wanted to quantify binding of **3.1** and **3.2** to DNA in the presence 0.1 mM TF. The changes in absorption of **3.1** and **3.2** upon addition of DNA in the presence of TF were measured in buffer (25 mM MOPS, pH 7.0, 50 mM NaCl) at 25 °C (Figure 3.38).

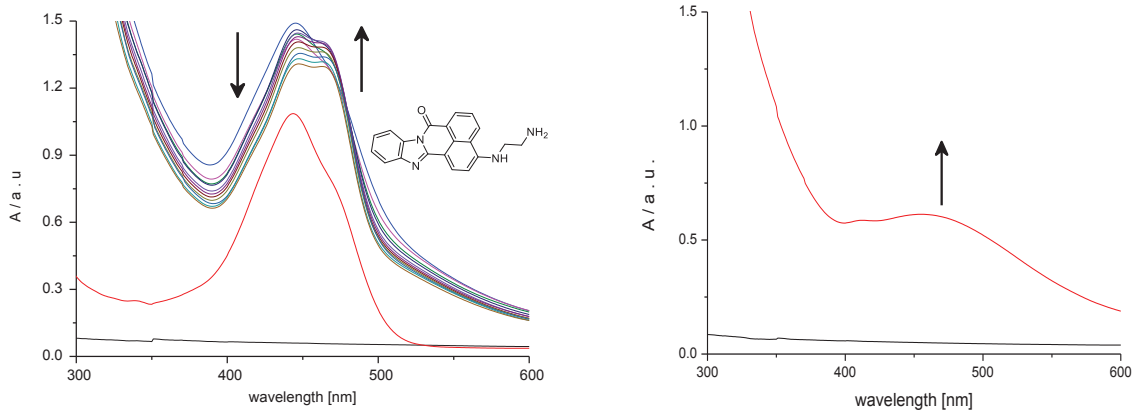

Figure 3.38: UV-visible spectra for 0.063 mM **3.1** upon addition of 0 – 2.3 mM DNA in the presence of 0.053 mM TF, at 25 °C in buffer (25 mM MOPS, pH 7, 50 mM NaCl) *(left)*. UV-visible spectra for 0.53 mM of TF in the absence of ligand **3.1** *(right)*.

The absorbance in the range of 400 − 600 nm increases upon addition of TF because of the high absorption and scattering of light by TF in the solution as confirmed by the spectrum for TF alone Figure 3.39 (right). Figure 3.39 then shows a hypochromic shift in absorbance at 444 nm followed by a hyperchromic shift at 444 nm upon addition of DNA in the presence of 0.053 mM TF. This change in UV-visible absorption at 444 nm may occur because of geometrical

distortion of **3.1** when it interacts with DNA in the presence of TF, but it may also be a local medium effect.

To quantify the affinity of **3.1** for DNA in the presence of TF, the absorbances at 444 nm were plotted as a function of the concentration of DNA after subtraction of the spectrum of TF alone (Figure 3.39, see appendix, Tables A55.49).

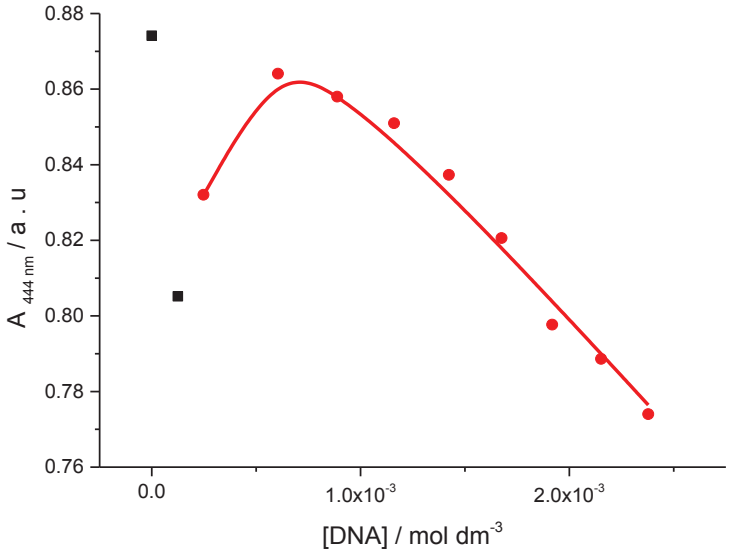

Figure 3.39: Absorbance at 444 nm for 0.063 mM **3.1** as a function of DNA concentration of 0 – 0.12 mM (■) and 0.24 – 2.3 mM (●), in the presence of 0.053 mM TF at 25 °C in buffer (25 mM MOPS pH 7, 50 mM NaCl). The solid line represents a fit of a multiple independent binding sites model to the data in the 0.24 – 2.3 mM range.

Figure 3.39 shows two events. The first event shows a fast decrease in the absorbance upon addition of DNA up to a concentration of 0.24 mM DNA (first two data points in Figure 3.38). We attribute this decline in absorbance to strong binding of **3.1** to the sugar-phosphate backbone of DNA at low concentration of DNA with a high concentration of ligand, leading to precipitation as a result of charge neutralisation of the **3.1**- DNA complex in the presence of TF, as also observed previously in the absence of TF. The second event shows a clear increase in the absorbance of **3.1** upon addition of 0.24– 2.3 mM of DNA in the presence of 0.053 mM of TF. The ligand strongly interacts with DNA, and the titration data in Figure 3.40 (with the first event not included) were analysed in terms of a multiple independent binding sites models, which also takes ligand dilution into account. The equilibrium constant K_{binding} was found to be $(5.0 \pm 7.5) \times 10^5\ M^{-1}$ for a binding site size of (11.7 ± 2.9) base pairs. The data were re analysed

with the stoichiometry restricted to 3.0 base pairs, giving an apparent equilibrium constant $K_{binding}$ of (7.6 ± 5.6) $\times 10^4\ M^{-1}$. A $K_{binding}$ of (1.5 ± 0.1) $\times\ 10^4\ M^{-1}$ for the binding site size restricted to 3.0 base pairs was observed for **3.1** binding to DNA in the absence of TF. From the similarity in the apparent binding constants in the absence of TF and the presence of TF[172], it appears that TF does not significantly compete with DNA for **3.1**. Unfortunately, our data show that TF does not help to avoid precipitation. On the other hand, the absence of this competition is beneficial if compound **3.1** were to be used in a biosensor because it means that TF will not cause false negatives. Similar data was observed for **3.2** (See appendix A16, Tables A55.50).

Summary

The results of UV-visible titrations for cationic compounds **3.1, 3.2, 3.3 3.4, 3.5, 3.6, 3.7, 3.8, 3.9, 3.10, 3.11** and **3.12** with DNA in the presence of SA are summarised in Table 3.3.

Table 3.3 Binding affinities and binding site sizes for binding of 3.1 - 3.12 to DNA and the effect of SA on DNA-binding in buffer (25 mM MOPS, pH 7.0, 50 mM NaCl) at 25 °C.

Ligands	*Binding affinities for SA* K / M^{-1}	*Binding affinities for DNA* K / M^{-1}	*Binding affinities for DNA +SA* K / M^{-1}	*Effect of SA on affinity for DNA*
3.1	$(1.5 \pm 1.2) \times 10^5$ n = 0.18 ± 0.06	$(1.5 \pm 0.1) \times 10^4$ n = 3* a	$(2.6 \pm 0.8) \times 10^4$ n = 3* a	No change
3.2	$(2.0 \pm 0.3) \times 10^4$ n = 0.1*	$(6.4 \pm 1.6) \times 10^4$ n =3* a	$(1.5 \pm 0.1) \times 10^4$ n = 3* a	Decrease
3.3	$(1.16 \pm 0.6) \times 10^4$ n = 0.5*	$(1.7 \pm 0.4) \times 10^4$ n = 3*	$(6.7 \pm 2.3) \times 10^4$ n = 3*	Increase
3.4	No binding	$(5.4 \pm 0.3) \times 10^4$ n = 3*	$(4.2 \pm 0.2) \times 10^4$ n = 3*	Decrease
3.5	No binding	$(8.9 \pm 2.3) \times 10^4$ n = 3*	$(6.5 \pm 0.4) \times 10^4$ n = 3*	No change
3.6	No binding	$(11.6 \pm 2.7) \times 10^4$ n = 1*	$(4.6 \pm 1.4) \times 10^3$ n = 1*	Decrease
3.7	$(2.2 \pm 0.5) \times 10^4$ n= 0.5 *	$(7.7 \pm 1.5) \times 10^5$ n =3*	$(7.9 \pm 6.2) \times 10^5$ n =3*	No change
3.8	No binding	$(4.4 \pm 0.5) \times 10^5$ n = 3*	$(2.5 \pm 1.6) \times 10^5$ n = 3*	No change
3.10	No binding	$(6.9 \pm 0.7) \times 10^3$ n = 3*	$(6.0 \pm 0.5) \times 10^3$ n = 3*	No change
3.11	No binding	$(1.6 \pm 0.6) \times 10^4$ n = 3*	$(1.6 \pm 0.2) \times 10^4$ n=3*	No change
3.12	No binding	$(1.8 \pm 0.38) \times 10^5$ n = 3*	$(7.5 \pm 1.0) \times 10^4$ n = 3*	Decrease

a. apparent binding constant for the event following initial precipitation.

b. *restricted**.**

To see if the affinities is increase or decrease, we need to compare affinities, taking their error margin into account. We did this as follows.

The confidence interval was taken as $\bar{x} \pm margin\ error$ and we checked whether the confidence intervals for the affinity in the absence and presence of the additive overlapped. For example, for the first entry in Table 3.3, the affinity in the absence of SA is $(1.5 \pm 0.1) \times 10^4$ which corresponds to a confidence interval of 1.6×10^4 M^{-1} to 1.7×10^4 M^{-1}. In the presence of SA, the confidence interval for the affinity is 1.8×10^4 M^{-1} to 3.4×10^4 M^{-1}. These two confidence intervals overlap, and the parameters are therefore considered the same within error.

Table 3.3 shows that all cationic oligoheteroaromatic compounds continue to interact with DNA in the presence of SA. We also compared the affinity between ligands and DNA in the presence and absence of serum albumin. We found ligands **3.1, 3.5, 3.7, 3.8, 3.10** and **3.11** do not show change in affinity for DNA. It appears that serum albumin does not significantly compete with DNA for these ligands. The absence of this competition is beneficial if these molecules were to be used in a biosensor because it means that SA would not cause false negatives. Decreases in affinity were observed for four ligands: **3.2, 3.4, 3.6** and **3.12**. This could mean that these sensitisers bind to SA and lead to a decrease in apparent K_{binding} and this could potentially give rise to false negative results. Another parameter to consider is the binding constant (a) for binding following initial precipitation of **3.1, 3.2** with DNA, which occurs through two events. The first event happens at low concentration of DNA and high concentration of ligand, leading to the precipitation of charge-neutralised ligands to form DNA complexes. The second event occurs at high concentration of DNA, where the ligand binds to main binding sites of DNA. Table 3.3 shows that binding of **3.1** to DNA is essentially unaffected by the presence of 0.1 mM SA. Binding of **3.2** to DNA is weaker in the presence of 0.1 mM SA. This observation is rather surprising because, according to Table 3.1, **3.1** has a higher affinity of SA than **3.2**. We therefore expected competition to be stronger in the case of **3.1**.

An increase in the affinity of **3.3** for DNA was observed in presence of SA, an effect attributed to sensitisers binding to SA instead of to the DNA backbone and increasing K_{binding} and this could cause false positives **3.3**.

Summary

The effect of the presence of TF on the affinities of **3.1** and **3.2** for DNA are summarised in Table 3.4.

Table 3.4 Binding affinities and binding site sizes for binding of 3.1 and 3.2 to DNA and the effect of TF on DNA-binding in buffer (25 mM MOPS, pH 7.0, 50 mM NaCl) at 25 °C.

Ligands	*Binding affinities for DNA* K / M^{-1}	*Binding affinities for DNA +TF* K / M^{-1}	*Binding site size* *n*
3.1	$(1.5 \pm 0.1) \times 10^4$ a	$(7.6 \pm 5.6) \times 10^4$ a	3*
3.2	$(6.4 \pm 1.6) \times 10^4$ a	$(1.1 \pm 0.4) \times 10^5$ a	3*

a) apparent binding constant for the event following initial precipitation.
b) *restricted.

Table 3.4 describes the binding that occurred between **3.1** and **3.2** and DNA in the presence of biomolecules TF. Compounds **3.1** and **3.2** shows an increase in the affinity.

3.3 Conclusion

This chapter presents the results of binding studies between ligands and (bio)macromolecules serum albumin, transferrin and the effect of serum albumin and transferrin on DNA-binding properties. Binding is accompanied by a change in optoelectronic properties of the compounds. The affinities for ligands were between 10^3 and 10^5 M^{-1} with different binding site and binding site sizes within a range of 0.1 to 6.0.

Compounds **3.1** and **3.2** bind to serum albumin and transferrin. These ligands interact with a hypochromic shift, and the binding site are (0.1- 0.5). The number of binding sites in SA and TF is measured by (1/n). The binding suggests that the ligands bind to the protein within hydrophobic pockets and also involving electrostatic interactions. The aromatic rings of the conjugated compounds probably interact with a hydrophobic area of albumin and transferrin. All titration curves had to be corrected to remove the scattering effect of SA and TF from absorbances.

As for the UV-visible results of **3.1** and **3.2** binding to DNA, the trends show two binding events with a low ratio of DNA/ligands interacting, leading to precipitation of ligand-DNA complex. During the second event with high ratio DNA/ligands, molecules bind to the main site in the minor groove or as an intercalator of DNA.

Our studies also demonstrated that the majority of cationic oligoheteroaromatics explored reveal good binding with DNA in the presence of serum albumin from the comparison of affinity which suggests that there is no effect of serum albumin on DNA biosensors. Four ligands **3.2, 3.4, 3.10, 3.11** and **3.12** exhibit decreased affinity, which could lead to false negatives. We also observed an increase in the binding constant of ligand **3.3**, which means false positives can exist.

3.4 Materials

Serum albumin SA and TF were purchased from Sigma-Aldrich as solids. The buffer components were purchased from Melford Laboratories Ltd and Sigma-Aldrich.

3.5 Solutions preparation

3.5.1 SA and TF preparation

The experiments were carried out in buffer (25 mM MOPS, 50 mM NaCl, pH 7.0, at 25 °C). Serum albumin solution was prepared by dissolving in MOPS buffer and sonicating for about

15 minutes. The SA solution was dialysed against 2000 mL of the buffer using a 3.5 kDa MWCO dialysis membrane for 24 hours. SA concentration was determined spectrophotometrically using $\varepsilon_{278\,nm}$ [178] = 43824 M^{-1} cm^{-1}. Transferrin was dissolved in MOPS buffer to prepare a 1.0 mM solution. Most experiments needed correction of the absorption to remove scattering of light by proteins as shown below.

3.5.2 DNA preparation

To prepare deoxyribonucleic acid (DNA), a stock solution of DNA was prepared by weight (around 0.12 g) by dissolving DNA in MOPS buffer. After that the solution of DNA was sonicated around 15 minutes. The solution of DNA was dialysed against 2.0 litre of MOPS buffer using a 3.5 kDa MWCO dialysis membrane for one day. The concentration of DNA was determined using UV-visible spectroscopy with the following extinction coefficient $\varepsilon_{260\,nm}$= 12800 M^{-1} cm^{-1} at 260 nm [177] by using Eqn 3.1.

$$A = \varepsilon \times C \times l \qquad \text{……. } \mathbf{3.1}$$

where, A= absorbance, l= path length, C= concentration, ε= extinction coefficient

$$\varepsilon = \frac{A}{C \times L} \qquad \text{…….. } \mathbf{3.2}$$

$$\varepsilon = M^{-1}\,cm^{-1} \qquad \text{…….. } \mathbf{3.3}$$

3.6 Calculations the binding site of macromolecules

The stoichiometry of the interaction between ligands and proteins is typically expressed in terms of numbers of binding sites. We calculated the binding site of protein and DNA.

1. Protein concentration is protein (folding) , not as an amino acid.
2. Binding site of protein = [Protein] / number of binding site per protein molecule.

$$Binding\ site = \frac{1}{n} \qquad \text{…..... } \mathbf{3.4}$$

3. Whereas binding site size for DNA concentration in [M] base pairs (b.p).

$$\boldsymbol{Binding\ site\ size} = \frac{[\boldsymbol{DNA}]}{\boldsymbol{base\ pairs}} \qquad \text{…….. 3.5}$$

$$[\boldsymbol{base\ pairs}] = \frac{[\boldsymbol{DNA}]}{\boldsymbol{n}} \qquad \text{…….. 3.6}$$

3.7 Corrected absorption

UV-visible titrations were carried out by adding aliquots of the concentrated stock solution of the protein to the buffer without adding a ligand.

The absorptivity of the (Bio)macromolecules in MOPS buffer at the absorbance of the ligand was recorded as a function of the concentration of (Bio)macromolecules. This provided ε at the wavelength of interest.

Predicted absorbances were calculated by multiplying molar absorptivity (ε) of biomolecules at the absorbance region for ligand by the concentration of the (Bio)macromolecules.

The corrected absorbances were calculated by subtracting the predict absorbances from the absorbances of macromolecules with the ligand.

Chapter Four

The effect of negatively charged biopolymers on DNA-binding properties of π-conjugated ligands

Abstract

Chapter four presents the results of our studies of the interactions of the negatively charged biopolymers hyaluronic acid (HA) and alginic acid (AA) with our π-conjugated compounds and the effect of the presence of HA and AA on the DNA − binding parameters of sensitisers for biosensors. We found that compounds **4.1** and **4.7** bind to HA in a moderately strong fashion and that **4.1** and **4.2** interact with AA.

We further studied the effect of these biopolymers on the DNA affinity of our potential sensitisers and compared the binding of ligands to DNA in the absence and in the presence of HA and AA. We found that ligands **4.4, 4.5, 4.10, 4.11** and **4.12** do not show any change in affinity for DNA in the presence of HA or AA. Our work also demonstrates a decrease in affinity of molecules **4.2, 4.7** and **4.8** for DNA in the presence AA, suggesting that these potential sensitisers could bind to the biopolymer and this binding leads to decreased apparent $K_{binding}$. Such a decrease could be a source for a false negative result. An increase in the apparent affinity of **4.1** for DNA in the presence of HA was also observed. This effect is attributed to sensitisers binding to biopolymers, suppressing weak binding in secondary binding sites on DNA thus increasing the apparent $K_{binding}$. This effect could cause false positives but could also be used to make these sensors more sensitive.

4.1 Introduction

4.1.1 The effect of biopolymers on biosensors

The presence of negatively charged biopolymers can affect the performance of biosensors involving a DNA probe and surface passivation using 6-mercapto -1-hexanol.

The interactions between sensitisers and biopolymers and how these interactions might affect biosensor functioning can be studied using several techniques such as UV-visible spectroscopy, isothermal titration calorimetry (ITC) and circular dichroism spectroscopy. These methods allow the study of the different parameters describing interactions of sensitisers with DNA and how they change upon potential binding of these sensitisers to added macromolecules.

4.1.2 Negatively charged biopolymers

In this chapter, we selected negatively charged biopolymers as shown in Scheme 4.1. HA $(C_{14}H_{21}NO_{11})_n$ is a biopolymer of disaccharides, which contains D-glucuronic acid and N-acetyl-D-glucosamine connected together by β-(1-4) and β-(1-3) glycoside bonds. HA has an average weight around 3–4 million Da.[179-180]

Alginic acid $(C_6H_8O_6)_n$ is a natural anionic polysaccharide composed of two types of uronic acid: mannuronic acid (M) and guluronic acid. (G). The polymer presents functional groups like carboxyl groups within the M and G units. These groups can be ion-exchanged and can bind to different types of cationic molecules. Alginic acid has many commercial applications including as an additive in the dehydrated product, waterproofing and pharmaceuticals.

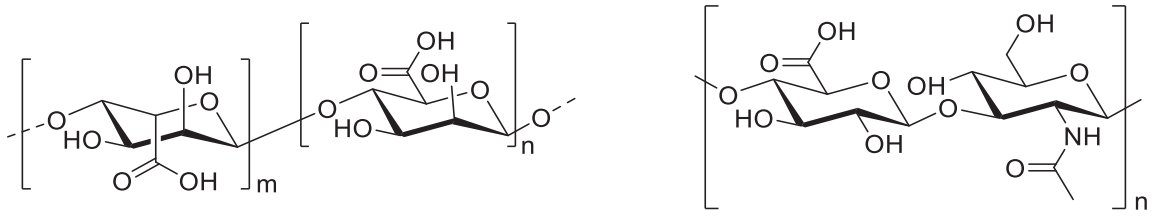

Scheme 4.1: Chemical structures of AA and HA

4.1.3 Aims

Our aims in Chapter four are to measure the binding parameters and binding site sizes for the molecules in Scheme 4.2 interacting with negative biopolymers HA and AA. We also study the effect of the presence of HA and AA on the DNA-binding parameters of these π-conjugated molecules.

4.2 Results and Discussion

The results of our binding studies for compounds **4.1-4.12** with biopolymers HA and AA, and the effect of these negatively charged biopolymers on interactions of small molecules with DNA will be provided and discussed for each compound.

Part A: Hyaluronic acid binding studies

4.2.1 Compound 4.1 binding to HA

We wanted to know whether **4.1** binds to HA, the changes in absorption of **4.1** upon addition of HA were measured in buffer (25 mM MOPS, 50 mM NaCl) at 25 °C (Figure 4.1).

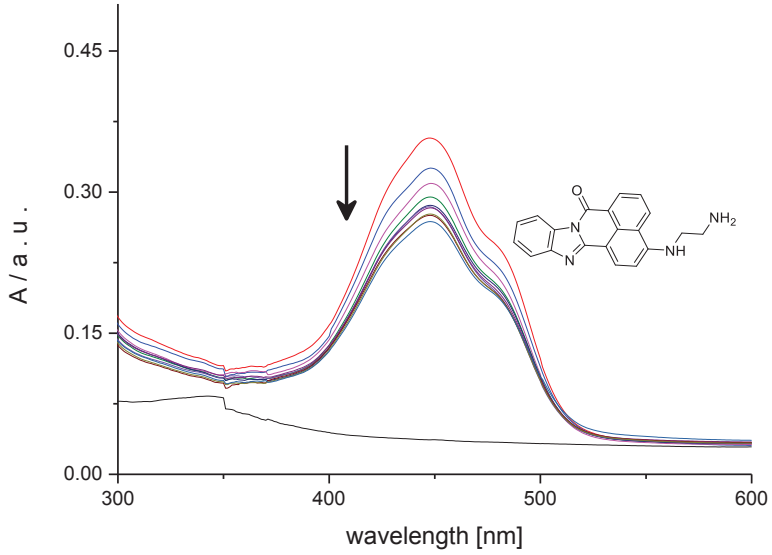

Figure 4.1: UV-visible spectra for 0.019 mM **4.1** upon addition of 0 - 0.35 mM HA, at 25 °C in buffer (25 mM MOPS, pH 7.0, 50 mM NaCl).

Figure 4.1 shows that compound **4.1** presents a hypochromic shift in absorbance upon addition of HA with a maximum change in absorbance at 448 nm. This decrease in UV-visible absorption may have occurred as a result of geometrical distortion of **4.1** when it interacts with HA, but it may also be as a consequence of a local medium effect exerted by the HA binding site.

To quantify the affinity of **4.1** for HA, the absorbance at 448 nm were plotted as a function of the concentration of HA (Figure 4.2, see Appendix, Tables A55.51).

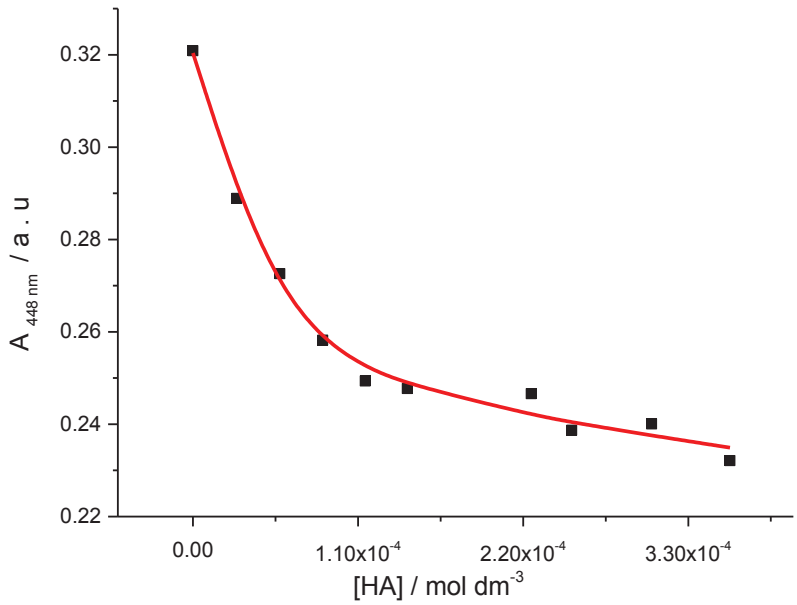

Figure 4.2: Absorbance at 448 nm for 0.019 mM **4.1** upon addition of 0 – 0.35 mM HA, at 25 °C in buffer (25 mM MOPS, pH 7.0, 50 mM NaCl). The solid line represents the best fit to the data fit in terms of a multiple independent binding sites model.

Figure 4.2 shows a decrease in the absorbance at 448 nm for **4.1** upon addition of HA. The binding affinity $K_{binding}$ and binding sites size n were determined by fitting a multiple independent binding sites model, which also takes ligand dilution into account, to the data. The fit reproduces the data well and gives a binding constant $K_{binding}$ of (3.0 ±0.96) × 10^5 M^{-1} for a binding site size restricted to 3 monomeric unit per molecule of **4.1**. The obtained values for the binding site size and binding constant seem reasonable. The fit suggests that **4.1** interacts with HA and we hypothesise that binding is due to electrostatic interaction.

4.2.2 Compound 4.7 binding to HA

We wanted to know the binding of **4.7** and HA was studied using UV-visible spectroscopy. The changes in absorption of **4.7** upon addition of HA were measured in buffer (25 mM MOPS, pH 7.0, 50 mM NaCl), at 25 °C (Figure 4.3).

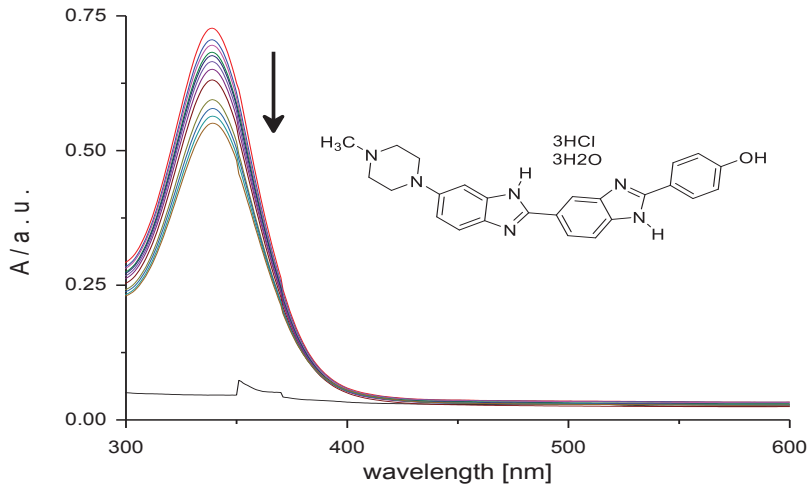

Figure 4.3: UV-visible spectra for 0.021 mM **4.7** upon addition of 0 – 1.8 mM HA, at 25 °C in buffer (25 mM MOPS, pH 7.0, 50 mM NaCl).

Figure 4.3 illustrates that **4.7** exhibits a hypochromic shift in its absorbance upon addition of HA, with a maximum change in absorbance at 339 nm. This decrease in UV-visible absorption may occur as a result of geometrical distortion of **4.7** when it interacts with HA, but it is more likely a result of a local medium effect considering λ_{max}does not change significantly.

To quantify the affinity of **4.7** for HA, we plotted the absorbance at 339 nm as a function of the concentration of HA (Figure 4.4, see Appendix, Tables A55.55).

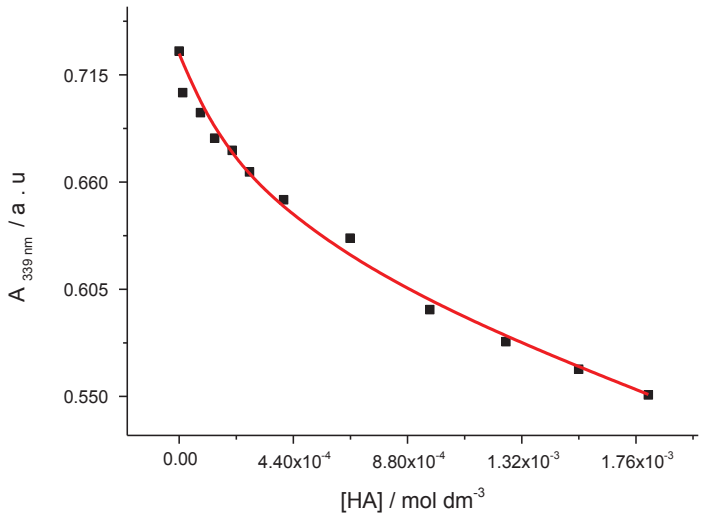

Figure 4.4: Absorbance at 339 nm for 0.021 mM **4.7** as a function of HA, at 25 °C in buffer (25 mM MOPS, pH 7.0, 50 mM NaCl). The solid line represents the best fit to the data in terms of a multiple independent binding sites model.

Figure 4.4 shows the decrease in absorbance at 339 nm for **4.7** upon addition HA. The binding affinity $K_{binding}$ and binding site size *n* were determined by fitting a multiple independent binding sites model, which also takes ligand dilution into account, to the data. The fit reproduces the data well and corresponds to an equilibrium constant $K_{binding}$ of $(2\times10^{-3}\pm1.2) \times10^{5}$ M^{-1} for a binding site size of $(1\times10^{-1} \pm 60.1)$ monomeric units per molecule of **4.7**. The obtained stoichiometry was unreasonably and had a large error margin. Therefore, the data were reanalysed with the stoichiometry restricted to 1, because this stoichiometry corresponds to each a positive charge on **4.7** engaging in electrostatic binding with a negative charge on HA. This an alysis gives anapparent bindingconstantof $(2.0 \pm 0.5) \times 10^{3}$ M^{-1}.Similarly, the interactions of **4.2, 4.4, 4.5, 4.8, 4.10**, **4.11** and **4.12** with HA were studied (see appendix A17-A23). These interactions were found to be negligible.

Summary

The results of UV-visible titrations for **4.1** and **4.7** with HA show that these molecules interact with HA. Compounds **4.2, 4.4, 4.5, 4.8, 4.10 - 4.12** do not show binding. The binding constant and stoichiometry for these ligands and HA are summarised in Table 4.1.

Table 4.1 Binding affinities and binding site sizes for the binding of 4.1, 4.2, 4.4, 4.5, 4.6, 4.7, 4.8, 4.9, 4.10, 4.11 and 4.12 to HA in buffer (25 mM MOPS, pH 7.0, 50 mM NaCl) at 25 °C.

Ligands	*Binding constant for HA* K / M^{-1}	*Binding site* n
4.1	$(3.09 \pm 0.96) \times 10^5$	3*
4.2	No binding	
4.4	No binding	
4.5	No binding	
4.7	$(2.0 \pm 0.5) \times 10^3$	1*
4.8	No binding	
4.10	No binding	
4.11	No binding	
4.12	No binding	
* restricted.		

Table 4.1 shows that only ligands **4.1** and **4.7** bind to hyaluronic acid. We attribute this binding to the interaction between the negatively charged COO^- on the biopolymer and the positively charged NH_3^+ on the molecules. The highest affinity is for **4.1** with a binding constant of 10^5 M^{-1}. The low affinity of **4.7** for HA may be attributed to the structure of ligand which does not fit with HA.

Part B: Effect of HA on DNA-binding

4.2.3 Compounds 4.1 and 4.2 binding to DNA in the presence of 0.3 mM HA

We wanted to evaluate the binding of **4.1** and **4.2** with DNA in the presence of 0.3 mM HA. The changes in absorption of **4.1** and **4.2** upon addition of DNA in the presence of 0.3 mM HA were measured in buffer (25 mM MOPS, pH 7.0, 50 mM NaCl) at 25° C. Data for **4.1** is shown in Figure 4.5. For the analogous data for **4.2,** see Appendix. A24 (Figure A24.1 and Figure A24.2, for data in tabular format, see appendix, Tables A55.60).

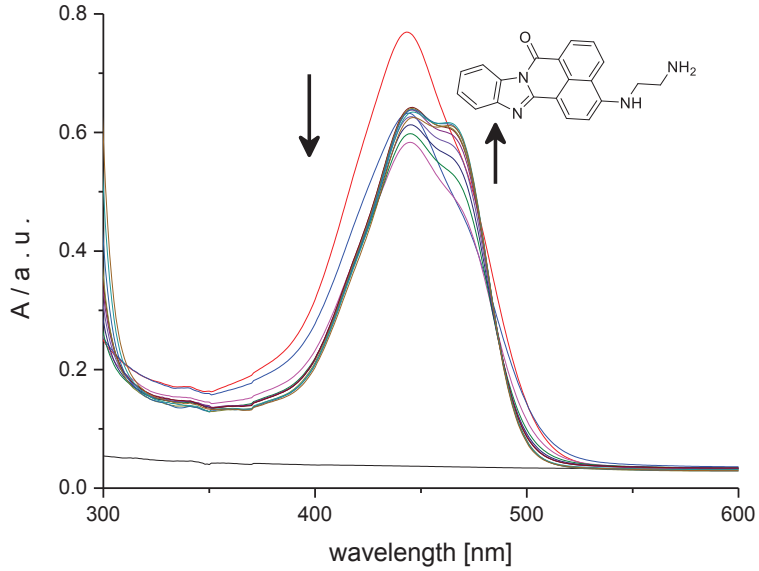

Figure 4.5: UV-visible spectra for 0.045 mM **4.1 (**red line**)** in buffer (25 mM MOPS, pH 7.0, 50 mM NaCl) in the absence of HA and subsequent spectra for **4.1** in the presence of 0.3 mM HA upon addition of 0 – 1.2 mM DNA, at 25 °C.

Figure 4.5 shows two events upon addition of DNA in the presence of 0.3 mM HA. The first event involves a hypochromic shift in absorbance at 443 nm upon addition HA. The second shows a hyperchromic shift at 443 nm of **4.1**. The change in UV-visible absorption may occur as a result of geometrical distortion of **4.1** when it interacts with DNA in presence HA, but it may also be a local medium effect. The observation of a rapid decrease in absorbance followed by increase suggests precipitation and subsequent dissolution of a DNA-ligand complex in the presence of 0.3mM HA. This, in turn, suggests that the two-species involved in the second equilibrium are **4.1** in primary and secondary sites.

To quantify the affinity of **4.1** for DNA in the presence of 0.3 mM HA, the absorbance at 443 nm were plotted as a function of the concentration of DNA (Figure 4.6, see Appendix, Tables A55.60).

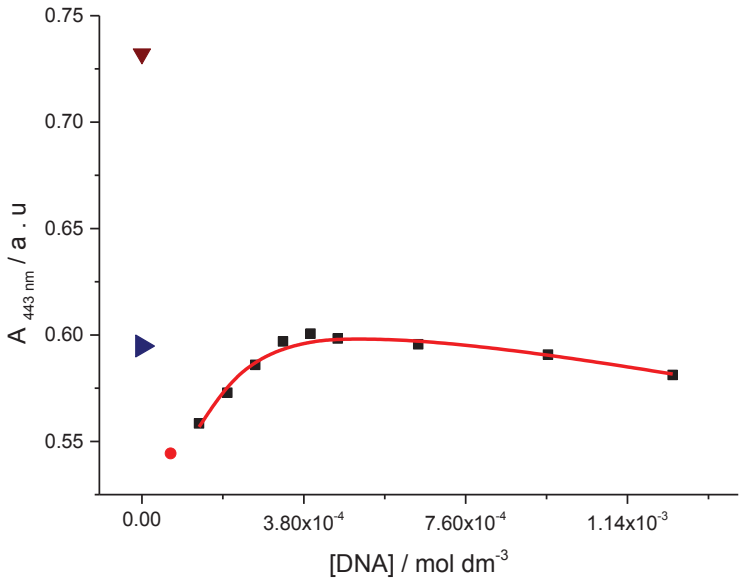

Figure 4.6: Absorbance at 443 nm for 0.045 mM **4.1** in the absence of HA (▼) and subsequent spectra for **4.1** in the presence of 0.3 mM HA (►) and as a function of DNA concentration of 0 - 0.067 mM (●) and 0.13 - 1.2 mM (■) both in the presence of 0.3 mM HA, at 25 °C in buffer (25 mM MOPS, pH 7, 50 mM NaCl). The solid red line represents a fit of a multiple independent sites model to the data in the 0.13 - 1.2 mM range (■).

Figure 4.6 shows two events. The first event corresponds to a fast decrease in absorbance upon addition 0.3 mM HA (►) with a subsequent continued decrease in absorbance upon addition of DNA up to a concentration of 0.067 mM (● in Figure 4.7). We attribute this decrease in absorbance to strong binding of **4.1** to HA and to the sugar-phosphate backbone of DNA at low concentration of DNA with a high concentration of ligand, i.e. a high ligand / DNA ratio. These conditions lead to precipitation as a result of charge neutralisation in the **4.1**-HA and **4.1**-DNA complexes. For the **4.1**-DNA complex, this is as also observed previously in the absence of HA.[172] The second event shows a clear increase in the absorbance of **4.1** upon addition of 0.13 - 1.2 mM DNA in the presence of 0.3 mM of HA. The ligand strongly interacts with DNA, and the titration data in Figure 4.7 (with the first event not included) were analysed in terms of a multiple independent binding sites models, which also takes ligand dilution into account. An apparent equilibrium constant $K_{binding}$ of (2.3 ± 1.5) $\times 10^5$ M^{-1} for a binding site size of (7.1 ± 1.5) base pairs was found. A $K_{binding}$ of (1.5 ± 0.1) × 10^4 M^{-1} for the binding site size restricted to 3.0 base pairs was observed for **4.1** to DNA in the absence of HA.[172] Therefore, the data were reanalysed with the stoichiometry restricted to 3.0 base pairs to allow comparison, giving an apparent equilibrium constant $K_{binding}$ of (5.3 ± 1.4) × 10^4 M^{-1}. From the difference in the apparent binding constant in the absence of HA[172] and in the presence of HA, it appears

that HA does compete with DNA for **4.1.** Unfortunately, HA does not help to avoid precipitation. On the other hand, the presence of this competition is beneficial if the compound **4.1** were to be used in a biosensor because it can be used to provide signals to detect DNA hybridization information and the presence of HA could avoid nonspecific interactions.

4.2.4 Compound 4.4 binding with DNA in the presence of 0.3 mM HA

We wanted to know whether the binding of **4.4** to DNA in the presence 0.3 mM HA. The changes in absorption of **4.4** upon addition of DNA were measured in buffer (25 mM MOPS pH 7.0, 50 mM NaCl) at 25 °C (Figure 4.7).

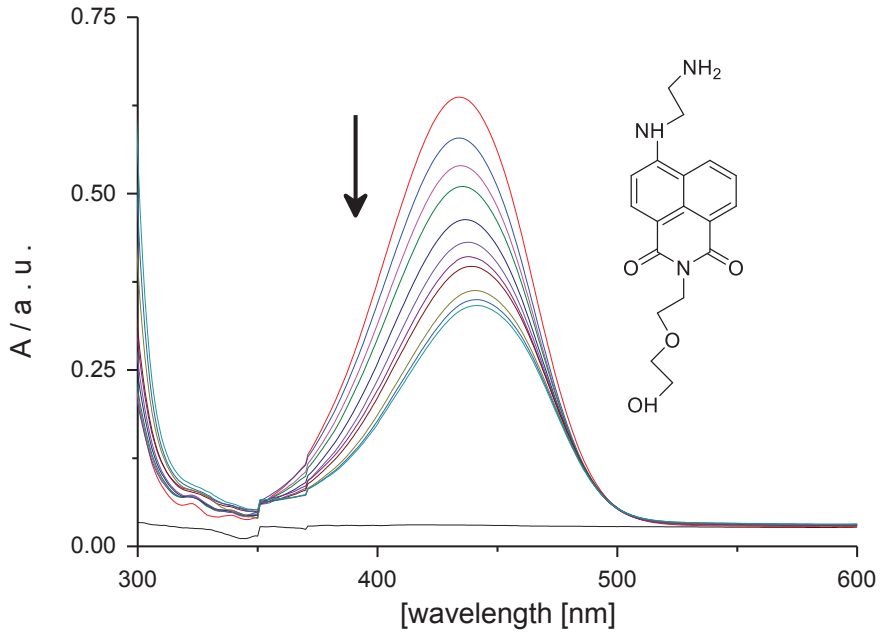

Figure 4.7: UV-visible spectra for 0.055 mM **4.4 (**red line**)** in buffer (25 mM MOPS, pH 7.0, 50 mM NaCl) in the absence of HA and subsequent spectra for **4.4** in the presence of 0.3 mM HA upon addition of 0 – 1.23 mM DNA, at 25 °C.

In the studies, **4.4** showed a hypochromic shift in absorbance with a maximum change in absorbance at 434 nm upon addition of DNA in the presence of 0.3 mM HA. This decrease in UV-visible absorption may have occurred as a result of geometrical distortion of **4.4** when it interacts with DNA in the presence of HA, but it may also be as a result of a local medium effect.

To quantify the affinity of **4.4** for DNA, the absorbance at 434 nm were plotted as a function of the concentration of DNA (Figure 4.8, see Appendix, Tables A55.62).

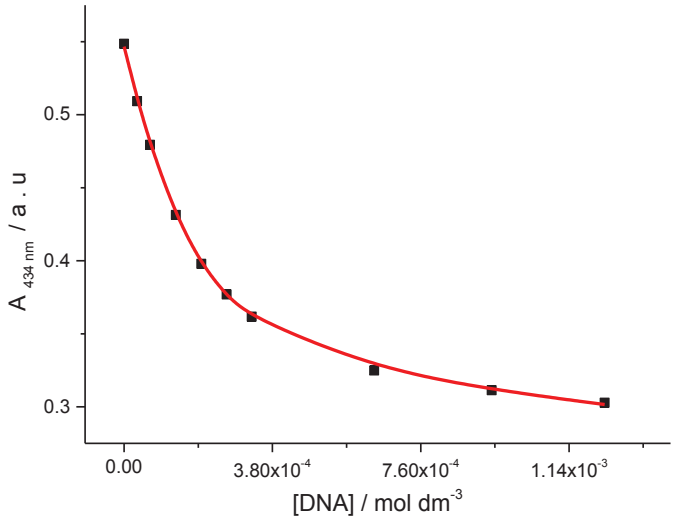

Figure 4.8: Absorbance at 434 nm for 0.055 mM **4.4** as a function of DNA concentration in the presence of 0.3 mM HA, at 25 °C in buffer (25 mM MOPS, pH 7, 50 mM NaCl). The solid line represents the best fit to the data in terms of a multiple independent binding sites model.

Figure 4.8 shows a decrease in the absorbance at 434 nm for **4.4** upon addition of DNA in the presence of HA. The binding affinity $K_{binding}$ and the binding sites size n were determined by fitting a multiple independent binding sites model, which also takes ligand dilution into account, to the data. The fit gives an equilibrium constant $K_{binding}$ of $(3.8 \pm 0.5) \times 10^4$ M^{-1} for a binding site size of (2.7 ± 0.2). A $K_{binding}$ of $(3.4 \pm 0.6) \times 10^4$ M^{-1} for a binding site size (2.3 ± 0.2) base pairs was observed for **4.4** interacting with DNA in the absence of HA. From the similarity in the binding constant, it appears that HA does not significantly compete with DNA for **4.4**.

4.2.5 Compound 4.5 binding with DNA in the presence of 0.2 mM HA

We wanted to know whether **4.5** binds to DNA in the presence 0.2 mM HA using UV-visible spectroscopy. The changes in absorption of **4.5** upon addition of DNA were measured in buffer (25 mM MOPS, pH 7.0, 50 mM NaCl) at 25 °C (Figure 4.9).

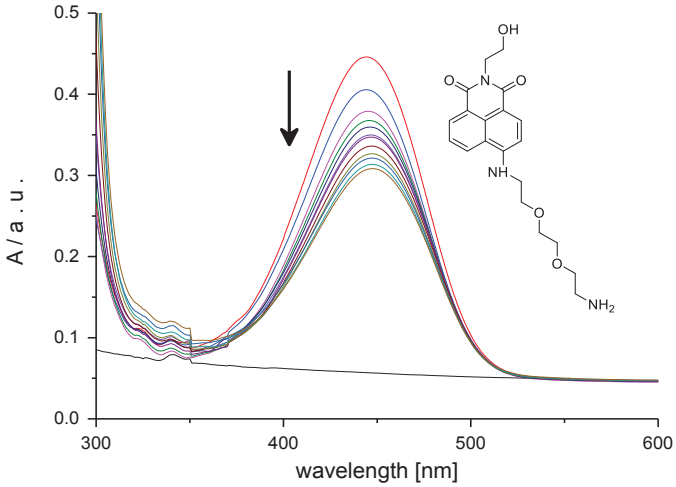

Figure 4.9: UV-visible spectra for 0.063 mM **4.5 (**red line**)** in buffer (25 mM MOPS, pH 7.0, 50 mM NaCl) in the absence of HA and subsequent spectra for **4.5** in the presence of 0.2 mM HA upon addition of 0 – 1.7 mM DNA, at 25 °C.

In the studies, **4.5** showed a decrease in absorbance upon addition of DNA with a maximum change in absorbance at 444 nm in the presence of 0.2 mM HA. This decrease in UV-visible absorption may have occurred as a result of geometrical distortion of **4.5** when it interacts with DNA without care to HA, but it may also be as a result of a local medium effect.

To quantify the affinity of **4.5** for DNA in the presence of 0.2 mM HA, the absorbance at 444 nm were plotted as a function of the concentration of DNA (Figure 4.10, see appendix, Tables A55.63).

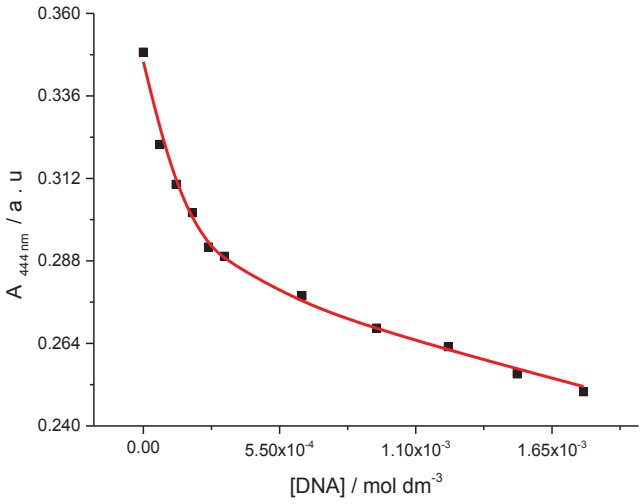

Figure 4.10: Absorbance at 444 nm for 0.063 mM **4.5** as a function of DNA in the presence of 0.2 mM HA, at 25 °C in buffer (25 mM MOPS, pH 7, 50 mM NaCl). The solid line represents the best fit to the data in terms of a multiple independent binding sites model, which also takes into account dilution (which causes the continued decrease in absorbance after binding of all ligand molecules).

Figure 4.10 shows the decrease in the absorbance at 444 nm for **4.5** upon addition of DNA in the presence of 0.2 mM HA. The binding affinity $K_{binding}$ and binding sites size *n* were determined by fitting a multiple independent binding sites model, which also takes ligand dilution into account, to the data, giving an equilibrium constant $K_{binding}$ of $(5.9 \pm 9.0) \times 10^3$ M^{-1} for a binding site size of (0.6 ± 0.7) base pairs. The obtained stoichiometry was unreasonable small, although in good agreement with data for **4.5** interacting with DNA in the absence of HA, which gives a binding constant of $(1.6 \pm 0.7) \times 10^4$ M^{-1} for a binding site size (1.2 ± 0.3). Therefore, the data were reanalysed with the stoichiometry restricted to 3.0 base pairs, giving an equilibrium constant $K_{binding}$ of $(6.3 \pm 1.3) \times 10^4$ M^{-1}. A $K_{binding}$ of $(8.9 \pm 2.3) \times 10^4$ M^{-1} for a binding site size restricted to 3.0 base pairs was observed for **4.5** DNA interacting within the absence of HA. From the similarity in the binding constants, it appears that HA does not significantly compete with DNA for **4.5.**

4.2.6 Compound 4.7 binding with DNA in the presence of 0.1 mM HA

We investigate the binding of **4.7** to DNA in the presence 0.1 mM HA. The changes in absorption of **4.7** upon addition of DNA were measured in buffer (25 mM MOPS, pH 7.0, 50 mM NaCl) at 25 °C (Figure 4.11).

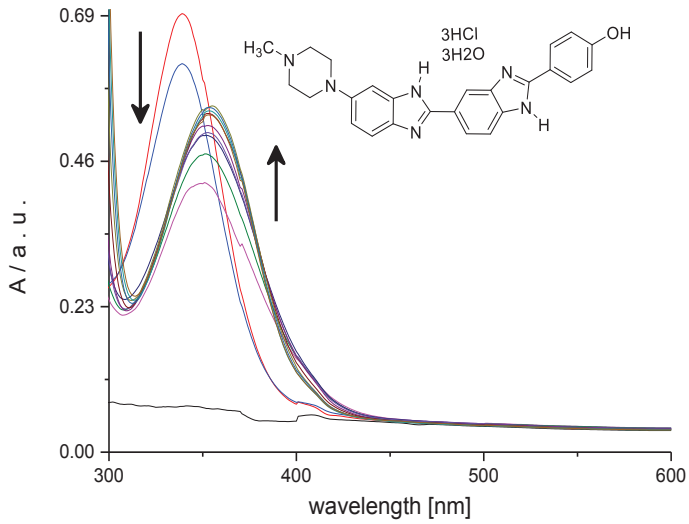

Figure 4.11: UV-visible spectra for 0.018 mM **4.7 (**red line**)** in buffer (25 mM MOPS, pH 7.0, 50 mM NaCl) in the absence of HA and subsequent spectra for **4.7** in the presence of 0.1 mM HA upon addition of 0 – 2.1 mM DNA, at 25 °C.

Figure 4.11 shows a hypochromic and hyperchromic shift in absorbance at 360 nm upon addition of DNA in the presence of 0.1 mM HA. The first rapid decrease is attributed to precipitation of **4.7** -DNA complexes at high **4.7** / DNA ratio. The subsequent increase in UV-visible absorption may occur as a result of geometrical distortion of **4.7** when it interacts with DNA in the presence of HA, but it may also be a local medium effect.

To quantify the apparent affinity of **4.7** for DNA in the presence of 0.1 mM HA, the absorbance at 360 nm were plotted as a function of the concentration of DNA (Figure 4.12, see Appendix, Tables A55.64).

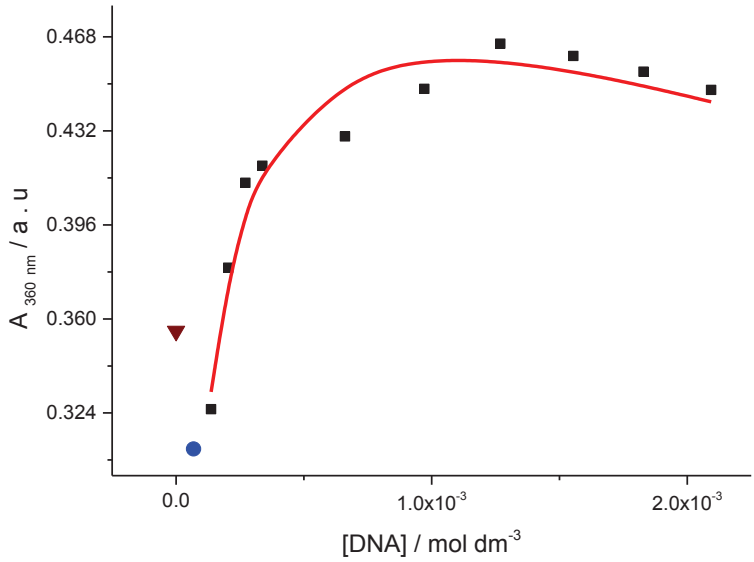

Figure 4.12: Absorbance at 360 nm for 0.018 mM **4.7** in the absence of HA (▼) and subsequent spectra for **4.7** in the presence of 0.1 mM HA (●) and upon addition of 0.013 – 2.1 mM DNA in the presence of HA (■), at 25 °C.in buffer (25 mM MOPS, pH 7, 50 mM NaCl). The solid line represents a fit of a multiple independent binding sites model to the data in the 0 013 – 2.1 mM range (■).

Figure 4.12 shows two events. The first event shows a decrease in absorbance upon addition 0.1 mM HA (●). We attribute this decline in absorbance to the binding of **4.7** - HA. These conditions lead to precipitation as a result of charge neutralisation of the **4.7** - HA complex. The first addition of DNA results in a further decrease in absorbance which we attribute to formation of an insoluble complex between **4.7** and DNA, as was also observed in the absence of HA. The second event shows a clear increase in the absorbance of **4.7** upon addition of 0.013 – 2.1 mM DNA in the presence of 0.1 mM of HA. The titration data in Figure 4.13 (with the first event not included) were analysed in terms of a multiple independent binding sites models, which also takes ligand dilution into account. The equilibrium constant

$K_{binding}$ of (8×10^{-3} ± 7.4) for a binding site size of (8×10^{-3} ± 7.1) base pairs were considered unreasonable. Therefore, the data were reanalysed with the stoichiometry restricted to 3.0 base pairs, giving an apparent equilibrium constant $K_{binding}$ of (2.8 ± 1.4) $\times10^4$ M^{-1}. A $K_{binding}$ of (7.7 ± 1.5) $\times10^5$ M^{-1} for the binding site size restricted to 3.0 base pairs was observed for **4.7** interacting with DNA in the absence of HA. From the differences in the apparent binding constant in the absence of HA and in the presence of HA, it appears that HA does significantly compete with DNA for **4.7**. The presence of this competition is beneficial if the compound **4.7** were to be used in a biosensor because it can be used to provide better signals to detect DNA hybridization because it could avoid nonspecific interactions.

4.2.7 Compound 4.8 binding with DNA in the presence of 0.3 mM HA

In order to explore the binding of **4.8** with DNA in the presence of 0.3 mM HA, the changes in absorption of **4.8** upon addition of DNA in the presence of 0.3 mM HA were measured in buffer (25 mM MOPS, pH 7.0, 50 mM NaCl and 10 vol-% DMSO) at 25 °C (Figure 4.13).

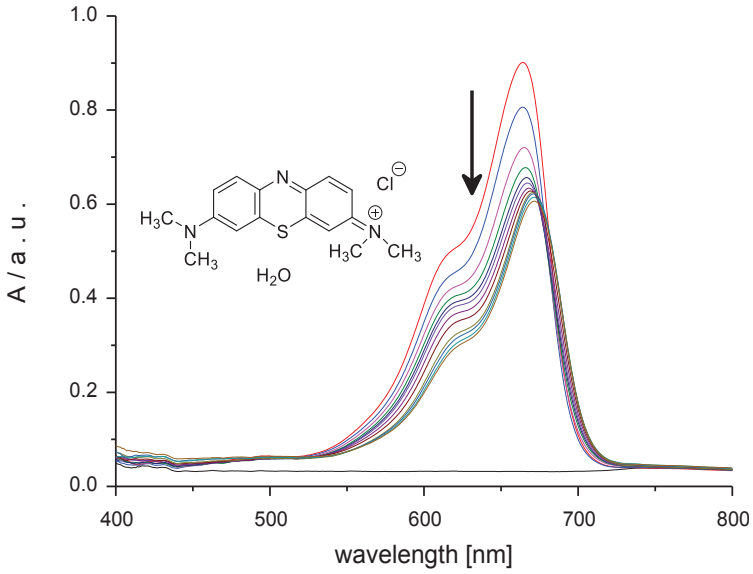

Figure 4.13: UV-visible spectra for 0.012 mM **4.8 (**red line**)** in buffer (25 mM MOPS, pH 7.0, 50 mM NaCl, 10 vol-% DMSO) in the absence of HA and subsequent spectra for **4.8** in the presence of 0.3 mM HA upon addition of 0 – 1.5 mM DNA, at 25 °C.

Figure 4.13 shows a hypochromic shift at 665 nm upon addition of DNA in the presence of 0.3 mM HA. The decrease in UV-visible absorption may occur because of geometrical distortion of **4.8** when it interacts with DNA, or it is a result of the different local medium provided by the binding sites.

To quantify the affinity of **4.8** for DNA in the presence of 0.3 mM HA, the absorbances at 665 nm were plotted as a function of the concentration of DNA (Figure 4.14, see Appendix, Tables A55.65).

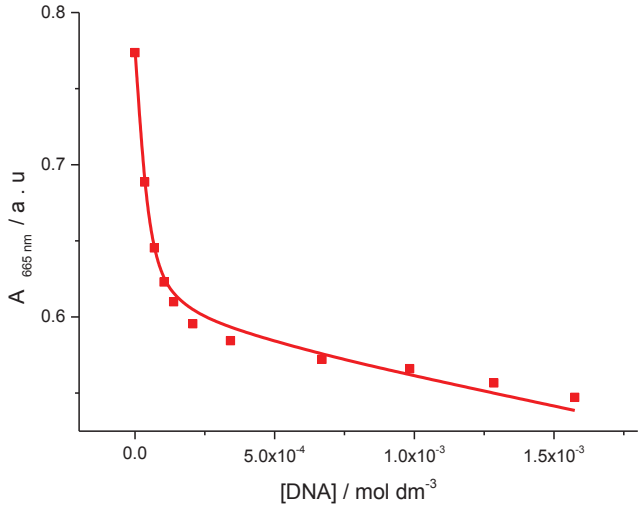

Figure 4.14: Absorbance at 665 nm for 0.012 mM **4.8** as a function of DNA concentration in the presence of 0.3 mM HA, at 25 C in buffer (25 mM MOPS, pH 7, 50 mM NaCl, 10 vol-% DMSO). The solid line represents the best fit to the data in terms of a multiple independent binding sites model, which also takes into account dilution which causes the continued decrease in absorbance after binding of all ligand molecules.

The titration curve in Figure 4.14 was evaluated by fitting a multiple independent binding sites model, which also takes simple dilution into account, to the data. The fit indicates a binding constant $K_{binding}$ of (5.7 ± 2.9) $\times 10^5$ M^{-1} for a binding site size of (5.3 ± 0.9) base pairs. The obtained value of binding constant and binding site size *n* were reasonable. For comparison with data obtained in the absence of HA, the data were reanalysed with the binding site size restricted to 3.0, giving an equilibrium constant $K_{binding}$ of (1.7 ± 0.37) $\times 10^5$ M^{-1}. A $K_{binding}$ of (4.4 ± 0.5) $\times$ 10^5 M^{-1} for a binding site size restricted to 3.0 base pairs was observed for **4.8** to DNA in the absence of HA. From the difference in binding constant in the presence and absence of HA, it appears that HA does compete with DNA for **4.8**. The presence of this competition is beneficial because it could reduce non-specific binding.

4.2.8 Compound 4.10 binding with DNA in the presence of 0.1 mM HA

We wanted to study the binding of **4.10** to DNA in the presence 0.1 mM HA. The changes in absorption of **4.10** upon addition of DNA were measured in buffer (25 mM MOPS, pH 7.0, 50 mM NaCl) at 25 °C (Figure 4.15).

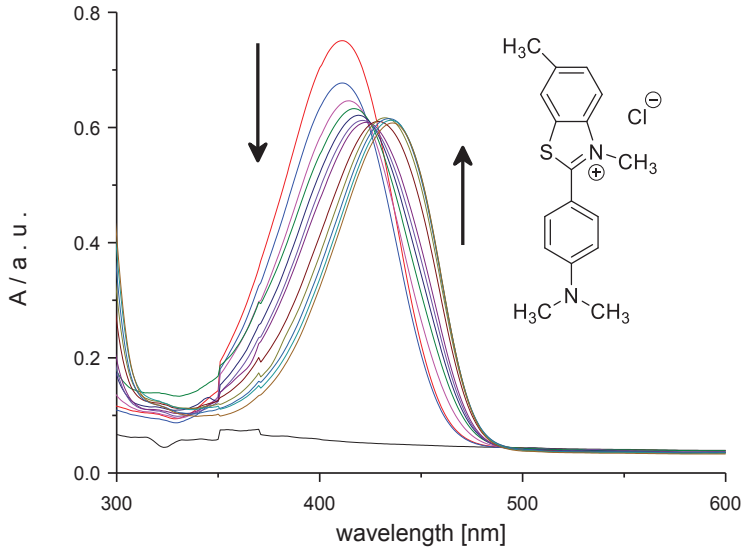

Figure 4.15: UV-visible spectra for 0.026 mM **4.10 (**red line**)** in buffer (25 mM MOPS, pH 7.0, 50 mM NaCl) in the absence of HA and subsequent spectra for **4.10** in the presence of 0.1 mM HA upon addition of 0 – 1.45 mM DNA, at 25 °C.

In the studies (Figure 4.15), **4.10** showed a red shift in absorbance upon addition of DNA with maximum changes in absorbance at 411 and 432 nm in the presence of 0.1 mM HA. This redshift UV-visible absorption has probably occurred as a result of geometrical distortion of **4.10** when it interacts with DNA in the presence of HA, but it may also be as a result of a local medium effect.

To quantify the affinity of **4.10** for DNA, the absorbance at 411 nm and 432 nm were plotted as a function of the concentration of DNA (Figure 4.16, see Appendix, Tables A55.66).

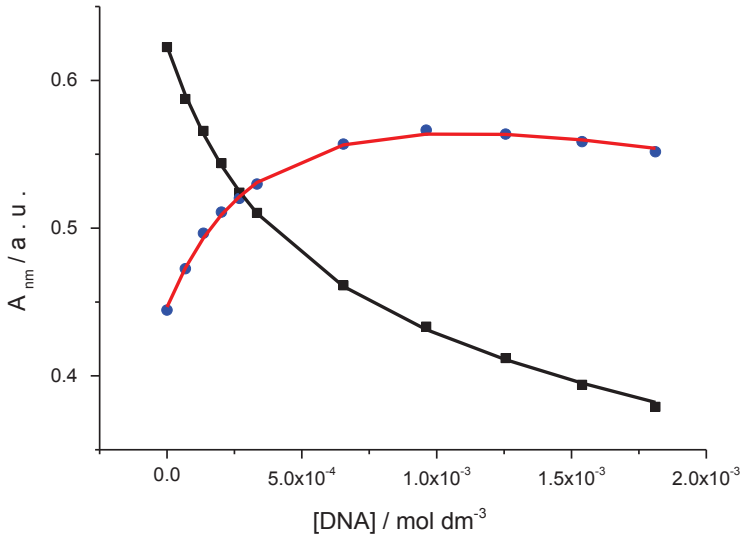

Figure 4.16: Absorbance at 411 nm (■) and at 432 nm (●) for 0.026 mM **4.10** as a function of DNA concentration in the presence of 0.1 mM HA, at 25 °C in buffer (25 mM MOPS, pH 7.0, 50 mM NaCl). The solid lines represent a global fit of a multiple independent binding sites model to the data.

Figure 4.16 shows a decrease in the absorbance of **4.10** at 411 nm (■) upon addition of DNA in the presence of 0.1 mM HA. The red line shows a clear increase in the absorbance of **4.10** at 432 nm (●) upon addition of DNA in the presence of 0.1 mM HA. The titration curves in Figure 4.17 were analysed globally by the fitting of a multiple independent binding sites model, which also takes simple dilution into account, to the data, giving an equilibrium constant $K_{binding}$ of $(2.0 \pm 8.8) \times 10^3$ M^{-1} for a binding site size of (0.8 ± 3.6) base pairs. The obtained value for the binding site size was unreasonable and had a large error margin. Therefore, the data of the titration curves were reanalysed, giving an equilibrium constant $K_{binding}$ of $(7.6 \pm 2.6) \times 10^3$ M^{-1} for a binding site size restricted to 3.0 base pairs. A $K_{binding}$ of $(6.7 \pm 0.7) \times 10^3$ M^{-1} for a binding site size restricted to 3.0 base pairs was observed for **4.10** to DNA in the absence of HA.

4.2.9 Compound 4.11 binding with DNA in the presence of 0.1 mM HA

We wanted to know whether the binding of **4.11** to DNA in the presence 0.1 mM HA. The changes in absorption of **4.11** upon addition of DNA were measured in buffer (25 mM MOPS, pH 7.0, 50 mM NaCl) at 25 °C (Figure 4.17).

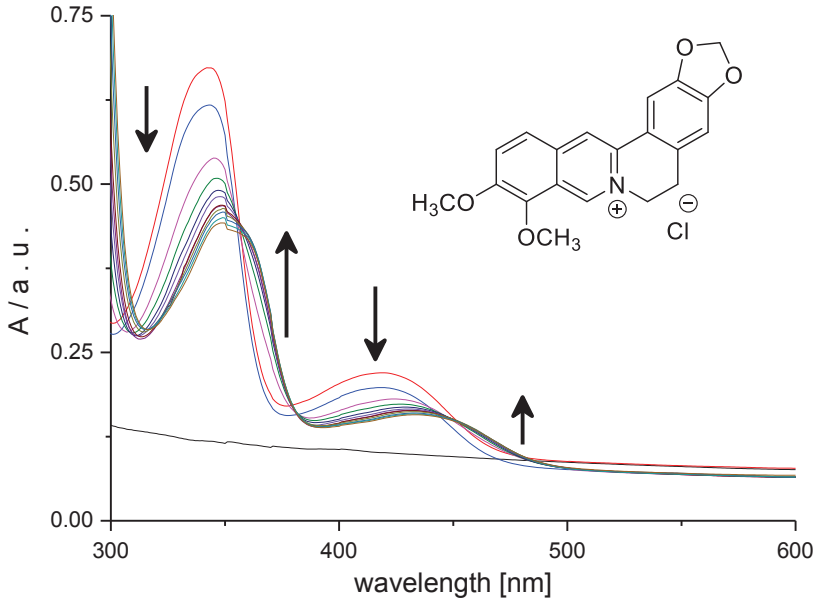

Figure 4.17: UV-visible spectra for 0.02 mM **4.11 (**red line**)** in buffer (25 mM MOPS, pH 7.0, 50 mM NaCl) in the absence of HA and subsequent spectra for **4.11** in the presence of 0.3 mM HA upon addition of 0 – 1.9 mM DNA, at 25 °C.

Figure 4.17 shows a hypochromic shift at 342 and 370 nm upon addition of DNA to **4.11** in the presence of 0.1 mM HA. This decrease in UV-visible absorption may occur as a result of geometrical distortion of **4.11** when it interacts with DNA in the presence of 0.1 mM HA or as a result of the different local medium provided by the binding sites.

To quantify the affinity of **4.11** for DNA in the presence of HA, the absorbances at 342 and 370 nm were plotted as a function of the concentration of DNA (Figure 4.18, see Appendix, Tables A55.67).

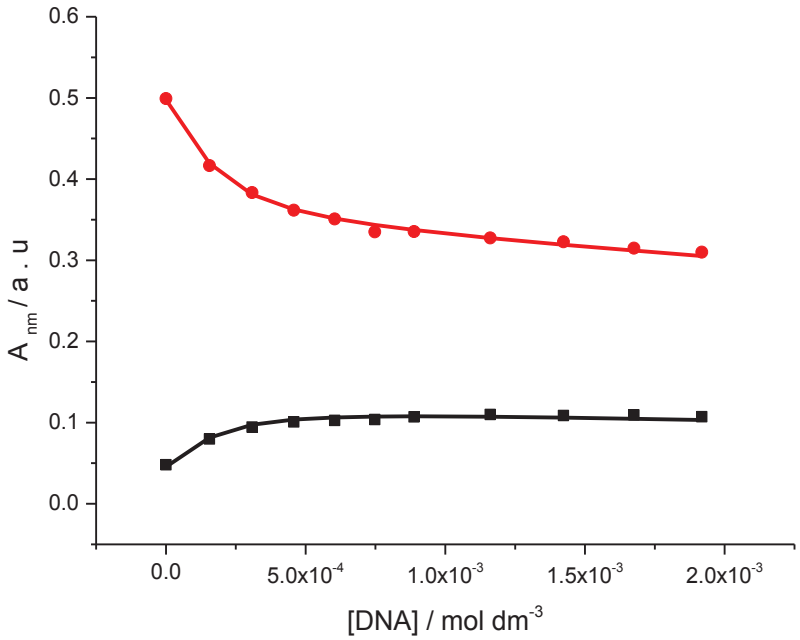

Figure 4.18: Absorbance at 342 nm and at 370 nm for 0.02 mM **4.11** as a function of DNA concentration in the presence of 0.1 mM HA, at 25 °C in buffer (25 mM MOPS, pH 7, 50 mM NaCl). The solid lines represent a global fit of a multiple independent binding sites model to the data.

Figure 4.18 shows an obvious decrease at 342 nm and an increase at 370 nm upon addition of DNA in the presence of 0.1 mM of HA, as also observed previously in the absence of HA. We attribute this decrease and increase in absorbance to strong binding of **4.11** to DNA in the presence of 0.1 mM HA. The binding affinity $K_{binding}$ and binding site size n were determined by fitting a multiple independent binding sites model, which also takes ligand dilution into account, to the data. The ligand strongly interacts with DNA giving an equilibrium constant $K_{binding}$ of $(2.2 \pm 0.2) \times 10^4\ M^{-1}$ for a binding site size restricted to 3 base pairs. A $K_{binding}$ of $(1.6 \pm 0.2) \times 10^4\ M^{-1}$ for a binding site size restricted to 3.0 base pairs was observed for **4.11** binding to DNA in the absence of HA.

4.2.10 Compound 4.12 binding with DNA in the presence of 0.1 mM HA

We wanted to study whether the binding of **4.12** to DNA in the presence 0.1 mM HA. The changes in absorption of **4.12** upon addition of DNA in the presence 0.1 mM HA were measured in buffer (25 mM MOPS, pH 7.0, 50 mM NaCl) at 25 °C (Figure 4.19).

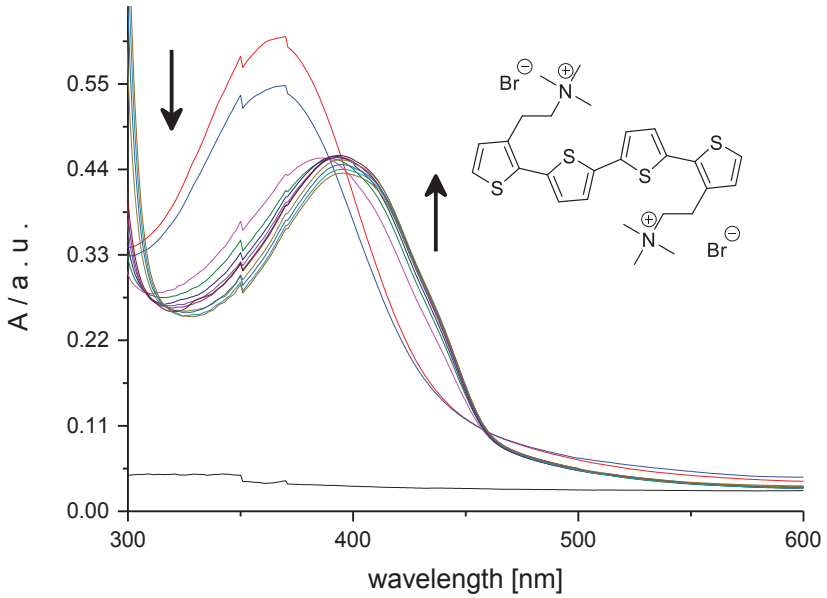

Figure 4.19: UV-visible spectra for 0.021 mM **4.12 (**red line**)** in buffer (25 mM MOPS, pH 7.0, 50 mM NaCl) in the absence of HA and subsequent spectra for **4.12** in the presence of 0.3 mM HA upon addition of 0 – 1.3 mM DNA, at 25 °C.

Figure 4.19 shows a hypochromic shift in absorbance at 367 nm and a hyperchromic shift at 430 nm of upon addition of DNA to **4.12** in the presence of 0.1 mM HA. The change in UV-visible absorption probably occurs as a result of geometrical distortion of **4.12** when it interacts with DNA in the presence of HA, but a local medium effect may also contribute.

To quantify the affinity of **4.12** for DNA in the presence of 0.1 mM HA the absorbance at 367 nm and 430 nm were plotted as a function of the concentration of DNA (Figure 4.20, see Appendix, Tables A55.68).

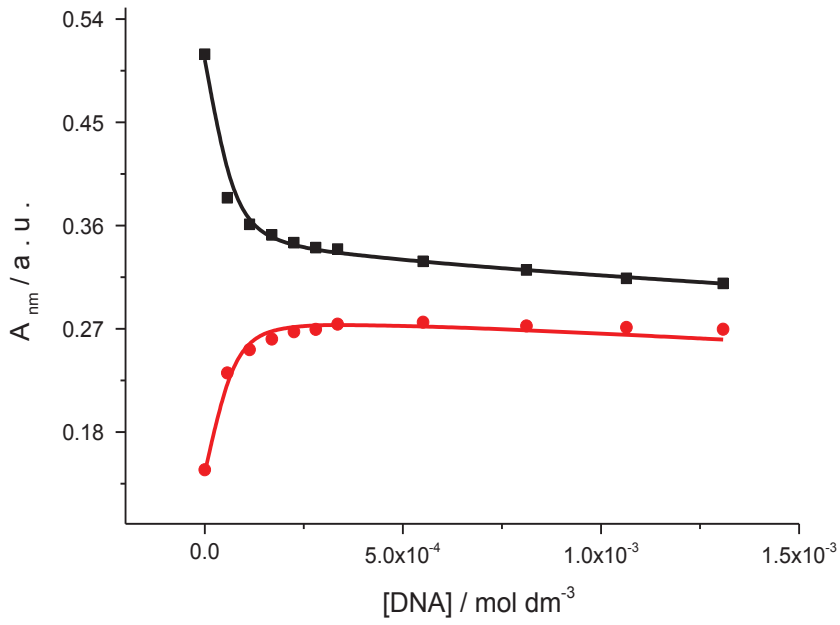

Figure 4.20: Absorbance at 367 nm (■) and at 430 nm (●) for 0.021 mM **4.12** as a function of DNA in the presence of 0.1 mM HA, at 25 °C in buffer (25 mM MOPS, pH 7.0, 50 mM NaCl). The solid lines represent a global fit of a multiple independent binding sites model to the data.

Figure 4.20 presents that ligand **4.12** displays a red-shift upon increasing the DNA concentration in the presence of 0.1 mM HA. The maximum decrease occurs at 367 nm, and the highest increase occurs at 430 nm. The absorbance at 367 nm corresponds to the free ligand, and the absorbance 430 nm is represented DNA-ligand complex. The binding affinity $K_{binding}$ and a binding site size n were determined by fitting a multiple independent binding sites model, which also takes ligand dilution into account, to the data. The two lines give an equilibrium constant $K_{binding}$ of $(4 \times 10^{-3} \pm 6.7) \times 10^5$ M^{-1} for a binding site size of $(1 \times 10^{-2} \pm 21)$ base pairs. The obtained binding stoichiometry was unreasonably small but had a significant error margin. Therefore, the data were reanalysed with the stoichiometry restricted to 2.0 base pairs[181] , giving an equilibrium constant $K_{binding}$ of $(1.0 \pm 0.13) \times 10^5$ M^{-1}. A $K_{binding}$ of $(8.2 \pm 1.06) \times 10^4$ M^{-1} for a binding site size restricted to 2.0 base pairs was observed for **4.12** binding to DNA in the absence of HA.

Summary

The results of UV-visible titrations for π-conjugated compounds with duplex DNA in the presence of HA show that ligands **4.1, 4.2, 4.4, 4.5, 4.7, 4.8, 4.10, 4.11** and **4.12** bind to DNA in the presence of HA. The affinities of these compounds for DNA are summarised in Table 4.2.

Table 4.2 Binding affinities and a binding site size for binding of 4.1, 4.2, 4.4, 4.5, 4.7, 4.8, 4.10, 4.11 and 4.12 to DNA in the presence of HA in buffer (25 mM MOPS, pH 7.0, 50 mM NaCl) at 25 °C.

Ligands	*Binding constant HA / M^{-1}*	*Binding constant DNA / M^{-1}*	*Binding constant DNA +HA / M^{-1}*	*Effect of HA on affinity for DNA*
4.1	$(3.1 \pm 2.7) \times 10^5$ 3.0 ± 0.7	$(1.5 \pm 0.1) \times 10^4$ n = 3*a	$(5.3 \pm 1.4) \times 10^4$ n = 3*a	Increase
4.2	No binding	$(6.4 \pm 1.6) \times 10^4$ n = 3*a	$(8.8 \pm 4.4) \times 10^3$ n = 3*a	Decrease
4.4	No binding	$(3.4 \pm 0.6) \times 10^4$ 2.3 ± 0.2	$(3.8 \pm 0.5) \times 10^4$ 2.7 ± 0.2	No change
4.5	No binding	$(8.9 \pm 3.2) \times 10^4$ n = 3*	$(6.3 \pm 1.3) \times 10^4$ n = 3*	No change
4.7	$(2.0 \pm 0.5) \times 10^3$ n = 1*	$(7.7 \pm 1.5) \times 10^5$ n = 3*	$(2.8 \pm 1.4) \times 10^4$ n = 3*a	Decrease
4.8	No binding	$(4.4 \pm 0.5) \times 10^5$ n = 3*	$(1.7 \pm 0.3) \times 10^5$ n = 3*	Decrease
4.10	No binding	$(6.9 \pm 0.7) \times 10^3$ n = 3*	$(7.6 \pm 0.2) \times 10^3$ n = 3*	No change
4.11	No binding	$(1.6 \pm 0.2) \times 10^4$ n = 3*	$(1.9 \pm 0.02) \times 10^4$ n = 3*	No change
4.12	No binding	$(1.8 \pm 0.38) \times 10^5$ n = 3*	(2.2 ± 0.4) x 10^5 n = 3*	No change

a) apparent binding constant for the event following initial precipitation.

b) * restricted**.**

Table 4.2 shows the binding that occurred between π-conjugated cationic compounds in our studies with biopolymer HA and the effect of HA on duplex DNA-binding. Compounds **4.1, 4.2** and **4.7** interact with DNA in the presence of HA with two events, the first event occurs when the concentration of ligand is high, and the concentration of DNA is still low under these condition ligand binds to both the highest affinity binding sites and to the negative sugar-phosphate backbone of DNA. As result of that precipitation will occur because of formation of a charge neutralised ligand-DNA complex. The second event occurs at a high concentration of DNA. In this case, the ligand binds to the main binding sites, viz. minor groove or intercalation site of DNA. Compounds **4.4, 4.5, 4.10, 4.11** and **4.12** do not show any change in affinity for DNA in the presence of HA. From the similarity in the binding constant, it appears that HA does not significantly compete with DNA for these ligands. This is in agreement with the observation that these compounds do not bind to HA. Decreases in binding constant were observed for **4.2**, **4.7** and **4.8.** That means the binding between these ligands and DNA in the presence of HA is not as easy as without polymer. For **4.7**, this observation is as expected, considering it binds to HA. For **4.2** and **4.8**, this is unexpected, considering that these compounds were not found to bind to HA. For **4.1** an increase in the apparent binding constant was observed. This increase is probably the result of excess ligand at the beginning of the titration binding to HA, rather than to secondary binding site on the DNA. This means that the second event now corresponds to **4.1** moving from HA to the primary site, rather than from precipitated complexes.

Part C: Alginic acid binding studies

4.2.11 Compounds 4.1 and 4.2 binding to AA

We wanted to know whether **4.1** and **4.2** bind to AA, the changes in absorption of **4.1** upon addition of AA were measured in buffer (25 mM MOPS, pH 7.0, 50 mM NaCl and 10 vol-% DMSO) at 25 °C (Figure 4.21). Similar experiments for compound **4.2** were carried out with AA (see appendix A25 Figure A25.1 and Figure A25.2, for data in tabular format see Appendix, Tables A55.70).

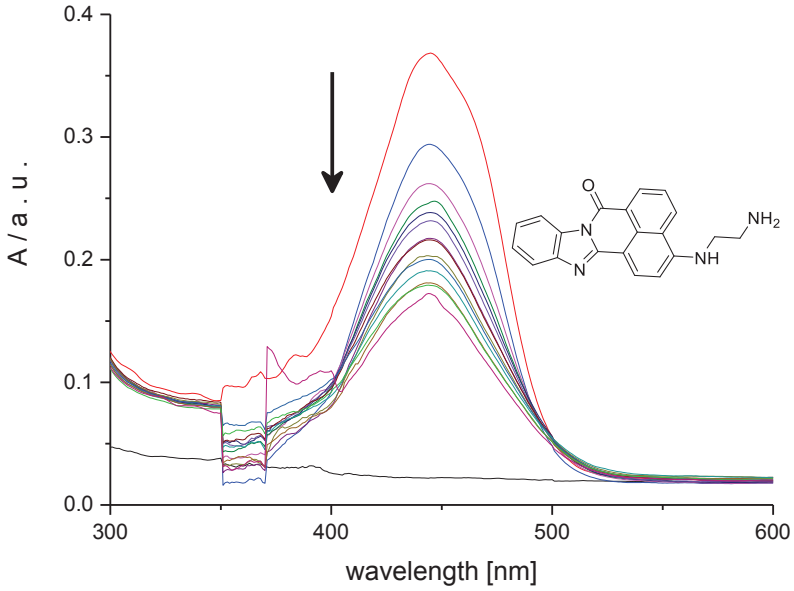

Figure 4.21: UV-visible spectra for 0.021 mM **4.1** upon addition of 0 – 1.34 mM AA, at 25 °C in buffer (25 mM MOPS, pH 7.0, 50 mM NaCl and 10 vol-% DMSO).

Figure 4.21 shows that **4.1** displays a hypochromic shift in absorbance upon addition of AA, with a maximum change in absorbance at 445 nm. This decrease in UV-visible absorption may have occurred as a result of geometrical distortion of **4.1** when it interacts with AA, but it may also be as a result of a local medium effect.

To quantify the affinity of **4.1** for AA, the absorbance at 445 nm was plotted as a function of the concentration of AA (Figure 4.22, see Appendix, Tables A55.69).

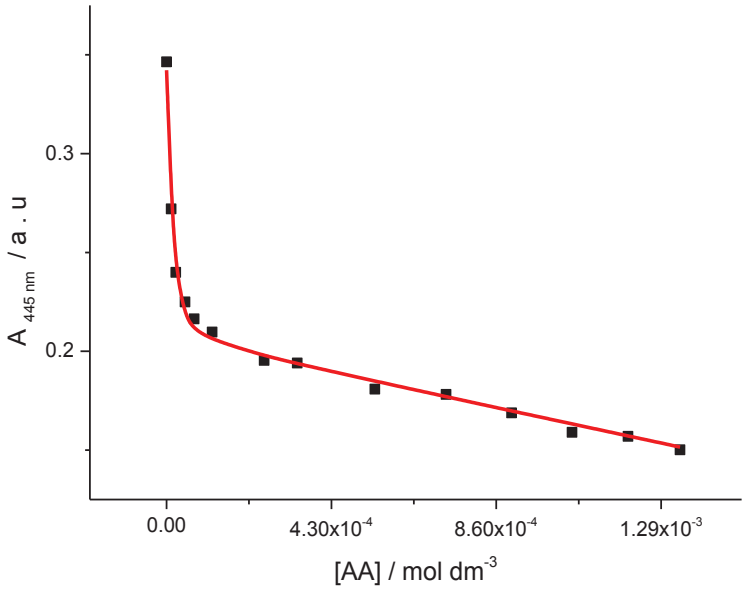

Figure 4.22: Absorbance at 445 nm for 0.021 mM **4.1** upon addition of 0.0 – 1.34 mM AA, at 25 °C in buffer (25 mM MOPS, pH 7.0, 50 mM NaCl and 10 vol-% DMSO). The solid line represents the best fit to the data in terms of multiple independent binding sites.

The titration curve in Figure 4.22 shows a decrease in the absorbance for **4.1** upon addition of AA. The binding affinity $K_{binding}$ and binding sites size n were determined by fitting a multiple independent binding sites model, which also takes ligand dilution into account, to the data. The fit reproduces the data well and gives an equilibrium constant $K_{binding}$ of $(4.5 \pm 2.4) \times 10^4$ M^{-1} for a binding site size of (0.3 ± 0.1) monomeric units per molecule of **4.1**. The obtained value of binding constant was reasonable. The binding site size is numerically well defined but looks unreasonable. We don't currently know why the apparent binding site size is so small. The fit suggests that **4.1** interacts and therefore that AA has a binding site size accessible to **4.1**.

In further experiments, compounds **4.4, 4.5, 4.7, 4.8, 4.10, 4.11** and **4.12** showed no interactions with AA (see appendixes A26-A32).

Summary

The affinities for AA of all tested compounds are summarised in Table 4.3.

Table 4.3 Binding affinities and binding site sizes for the binding of 4.1- 4.12 with AA in buffer (25 mM MOPS, pH 7.0, 50 mM NaCl) at 25 °C.

Ligands	*Binding constant AA* K / M^{-1}	*Binding site size* n
4.1	$(4.5 \pm 2.4) \times 10^4$	0.3 ± 0.1
4.2	$(6.9 \pm 1.5) \times 10^4$	3^*
4.4	No binding	
4.5	No binding	
4.7	No binding	
4.8	No binding	
4.10	No binding	
4.11	No binding	
4.12	No binding	
* restricted.		

Table 4.3 shows that only **4.1** and **4.2** cationic ligands bind with negative natural polymer alginic acid AA. We attribute this binding to the interaction between the negatively charged COO^- on the biopolymer AA and the positively charged on molecules. The affinity for **4.1** and **4.2** is quantified by a binding constant of $10^4\ M^{-1}$.

Part D: Effect of AA on DNA-binding properties

4.2.12 Compound 4.1 binding to DNA in the presence of AA.

We studied the interactions of **4.1** with DNA in the presence of 0.1 mM AA. The changes in absorption of **4.1** upon addition of DNA in the presence of 0.1 mM AA were measured in buffer (25 mM MOPS, pH 7.0, 50 mM NaCl) at 25 °C (Figure 4.23)

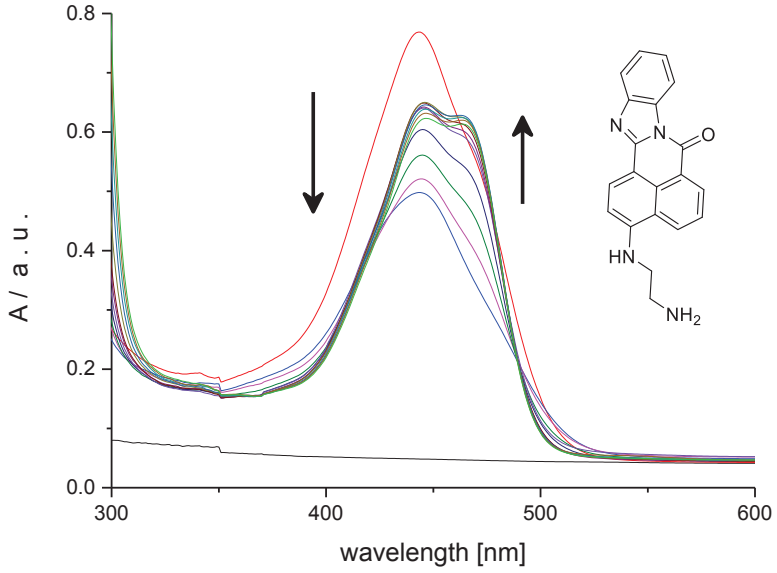

Figure 4.23: UV-visible spectra for 0.044 mM **4.1 (**red line**)** in buffer (25 mM MOPS, pH 7.0, 50 mM NaCl) in the absence of AA and subsequent spectra for **4.1** in the presence of 0.1 mM AA upon addition of 0 – 1.5 mM DNA, at 25 °C.

In the studies, **4.1** shows a hypochromic shift in absorbance at 443 nm upon addition of 0.1 mM AA, followed by a hyperchromic shift at 443 nm upon addition of DNA in the presence of 0.1 mM AA. This observation suggests precipitation and subsequent dissolution of a DNA ligand complex in the presence of AA, similar to observations in the absence of AA.[172] The change in UV-visible absorption during the second phase of the titration may occur because of geometrical distortion of **4.1** when it interacts with DNA in the presence of AA, but considering the rigidity of **4.1** it is more likely a local medium effect.

To quantify the apparent affinity of **4.1** for DNA in the presence of 0.1 mM AA, the absorbance at 443 nm were plotted as a function of the concentration of DNA (Figure 4.24, see Appendix, Tables A55.78).

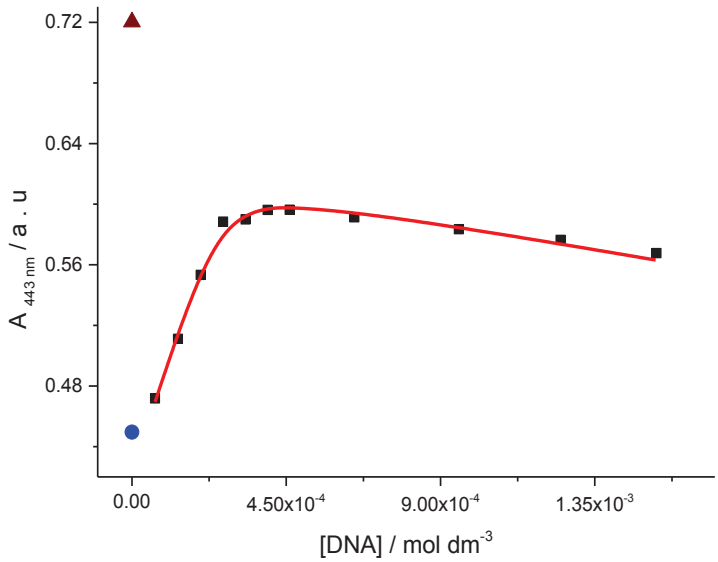

Figure 4.24: Absorbance at 443 nm for 0.044 mM **4.1** in the absence of AA (▲) and subsequent spectra for **4.1** in the presence of 0.1 mM AA (●) and upon addition of 0 067 – 1.5 mM DNA (■) in the presence of AA, at 25 °C in buffer (25 mM MOPS, pH 7, 50 mM NaCl). The solid line represents a fit of a multiple independent sites model to the data in the 0.067 – 1.5 mM range (■).

Figure 4.24 shows two events. The first event shows a fast decrease in absorbance upon addition 0.1 mM AA (●). We attribute this decrease in absorbance to strong binding of **4.1** to AA. The second event shows a clear increase in the absorbance of **4.1** upon addition of DNA (■) in the presence of 0.1 mM of AA. According to data analysis, the ligand strongly interacts with DNA in the presence of AA, giving an apparent equilibrium constant $K_{binding}$ of $(6.3 \pm 3.2) \times 10^5\ M^{-1}$ for a binding site size of (6.5 ± 0.5) base pairs. The obtained binding parameters were reasonable for both stoichiometry and binding constant. A $K_{binding}$ of $(1.5 \pm 0.1) \times 10^4\ M^{-1}$ for the binding site size restricted to 3 base pairs was observed for **4.1** to DNA in absence AA[172]. For comparison, the data were reanalysed with the stoichiometry restricted to 3.0 base pairs, giving an apparent equilibrium constant $K_{binding}$ of $(7.1 \pm 1.8) \times 10^4\ M^{-1}$. From the difference in the apparent binding constant in the absence of AA[172] and in the presence of AA, it appears that AA does significantly compete with DNA for **4.1**. Unfortunately, AA does not help to avoid precipitation. On the other hand, the presence of this competition may be beneficial if compound **4.1** were to be used in a biosensor because AA could be used to compete with the non-specific binding of **4.1** as a sensitiser. Our analogous experiments showed that there is no binding between DNA and **4.2** in the presence of AA (See appendix A33 for Compound **4.2** with DNA. Figure A33.1 and Figure A33.2, see appendix, Tables A55.79).

4.2.13 Compound 4.4 binding with DNA in the presence of 0.1 mM AA

We wanted to know the binding of **4.4** to DNA in the presence 0.1 mM AA. The changes in absorption of **4.4** upon addition of DNA were measured in buffer (25 mM MOPS, pH 7.0, 50 mM NaCl) at 25 °C (Figure 4.25).

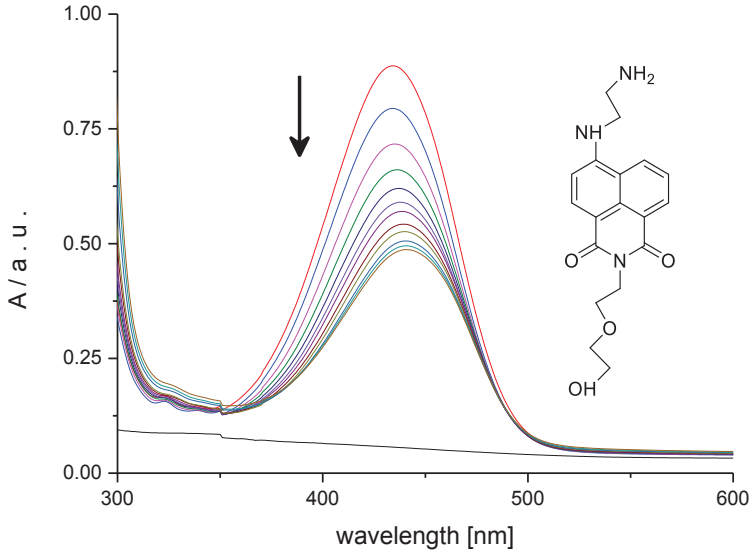

Figure 4.25: UV-visible spectra for 0.076 mM **4.4 (**red line**)** in buffer (25 mM MOPS, pH 7.0, 50 mM NaCl) in the absence of AA and subsequent spectra for **4.4** in the presence of 0.1 mM AA upon addition of 0 – 1.2 mM DNA, at 25 °C.

In the studies, **4.4** showed a hypochromic shift in absorbance upon addition of DNA with a maximum change in absorbance at 434 nm in the presence of 0.1 mM AA. This decrease in UV-visible absorption may have occurred as a result of geometrical distortion of **4.4** when it interacts with DNA in the presence of AA, but it may also be as a result of a local medium effect.

To quantify the affinity of **4.4** for DNA, the absorbance at 434 nm were plotted as a function of the concentration of DNA (Figure 4.26, see Appendix, Tables A55.80).

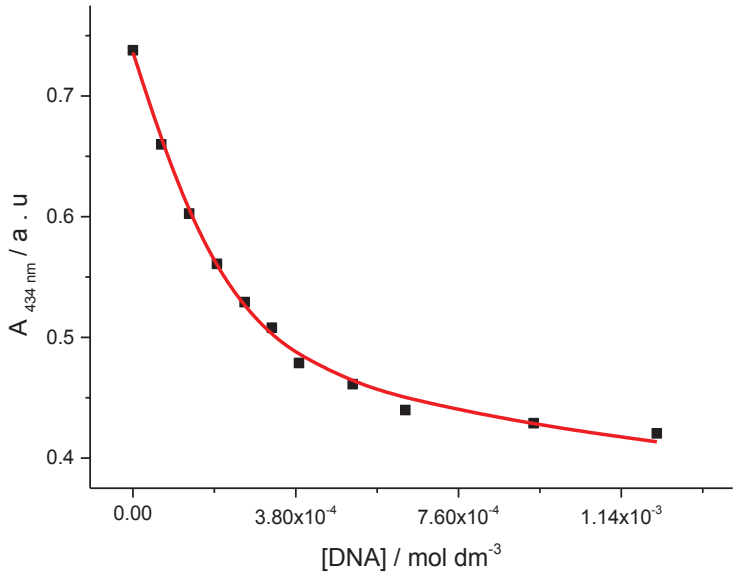

Figure 4.26: Absorbance at 434 nm for 0.076 mM **4.4** as a function of DNA concentration in the presence of 0.1 mM AA, at 25 °C in buffer (25 mM MOPS, pH 7, 50 mM NaCl). The solid line represents the best fit to the data in terms of a multiple independent binding sites model.

Figure 4.26 shows a clear decrease in absorbance at 434 nm upon addition of DNA in the presence of AA. The binding affinity $K_{binding}$ and the binding site size *n* were determined by fitting a multiple independent binding sites model, which also takes ligand dilution into account, to the data. A binding constant $K_{binding}$ of (4.6 ± 0.5) $\times 10^4$ M^{-1} was found for binding site size restricted to 3 base pairs. A $K_{binding}$ of (5.3 ± 0.2) $\times$ 10^4 M^{-1} for a binding site size restricted to 3.0 base pairs was observed for **4.4** interacting with DNA in the absence of AA.

4.2.14 Compound 4.5 binding with DNA in the presence of 0.1 mM AA

The binding of **4.5** to DNA in the presence 0.1 mM AA was studied using UV-visible spectroscopy. The changes in absorption of **4.5** upon addition of DNA were measured in buffer (25 mM MOPS, pH 7.0, 50 mM NaCl) at 25 °C (Figure 4.27).

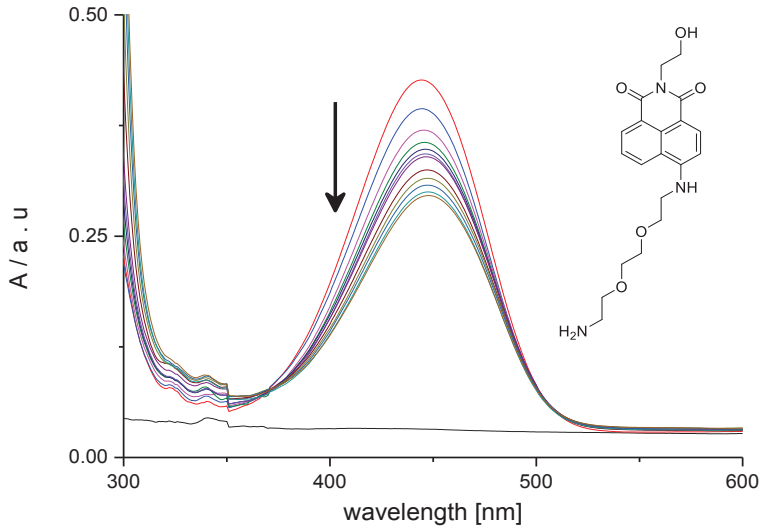

Figure 4.27: UV-visible spectra for 0.063 mM **4.5 (**red line**)** in buffer (25 mM MOPS, pH 7.0, 50 mM NaCl) in the absence of AA and subsequent spectra for **4.5** in the presence of 0.1 mM AA upon addition of 0 – 1.2 mM DNA, at 25 °C.

In the studies, **4.5** showed a red shift in absorbance upon addition of DNA with a maximum change in absorbance at 444 nm in the presence of 0.1 mM AA. This red-shift UV-visible absorption has probably occurred as a result of geometrical distortion of **4.5** when it interacts with DNA in the presence of AA, but it may also be as a result of a local medium effect.

To quantify the affinity of **4.5** for DNA, the absorbance at 444 nm were plotted as a function of the concentration of DNA (Figure 4.28, see Appendix, Tables A55.81).

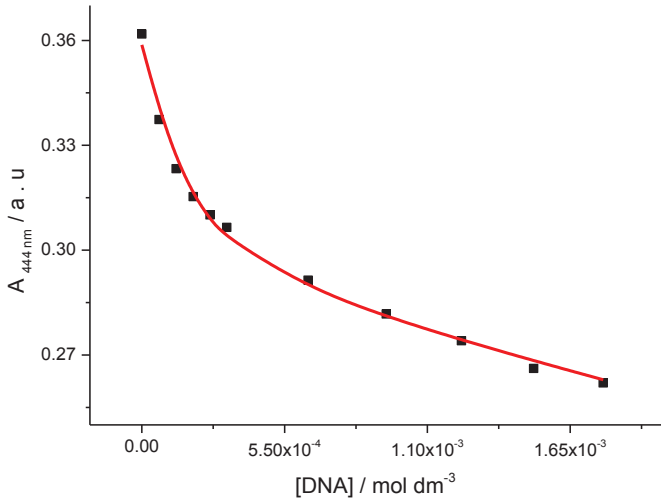

Figure 4.28: Absorbance at 444 nm for 0.063 mM **4.5** as a function of DNA concentration in the presence of 0.1 mM AA, at 25 °C in buffer (25 mM MOPS, pH 7, 50 mM NaCl). The solid line represents the best fit to the data in terms of a multiple independent binding sites model.

Figure 4.28 shows a decrease in absorbance at 444 nm upon addition of DNA in the presence of AA. The binding affinity $K_{binding}$ and the binding site size *n* were determined by fitting a multiple independent binding sites model, which also takes ligand dilution into account, to the data. The fit gives an equilibrium constant $K_{binding}$ of (4.5 ± 0.98) $\times 10^4$ M^{-1} for a binding site size restricted to 3 base pairs. A $K_{binding}$ of (8.9 ± 2.3) $\times 10^4$ M^{-1} for a binding site size restricted to 3.0 base pairs was previously observed for **4.5** binding to DNA in the absence of AA. From the similarity in the binding constants, it appears that AA does not significantly compete with DNA for **4.5**.

4.2.15 Compound 4.7 binding with DNA in the presence of 0.1 mM AA

We wanted to study the binding of **4.7** to DNA in the presence of 0.1 mM AA. The changes in absorption of **4.7** upon addition of DNA were measured in buffer (25 mM MOPS, pH 7.0, 50 mM NaCl) at 25 °C (Figure 4.29).

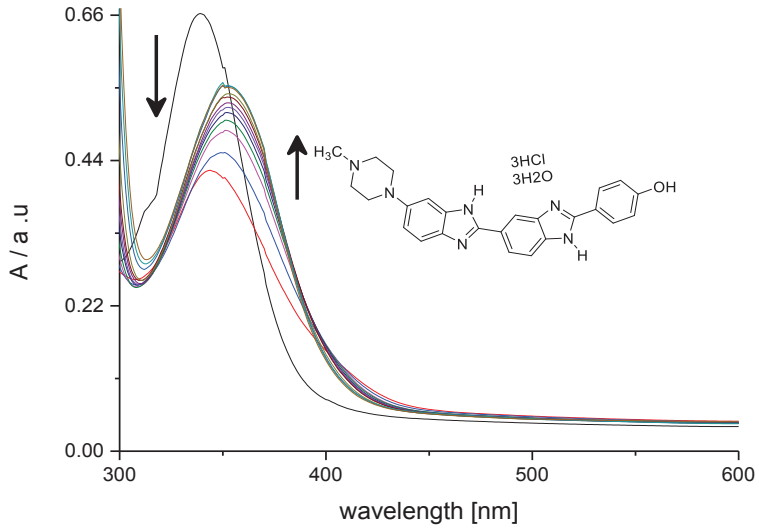

Figure 4.29: UV-visible spectra for 0.017 mM **4.7 (**red line**)** in buffer (25 mM MOPS, pH 7.0, 50 mM NaCl) in the absence of AA and subsequent spectra for **4.7** in the presence of 0.1 mM AA upon addition of 0 – 2.09 mM DNA, at 25 °C.

In the studies, **4.7** shows a hypochromic shift in absorbance at 360 nm upon addition 0.1 mM AA followed by a hyperchromic shift at 360 nm of **4.7** upon addition of DNA. The slight red shift suggests an increase in effective conjugation length, which attributed to increase in the planarity of **4.7** upon interaction with DNA in the presence of AA.

To quantify the apparent affinity of **4.7** for DNA in the presence of AA, the absorbance at 360 nm were plotted as a function of the concentration of DNA (Figure 4.30, see Appendix, Tables A55.82).

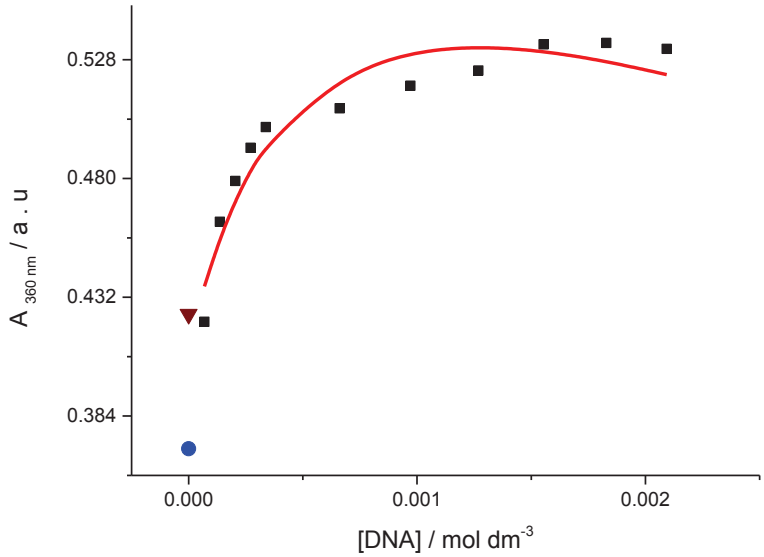

Figure 4.30: Absorbance at 360 nm for 0.017 mM **4.7** in the absence of AA **(▼)** and subsequent spectra for **4.7** in the presence of 0.1 mM AA (●) and upon addition of 0.068 – 2.1 mM DNA (■) in the presence of AA, at 25 °C.in buffer (25 mM MOPS, pH 7, 50 mM NaCl). The solid line represents a fit of a multiple independent sites model to the data in the 0 068 – 2.1 mM range (■).

Figure 4.30 shows two events. The first event shows a large decrease in absorbance upon addition of 0.1 mM AA. We attribute this decrease in absorbance to strong binding of **4.7** to AA, leading to charge neutralisation of **4.7**-AA complexes and eventually precipitation. The second event shows a clear increase in the absorbance of **4.7** upon addition of DNA (■) in the presence of 0.1 mM of AA. The ligand strongly interacts with DNA in the presence of AA. Data analysis gives an apparent equilibrium constant $K_{binding}$ of $(2\times10^{-5} \pm 1.1) \times10^{5}\ M^{-1}$ for a binding site size of $(1\times10^{-1} \pm 51)$ base pairs. A $K_{binding}$ of $(7.7 \pm 1.5) \times 10^{5}\ M^{-1}$ for a binding site size restricted to 3.0 base pairs was observed for **4.7** binding to DNA in the absence of AA. The data were therefore reanalysed with the stoichiometry restricted to 3.0 base pairs to allow comparison, giving an apparent equilibrium constant $K_{binding}$ of $(1.1 \pm 0.2) \times10^{4}\ M^{-1}$. From the differences in the binding constants in the absence of AA and in the presence of AA, it appears that AA significantly competes with DNA for **4.7**. The presence of this competition may be beneficial if the compound **4.7** were to be used in a biosensor because it can be used to provide cleaner signals to detect DNA hybridization.

4.2.16 Compound 4.8 binding with DNA in the presence of 0.1 mM AA

We wanted to study the binding of **4.8** with DNA in the presence of 0.1 mM AA. The changes in absorption of **4.8** upon addition of DNA were measured in buffer (25 mM MOPS, pH 7.0, 50 mM NaCl) at 25 °C (Figure 4.31).

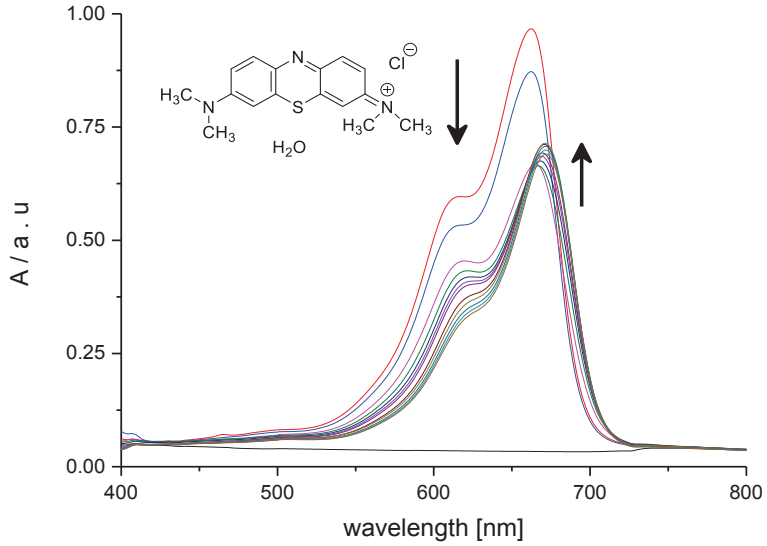

Figure 4.31: UV-visible spectra for 0.013 mM **4.8 (**red line**)** in buffer (25 mM MOPS, pH 7.0, 50 mM NaCl) in the absence of AA and subsequent spectra for **4.8** in the presence of 0.1 mM AA upon addition of 0 – 1.8 mM DNA, at 25 °C.

Figure 4.31 shows a red-shift in absorbance upon addition of DNA in the presence of 0.1 mM AA (at the λ_{max} of 663 nm) of **4.8**. The change in UV-visible absorption may occur as a result of geometrical distortion of **4.8** when it interacts with DNA, but it may also be a local medium effect.

To quantify the affinity of **4.8** for DNA in the presence of 0.1 mM AA the absorbance at 663 nm were plotted as a function of the concentration of DNA (Figure 4.323, see Appendix, Tables A55.83).

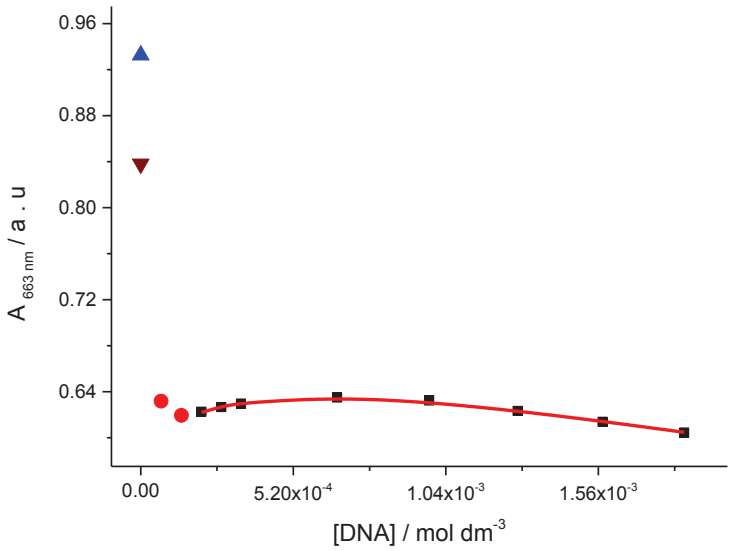

Figure 4.32: Absorbance at 663 nm for 0.013 mM **4.8** in the absence of AA **(▲)** and subsequent spectra for **4.8** in the presence of 0.1 mM AA (▼) and upon addition of 0.0 – 0.013 mM DNA (●) and for 0.02 – 1.8 mM DNA (■) both in the presence of AA, at 25 °C in buffer (25 mM MOPS, pH 7, 50 mM NaCl. The solid line represents a fit of a multiple independent sites model to the data in the 0.02 – 1.8 mM range.

Figure 4.32 shows two binding events. The first binding event shows a decrease in the absorbance upon addition 0.1 mM AA (▼) with a subsequent continued decrease in absorbance up to a concentration of 0 – 0.013 mM DNA (● first two data points in Figure 4.33). We attribute this decline in absorbance to strong binding of **4.8** to AA and DNA, leading to precipitation as a result of charge neutralisation of the **4.8 -** DNA in the presence of AA. The second binding event shows an increase in the absorbance of **4.8** upon addition 0.020 - 1.8 mM DNA in the presence of 0.1 mM of AA. Data analysis in the usual manner yields an apparent equilibrium constant $K_{binding}$ of (9.2 ± 1.1) $\times 10^3$ M^{-1} for a binding site size restricted to 3.0 base pairs. A $K_{binding}$ (4.4 ± 0.5) $\times 10^5$ M^{-1} for a binding site size restricted to 3.0 base pairs was observed for **4.8** interacting with AA therefore clearly there is a decrease in the affinity of **4.8** for DNA in the presence of AA.

4.2.17 Compound 4.10 binding with DNA in the presence of 0.1 mM AA

We desired to know whether **4.10** and DNA interact in the presence 0.1 mM AA. The changes in absorption of **4.10** upon addition of DNA in the presence 0.1 mM AA were measured in buffer (25 mM MOPS, pH 7.0, 50 mM NaCl) at 25 °C (Figure 4.33).

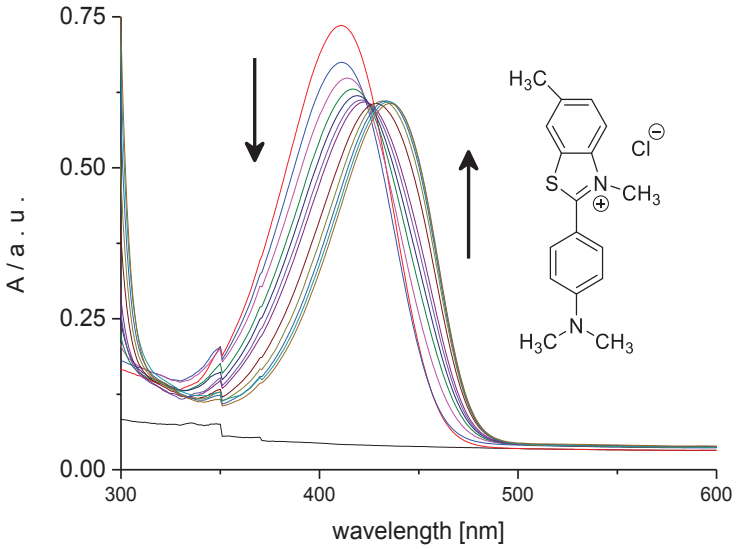

Figure 4.33: UV-visible spectra for 0.026 mM **4.10 (**red line**)** in buffer (25 mM MOPS, pH 7.0, 50 mM NaCl) in the absence of AA and subsequent spectra for **4.10** in the presence of 0.1 mM AA upon addition of 0 – 1.5 mM DNA, at 25 °C.

Figure 4.33 shows a red shift in absorbance of **4.10** upon addition of DNA in the presence of 0.1 mM AA. This change in UV-visible absorption may occur as a result of geometrical distortion of **4.10** when it interacts with DNA, but it may also be a local medium effect.

To quantify the affinity of **4.10** for DNA in the presence of 0.1 mM AA, the absorbance at 411 nm and at 432 nm were plotted as a function of the concentration of DNA in the presence of 0.1 mM AA (Figure 4.34, see Appendix, Tables A55.84).

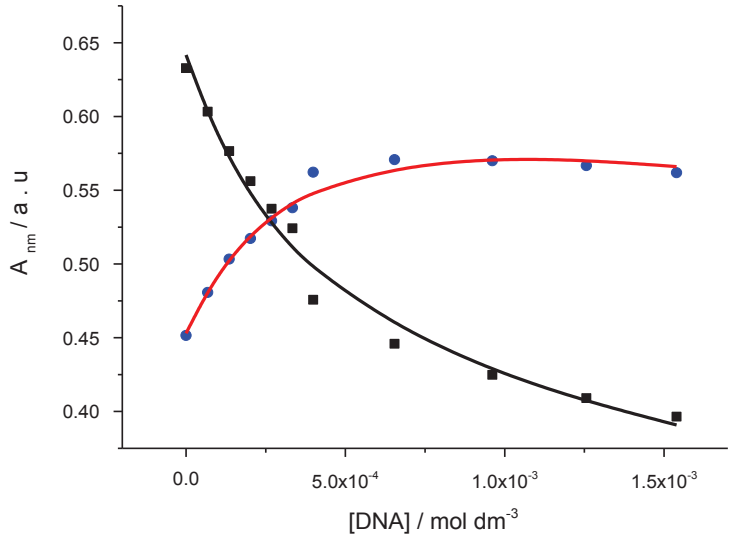

Figure 4.34: Absorbance at 411 nm (■) and at 432 nm (●) for 0.026 mM **4.10** as a function of DNA in the presence of AA, at 25 °C in buffer (25 mM MOPS, pH 7.0, 50 mM NaCl). The solid lines represent a global fit of a multiple independent sites model to the data.

The titration curves in Figure 4.34 were analysed globally in terms of a multiple independent binding sites model, which also takes ligand dilution into account, giving an equilibrium constant $K_{binding}$ of $(8.6 \pm 0.12) \times 10^3$ M^{-1} for a binding site size restricted to 3.0 base pairs. A $K_{binding}$ of $(6.9 \pm 0.7) \times 10^3$ M^{-1} for a binding site size restricted to 3.0 base pairs was observed for **4.10** interacting with DNA in the absence of AA. From the similarity in the binding constants, it appears that AA does not significantly compete with DNA for **4.10**.

4.2.18 Compound 4.11 binding with DNA in the presence of 0.1 mM AA

The binding of **4.11** to DNA in the presence 0.1 mM AA was studied using UV-visible spectroscopy. The changes in absorption of **4.11** upon addition of DNA in the presence 0.1 mM AA were measured in buffer (25 mM MOPS, pH 7.0, 50 mM NaCl) at 25 °C (Figure 4.35).

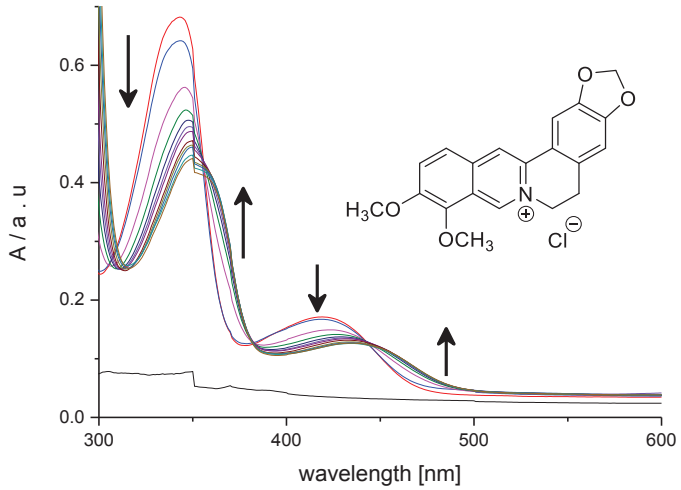

Figure 4.35: UV-visible spectra for 0.022 mM **4.11 (**red line**)** in buffer (25 mM MOPS, pH 7.0, 50 mM NaCl) in the absence of AA and subsequent spectra for **4.11** in the presence of 0.1 mM AA upon addition of 0 – 1.9 mM DNA, at 25 °C.

Figure 4.35 shows a redshift of **4.11** upon addition of DNA in the presence of 0.1 mM AA. This red shift in UV-visible absorption may occur as a result of geometrical distortion of **4.11** when it interacts with DNA in the presence of 0.1 mM AA, or as a result of the different local medium provided by the binding sites.

To quantify the affinity of **4.11** for DNA in the presence of 0.1 mM AA. The absorbances at 342 nm and 370 nm were plotted as a function of concentration of DNA in the presence of 0.1 mM AA (Figure 4.36, see Appendix, Tables A55.85).

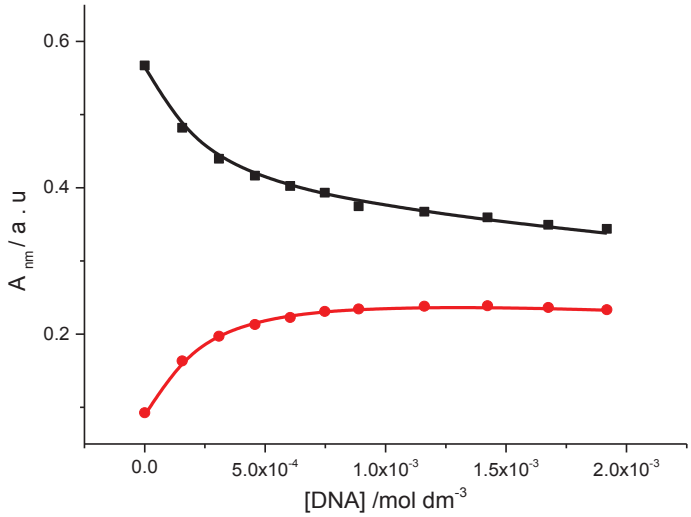

Figure 4.36: Absorbance at 343 nm and at 375 nm for 0.022 mM **4.11** as a function of DNA concentration in the presence of 0.1 mM AA, at 25 °C in buffer (25 mM MOPS, pH 7, 50 mM NaCl). The solid lines represent a global fit of a multiple independent binding sites model to the data.

The titration data in Figure 4.36 were analysed in terms of a multiple independent binding sites model, which also takes ligand dilution into account. The ligand interacts with DNA, giving an equilibrium constant $K_{binding}$ of (1.5 ± 0.08) ×10^4 M^{-1} for a binding site size restricted to 3 base pairs. A $K_{binding}$ of (1.6 ± 0.2) × 10^4 M^{-1} for a binding site size restricted to 3.0 base pairs was observed for **4.11** binding to DNA in the absence of AA. From the similarity in the binding constants, it appears that AA does not significantly compete with DNA for **4.11**.

4.2.19 Compound 4.12 binding with DNA in the presence of 0.1 mM AA

We wanted to evaluate whether **4.12** and DNA interact in the presence 0.1 mM AA. The changes in absorption of **4.12** upon addition of DNA were measured in buffer (25 mM MOPS, pH 7.0, 50 mM NaCl) at 25 °C (Figure 4.37).

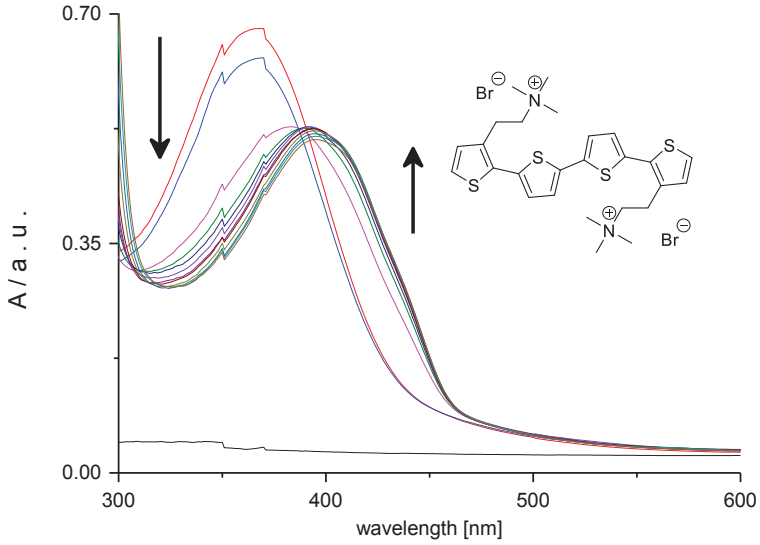

Figure 4.37: UV-visible spectra for 0.023 mM **4.12 (**red line**)** in buffer (25 mM MOPS, pH 7.0, 50 mM NaCl) in the absence of AA and subsequent spectra for **4.12** in the presence of 0.1 mM AA upon addition of 0 – 1.3 mM DNA, at 25 °C.

Figure 4.37 shows a red shift of **4.12** upon addition of DNA in the presence of 0.1 mM AA. A hypochromic shift at one wavelength that happens simultaneously to a hyperchromic shift at a higher wavelength is actually a red shift. This change in UV-visible absorption probably occurs as a result of geometrical distortion of **4.12** when it interacts with DNA, although a local medium effect may also contribute.

To quantify the affinity of **4.12** for DNA in the presence of 0.1 mM AA, the absorbance at 367 nm and 430 nm were plotted as a function of the concentration of DNA in the presence of 0.1 mM AA (Figure 4.38, see Appendix, Tables A55.86).

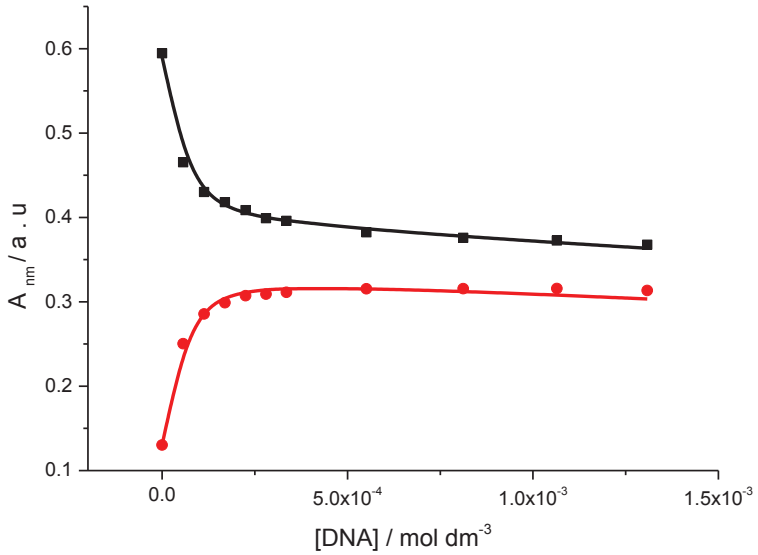

Figure 4.38: Absorbance at 367 nm (■) and at 430 nm (●) of a solution of 0.023 mM **4.12** as a function of DNA concentration in the presence of 0.1 mM AA, in buffer (25 mM MOPS, pH 7.0, 50 mM NaCl) at 25 °C. The solid lines represent a global fit of a multiple independent binding sites model to the data.

In Figure 4.38, the black line shows the decrease in the absorbance at 367 nm (■) of **4.12** upon addition of DNA in the presence of 0.1 mM AA while, the red line shows the increase in the absorbance at 430 nm (●) of **4.12** upon addition of DNA in the presence of 0.1 mM AA. The solid lines represent a global fit of the multiple independent sites model to the data. This fit also takes ligand dilution into account. The fit gives an equilibrium constant $K_{binding}$ of (1.9 ± 0.25) x 10^5 M^{-1} for a binding site size was restricted to 3.0. A $K_{binding}$ of (1.8 ± 0.34) x10^5 M^{-1} for a binding site size restricted to 3.0 base pairs was observed for **4.12** interacting with DNA in the absence of AA. From the similarity in the binding constants, it appears that AA does not significantly compete with DNA for **4.12**.

Summary

The UV-visible titrations for cationic molecules interacting with duplex DNA in the presence of AA are summarised in Table 4.6.

Table 4.6 Binding affinities and binding site sizes for binding of 4.1, 4.2, 4.4, 4.5, 4.7, 4.8, 4.10, 4.11 and 4.12 to DNA in buffer (25 mM MOPS, pH 7.0, 50 mM NaCl) at 25 °C.

Ligands	*Binding constant AA / M^{-1} N*	*Binding constant DNA / M^{-1} n*	*Binding constant DNA +AA / M^{-1} n*	*Effect of AA on affinity for DNA*
4.1	$(4.5\pm 2.4) \times 10^4$ 0.3 ± 0.1	$(1.5 \pm 0.1) \times 10^4$ n =3*a	$(7.1 \pm 1.8) \times 10^4$ n =3*a	Increase
4.2	$(6.9 \pm 1.5) \times 10^4$ n =3*	$(6.4 \pm 1.6) \times 10^4$ n =3*a	No binding	Decrease
4.4	No binding	$(5.4 \pm 0.3) \times 10^4$ n =3*	$(4.6 \pm 0.5) \times 10^4$ n =3*	No change
4.5	No binding	$(8.9 \pm 3.2) \times 10^4$ n =3*	$(4.0 \pm 0.4) \times 10^4$ n =3*	No change
4.7	No binding	$(7.7 \pm 1.5) \times 10^5$ n =3*	$(1.1 \pm 0.2)\ 10^4$ n =3* a	Decrease
4.8	No binding	$(4.4 \pm 0.5) \times 10^5$ n =3*	$(9.2 \pm 1.1) \times 10^3$ n =3*a	Decrease
4.10	No binding	$(6.9 \pm 0.7) \times 10^3$ n =3*	$(8.6 \pm 0.1) \times 10^3$ n =3*	No change
4.11	No binding	$(2.0 \pm 0.2) \times 10^4$ n =3*	$(1.7 \pm 0.1) \times 10^4$ n =3*	No change
4.12	No binding	$(1.8 \pm 0.38) \times 10^5$ n =3*	(1.9 ± 0.25) x 10^5 n =3*	No change
a) apparent binding constant for the event following initial precipitation. b) * restricted				

Table 4.6 describes the ligands that can bind to DNA in presence negative natural biopolymers alginic acid AA and the interaction is joined by changing their spectroscopic and electronic properties. Compounds **4.4, 4.5, 4.10, 4.11** and **4.12** do not show any change in affinity for

DNA in the presence of AA. From the similarity in the binding constant, it appears that AA does not significantly compete with DNA for these ligands. The decrease in binding constant of **4.7** and **4.8** to DNA means the binding between the ligands and DNA in the presence of AA is not easy like without polymer. In a biosensor, the presence of AA might, therefore, lead to a false negative for these compounds. The increasing binding constant for **4.1** means a false positive readout could occur. Compound **4.2** shows no binding to DNA in presence AA as result of strong binding between **4.2** and AA.

4.3 Conclusion

From the results that we obtained, **4.1** and **4.2** interact with both HA and AA with good binding affinity, while **4.7** and **4.8** just bind to HA. Most ligands bind to DNA in the presence of these biopolymers without any change in a binding constant, that means no effect on DNA biosensors. Three molecules, viz. **4.2, 4.7** and **4.8** show decreasing in affinity for DNA while **4.1** binds more strongly to DNA in the presence of these biopolymers.

4.4 Materials and Methods

4.4.1 Materials

A solution of the negative natural polymers hyaluronic acid HA and alginic acid AA were prepared by dissolving the solids in MOPS buffer. Natural polymers were purchased from Acros and Sigma-Aldrich. HA and AA concentrations were determined by weight using one monomer unit from polymers as molecular weight.

4.5 Solutions preparation

4.5.1 Biopolymers HA and AA preparation

All experiments were carried out in buffer (25 mM MOPS, 50 mM NaCl, pH 7.0, at 25 °C). HA and AA with high molecular weight were dissolved in MOPS buffer. To prepare different concentration, we use a molecular weight of one monomeric unit for each polymer AA and HA, then prepare the stock solution with concentrations expressed in terms of monomeric units.

4.6 Spectroscopy studies

2.0 ml of MOPS buffer was added in a 1.0 cm path length cuvette. The stock solutions of all molecules in MOPS buffer, sometimes involving 10 vol.-% DMSO were prepared as mentioned before (Section 4.2.7). All UV-visible titrations were carried out by adding aliquots of the macromolecules, such as HA and AA and DNA, stock solutions into the 1.0 cm path length cuvette which contains the ligand solution in MOPS, recording the absorption in the range of 200 - 800 nm after each addition. Absorptions were kept in the range of (0.0 - 1.0). Furthermore, when studying the effect of AA and HA on DNA - binding, the same steps were carried out as before except adding HA and AA after the ligand before continuing with the addition of DNA. The absorption at selected wavelengths were plotted against macromolecule concentrations, and a multiple independent binding sites model was used to analyse the UV-visible data using Origin 9.0 software.

Chapter Five

Effect of negatively charged synthetic polymers on DNA-binding properties of π-conjugated ligands

Abstract

Chapter five discusses the binding between negatively charged synthetic polymers (sodium polystyrene sulfonic acid POSA and polyacrylic acid PAA see Scheme 5.1) with ligands (Scheme 1.5). These interactions were studied using UV-visible spectroscopy. We also studied the effect of synthetic negative polymers on DNA binding constants $K_{binding}$ and binding site sizes n of our sensitisers. We studied this because added polymers may reduce or stop nonspecific interactions. In these systems the ligands are in equilibrium between binding with DNA or with negatively charged polymers. If binding to polymers is stronger than nonspecific binding, then we could avoid any nonspecific binding which might lead to false positives as shown in Figure 1.16. Our studies found that compounds **5.1, 5.2, 5.7** and **5.8** bind to both PAA and POSA. In contrast, cationic molecules **5.4, 5.5, 5.10** and **5.12** bind to POSA only.

We further compared the affinity of these molecules for DNA in the absence and presence of PAA and POSA. All compounds demonstrated a decrease in affinity for DNA in the presence of POSA, suggesting that potential sensitisers could bind to POSA polymer which leads to decreased apparent $K_{binding}$ and this may be a source of false negative results.

We found that ligands **5.1** and **5.7** bind to DNA in the presence of PAA and POSA. Compound **5.2** interacts with DNA in the presence of PAA with precipitation and **5.8** binds to DNA with precipitation in the presence of POSA. However, compounds **5.4, 5.10, 5.11** and **5.12** do not indicate any change in affinity for DNA in the presence of PAA. That means there is no effect of PAA on DNA biosensors. An increase in the affinity of **5.1** for DNA in the presence of POSA was also observed. This initially surprising an effect was attributed to sensitisers binding to polymers instead of to secondary binding sites on the DNA backbone and increasing the apparent $K_{binding.}$

5.1 Introduction

The binding of a sensitiser to synthetic polymers such as PAA and POSA can affect the sensitisers DNA-binding properties. Such interactions may therefore offer a new flexible method to improve biosensors with high detection sensitivity, selectivity and reduced nonspecific interaction. The advantage of using synthetic polymers is that they are easy to use and cheap. The way in which a negatively charged polymer can improve a biosensor.

The interactions between sensitisers and polymers and how these interactions affect biosensor functioning can be studied using several techniques such as UV-visible spectroscopy, isothermal titration calorimetry (ITC) and circular dichroism spectroscopy. These methods allow the study of how different parameters describing interactions of sensitisers with DNA change upon potential binding of these sensitisers to added macromolecules.

Polymers can be classified into two types according to the repeating unit that is found in the polymer. Homopolymers are made of only one kind of monomer, for example polyacrylic acid PAA Figure 5.2. If a homopolymer is linked to another homopolymer B a so-called block copolymer is formed.

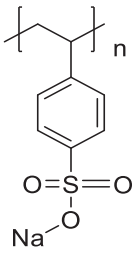

Sodium Poly styrene sulfonate (POSA)

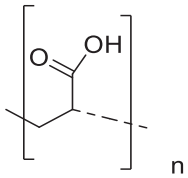

Poly acrylic acid (PAA)

Scheme 5.1: Chemical structures of POSA and PAA

We have selected two negatively charged synthetic polymers, viz POSA and PAA (Scheme 5.1), for studies. The sodium salt of Poly (4-styrene sulfonic acid) $(CH_2CHC_6H_4SO_3H)_n$ is a water-soluble polymer with a molecular weight 75000 gm/mole. Polyelectrolyte properties with high stability in water and high conductivity.[182-184] Poly acrylic acid PAA is a weak anionic polymer and polyelectrolyte with chemical formula $(C_3H_4O_2)_n$.

Homopolymer (A): PAA-PAA-PAA-PAA-PAA-PAA-PAA-PAA-PAA-PAA
Block copolymer (AB): PAA-PAA-PAA-PAA-PAA-POSA-POSA-POSA-POSA-POSA

Figure 5.2: Schematic representation of various types of synthetic polymer structures. Homopolymer (A) is formed solely of monomers of acrylic acid A. Block copolymer (AB) is formed from acrylic acid and styrene sulfonate monomers, connected as blocks.

5.2 Aim

Our objectives in Chapter five are to determine binding parameters and binding site sizes for various molecules (Scheme 1.5) interacting with POSA and PAA. Moreover, we investigate the effect of the presence of negatively charged synthetic polymers POSA and PAA on the DNA binding parameter of these molecules.

5.3 Results and Discussion

The results of the binding studies for different molecules **5.1**−**5.12** with negatively charged synthetic polymers POSA and PAA and the effect of the negatively charged polymers on DNA−binding will be shown and discussed for each compound.

Part A: POSA binding studies

5.3.1 Compounds 5.1 and 5.2 binding to POSA

We wanted to know whether **5.1** and **5.2** interact with POSA. The changes in absorption of **5.1** and **5.2** upon addition of POSA were measured in buffer (25 mM MOPS, pH 7.0, 50 mM NaCl and 10 vol-% DMSO) at 25 °C. Figure 5.1 shows the results for **5.1** see Appendix A34. We used DMSO to prevent the precipitation that often occurs when POSA interacts with molecules of opposite charge. The ratio of added DMSO was selected to keep the DNA in its duplex form[185].

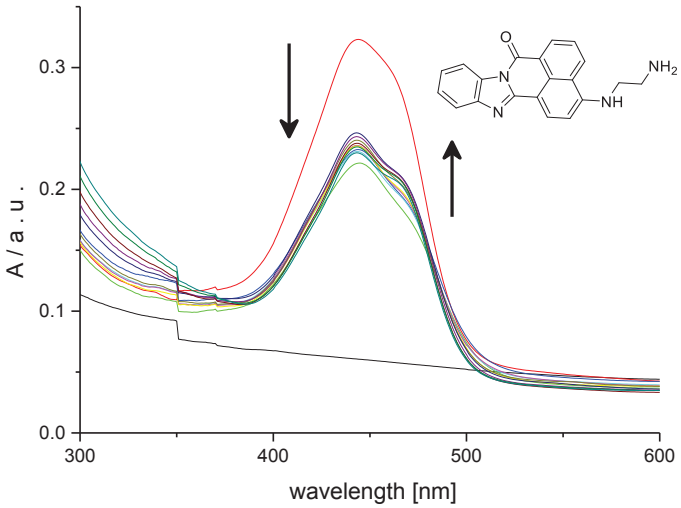

Figure 5.1: UV-visible spectra for 0.016 mM **5.1** upon addition of 0–1.9 mM POSA, at 25 °C in buffer (25 mM MOPS, pH 7.0, 50 mM NaCl and 10 vol-% DMSO).

Figure 5.1 shows a hypochromic shift in absorbance at 444 nm followed by a hyperchromic shift at 444 nm upon addition of POSA. This change in UV-visible absorption may occur as a result of geometrical distortion of **5.1** when it interacts with POSA, but it may also be a local medium effect.

To quantify the apparent affinity of **5.1** for POSA we plotted the absorbances at 444 nm as a function of the concentration of POSA (Figure 5.2, see Appendix, Tables A55.87).

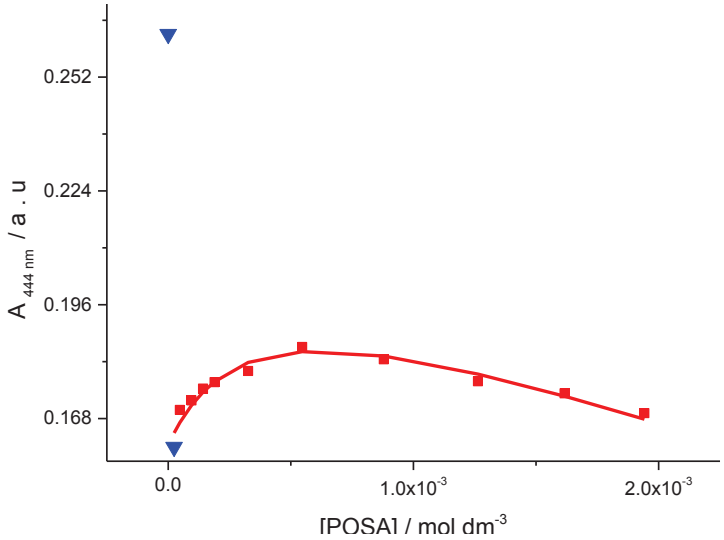

Figure 5.2: Absorbance at 444 nm for 0.016 mM **5.1** as a function of POSA concentration of 0 – 0.024 mM (▼) and 0.074–1.9 mM (■), at 25 °C in buffer (25 mM MOPS, pH 7.0, 50 mM NaCl and 10 vol-% DMSO). The solid lines represent the best fit to the data of a multiple independent binding sites model in the 0.074–1.9 mM range (■).

Figure 5.2 shows two events. The first event is a rapid decrease in absorbance upon addition of POSA. We attribute this rapid decline in absorption to strong binding of **5.1** to the POSA at low POSA / ligand ratios, leading to charge neutralisation of **5.1**-POSA complexes and eventually precipitation. This is in agreement with the changing baseline between 550 and 600 nm. The second event is accompanied by an increase in absorbance at high ratio POSA / ligand. The second phase was analysed in terms of the multiple independent binding sites model. The fit gives an apparent equilibrium constant $K_{binding}$ of (1.4 ± 7.0) $\times 10^4$ M^{-1} for a binding site size of (6.6 ± 27) monomeric units per molecule of **5.1**. The error on the binding site size was unreasonable. Therefore, the titration data were reanalysed as shown in Figure 5.4 (without the first event involved) in terms of a multiple independent binding sites models, which also takes ligand dilution into account. The fit gives an apparent equilibrium constant $K_{binding}$ of (6.8 ± 1.1) $\times 10^3$ M^{-1} for a binding site size restricted to 3.0 monomeric unites per molecule of **5.1**. Similar results were found for **5.2 i**nteracting with POSA (see appendix. Figure A34.1 and Figure A34.2, Tables A44.88).

5.3.2 Compound 5.4 binding to POSA

We also wanted to know whether **5.4** binds to POSA. The changes in absorption of **5.4** upon addition of POSA were measured in buffer (25 mM MOPS, pH 7.0, 50 mM NaCl and 10 vol-% DMSO) at 25 °C (Figure 5.3).

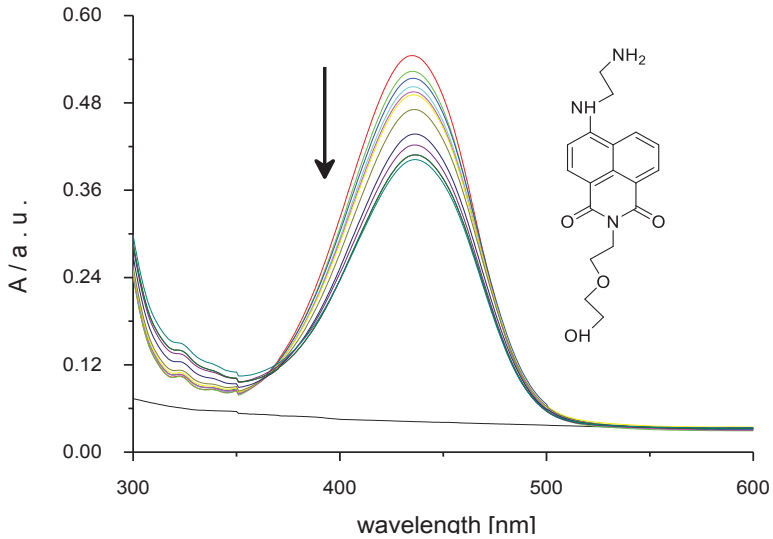

Figure 5.3: UV-visible spectra for 0.042 mM **5.4** upon addition of 0 – 2.0 mM POSA, at 25 °C in buffer (25 mM MOPS, pH 7.0, 50 mM NaCl and 10 vol-% DMSO).

Figure 5.3 shows a hypochromic shift in absorbance of **5.4** upon addition of POSA. This change in UV-visible absorption may occur as a result of geometrical distortion of **5.4** when it interacts with POSA, but it may be also a local medium effect.

To quantify the affinity of **5.4** for POSA, the absorbances at 435 nm was plotted as a function of the concentration of POSA (Figure 5.4, see Appendix, Tables A55.89).

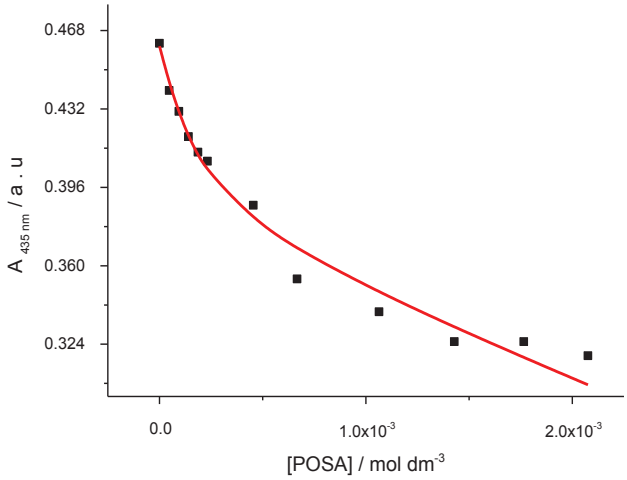

Figure 5.4: Absorbance at 435 nm for 0.042 mM **5.4** as a function of POSA concentration, at 25 °C in buffer (25 mM MOPS, pH 7.0, 50 mM NaCl and 10 vol-% DMSO). The solid line represents the best fit to the data fit in terms of a multiple independent binding sites model.

Figure 5.4 shows a decrease in the absorbance at 435 nm for **5.4** upon addition of POSA. The binding affinity $K_{binding}$ and the binding sites size n were determined by fitting a multiple independent binding sites model, which also takes ligand dilution into account, to the data. The fit gives an equilibrium constant $K_{binding}$ of (0.9 ± 2.3) $\times 10^5$ M^{-1} for a binding site size (5.7 ± 4.4) monomeric units per molecule of **5.4**. The data were reanalysed with the stoichiometry restricted to 1, giving an apparent equilibrium constant $K_{binding}$ of (7.0 ± 2.0) $\times 10^3$ M^{-1}.The stoichiometry was restricted because the fit does not provide reasonable parameters with variable stoichiometry. The fit suggests that one positive molecule of **5.4** binds with one negative monomeric unit of POSA. The positive charge on **5.4** allows electrostatic binding with negatively charged POSA.

5.3.3 Compound 5.5 binding to POSA

We wanted to study the binding of **5.5** to POSA. The changes in absorption of **5.5** upon addition of POSA were measured in buffer (25 mM MOPS, pH 7.0, 50 mM NaCl) at 25 °C (Figure 5.5).

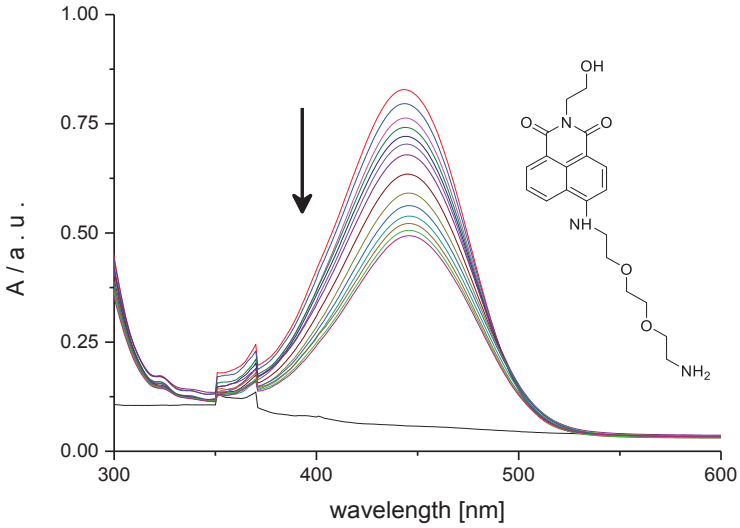

Figure 5.5: UV-visible spectra for 0.074 mM **5.5** upon addition of 0 – 0.24 mM POSA, at 25 °C in buffer (25 mM MOPS, pH 7.0, 50 mM NaCl).

Figure 5.5 shows a hypochromic shift in absorbance of **5.5** upon addition of POSA. This change in UV-visible absorption may occur as a result of geometrical distortion of **5.5** when it interacts with POSA, but it is most likely a local medium effect considering the rigidity of **5.5** and absence of a clear shift in λ_{max}.

To quantify the affinity of **5.5** for POSA, the absorbances at 443 nm was plotted as a function of the concentration of POSA (Figure 5.6, see Appendix, Tables A55.90).

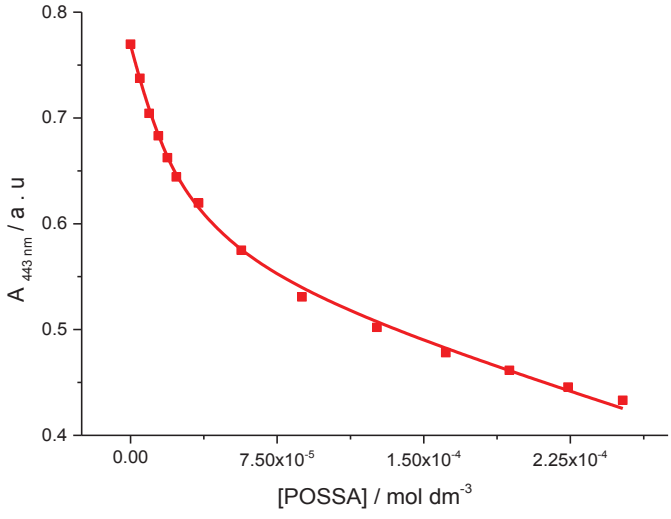

Figure 5.6: Absorbance at 443 nm for 0.074 mM **5.5** as a function of POSA concentration, at 25 °C in buffer (25 mM MOPS, pH 7.0, 50 mM NaCl). The solid lines represent the best fit to the data in terms of a multiple independent binding sites model.

Figure 5.6 shows a decrease in the absorbance at 444 nm for **5.5** upon addition of POSA. The binding affinity $K_{binding}$ and binding site size n were determined by fitting a multiple independent binding sites model, which also takes ligand dilution into account, to the data. The fit gives an equilibrium constant $K_{binding}$ of (2.0 ± 1.7) $\times 10^4$ M^{-1} for a binding site size of ($2.6\times10^{-1} \pm 8.2\times10^{-2}$) monomeric units. The obtained binding parameters were reasonable but small for binding site size. Therefore; the data were reanalysed with the stoichiometry restricted to 3.0, giving an equilibrium constant $K_{binding}$ of ($6\times10^{-1} \pm 5.6$) $\times 10^5$ M^{-1}. The obtained binding constant now has unreasonable error margin. We therefore know that **5.5** binds to POSA but binding cannot reliable be quantified. *T*he binding of **5.5** could be due to electrostatic interactions. Because of a positively charged on **5.5** lead to the electrostatic binding with negatively charged of POSA.

5.3.4 compound 5.7 binding to POSA

UV-visible spectroscopy has been used to determine the affinity and stoichiometry for **5.7** interacting with POSA; the changes in absorption of **5.7** upon addition of POSA were measured in buffer (25 mM MOPS, pH 7.0, 50 mM NaCl and 10 vol-% DMSO) at 25 °C (Figure 5.7).

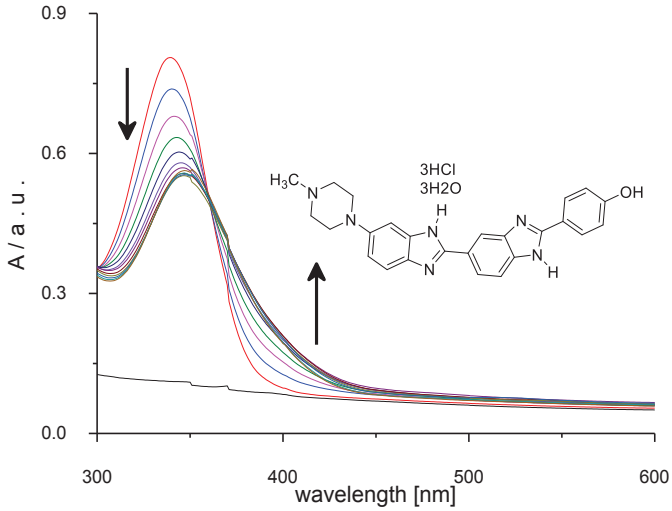

Figure 5.7: UV-visible spectra for 0.020 mM **5.7** upon addition of 0 – 0.067 mM POSA at 25 °C in buffer (25 mM MOPS, pH 7.0, 50 mM NaCl and 10 vol- % DMSO).

The isosbestic point in Figure 5.9 suggests that only two forms of the ligands are involved in the titration, *viz.* the free and bound ligand. This change in UV-visible absorption may occur as a result of geometrical distortion of **5.7** when it interacts with POSA, but it may also be a local medium effect. The observation of rapid decrease in absorbance followed by increase suggests

precipitation and subsequent dissolution of a POSA-ligand complex. This, in turn, suggests that the two-species involved in the second equilibrium are **5.7** in primary and secondary sites

To quantify the apparent affinity of **5.7** for POSA, the absorbances at 340 and 388 nm were plotted as a function of the concentration of POSA (Figure 5.8, see appendix, Tables A55.91).

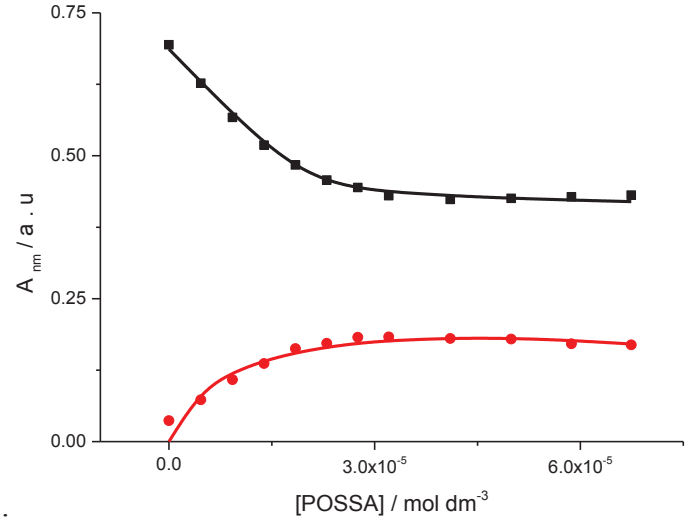

Figure 5.8: Absorbance at 340 nm (■) and at 388 nm (●) for 0.020 mM **5.7** as a function of POSA, at 25 °C in buffer (25 mM MOPS, pH 7.0, 50 mM NaCl and 10 vol-% DMSO). The solid lines represent a global fit of a multiple independent binding sites model to the data.

The titration curves in Figure 5.8 were analysed globally in terms of a multiple independent binding sites model, which also takes ligand dilution into account. The equilibrium constant $K_{binding}$ was found to be (1.6 ± 0.7) $\times 10^6$ M^{-1} for a binding site size of ($9\times10^{-1} \pm 4\times10^{-2}$). The obtained binding parameters were reasonable, although with a small stoichiometry. Therefore, the data were reanalyzed with a stoichiometry restricted to 1, giving an equilibrium constant $K_{binding}$ of (1.4 ± 0.8) × 10^6 M^{-1}. The obtained value of binding site size and affinity were reasonable, and the fit suggests that **5.7** binds strongly with POSA and has a binding site size accessible to **5.7**.

5.3.5 Compound 5.8 binding to POSA

We wanted to know the binding of **5.8** to POSA, the changes in absorption of **5.8** upon addition of POSA were measured in buffer (25 mM MOPS, pH 7.0,50 mM NaCl and 10 vol-% DMSO) at 25 °C (Figure 5.9).

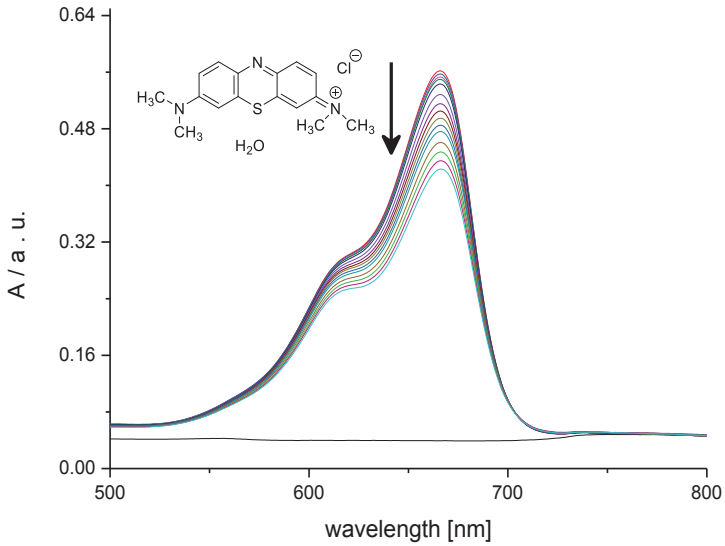

Figure 5.9: UV-visible spectra for 0.0078 mM **5.8** upon addition of 0 – 0.16 mM POSA, at 25 °C in buffer (25 mM MOPS pH 7.0, 50 mM NaCl and 10 vol-% DMSO).

Figure 5.9 shows a hypochromic shift in absorbance at 666 nm of **5.8** upon addition of POSA. This change in UV-visible absorption may occur as a result of geometrical distortion of **5.8** when it interacts with POSA, but it may also be a local medium effect.

To quantify the affinity of **5.8** for POSA, the absorbances at 666 nm was plotted as a function of the concentration of POSA (Figure 5.10, see Appendix, Tables A55.92).

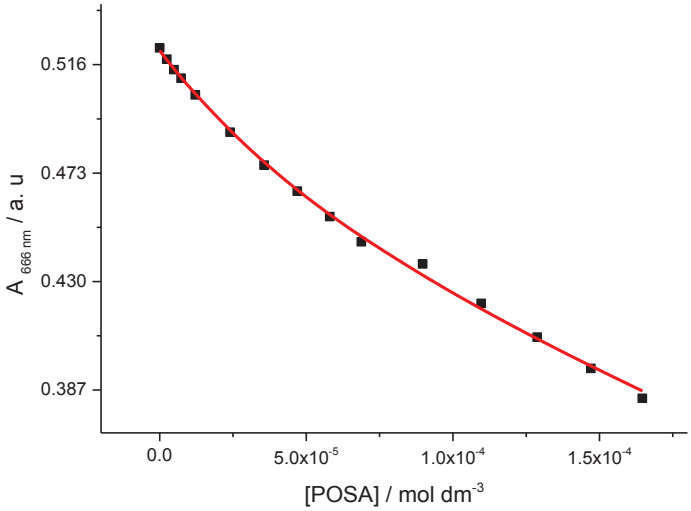

Figure 5.10: Absorbance at 666 nm for 0.0078 mM **5.8** as a function of POSA concentration, at 25 °C in buffer (25 mM MOPS, pH 7.0, 50 mM NaCl and 10 vol-% DMSO). The solid line represents the best fit to the data fit in terms of a multiple independent binding sites model.

The titration curve in Figure 5.10 was analysed in terms of a multiple independent binding sites model, which also takes simple dilution into account. The fit provides an equilibrium constant $K_{binding}$ of $(1\times10^{-2} \pm 2.4) \times10^{6}$ M^{-1} for a binding site size of $(8\times10^{-2} \pm 190)$ monomers per molecule of **5.8**. The obtained binding parameters were unreasonable for both binding constant and binding site. Size. The data were reanalysed with the stoichiometry restricted to 1 monomers per molecule of **5.8**, giving an equilibrium constant $K_{binding}$ of $(1. \pm 0.2) \times10^{4}$ M^{-1}. The fit suggests that one monomeric unit of POSA interacts with one molecule of **5.8.**

5.3.6 Compound 5.10 binding to POSA

We wanted to study the binding of **5.10** to POSA.The changes in absorption of **5.10** upon addition of POSA were measured in buffer (25 mM MOPS, pH 7.0, 50 mM NaCl) at 25 °C (Figure 5.11).

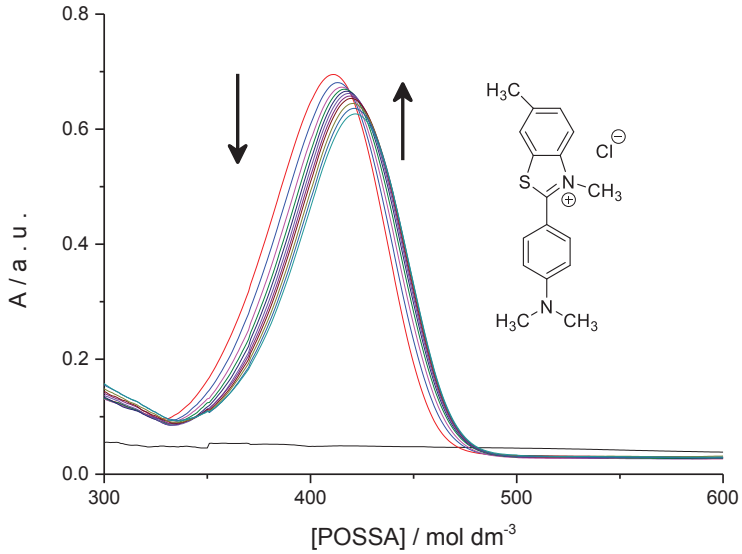

Figure 5.11: UV-visible spectra for 0.024 mM **5.10** upon addition of 0 – 0.68 mM POSA, at 25 °C in buffer (25 mM MOPS, pH 7.0, 50 mM NaCl).

Figure 5.11 shows that **5.10** exhibits a slight red-shift in absorbance of **5.10** upon addition of POSA. This redshift suggests an increase in effective conjugation length, which is attributed to increase in planarity of **5.10** upon interaction with POSA. The red-shift in absorption may have occurred as a result of geometrical distortion of **5.10** when it interacts with POSA, but it may also be as a result of a local medium effect.

To quantify the affinity of **5.10** for POSA, the absorbances at 411 and 439 nm were plotted as a function of the concentration of POSA (Figure 5.12, see Appendix, Tables A55.93).

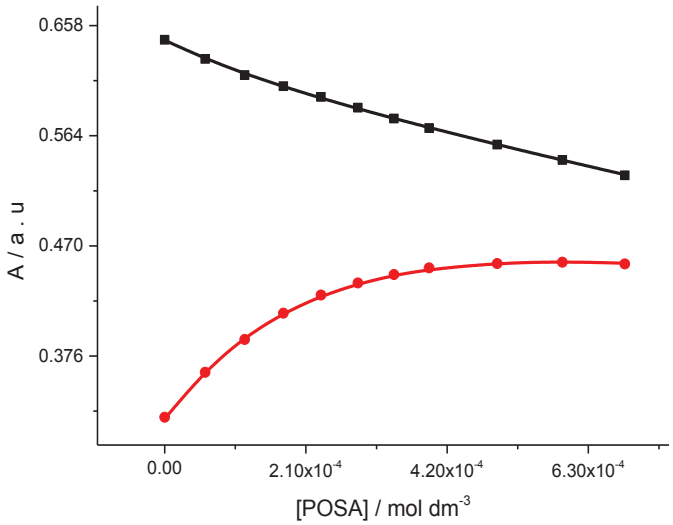

Figure 5.12: Absorbance at 411 nm (■) and 439 nm (●) for 0.024 mM **5.10** as a function of POSA concentration, at 25 °C in buffer (25 mM MOPS, pH 7.0, 50 mM NaCl). The solid lines represent a global fit of a multiple independent sites model to the data.

In the Figure 5.12, the black line shows a clear decrease in the absorbance at 411 nm (■) upon addition of POSA. The red line shows a clear increase in the absorbance of **5.10** at 439 nm (●) upon addition of POSA. The titration curves in Figure 5.14 were analysed globally by the fitting of a multiple independent binding site model of the data, which also takes simple dilution into account. The fit provides an equilibrium constant $K_{binding}$ of (3.2 ± 0.7) $\times 10^4$ M^{-1} for a binding site size of (6.1 ± 0.7) monomeric units per molecule of **5.10**. The obtained value of binding site size and affinity were reasonable; the fit suggests that **5.10** interacts with POSA

5.3.7 Compound 5.12 binding with POSA

We wanted to measure the binding of **5.12** to POSA.The changes in absorption of **5.12** upon addition of POSA were measured in buffer (25 mM MOPS, pH 7.0, 50 mM NaCl and 10 vol% DMSO) at 25 °C (Figure 5.13).

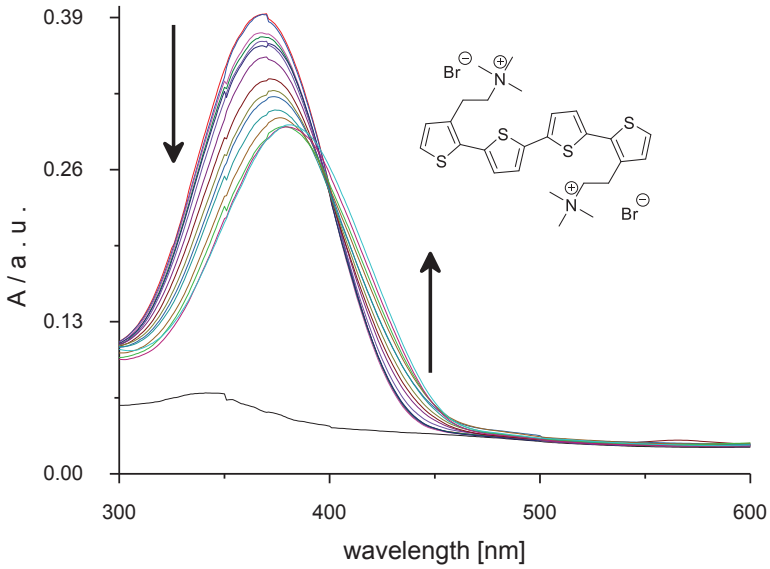

Figure 5.13: UV-visible spectra for 0.012 mM **5.12** upon addition of 0 – 0.37 mM POSA, at 25 °C in buffer (25 mM MOPS, pH 7.0, 50 mM NaCl and 10 vol-% DMSO).

Figure 5.13 shows a red-shift in absorbance of **5.12** upon addition of POSA. The change in UV-visible absorption may occur as a result of geometrical distortion of **5.12** when it interacts with POSA, but it may also be a local medium effect.

To quantify the affinity of **5.12** for POSA, the absorbances at 369 and 435 nm were plotted as a function of the concentration of POSA (Figure 5.14, see Appendix, Tables A55.94).

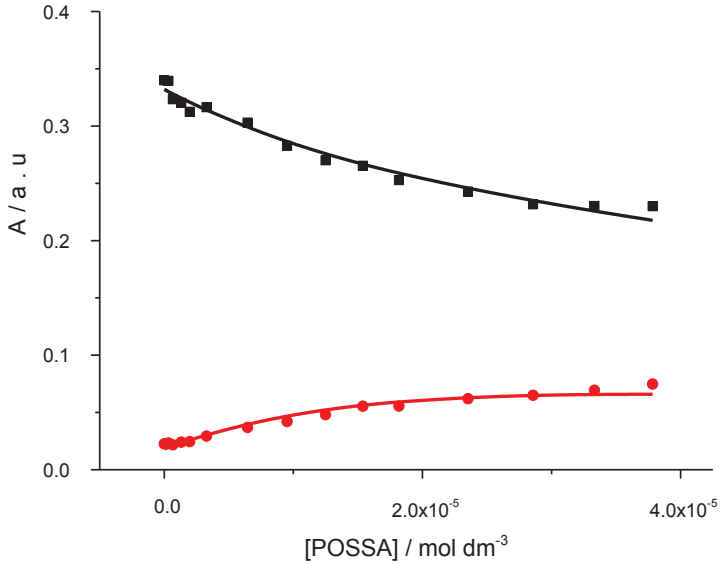

Figure 5.14: Absorbance at 369 nm (■) and at 435 nm (●) for 0.012 mM **5.12** as a function of POSA concentration, at 25 °C in buffer (25 mM MOPS, pH 7.0, 50 mM NaCl and 10 vol-% DMSO). The solid lines represent a global fit of a multiple independent sites model to the data.

Figure 5.14 shows that ligand **5.12** display a decrease in absorbance at 369 nm and an increase in absorbance at 435 nm upon addition of POSA. The absorbance at 369 nm corresponds mainly to free ligand, and the absorbance at 435 nm is dominated by the complex of POSA-ligand. Therefore, by adding more POSA, the amount of free ligand decreases as the ligand binds. The binding affinity $K_{binding}$ and a binding sites size n were determined by fitting a multiple independent binding sites model, which also takes ligand dilution into account, to the data. The fit gives an equilibrium constant $K_{binding}$ of $(3.9 \pm 7.0) \times 10^5$ M^{-1} for a binding site size of (1.3 ± 0.5) monomeric units per molecule of **5.12**. The data were reanalysed with the stoichiometry restricted to 1.0, giving an apparent equilibrium constant $K_{binding}$ of $(1.3 \pm 0.6) \times 10^5$ M^{-1}. The fit suggests that one molecule of **5.12** binds with one monomeric unit of POSA. This is in agreement with the positives charges on **5.12** leading to electrostatic binding with negatively charged of POSA.

Compound **5.11** shows no binding to POSA (see appendix A36 for compound **5.11** with POSA).

Summary

The results from UV-visible titrations for **5.1, 5.2, 5.4, 5.5, 5.7, 5.8, 5.10, 5.11** and **5.12** with POSA are summarised in Table 5.1.

Table 5.1 Binding affinities and binding site sizes for binding of 5.1, 5.2, 5.4, 5.5, 5.7, 5.8, 5.10, 5.11 and 5.12 to POSA in buffer (25 mM MOPS, pH 7.0, 50 mM NaCl) at 25 °C.

Ligands	*Binding constant for POSA* K / M^{-1}	*Binding site size* *n*
5.1	$(6.8 \pm 1.1) \times 10^3$ a	3*
5.2	$(2.2 \pm 0.8) \times 10^3$ a	3*
5.4	$(7.0 \pm 2.0) \times 10^3$	1*
5.5	$(2.0 \pm 1.1) \times 10^4$	(0.27 ± 0.08)
5.7	$(1.4 \pm 0.8) \times 10^6$	1*
5.8	$(1.4 \pm 0.2) \times 10^4$	1*
5.10	$(3.1 \pm 0.7) \times 10^4$	(6.1 ± 0.7)
5.11	No binding	
5.12	$(1.3 \pm 0.67) \times 10^5$	1*

a) apparent binding constant for the event following initial precipitation

b) ∗ restricted

Table 5.1 shows the interactions that happen between positively charged molecules and POSA. We attribute this binding to the presence of positive charges on the ammonium NH_3^+ groups of **5.1, 5.2, 5.4, 5.5, 5.7, 5.8, 5.10** and **5.12** interacting with the negative charges on POSA. The electrostatic interaction between the ammonium groups and the negative sulfate groups on

POSA are the main driving force responsible for the formation of the ligand-POSA complex. In addition, it is possible that hydrophobicity also plays a role.

Cationic conjugated oligoheteraromatics **5.1** and **5.2** interact with POSA and show two events, with a high ligands / POSA ratio leading to a sharp decrease in absorbances as result of precipitation of ligand-POSA complexes. The next event at low concentration of ligand and high concentration of POSA leads to an increase in absorbance where the ligands bind to the main binding sites of POSA.

The highest affinity is observed for the complex of POSA **5.7** and **5.12,** with a binding constant 10^5 M^{-1}. We attribute this high affinity to the presence of more positive charges and aromatics rings in these molecules, which lead to an increase in electrostatic interactions and hydrophobic interactions between ligands and POSA. The weakest binders are **5.1**−**5.2** with apparent binding constant ~ 10^3 M^{-1}. These low affinities of **5.1**−**5.2** for POSA may be attributed to precipitation and subsequent dissolution of a POSA-ligand complex, leading to decreased apparent affinity.

In contrast, compound **5.11** does not show any affinity for POSA. We might attribute this to the presence of negative charges on COO^- which leads to electrostatic repulsion between **5.11** and POSA. This indicate that the electrostatic repulsion is stronger than the hydrophobic interaction between **5.11** and POSA.

Part B: Effect of POSA on DNA-binding properties

5.3.8 Compounds 5.1 and 5.2 binding with DNA in the presence of 0.1 mM POSA

We wanted to evaluate the binding of **5.1** and **5.2** with DNA in the presence of 0.1 mM POSA. The changes in absorption of **5.1** upon addition of DNA in the presence of 0.1 mM POSA were measured in buffer (25 mM MOPS, pH 7.0, 50 mM NaCl) at 25° C (Figure 5.15). A similar experiment for compound **5.2** was carried out with DNA in the presence of POSA (see appendix A37. Figure A37.1 and Figure A37.2, Table A55.98).

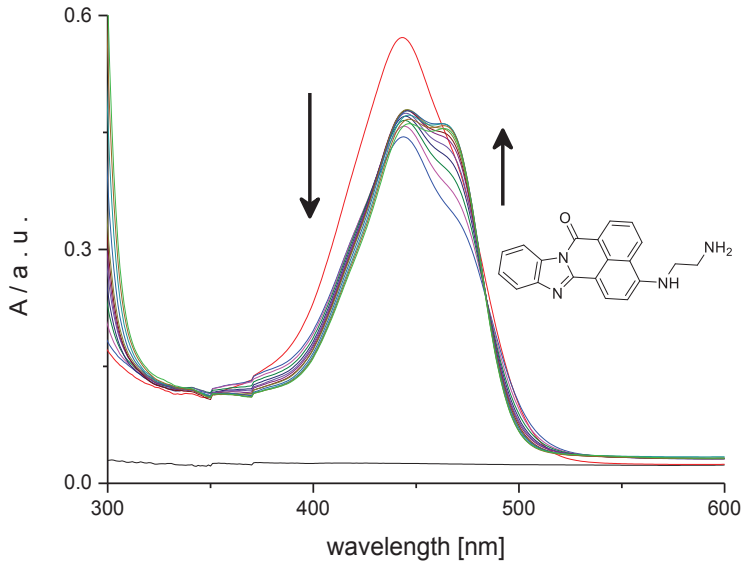

Figure 5.15: UV-visible spectra for 0.034 mM **5.1 (**red line**)** in buffer (25 mM MOPS, pH 7.0, 50 mM NaCl) in the absence of POSA and subsequent spectra for **5.1** in the presence of 0.1 mM POSA and upon addition of 0 – 1.5 mM DNA, at 25 °C.

Figure 5.15 shows two events. The first event involves a hypochromic shift in absorbance at 443 nm upon addition of POSA. The second event involved a hyperchromic shift at 443 nm upon addition of DNA. The isosbestic point for the second event indicates that two forms of the DNA binder are involved in the titration during the second event. The change in UV-visible absorption may occur as a result of geometrical distortion of **5.1** when it interacts with DNA in the presence of POSA, but it may also be a local medium effect. The observation of a rapid decrease in absorbance followed by an increase suggests precipitation and subsequent dissolution of DNA-ligand complex in the presence of 0.1 mM POSA. This, in turn, suggests that the two-species involved in the second equilibrium are **5.1** bound to POSA and **5.1** bound to DNA.

To quantify the apparent affinity of **5.1** for DNA in the presence of 0.1 mM POSA, the absorbances at 443 nm were plotted as a function of the concentration of DNA in the presence of 0.1 mM POSA (Figure 5.16, Table A55.97).

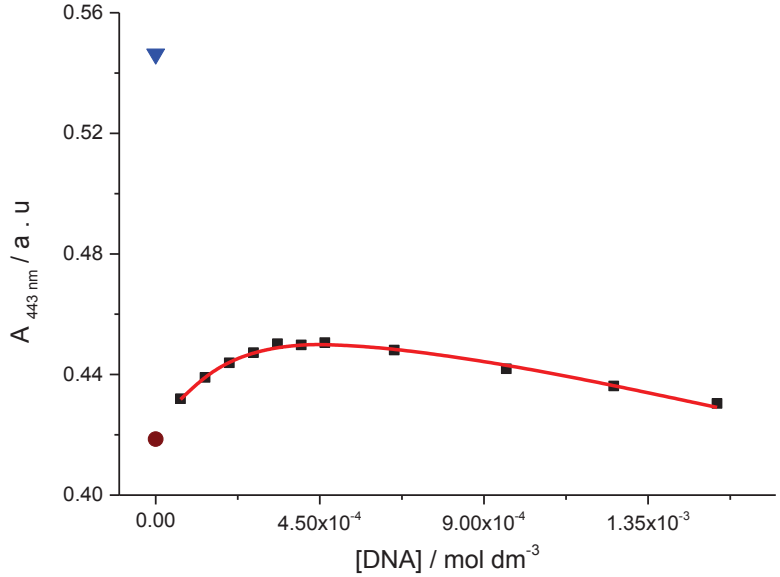

Figure 5.16: Absorbance at 443 nm for 0.034 mM **5.1** in absence of POSA (▼) and subsequent spectra for **5.1** in the presence of POSA (●) and upon addition of DNA concentration of 0.067 – 1.5 mM (■), at 25 °C in buffer (25 mM MOPS, pH 7, 50 mM NaCl). The solid red line represents a fit of a multiple independent sites model to the data in the 0.067 – 1.5 mM range (■).

Figure 5.16 shows two events. The first event corresponds to the large initial decrease in the absorbance upon addition of 0.1 mM POSA (●). We attribute this decrease in absorbance to strong binding of **5.1** to POSA, leading to precipitation as a result of charge neutralisation of the **5.1**− POSA complex as also observed previously when titrating **5.1** with POSA in the absence of DNA. A similar initial precipitation occurs when titrating **5.1** with DNA in the absence of POSA.[172] The second event shows a clear increase in the absorbance of **5.1** upon addition of DNA (■) in the presence of 0.1 mM of POSA. The ligand interacts with DNA, giving an apparent equilibrium constant $K_{binding}$ of (1.7 ± 3.0) $\times 10^4$ M^{-1} for a binding site size of (2.8 ± 4.31) base pairs. A $K_{binding}$ of (1.5 ± 0.1) $\times 10^4$ M^{-1} for the binding site size restricted to 3.0 base pairs was observed for **5.1** binding to DNA in the absence of POSA[172]. Therefore, the data were reanalysed with the stoichiometry restricted to 3.0 base pairs to allow comparison, giving an apparent equilibrium constant $K_{binding}$ of (1.8 ± 0.14) $\times 10^4$ M^{-1}. From the similarity in the apparent binding constant in the absence of POSA[172] and in the presence of POSA, it appears that POSA does not significantly compete with DNA for **5.1**. This observation

suggesting that **5.1** binding to POSA is similar to **5.1** binding non-selectively to the phosphate ester backbone of DNA.

5.3.9 Compound 5.4 binding with DNA in the presence of 0.1 mM POSA

We wanted to know whether of the binding of **5.4** with DNA is affected by the presence of 0.1 mM POSA. The changes in absorption of **5.4** upon addition of DNA were measured in buffer (25 mM MOPS, pH 7.0, 50 mM NaCl) at 25° C in the presence of 0.1 mM POSA (Figure 5.17).

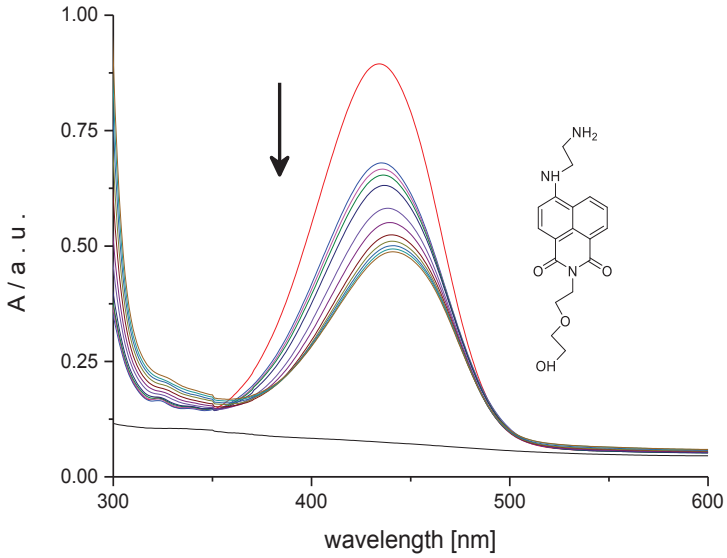

Figure 5.17: UV-visible spectra for 0.076 mM **5.4 (**red line**)** in buffer (25 mM MOPS, pH 7.0, 50 mM NaCl) in the absence of POSA and subsequent spectra for **5.4** in the presence of 0.1 mM POSA upon addition of 0 – 1.9 mM DNA, at 25 °C.

Figure 5.17 shows that **5.4** displays a hypochromic shift in its absorbance upon addition of DNA in the presence of 0.1 mM POSA with a maximum change in absorbance at 434 nm. This decrease in UV-visible absorption may have occurred as a result of geometrical distortion of **5.4** when it interacts with DNA, but it may also be as a result of a local medium effect.

To quantify the affinity of **5.4** for DNA in the presence of 0.1 mM POSA, the absorbances at 434 nm were plotted as a function of the concentration of DNA in the presence of 0.1 mM POSA (Figure 5.18, Table A55.99).

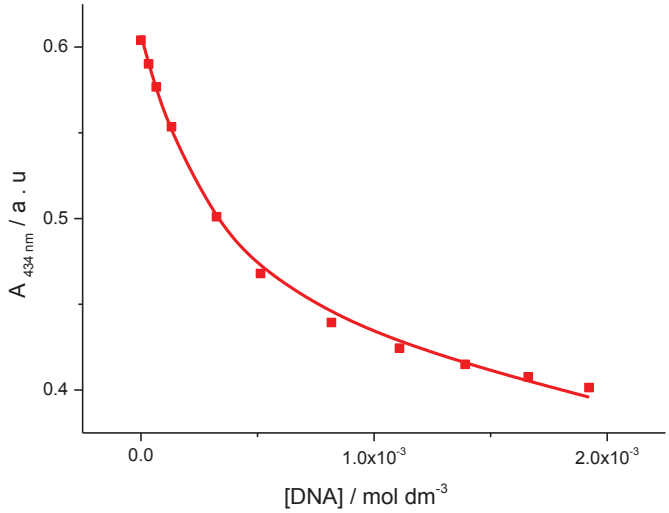

Figure 5.18: Absorbance at 434 nm for 0.076 mM **5.4** as a function of DNA concentration of 0 – 1.9 mM, in the presence of 0.1 mM POSA at 25 °C in buffer (25 mM MOPS pH 7, 50 mM NaCl). The solid line represents the best fit to the data fit in terms of a multiple independent binding sites model.

Figure 5.18 shows a clear decrease in the absorbances at 434 nm upon addition of DNA in the presence of 0.1 mM POSA. The binding affinity $K_{binding}$ and binding sites n were determined by fitting a multiple independent binding sites model, which also takes ligand dilution into account, to the data. A binding constant $K_{binding}$ of (9.1 ± 3.0) $\times 10^4$ M^{-1} for a binding site size of (5.7 ± 0.5) base pairs was found. A $K_{binding}$ of (5.3 ± 0.2) $\times 10^4$ M^{-1} for a binding site size restricted to 3.0 base pairs was observed for **5.4** interacting with DNA in the absence of POSA. Therefore, the data were reanalysed with the stoichiometry restricted to 3.0 base pairs to allow comparison, giving an apparent equilibrium constant $K_{binding}$ of (1.9 ±0.28) $\times 10^4$ M^{-1}. From the difference in the binding constants in the presence and absence of POSA, it appears that POSA competes with DNA for **5.4**. The presence of competition is beneficial because it could reduce a non-specific interaction, but it may also cause a false negative.

5.3.10 Compound 5.5 binding with DNA in the presence of 0.5 mM POSA

We studied the interactions of **5.5** with DNA in the presence of 0.5 mM POSA. The changes in absorption of **5.5** upon addition of DNA were measured in buffer (25 mM MOPS, pH 7.0, 50 mM NaCl) at 25 °C (Figure 5.19).

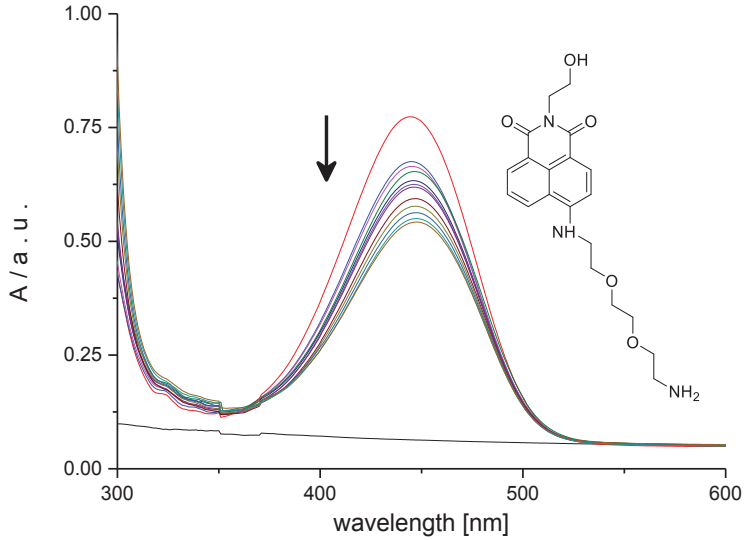

Figure 5.19: UV-visible spectra for 0.098 mM **5.5 (**red line**)** in buffer (25 mM MOPS, pH 7.0, 50 mM NaCl) in the absence of POSA and subsequent spectra for **5.5** in the presence of 0.5 mM POSA upon addition of 0 – 1.7 mM DNA, at 25 °C.

Figure 5.19 shows that **5.5** displays a hypochromic shift in absorbance upon addition of DNA in the presence of 0.5 mM POSA, with maximum change in absorbance at 444 nm. This decrease in UV-visible absorption may have occurred as a result of geometrical distortion of **5.5** when it interacts with DNA in the presence of 0.5 mM POSA, but it may also be as a result of a local medium effect.

To quantify the affinity of **5.5** for DNA in the presence of 0.5 mM POSA, the absorbances at 444 nm were plotted as a function of the concentration of DNA in the presence of 0.5 mM POSA (Figure 5.20, see appendex Table A55.100).

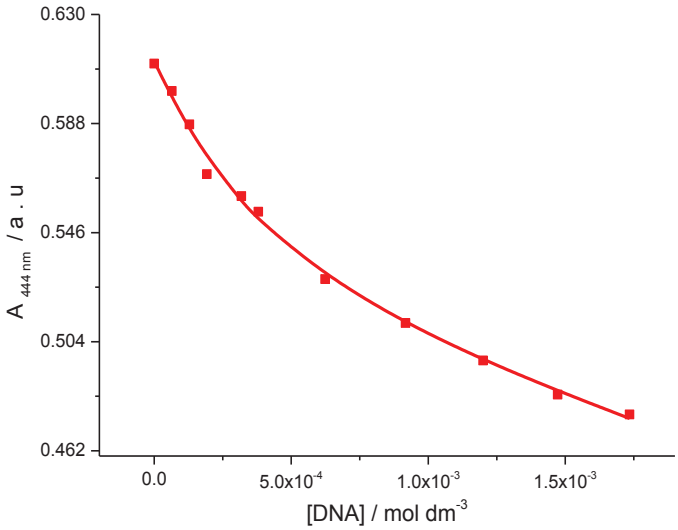

Figure 5.20: Absorbance at 444 nm for 0.098 mM **5.5** as a function of DNA concentration of 0 – 1.7 mM, in the presence of 0.1 mM POSA, at 25 °C in buffer (25 mM MOPS pH 7, 50 mM NaCl). The solid line represents the best fit to the data fit in terms of a multiple independent binding sites model.

Figure 5.20 shows that interaction of **5.5** with DNA produces a hypochromic shift at 444 nm in the UV-visible spectrum. Titration curves were extracted from the data in Figure 5.22, and these were analysed in terms of a multiple independent binding sites model, which also takes ligand dilution into account. A binding constant $K_{binding}$ of (1.0 ± 1.7) $\times 10^4$ M^{-1} for a binding site size of (2.62 ± 2.63) base pairs was found. A $K_{binding}$ of (8.9 ± 2.3) $\times 10^4$ M^{-1} for the binding site size restricted to 3.0 base pairs was previously observed for **5.5** interacting with DNA in the absence of POSA. Therefore, the data were reanalysed with the stoichiometry restricted to 3.0 base pairs to allow comparison, giving an apparent equilibrium constant $K_{binding}$ of (1.3 ± 0.3) $\times 10^4$ M^{-1}. From the difference in binding constants in the presence and absence of POSA, it appears that POSA competes with DNA for **5.5**.

5.3.11 Compound 5.7 binding with DNA in the presence of 0.1 mM POSA

We wanted to quantify the binding of **5.7** with DNA in the presence of 0.1 mM POSA. The changes in absorption of **5.7** upon addition of DNA were measured in buffer (25 mM MOPS, pH 7.0, 50 mM NaCl) at 25° C in the presence of 0.1 mM POSA (Figure 4.21).

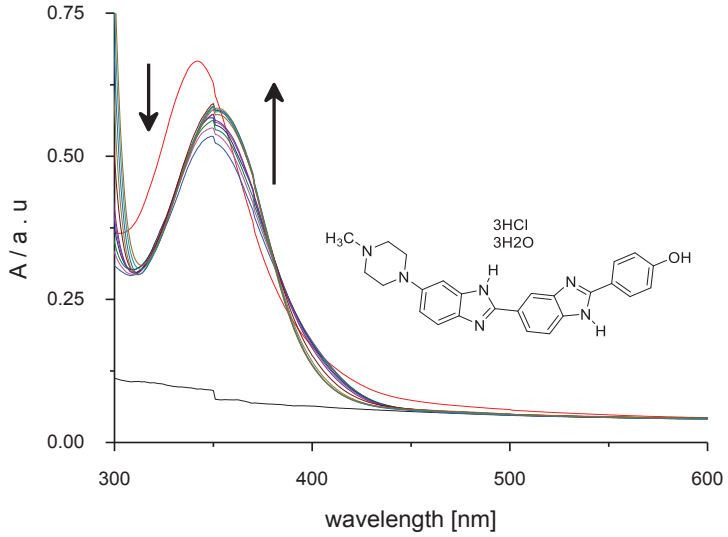

Figure 5.21: UV-visible spectra for 0.017 mM **5.7 (**red line**)** in buffer (25 mM MOPS, pH 7.0, 50 mM NaCl) in the absence of POSA and subsequent spectra for **5.7** in the presence of 0.1 mM POSA upon addition of 0 – 2.0 mM DNA, at 25 °C.

Figure 5.21 shows a hypochromic shift in absorbance at 339 nm upon addition of 0.1 mM POSA followed by a hyperchromic shift at 339 nm upon addition of DNA in the presence of 0.1 mM POSA. This change in UV−visible absorption may occur as a result of geometrical distortion of **5.7** when it interacts with DNA, but it may also be a local medium effect. This observation suggests precipitation of a POSA-ligand complex and subsequent dissolution of a DNA−ligand complex in the presence of 0.1 mM POSA.

To quantify the apparent affinity of **5.7** for DNA, the absorbances at 339 nm were plotted as a function of the concentration of DNA (Figure 5.22, Table A55.101).

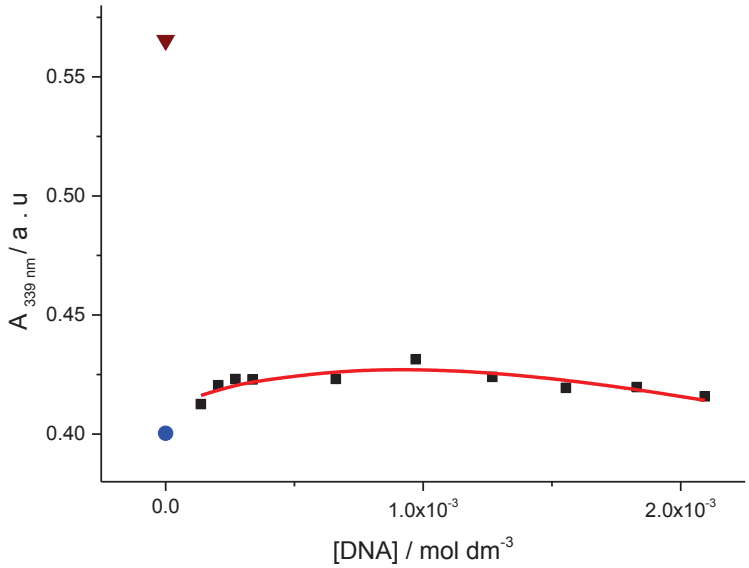

Figure 5.22: Absorbance at 339 nm for 0.017 mM **5.7** in the absence of POSA (▼) and subsequent spectra for **5.7** in the presence of POSA (●) and upon addition of DNA concentration of 0.068 – 1.8 mM DNA (■), at 25 °C in buffer (25 mM MOPS, pH 7, 50 mM NaCl). The solid line represents the best fit of a multiple independent binding sites model to the data in the 0.068 – 1.8 mM DNA range (■).

Figure 5.22 shows two events. The first event shows a decrease in the absorbance upon addition 0.1 mM POSA (●). We attribute this decrease in absorbance to strong binding of **5.7** to POSA which as result of charge neutralisation, leads to precipitation. The second binding event shows a clear increase in the absorbance of **5.7** upon addition of 0.068–1.8 mM DNA (■) in the presence of 0.1 mM of POSA. The ligand interacts with DNA, giving an apparent equilibrium constant $K_{binding}$ of $(0.004 \pm 4.5) \times 10^5$ M^{-1} for a binding site size (0.6 + 710) base pairs. A $K_{binding}$ of $(7.7 \pm 1.5) \times 10^5$ M^{-1} for a binding site size restricted to 3.0 base pairs was observed for **5.7** binding to DNA in the absence of POSA. Therefore, the data were reanalysed with the stoichiometry restricted to 3.0 base pairs to allow comparison, giving an apparent equilibrium constant $K_{binding}$ of $(1.9 \pm 0.9) \times 10^3$ M^{-1}. From the big difference in binding constants in the presence and absence of POSA, it appears that POSA does significantly compete with DNA for **5.7**. The presence of this competition is beneficial because it could reduce non-specific binding events.

5.3.12 Compound 5.8 binding with DNA in the presence of 0.1 mM POSA

We wanted to study the binding of **5.8** with DNA in the presence of 0.1 mM POSA. The changes in absorption of **5.8** upon addition of DNA were measured in buffer (25 mM MOPS, pH 7.0, 50 mM NaCl) at 25°C in the presence of 0.1 mM POSA (Figure 5.23).

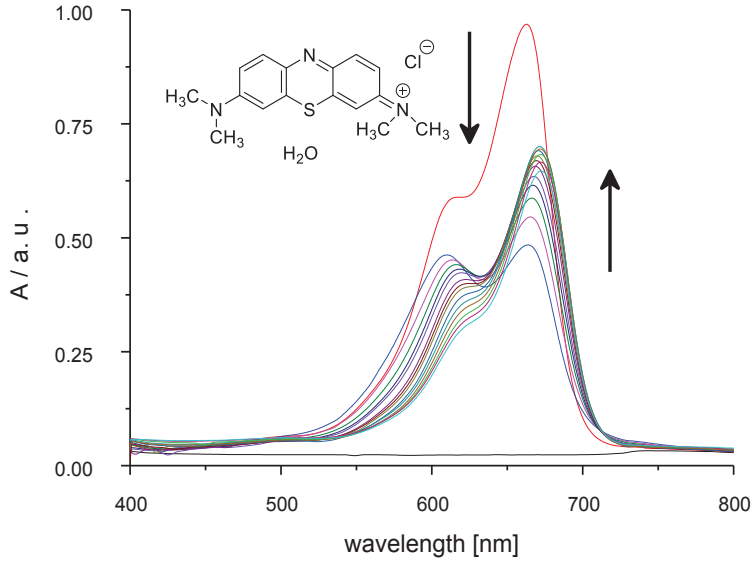

Figure 5.23: UV-visible spectra for 0.017 mM **5.8 (**red line**)** in buffer (25 mM MOPS, pH 7.0, 50 mM NaCl) in the absence of POSA and subsequent spectra for **5.8** in the presence of 0.1 mM POSA upon addition of 0 – 2.7 mM DNA, at 25 °C.

Figure 5.23 shows a red shift in absorbance at 663 nm upon addition of 0.1 mM POSA followed by a hyperchromic shift at 663 nm upon addition of DNA in the presence of 0.1 mM POSA. This change in UV-visible absorption may occur as a result of geometrical distortion of **5.8** when it interacts with DNA, but it may also be a local medium effect. This observation suggests precipitation of **5.8**-POSA and subsequent dissolution of a DNA-ligand complex in the presence of 0.1 mM POSA.

To quantify the affinity of **5.8** for DNA, the absorbance at 663 nm was plotted as a function of the concentration of DNA (Figure 5.24, see Appendix, Tables A55.102).

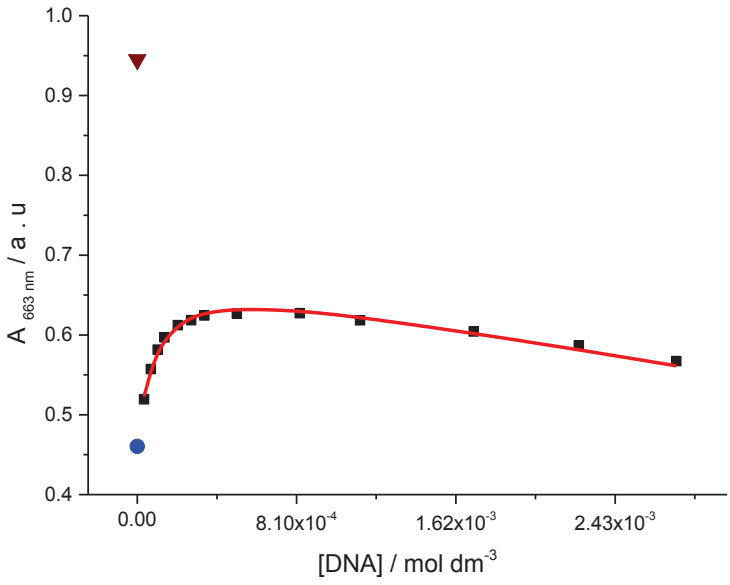

Figure 5.24: Absorbance at 663 nm for 0.014 mM **5.8** in the absence of POSA (▼) and subsequent spectra for **5.8** in the presence of 0.1 mM POSA (●) and as a function of DNA concentration of 0 – 1.5 mM (■), at 25 °C in buffer (25 mM MOPS, pH 7, 50 mM NaCl). The solid line represents a fit of a multiple independent binding sites model to the data in the 0 – 1.5 mM range (■).

Figure 5.24 shows two events. The first event shows a large initial decrease in the absorbance upon addition 0.1 mM POSA (●). We attribute this decrease in absorbance to strong binding of **5.8** to POSA, leading to precipitation as a result of charge neutralization of the **5.8**–POSA complex. The second binding event shows a clear increase in the absorbance of **5.8** upon addition of DNA (■) in the presence of 0.1 mM of POSA. The ligand interacts with DNA, giving an apparent equilibrium constant of $(4.9 \times 10^{-4} \pm 3.5 \times 10^{-1})$ M^{-1} for a binding site size of $(4.1 \times 10^{-7} \pm 2.9 \times 10^{-5})$ base pairs. A $K_{binding}$ of $(4.4 \pm 0.5) \times 10^{5}$ M^{-1} for the binding site size restricted to 3.0 base pairs was observed for **5.8** binding to DNA in the absence of POSA. Therefore, the data were reanalysed with the stoichiometry restricted to 3.0 base pairs to allow comparison, giving an apparent equilibrium constant $K_{binding}$ of $(3.7 \pm 0.4) \times 10^{4}$ M^{-1}. From the big difference in binding constant in the presence and absence of POSA, it appears that POSA does significantly compete with DNA for **5.8**. The presence of competition is beneficial because it could reduce non-specific binding.

5.3.13 Compound 5.10 binding with DNA in the presence of 0.5 mM POSA

We wanted to quantify the binding of **5.10** with DNA in the presence of 0.5 mM POSA. The changes in absorption of **5.10** upon addition of DNA were measured in buffer (25 mM MOPS pH 7.0, 50 mM NaCl) at 25° C in the presence of 0.5 mM POSA (Figure 5.25).

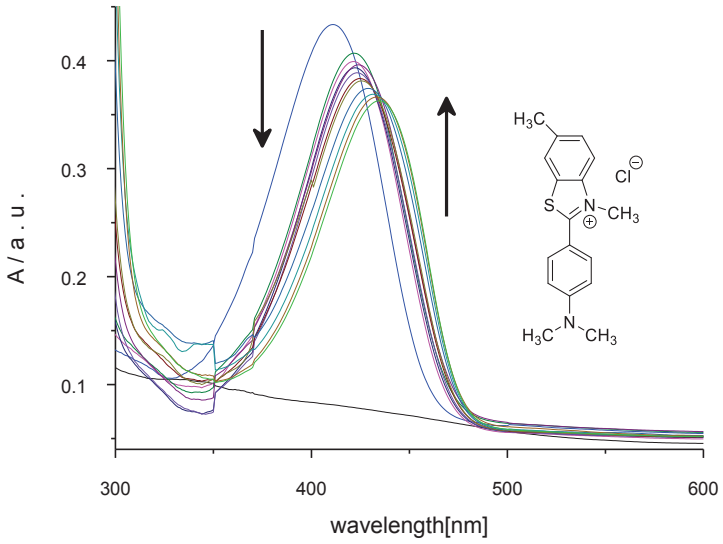

Figure 5.25: UV-visible spectra for 0.013 mM **5.10 (**blue line**)** in buffer (25 mM MOPS, pH 7.0, 50 mM NaCl) in the absence of POSA and subsequent spectra for **5.10** in the presence of 0.5 mM POSA upon addition of 0 – 1.5 mM DNA, at 25 °C.

Figure 5.25 shows a redshift in absorbance of **5.10** upon addition of DNA in the presence of 0.5 mM POSA. This change in UV-visible absorption may occur as a result of geometrical distortion of **5.10** when it interacts with DNA, but it may also be a local medium effect.

To quantify the affinity of **5.10** for DNA in the presence of 0.5 mM POSA, the absorbances at 411nm and 425 nm were plotted as a function of the concentration of DNA (Figure 5.26, see Appendix, Tables A55.103).

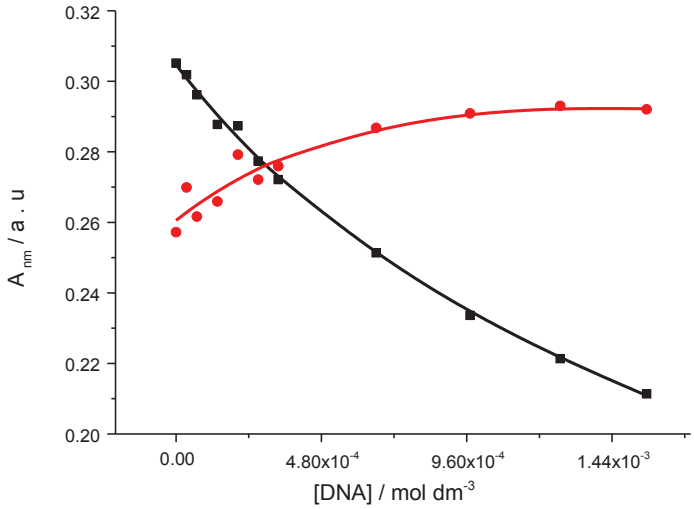

Figure 5.26: Absorbance at 411 nm (■) and at 425 nm (●) for 0.013 mM **5.10** as a function of DNA, in the presence of 0.5 mM POSA, at 25 °C in buffer (25 mM MOPS, pH 7.0, 50 mM NaCl). The solid lines represent a global fit of a multiple independent binding sites model to the data.

The values of binding affinity and binding site size were determined by fitting a multiple independent binding sites model, which also takes ligand dilution into account, to the data in Figure 5.28. The fit gives an equilibrium constant $K_{binding}$ of $(6.5\times10^{-2} \pm 9.5) \times10^{5}$ M^{-1} for a binding site size of $(9\times10^{-3} \pm 1.3) \times10^{3}$ base pairs. A $K_{binding}$ of $(6.9 \pm 0.7) \times10^{3}$ M^{-1} for a binding site size restricted to 3.0 base pairs was observed for **5.10** binding to DNA in the absence of POSA. Therefore, the data were reanalysed with the stoichiometry restricted to 3.0 base pairs to allow comparison, giving an apparent equilibrium constant $K_{binding}$ of $(2.1 \pm 0.5) \times10^{3}$ M^{-1}. From the big difference in binding constants in the presence and absence of POSA, it appears that POSA does significantly compete with DNA for **5.10**.

5.3.14 Compound 5.11 binding with DNA in the presence of 0.1 mM POSA

We wanted to know whether of **5.11** binds with DNA in the presence of 0.1 mM POSA. The changes in absorption of **5.11** upon addition of DNA were measured in buffer (25 mM MOPS, pH 7.0, 50 mM NaCl) at 25 °C in the presence of 0.1 mM POSA (Figure 5.27).

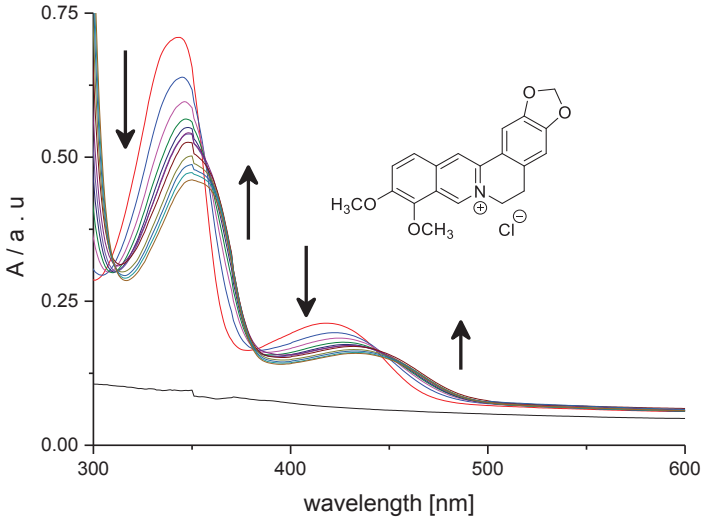

Figure 5.27: UV-visible spectra for 0.019 mM **5.11 (**red line**)** in buffer (25 mM MOPS, pH 7.0, 50 mM NaCl) in the absence of POSA and subsequent spectra for **5.11** in the presence of 0.1 mM POSA upon addition of 0 – 1.9 mM DNA, at 25 °C.

Figure 5.27 shows that **5.11** displays a red-shift in its absorbance upon addition of DNA in the presence of 0.1 mM POSA. This decrease in UV-visible absorption may have occurred as a result of geometrical distortion of **5.11** when it interacts with DNA in the presence of POSA, but it may also be as a consequence of a local medium effect.

To quantify the affinity of **5.11** for DNA in the presence of POSA, the absorbances at 343 and 375 nm were plotted as a function of the concentration of DNA (Figure 5.28, see Appendix, Tables A55.104).

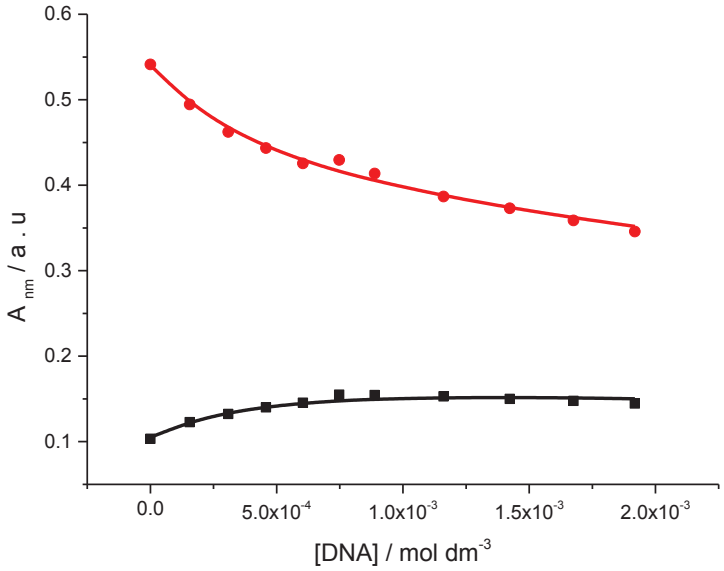

Figure 5.28: Absorbance at 343 nm and at 375 nm for 0.021 mM **5.11** as a function of DNA concentration of 0 – 1.9 mM in the presence of 0.1 mM POSA, at 25 °C in buffer (25 mM MOPS, pH 7, 50 mM NaCl). The solid lines represent the best fit to the data fit in terms of a multiple independent binding sites model.

Figure 5.28 shows a clear decrease in the absorbances at 343 nm and increase at 375 nm upon addition of DNA in the presence of POSA. The binding affinity $K_{binding}$ and binding site size *n* were determined by fitting a multiple independent binding sites model, which also takes ligand dilution into account, to the data. The fit produces a binding constant $K_{binding}$ of $(4\times10^{-4} \pm 1.7) \times10^{6}$ M^{-1} for a binding site size of $(2\times10^{-1} \pm 918)$. The obtained binding parameters were unreasonable for both stoichiometry and binding constant. Therefore, the data were reanalysed with the stoichiometry restricted to 3.0 base pairs, giving an apparent equilibrium constant $K_{binding}$ of $(6.1 \pm 0.9) \times10^{3}$ M^{-1}. A $K_{binding}$ of $(1.6 \pm 0.2) \times10^{4}$ M^{-1} for the binding site size restricted to 3.0 base pairs was observed for **5.11** binding to DNA in the absence of POSA. From the difference in binding constants in the presence and absence of POSA, it appears that POSA does significantly compete with DNA.

The same experiment was carried out with **5.12** and this showed no interactions between **5.12** and DNA in the presence of POSA (See appendix A38, Figure A38.1 and Figure A38.2, see Appendix, Tables A44.105).

Summary

The results from UV- visible titrations for these cationic compounds with DNA in the presence of POSA show that ligands **5.1, 5.2, 5.4, 5.5, 5.7, 5.8, 5.10,** and **5.11** bind to DNA in the presence of POSA (results are summarised in Table 5.2). Compound **5.12** does not show binding with DNA in the presence of POSA.

Table 5.2 Binding affinities and binding site sizes for binding of 5.1, 5.2, 5.4, 5.5, 5.7, 5.8, 5.10, 5.11 and 5.12 to POSA and effect of POSA on DNA-binding at 25 °C in buffer (25 mM MOPS, pH 7.0, 50 mM NaCl).

Ligands	*Binding constant for POSA* K/M^{-1} *n*	*Binding constant for DNA* K/M^{-1} *N*	*Binding constant for DNA+POSA* K/M^{-1} *N*	*Effect of POSA on affinity for DNA*
5.1	$(6.8 \pm 1.1) \times 10^3$ a 3*	$(1.5 \pm 0.1) \times 10^4$ 3*a	$(1.8 \pm 0.14) \times 10^4$ 3*a	No change
5.2	$(2.2 \pm 0.8) \times 10^3$ a 3*	$(6.4 \pm 1.6) \times 10^4$ 3*a	No binding	Decrease
5.4	$(7.0 \pm 2.0) \times 10^3$ 1*	$(5.3 \pm 0.2) \times 10^4$ 3*	$(1.9 \pm 0.28) \times 10^4$ 3*	Decrease
5.5	$(2.0 \pm 1.1) \times 10^4$ 0.27 ± 0.08	$(8.9 \pm 2.3) \times 10^4$ 3*	$(1.3 \pm 0.3) \times 10^4$ 3*	Decrease
5.7	$(1.4 \pm 0.8) \times 10^6$ 1*	$(7.7 \pm 1.5) \times 10^5$ 3*	$(4.5 \pm 1.6) \times 10^3$ 3*a	Decrease
5.8	$(1.4 \pm 0.2) \times 10^4$ 1*	$(4.4 \pm 0.5) \times 10^5$ 3*	$(4.2 \pm 0.3) \times 10^4$ 3*a	Decrease
5.10	$(3.1 \pm 0.7) \times 10^4$ 6.1 ± 0.7	$(6.9 \pm 0.7) \times 10^3$ 3*	$(2.1 \pm 0.5) \times 10^3$ 3*	Decrease
5.11	No binding	$(1.6 \pm 0.2) \times 10^4$ 3*	$(6.1 \pm 0.9) \times 10^3$ 3*	Decrease
5.12	$(1.3 \pm 0.67) \times 10^5$ 1*	$(1.8 \pm 0.38) \times 10^5$ 3*	No binding	Decrease

a. a) apparent binding constant for the event following initial precipitation.
b. b) * restricted.

Table 5.2 shows the interaction between π-conjugated oligoheteroaromatic molecules and DNA in the presence of POSA. **5.1, 5.7** and **5.8** interacting with DNA in the presence of POSA two events are observed. The first event occurs when the concentration of ligand is high, and the concentration of DNA is still low under these condition ligand binds to both the highest affinity binding sites and to the negative sugar-phosphate backbone of DNA. As result of that, precipitation will occur because of formation of a charge neutralised ligand-DNA complex. The second event occurs at high concentration of DNA. In this case, the ligand binds to the main binding sites, viz. in the minor groove or an intercalation sites of DNA.

The main binding forces between molecules and DNA in the presence of POSA may involve hydrophobic forces, electrostatic interactions, Van der Waals interactions and hydrogen-bonds interactions. Compound **5.1** does not show any change in affinity in the presence of POSA. The absence of this competition is beneficial if we need to use **5.1** in a biosensor. Decreases in affinity for DNA are observed for most ligands in the presence of POSA, viz. for **5.2, 5.4, 5.5, 5.7, 5.8, 5.11** and **5.12**. That means the binding between these ligands and DNA in the presence of POSA is not as easy as without polymer. For **5.2, 5.4, 5.5, 5.7, 5.8** and **5.12,** this observation is as expected, considering these ligands bind to POSA. For **5.11** this is unexpected, considering that this compound was not found to bind to POSA. From the differences in the binding constant, it appears that POSA does significantly compete with DNA for these ligands as result of strong binding to POSA. There is no binding to DNA for **5.2** and **5.12** in the presence of POSA with DNA. The presence of this competition is harmful if we need to use these compounds in a biosensor.

Part C: PAA binding studies

5.3.15 Compound 5.1 and 5.2 binding to PAA

We wanted to know whether **5.1** and **5.2** bind to PAA. The changes in absorption of **5.1** upon addition of PAA were measured in buffer (25 mM MOPS pH 7.0, 50 mM NaCl and 10 vol-% DMSO) at 25 °C (Figure 5.29).

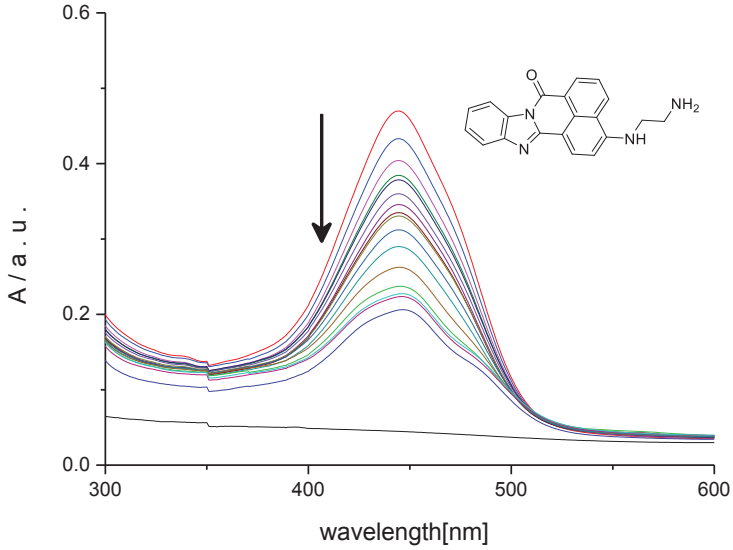

Figure 5.29: UV-visible spectra for 0.026 mM **5.1** upon addition of 0 – 0.056 mM PAA, at 25 °C in buffer (25 mM MOPS, pH 7.0, 50 mM NaCl and 10 vol-% DMSO).

Figure 5.29 shows that **5.1** displays a hypochromic shift in the absorbance upon addition of PAA with a maximum change in absorbance at 445 nm. This decrease in UV-visible absorption may have occurred as a result of geometrical distortion of **5.1** when it interacts with PAA, but it may also be as a consequence of a local medium effect.

To quantify the affinity of **5.1** for PAA, the absorbances at 445 nm were plotted as a function of the concentration of PAA (Figure 5.30, see Appendix, Tables A55.106).

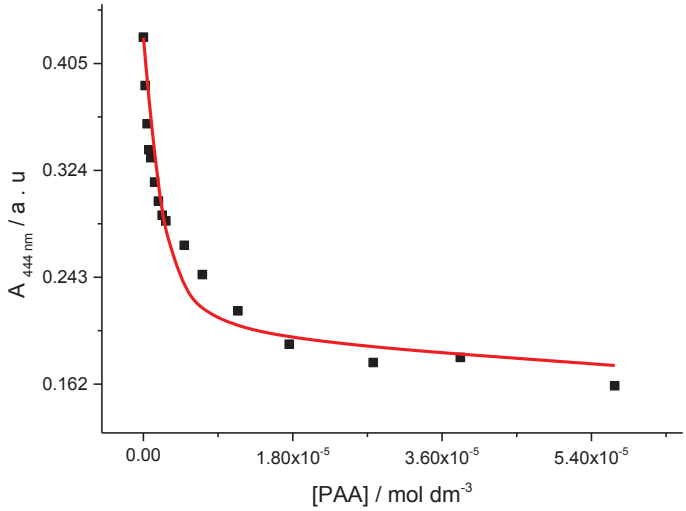

Figure 5.30: Absorbance at 445 nm for 0.026 mM **5.1** upon addition of 0 – 0.056 mM PAA, at 25 °C in buffer (25 mM MOPS, pH 7.0, 50 mM NaCl and 10 vol- % DMSO). The solid lines represent the best fit to the data fit in terms of a multiple independent binding sites model.

Figure 5.30 shows a clear decrease in the absorbances of **5.1** at 445 nm upon addition of PAA. The binding affinity $K_{binding}$ and binding sites size n were determined by fitting a multiple independent binding sites model, which also takes ligand dilution into account, to the data. The fit gives a binding constant $K_{binding}$ of $(18\times10^{-2} \pm 2.2) \times 10^4$ M^{-1} for a binding site size of $(4\times10^{-3} \pm 3\times10^{-2})$ monomeric units per molecule of **5.1**. The obtained stoichiometry was unreasonable; therefore, the data were reanalysed with a stoichiometry restricted to 0.1, giving an equilibrium constant $K_{binding}$ of $(7.3 \pm 2.6) \times10^4$ M^{-1}. The fit suggests that **5.1** interacts and that PAA has a binding site size reachable to **5.1**. Nevertheless, the binding site size is unreasonably small. We do not know why this is the case. Further experiments showed that **5.2, 5.4** and **5.5** did not show any binding with PAA (see appendixes A39 - A 41).

5.3.16 Compound 5.7 binding to PAA

We wanted to know whether **5.7** binds to PAA. The changes in absorption of **5.7** upon addition of PAA were measured in buffer (25 mM MOPS pH 7.0, 50 mM NaCl) at 25 °C (Figure 5.31).

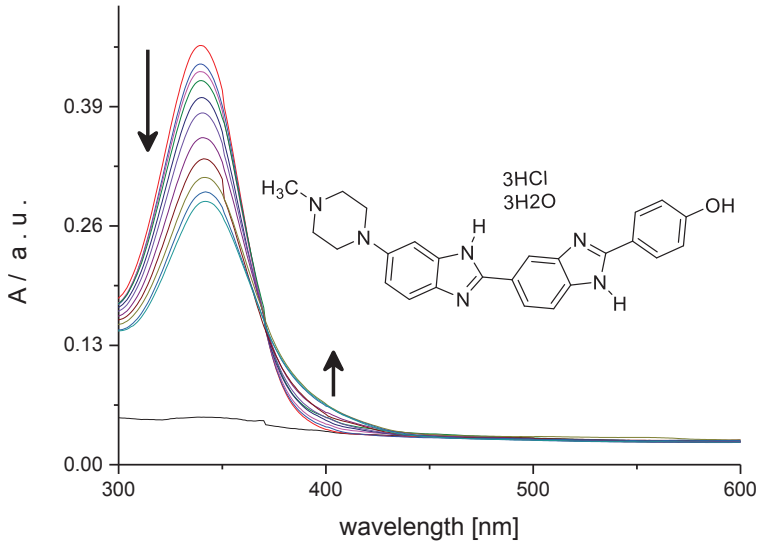

Figure 5.31: UV-visible spectra for 0.012 mM **5.7** upon addition of 0 – 0.13 mM PAA, at 25 °C in buffer (25 mM MOPS, pH 7.0, 50 mM NaCl).

Figure 5.31 shows a red shift in absorbance of **5.7** upon addition of PAA. The change in UV-visible absorption may occur as a result of geometrical distortion of **5.7** when it interacts with PAA, but it may also be a local medium effect.

To quantify the affinity of **5.7** for PAA, the absorbances at 339 and 390 nm were plotted as a function of the concentration of PAA (Figure 5.32, see Appendix, Tables A55.110).

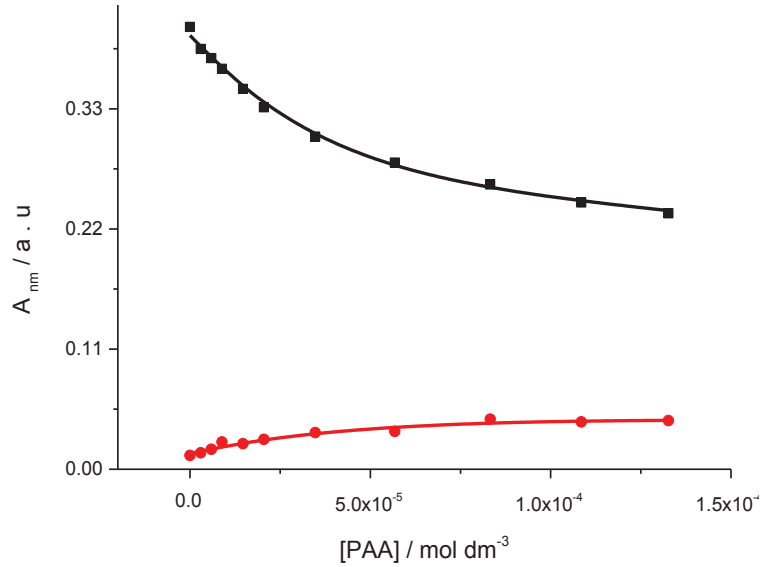

Figure 5.32: Absorbance at 340 nm (■) and at 390 nm (●) for 0.012 mM **5.7** as a function of PAA concentration, at 25 °C in buffer (25 mM MOPS, pH 7.0, 50 mM NaCl). The solid lines represent a global fit of a multiple independent sites model to the data.

The titration curves in Figure 5.32 were analysed globally in terms of a multiple independent binding sites model, which also takes ligand dilution into account, giving an equilibrium constant $K_{binding}$ of $(6\times10^{-3} \pm 1.2) \times10^{5}$ M^{-1} for a binding site size of $(2\times10^{-2} \pm 4.2)$ monomeric units per molecule of **5.7**. The obtained binding parameters were unreasonable, in particular the stoichiometry is ill-defined. Therefore, the data were reanalysed with a stoichiometry restricted to 3.0 monomeric units per molecule of **5.7**, giving an apparent equilibrium constant $K_{binding}$ of $(2.5\pm 0.58) \times10^{5}$ M^{-1}.

5.3.17 Compound 5.8 binding to PAA

We need to quantify the interactions of **5.8** with PAA. The changes in absorption of **5.8** upon addition of PAA were measured in buffer (25 mM MOPS, pH 7.0, 0 mM NaCl) at 25 °C (Figure 5.33).

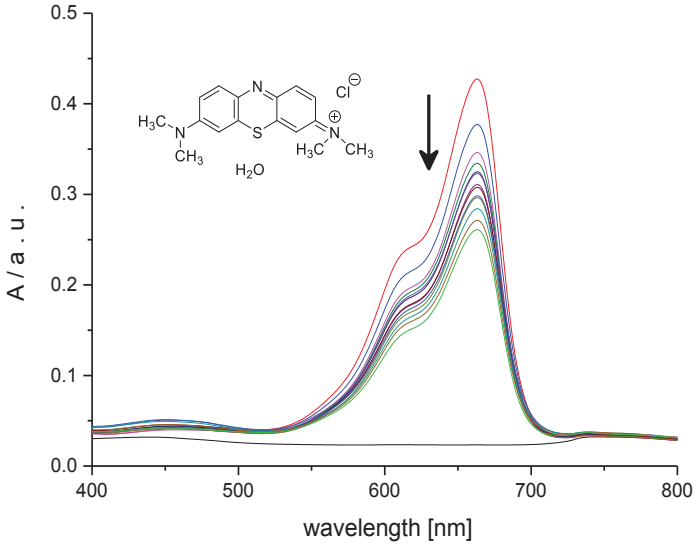

Figure 5.33: UV-visible spectra for 0.006 mM **5.8** upon addition of 0 – 1.8 mM PAA, at 25 °C in buffer (25 mM MOPS, pH 7.0, 50 mM NaCl).

Figure 5.33 displays a hypochromic shift in the absorbance upon addition of PAA, with a maximum change in absorbance at 665 nm. This decrease in UV-visible absorption may have occurred as a result of geometrical distortion of **5.8** when it interacts with PAA, but it may also be as a result of a local medium effect.

To quantify the affinity of **5.8** for PAA we plotted the absorbances at 665 nm as a function of the concentration of PAA (Figure 5.34, see Appendix, Tables A55.111).

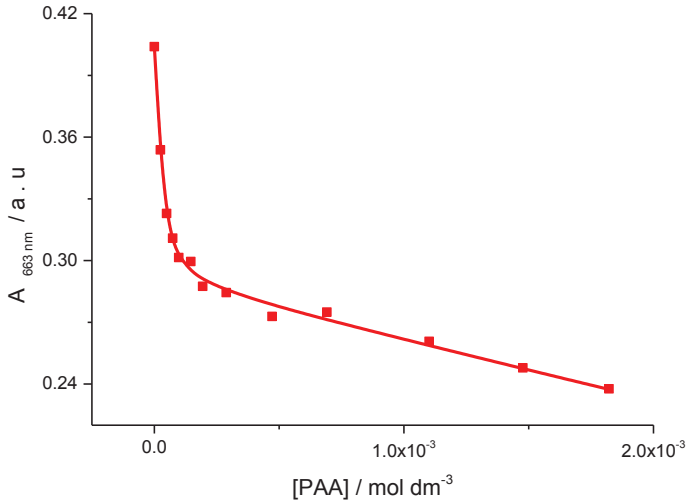

Figure 5.34: Absorbance at 665 nm for 0.006 mM **5.8** upon addition of 0 – 1.8 mM PAA concentration, at 25 °C in buffer (25 mM MOPS, pH 7.0, 50 mM NaCl). The solid lines represent the best fit to the data fit in terms of a multiple independent binding sites model.

Figure 5.34 shows a clear decrease in the absorbances at 665 nm for **5.8** upon addition of PAA. The binding affinity $K_{binding}$ and binding sites size n were determined by fitting a multiple independent binding sites model, which also takes ligand dilution into account, to the data. A binding constant $K_{binding}$ of $(6.1 \pm 2.7) \times 10^5$ M^{-1} for a binding site size of (6.4 ± 1.2) monomeric units per molecule of **5.8** was found. The fit suggests that **5.8** interacts and that PAA has a binding site reachable to **5.8**. Ligands **5.10, 5.11** and **5.12** showed no binding with PAA (See appendixes A42-A44)

Summary

The UV-visible titrations for oligoheteroaromatic compounds with PAA show that ligands **5.1, 5.2, 5.7** and **5.8** bind to PAA and the binding parameters are summarised in Table 5.3.

Table 5.3 Binding affinities and binding site sizes for binding of 5.1, 5.2, 5.4, 5.5, 5.7, 5.8, 5.10, 5.11 and 5.12 to PAA in buffer (25 mM MOPS, pH 7.0, 50 mM NaCl) at 25 °C.

Ligands	***Binding constant for PAA*** K / M^{-1}	***Stoichiometry*** N
5.1	$(7.3 \pm 2.6) \times 10^4$	0.1*
5.2	$(2.9 \pm 1.9) \times 10^5$	(0.7 ± 0.08)
5.4	No binding	
5.5	No binding	
5.7	$(2.7 \pm 0.6) \times 10^5$	3*
5.8	$(6.1 \pm 2.7) \times 10^5$	(6.4 ± 1.2).
5.10	No binding	
5.11	No binding	
5.12	No binding	
* restricted		

Table 5.3 shows that **5.1, 5.2, 5.7** and **5.8** bind to negative synthetic polymer polyacrylic acid and the interaction is accompanied by a change in optoelectronic properties of the ligands. For example, binding of several ligands to PAA is accompanied by red-shift in UV-visible absorption. This red shift suggests an increase in effective conjugation, *i.e.,* an increase in the planarity of the molecules upon interaction with PAA. We attribute the affinity for PAA to the presence of positive charge on the ammonium NH_3^+ group of **5.1, 5.2, 5.7** and **5.8** which interacts with the negative charge on the $RCOO^-$ of PAA. The electrostatic interaction between the ammonium group and the negative charged PAA are presumably the main driving forces responsible for the arrangement of ligand-PAA complex. It is possible that hydrophobicity also plays a role. However, positive compounds **5.4, 5.5, 5.10, 5.11** and **5.12** do not show any affinity for PAA, indicating that electrostatic interactions only are not enough for interaction to occur.

Part D: Effect of PAA on DNA-binding properties.

5.3.19 Compound 5.1 binding with DNA in the presence of 0.5 mM PAA

We studied the interactions of **5.1** with DNA in the presence of 0.5 mM PAA. The changes in absorption of **5.1** upon addition of DNA in the presence of 0.5 mM PAA were measured in buffer (25 mM MOPS, pH 7.0, 50 mM NaCl) at 25 °C (Figure 5.35).

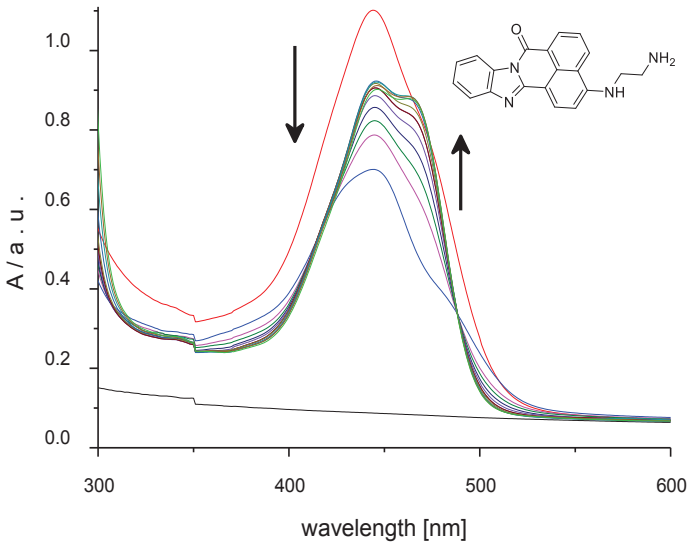

Figure 5.35: UV-visible spectra for 0.063 mM **5.1 (**red line**)** in buffer (25 mM MOPS, pH 7.0, 50 mM NaCl) in the absence of PAA and subsequent spectra for **5.1** in the presence of 0.5 mM PAA upon addition of 0 – 1.5 mM DNA, at 25 °C.

Figure 5.35 shows a hypochromic shift in absorbance at 444 nm upon addition of PAA followed by a hyperchromic shift at 444 nm upon addition of DNA in the presence of 0.5 mM PAA. This observation suggests precipitation of the **5.1**-PAA complex and subsequent dissolution of DNA-ligand complex in the presence of 0.5 mM PAA, similar to the observation in the absence of PAA. The change in UV-visible absorption during the second phase of the titration may occur as a result of geometrical distortion of **5.1** when it interacts with DNA, but it may also be a local medium effect.

To quantify the affinity of **5.1** for DNA in the presence of 0.5 mM PAA, the absorbances at 444 nm were plotted as a function of the concentration of DNA (Figure 5.36, see Appendix, Tables A55.115).

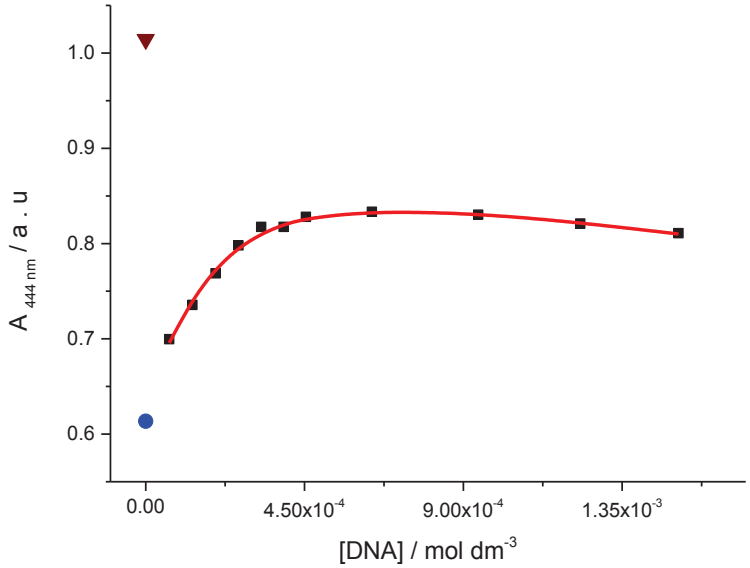

Figure 5.36: Absorbance at 444 nm for 0.063 mM **5.1** in the absence of PAA (▼) and subsequent spectra for **5.1** in the presence of 0.5 mM PAA (●) and as a function of DNA concentration of 0 – 1.5 mM (■) at 25 °C in buffer (25 mM MOPS, pH 7, 50 mM NaCl). The solid line represents the best fit to the data fit in terms of a multiple independent binding sites model in the 0 – 1.5 mM range (■).

Figure 5.36 shows two events. The first event shows a large initial decrease in the absorbance upon addition 0.5 mM PAA (●). We attribute this decline in absorbance to strong binding of **5.1** to PAA, leading to precipitation as a result of charge neutralisation of the **5.1** – PAA complexes, as also observed previously in the absence of PAA. The second event shows a clear increase in the absorbance of **5.1** upon addition of 0 – 1.5 mM (■) of DNA in the presence of 0.5 mM of PAA. The ligand strongly interacts with DNA in the presence of PAA, giving an apparent equilibrium constant $K_{binding}$ of (6.2 ± 2.6) $\times 10^4$ M^{-1} for a binding site size of (4.3 ± 0.8) base pairs. A $K_{binding}$ of (1.5 ± 0.1) $\times 10^4$ M^{-1} for a binding site size restricted to 3.0 base pairs was observed for **5.1** binding to DNA in the absence of PAA[172]. Therefore, the data were reanalysed with a stoichiometry restricted to 3.0 base pairs to compare the affinities, giving an apparent equilibrium constant $K_{binding}$ of (3.7 ± 0.4) $\times 10^4$ M^{-1}. From the difference in the apparent binding constant in the absence of PAA[172] and in the presence of PAA, it appears that PAA does significantly compete with DNA for **5.1**. Unfortunately, PAA does not help to avoid precipitation. The presence of this competition is beneficial if **5.1** were to be used in a biosensor because it can be used to stop non-specific interaction that may lead to a false positive signal. In addition, it may provide signals to detect DNA hybridization when used in biosensors.

Similar data were observed for compound **5.2** (See Appendix A45 for compound **5.2** with DNA in presence of PAA. Figure A45.1 and Figure A45.2, Tables A55.116).

5.3.20 Compound 5.4 binding with DNA in the presence of 0.7 mM PAA

We wanted to study the binding of **5.4** with DNA in the presence of 0.7 mM PAA. The changes in absorption of **5.4** upon addition of DNA were measured in buffer (25 mM MOPS, pH 7.0, 50 mM NaCl) at 25 °C (Figure 5.37).

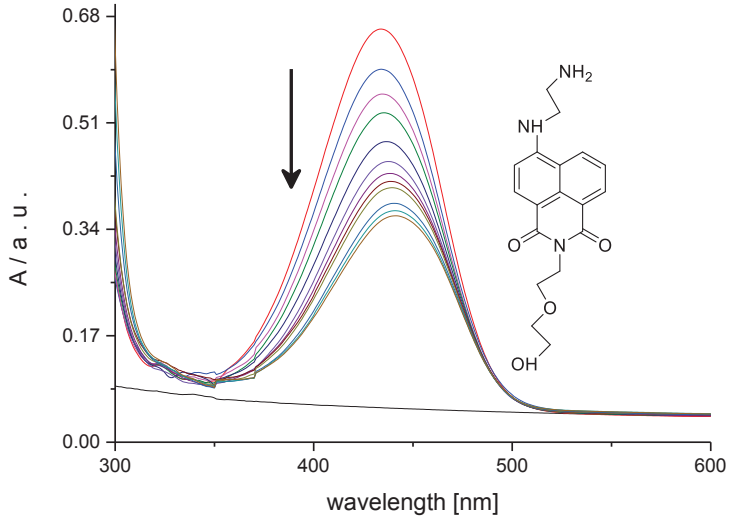

Figure 5.37: UV-visible spectra for 0.055 mM **5.4 (**red line**)** in buffer (25 mM MOPS, pH 7.0, 50 mM NaCl) in the absence of AA and subsequent spectra for **5.4** in the presence of 0.7 mM AA upon addition of 0 – 1.5 mM DNA, at 25 °C.

Figure 5.37 shows a hypochromic shift with a maximum change at 434 nm upon addition of DNA in the presence of 0.7 mM PAA. This decrease in UV-visible absorption may occur because of geometrical distortion of **5.4** when it interacts with DNA, or as a result of the different local medium affected by the binding sites.

To quantify the affinity of **5.4** for DNA in the presence of 0.7 mM PAA, the absorbances at 434 nm was plotted as a function of the concentration of DNA (Figure 5.38, see Appendix, Tables A55.117).

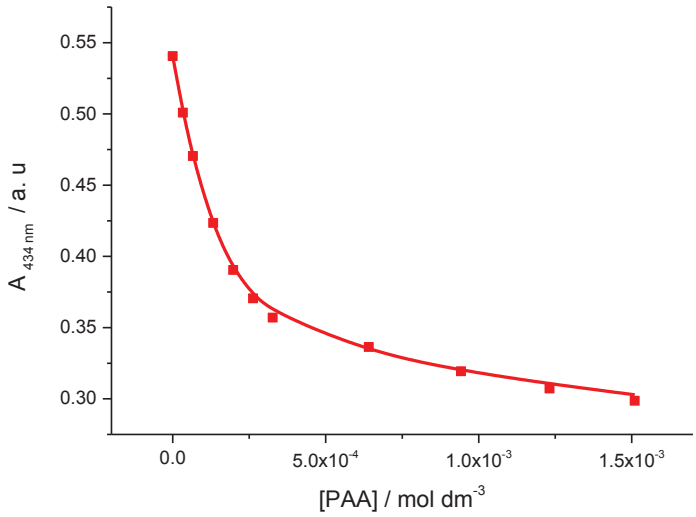

Figure 5.38: Absorbance at 434 nm for 0.055 mM **5.4** as a function of DNA concentration in the presence of 0.7 mM PAA, at 25 °C in buffer (25 mM MOPS, pH 7.0, 50 mM NaCl). The solid line represents the best fit to the data in terms of a multiple independent binding sites model.

Figure 5.38 shows a decrease in the absorbance for **5.4** upon addition of DNA in the presence of 0.7 mM PAA. The binding affinity $K_{binding}$ and binding sites size *n* were obtained by analysis of the titration curves in terms of a multiple independent binding sites model, correcting for dilution of **5.4**. The fit produces an equilibrium constant $K_{binding}$ of (4.2 ± 1.1) $\times 10^4$ M^{-1} for a binding site size of (2.3 ± 0.3) base pairs. A binding constant $K_{binding}$ of (3.4 ± 0.67) $\times 10^4$ M^{-1} for a binding site size of (2.3 ± 0.25) base pairs was found for **5.4** binding with DNA in the absence of PAA. The obtained binding parameters were reasonable for both stoichiometry and binding constant to both experiments. From the similarity in the binding constants, it appears that PAA does not significantly compete with DNA for **5.4**.

5.3.21 Compound 5.5 binding with DNA in the presence of 0.1 mM PAA

We wanted to study the binding of **5.5** with DNA in the presence of 0.1 mM PAA. The changes in absorption of **5.5** upon addition of DNA in the presence of 0.1 mM PAA were measured in buffer (25 mM MOPS, pH 7.0, 50 mM NaCl) at 25 °C (Figure 5.39).

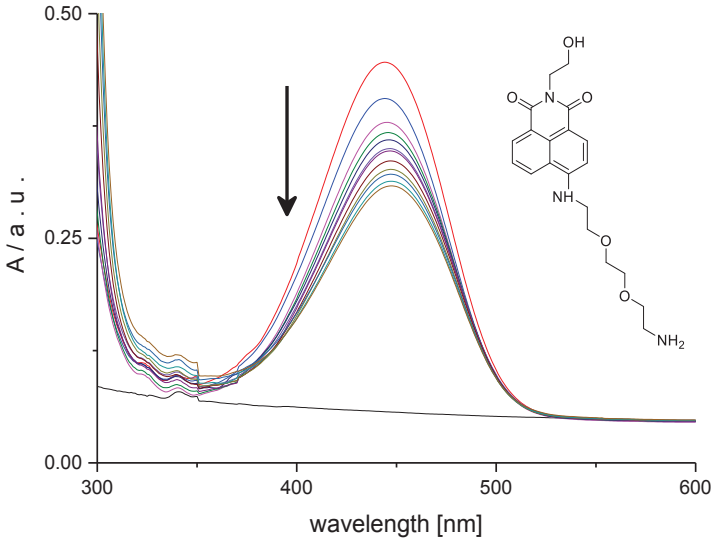

Figure 5.39: UV-visible spectra for 0.032 mM **5.5 (**red line**)** in buffer (25 mM MOPS, pH 7.0, 50 mM NaCl) in the absence of PAA and subsequent spectra for **5.5** in the presence of 0.1 mM PAA upon addition of 0 – 1.7 mM DNA, at 25 °C.

Figure 5.39 shows a hypochromic shift (with a maximum at 444 nm) of **5.5** upon addition of DNA in the presence of 0.1 mM PAA. The decrease in UV-visible absorption may occur because of geometrical distortion of **5.5** when it interacts with DNA, or as a result of the different local medium provided by the binding sites.

To quantify the affinity of **5.5** for DNA in the presence of PAA, the absorbances at 444 nm were plotted as a function of the concentration of DNA in the presence of PAA (Figure 5.40, see Appendix, Tables A55.118).

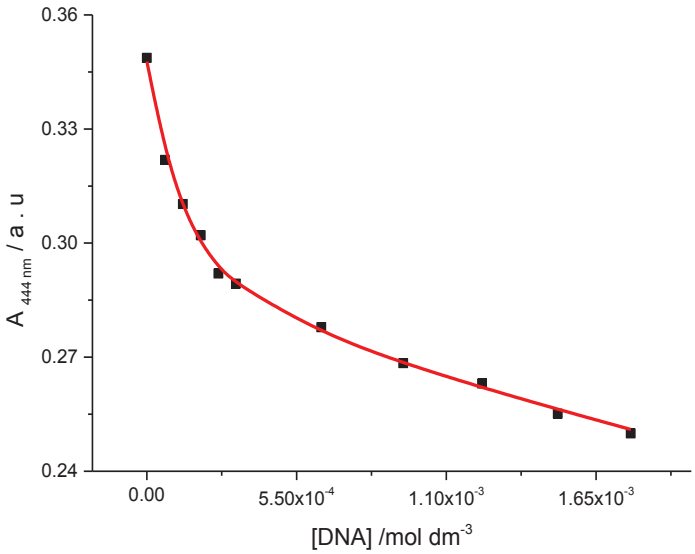

Figure 5.40: Absorbance at 444 nm for 0.032 mM **5.5** as a function of DNA concentration in the presence of 0.1 mM PAA, at 25 °C in buffer (25 mM MOPS pH 7.0, 50 mM NaCl). The solid line represents the best fit to the data in terms of a multiple independent binding sites model.

The figure 5.40 shows a decrease in the absorbance for **5.5** on the addition of DNA in the presence of 0.1 mM PAA. The binding affinity $K_{binding}$ and binding site size *n* were determined by fitting a multiple independent binding sites model, which also takes ligand dilution into account, to the data. A binding constant $K_{binding}$ of (1.0 ± 1.5) $\times 10^4$ M^{-1} for a binding site size of (1.0 ± 1.3) base pairs was found. A $K_{binding}$ of (8.9 ± 3.2) $\times 10^4$ M^{-1} for a binding site size restricted to 3.0 base pairs was observed for **5.5** binding to DNA in the absence of PAA. Therefore, the data were reanalysed with the stoichiometry restricted to 3.0 base pairs to allow comparison, giving an equilibrium constant $K_{binding}$ of (4.0 ± 0.46) $\times 10^4$ M^{-1}. From the similarity in the binding constants, it appears that PAA does not significantly compete with DNA for **5.5**.

5.3.22 Compound 5.7 binding with DNA in the presence of 0.1 mM PAA

We studied the interactions of **5.7** with DNA in the presence of 0.1 mM PAA. The changes in absorption of **5.7** upon addition of DNA were measured in buffer (25 mM MOPS, pH 7.0, 50 mM NaCl) at 25 °C (Figure 5.41).

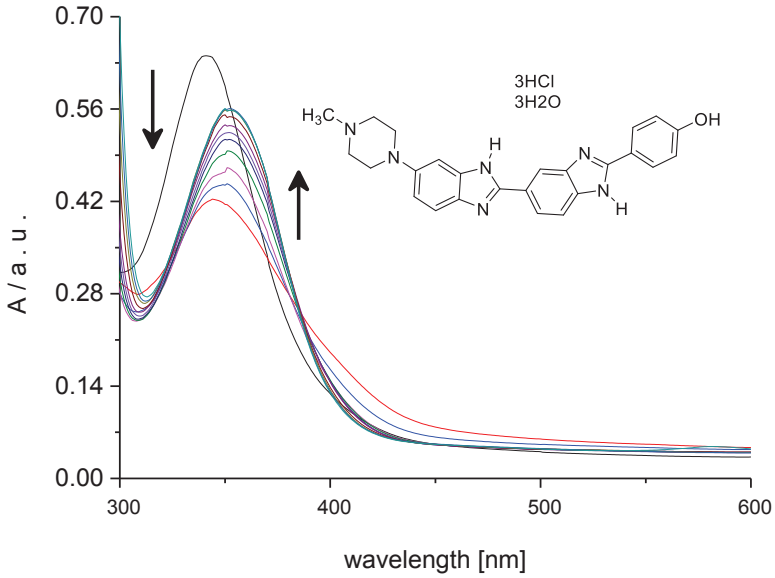

Figure 5.41: UV-visible spectra for 0.019 mM **5.7 (**red line**)** in buffer (25 mM MOPS, pH 7.0, 50 mM NaCl) in the absence of PAA and subsequent spectra for **5.7** in the presence of 0.1 mM PAA upon addition of 0 – 2.2 mM DNA, at 25 °C.

Figure 5.41 shows two events upon addition of DNA in the presence of 0.1 mM PAA. The first event involves a hypochromic shift in absorbance at 339 nm upon addition of PAA with a subsequent continued decrease in absorbance upon addition of DNA up to a concentration of 0.074 mM DNA (round data point in Figure 5.44). The second event involved a hyperchromic shift at 339 nm. The isosbestic point indicates that two forms of the DNA binder are involved in the titration during the second event. The change in UV-visible absorption may occur as a result of geometrical distortion of **5.7** when it interacts with DNA in presence PAA, but it may also be a local medium effect. The observation of rapid decrease in absorbance followed by an increase suggests precipitation and subsequent dissolution of DNA-ligand complex in the presence of 0.1 mM PAA. This, in turn, suggests that the two-species involved in the second equilibrium are **5.7** in primary and secondary sites on the DNA.

To quantify the affinity of **5.7** for DNA in the presence of 0.1 mM PAA, the absorbance at 339 nm was plotted as a function of the concentration of DNA (Figure 5.42, see Appendix, Tables A55.119).

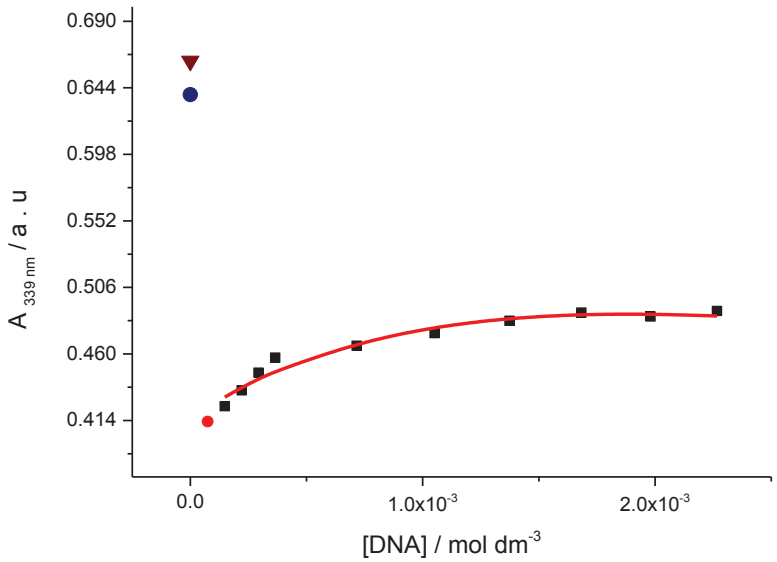

Figure 5.42: Absorbance at 339 nm for 0.019 mM **5.7** in the absence of PAA (▼) and subsequent spectra for **5.7** in the presence of 0.1 mM PAA (●) and upon addition of DNA of 0.0 – 0.075 mM (●) and 0.14 – 2.2 mM (■) of DNA concentration both in presence of 0.1 mM PAA, at 25 °C in buffer (25 mM MOPS pH 7, 50 mM NaCl). The solid line represents a fit of a multiple independent sites model to the data in the 0.14 – 2.2 mM range (■).

Figure 5.42 shows two events. The first event shows a decrease in the absorbance upon addition of 0.1 mM PAA (●) with a subsequent continued decrease in absorbance up to a concentration of 0.075 mM DNA (● in Figure 5.42). We attribute this decline in absorbance to strong binding of **5.7** to DNA, leading to precipitation as a result of charge neutralisation of the **5.7** – DNA complex. The second event shows an increase in the absorbance of **5.7** upon addition of 0.14 – 2.2 mM of DNA (■) in the presence of 0.1 mM of PAA. The ligand of interacts with DNA, giving an apparent equilibrium constant $K_{binding}$ of $(3.6\times10^{-3} \pm 3.9) \times10^{5}$ M^{-1} for a binding site size $(6\times10^{-1} \pm 745)$ base pairs. A $K_{binding}$ of $(9.2 \pm 1.9) \times10^{5}$ M^{-1} for the binding site size restricted to 3.0 base pairs was observed for **5.7** binding to DNA in the absence of PAA. Therefore, the data were reanalysed with the stoichiometry restricted to 3.0 base pairs to allow comparison, giving an apparent equilibrium constant $K_{binding}$ of $(1.6 \pm 0.5) \times10^{3}$ M^{-1}. From the difference in the binding constants, it appears that PAA does significantly compete with DNA for **5.7**.

5.3.23 Compound 5.8 binding with DNA in the presence of 0.5 mM PAA

We studied the interactions of **5.8** with DNA in the presence of 0.5 mM PAA. The changes in absorption of **5.8** upon addition of DNA were measured in buffer (25 mM MOPS, pH 7.0, 50 mM NaCl, 10 vol- %DMSO) at 25 °C (Figure 5.43).

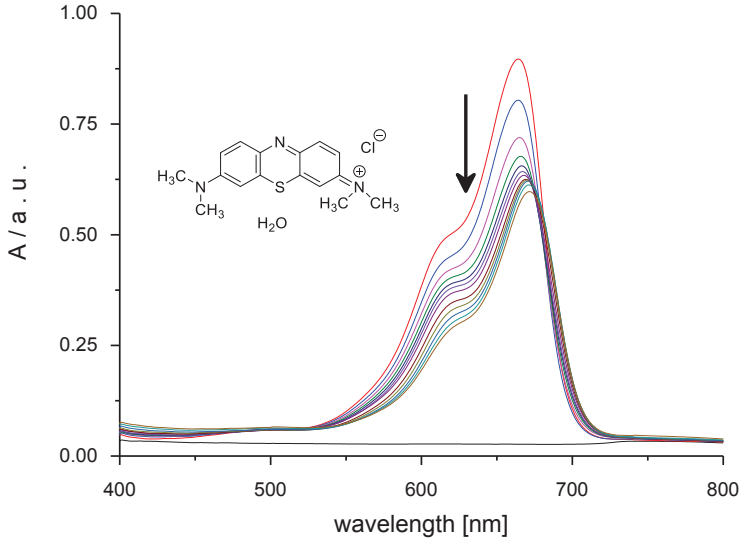

Figure 5.43: UV-visible spectra for 0.012 mM **5.8 (**red line**)** in buffer (25 mM MOPS, pH 7.0, 50 mM NaCl, 10 vol-% DMSO) in the absence of PAA and subsequent spectra for **5.8** in the presence of 0.5 mM PAA upon addition of 0 – 1.8 mM DNA, at 25 °C.

Figure 5.43 shows that **5.8** displays a hypochromic shift in absorbance upon addition of DNA in the presence of 0.5 mM PAA with a maximum change in absorbance at 664 nm. This decrease in UV-visible absorption may have occurred as a result of geometrical distortion of **5.8** when it interacts with DNA, but it may also be as a result of a local medium effect.

To quantify the affinity of **5.8** for DNA in the presence of 0.5 mM PAA, the absorbances at 664 nm was plotted as a function of the concentration of DNA in the presence of 0.5 mM PAA (Figure 5.44, see Appendix, Tables A55.120).

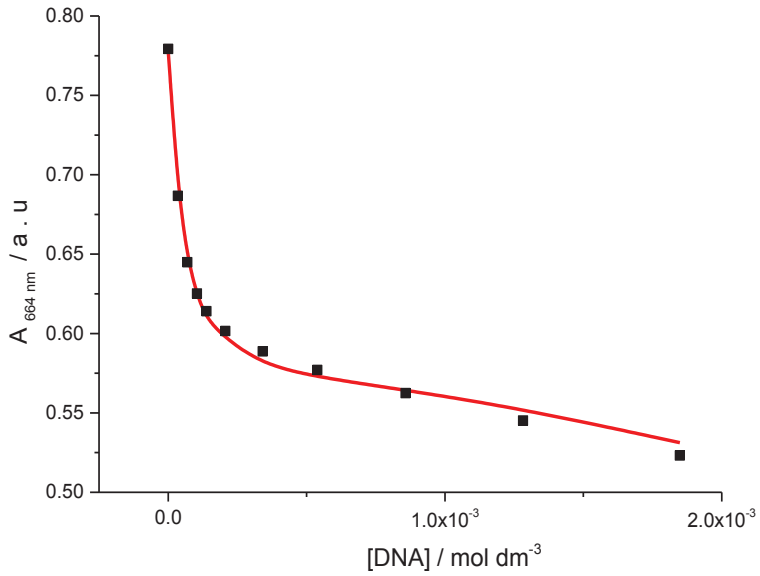

Figure 5.44: Absorbance at 664 nm for 0.012 mM **5.8** as a function of DNA concentration of 0 – 1.8 mM, in the presence of 0.5 mM PAA, at 25 °C in buffer (25 mM MOPS, pH 7, 50 mM NaCl, 10 vol-%DMSO). The solid line represents the best fit to the data in terms of a multiple independent binding sites model.

Figure 5.44 shows decrease in the absorbances at 664 nm for **5.8** upon addition DNA in the presence of 0.5 mM PAA. The binding affinity $K_{binding}$ and binding site size *n* were determined by fitting a multiple independent binding sites model, which also takes ligand dilution into account, to the data. The fit provides an equilibrium constant $K_{binding}$ of (1.1 ± 0.79) $\times 10^6$ M^{-1} for a binding site size of (8.8 ± 1.8) base pairs. A $K_{binding}$ of (4.5 ± 1.8) $\times 10^5$ M^{-1} for a binding site size of (3.0 ± 0.5) base pairs was observed for **5.8** binding to DNA in the absence of PAA. The data were reanalysed with the stoichiometry restricted to 3.0 base pairs to allow comparison, giving an apparent equilibrium constant $K_{binding}$ of (1.4 ± 0.2) $\times 10^5$ M^{-1}. A $K_{binding}$ of (4.4 ± 0.5) $\times 10^5$ M^{-1} for the binding site size restricted to 3.0 base pairs was observed for **5.8** to DNA in the absence of PAA. From the difference in the binding constant in the presence and absence of PAA, it appears that PAA does significantly compete with DNA for **5.8**. The presence of competition is beneficial because it could reduce a nonspecific binding.

5.3.24 The interaction of compound 5.10 and DNA in the presence of 0.1 mM PAA

We studied the interactions of **5.10** with DNA in the presence of 0.1 mM PAA. The changes in absorption of **5.10** upon addition of DNA were measured in buffer (25 mM MOPS, pH 7.0, 50 mM NaCl, at 25 °C) (Figure 5.45).

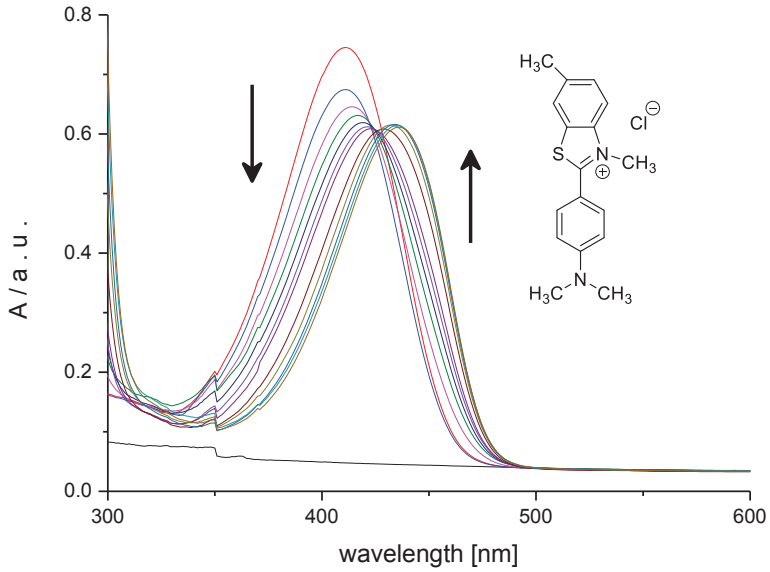

Figure 5.45: UV-visible spectra for 0.026 mM **5.10 (**red line**)** in buffer (25 mM MOPS, pH 7.0, 50 mM NaCl) in the absence of PAA and subsequent spectra for **5.8** in the presence of 0.1 mM PAA upon addition of 0 – 1.8 mM DNA, at 25 °C.

Figure 5.45 shows a red shift in absorbance of **5.10** upon addition of DNA in the presence of 0.1 mM PAA. This change in UV-visible absorption may occur as a result of geometrical distortion of **5.10** when it interacts with DNA in the presence of 0.1 mM PAA, but it may also be a local medium effect.

To quantify the affinity of **5.10** for DNA in the presence of 0.1 mM PAA, the absorbances at 411 and 432 nm were plotted as a function of the concentration of DNA (Figure 5.46, see appendix, Tables A55.121).

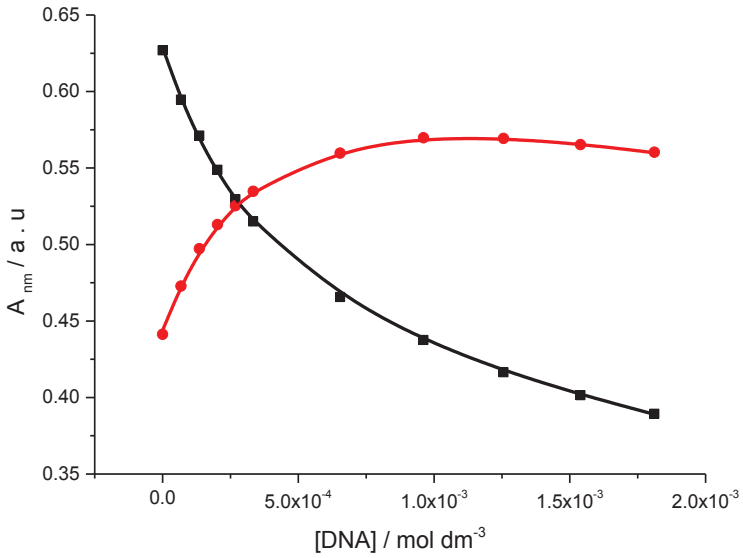

Figure 5.46: Absorbance at 411 nm (■) and at 432 nm (●) for 0.026 mM **5.10** as a function of DNA concentration in the presence of 0.1 mM PAA, at 25 °C in buffer (25 mM MOPS, pH 7.0, 50 mM NaCl). The solid lines represent a global fit of a multiple independent binding sites model to the data.

Figure 5.46 shows a decrease in the absorbance of at 411 nm (■) upon addition of DNA in the presence of 0.1 mM PAA. The red line shows a clear increase in the absorbance of **5.10** at 432 nm (●) upon addition of DNA in the presence of 0.1 mM PAA. The titration curves in Figure 5.48 were analysed globally by the fitting of a multiple independent binding sites model, which also takes simple dilution into account, to the data. The fit gives an equilibrium constant $K_{binding}$ of $(3\times10^{-2} \pm 3.1) \times10^{4}$ M^{-1} for a binding site size of $(5\times10^{-1} \pm 13)$ base pairs. A $K_{binding}$ of $(6.9 \pm 0.7) \times10^{3}$ M^{-1} for the binding site size restricted to 3.0 base pairs was observed for **5.10** binding to DNA in the absence of PAA. Therefore, the data were reanalyzed with the stoichiometry restricted to 3.0 base pairs to allow comparison, giving an apparent equilibrium constant $K_{binding}$ of $(8.0 \pm 1.9) \times10^{3}$ M^{-1}. From the similarity in the binding constant, it appears that PAA does not significantly compete with DNA for **5.10**. The absence of this competition is beneficial if **5.10** were to be used in a biosensor.

5.3.25 Compound 5.11 binding with DNA in the presence of 0.1 mM PAA

We studied the interactions of **5.11** with DNA in the presence of 0.1 mM PAA. The changes in absorption of **5.11** upon addition of DNA were measured in buffer (25 mM MOPS, pH 7.0, 50 mM NaCl) at 25 °C (Figure 5.47).

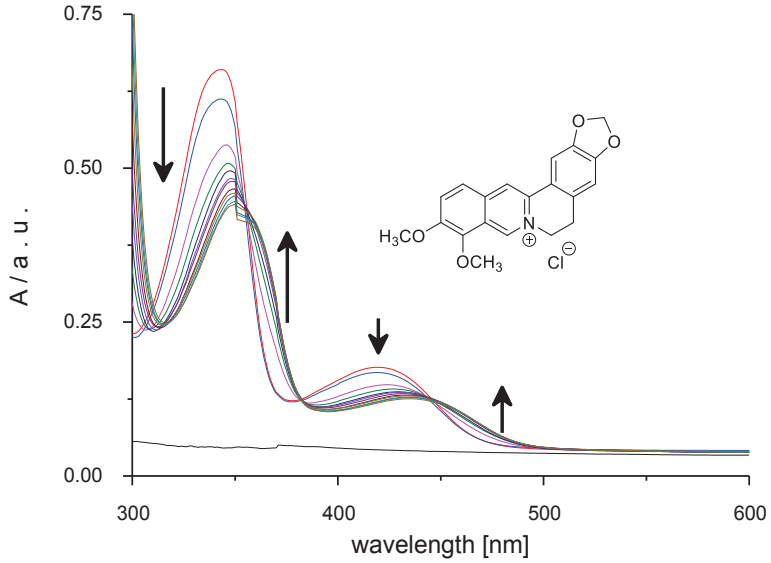

Figure 5.47: UV-visible spectra for 0.022 mM **5.11 (**red line**)** in buffer (25 mM MOPS, pH 7.0, 50 mM NaCl) in the absence of PAA and subsequent spectra for **5.11** in the presence of 0.1 mM PAA upon addition of 0 – 1.9 mM DNA, at 25 °C.

In the studies, **5.11** showed a red shift in absorbance upon addition of DNA with maximum changes in absorbance at 343 and at 375 nm in the presence of 0.1 mM PAA. This decrease in UV-visible absorption may have occurred as a result of geometrical distortion of **5.11** when it interacts with DNA in the presence of 0.1 mM PAA, but it may also be as a consequence of a local medium effect.

To quantify the affinity of **5.11** for DNA, the absorbances at 343 and 375 nm were plotted as a function of the concentration of DNA in the presence of PAA (Figure 5.48, see Appendix, Tables A55.122).

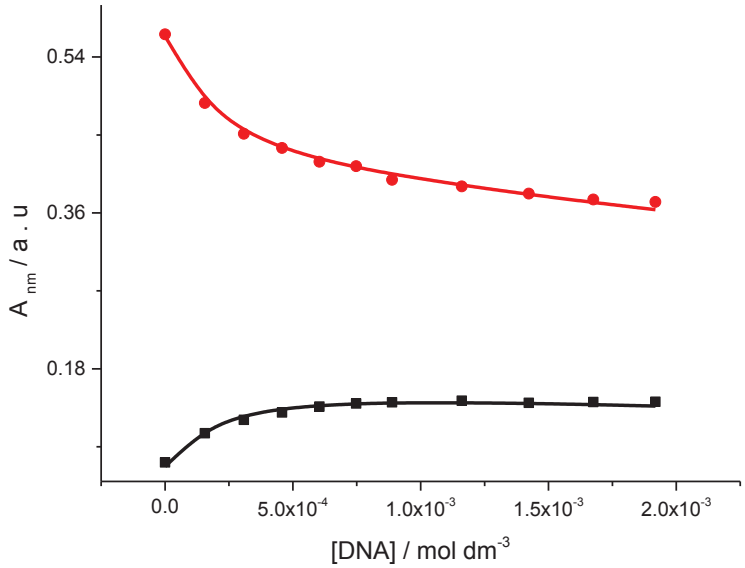

Figure 5.48: Absorbance at 343 nm and at 375 nm for 0.022 mM **5.11** as a function of DNA concentration in the presence of 0.1 mM PAA, at 25 °C in buffer (25 mM MOPS, pH 7.0, 50 mM NaCl). The solid lines represent the best fit to the data fit in terms of a multiple independent binding sites model.

Figure 5.48 shows a decrease in absorption at 343 nm and an increase at 375 nm upon addition DNA in the presence of 0.1 mM PAA. We attribute this decrease and increase in absorbance to binding of **5.11** to DNA in the presence of 0.1 mM PAA. The binding affinity $K_{binding}$ and binding site size *n* were determined by fitting a multiple independent binding sites model, which also takes ligand dilution into account, to the data. The binding constant $K_{binding}$ of $(5.6 \pm 4.7) \times 10^4$ M^{-1} for a binding site size of (6.7 ± 3.6) base pairs was found. A $K_{binding}$ of $(1.6 \pm 0.2) \times 10^4$ M^{-1} for a binding site size restricted to 3.0 base pairs was observed for **5.11** binding to DNA in the absence of PAA. The data were reanalysed with the stoichiometry restricted to 3.0 base pairs to allow comparison, giving an apparent equilibrium constant $K_{binding}$ of $(1.9 \pm 0.2) \times 10^4$ M^{-1}. From the similarity in the binding constants, it appears that PAA does not significantly compete with DNA for **5.11**. The absence of this competition is beneficial if **5.11** were to be used in a biosensor.

5.3.26 Compound 5.12 binding with DNA in the presence of 0.5 mM PAA

We wanted to study the binding of **5.12** to DNA in the presence 0.5 mM PAA. The changes in absorption of **5.12** upon addition of DNA were measured in buffer (25 mM MOPS, pH 7.0, 50 mM NaCl) at 25 °C (Figure 5.49).

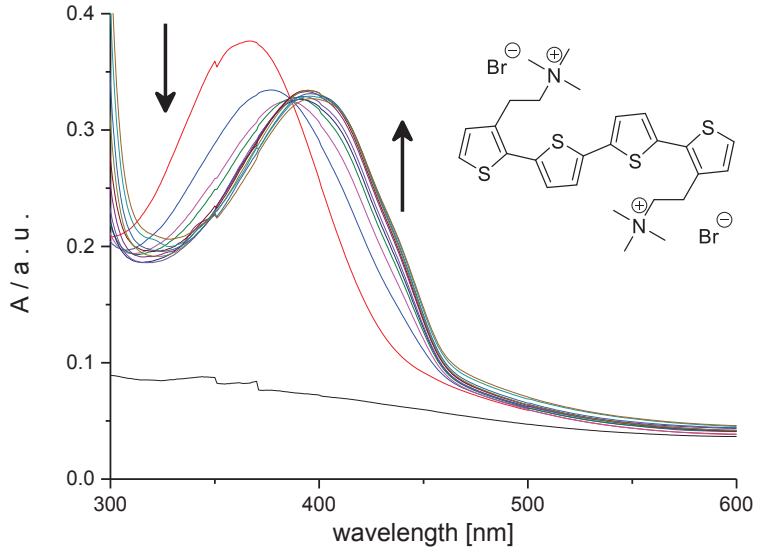

Figure 5.49: UV-visible spectra for 0.014 mM **5.12 (**red line**)** in buffer (25 mM MOPS, pH 7.0, 50 mM NaCl) in the absence of PAA and subsequent spectra for **5.12** in the presence of 0.5 mM PAA upon addition of 0 – 0.68 mM DNA, at 25 °C.

In the studies, **5.12** showed a red shift in absorbance upon addition of DNA in the presence of 0.5 mM PAA. The change in UV-visible absorption probably occurs as a result of geometrical distortion of **5.12** when it interacts with DNA in the presence of PAA, but a local medium effect may also contribute.

To quantify the affinity of **5.12** for DNA, the absorbances at 367 and 430 nm were plotted as a function of the concentration of DNA (Figure 5.50, see Appendix, Tables A55.123).

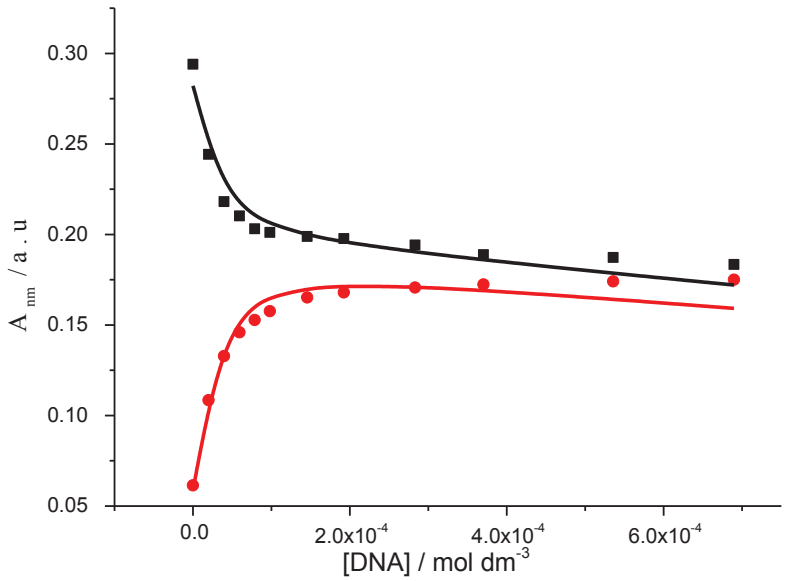

Figure 5.50: Absorbance at 367 nm (■) and at 430 nm (●) for 0.014 mM **5.12** as a function of DNA concentration in the presence of 0.5 mM PAA, at 25 °C in buffer (25 mM MOPS, pH 7.0, 50 mM NaCl). The solid lines represent a global fit of a multiple independent binding sites model to the data.

The binding affinity $K_{binding}$ and binding sites size n were determined by globally fitting a multiple independent binding sites model, which also takes ligand dilution into account, to the data in Figure 5.50. A binding constant $K_{binding}$ of (4.0 ± 9.3) × 10^4 M^{-1} for a binding site size of (0.8 ± 1.6) base pairs was found. A $K_{binding}$ of (8.3 ± 1.7) ×10^4 M^{-1} for a binding site size restricted to 2.0 base pairs was observed for **5.12** binding to DNA in absence PAA. The data were reanalysed with a stoichiometry restricted to 2.0 base pairs to allow comparison, giving an apparent equilibrium constant $K_{binding}$ of (1.3 ± 0.3) ×10^5 M^{-1}. From the similarity in the binding constant, it appears that PAA does not significantly compete with DNA for **5.12**. The lack of this competition is beneficial if **5.12** were to be used in a biosensor.

Summary

The results of UV-visible titrations show that ligands **5.1, 5.2, 5.4, 5.5, 5.7, 5.8, 5.10, 5.11** and **5.12** bind to DNA in the presence of PAA. Binding parameters are summarised in Table 5.4.

Table 5.4 Binding affinities and binding site sizes for binding of 5.1, 5.2, 5.4, 5.5, 5.7, 5.8, 5.10, 5.11 and 5.12 to DNA in the presence of PAA in buffer (25 mM MOPS, pH 7.0, 50 mM NaCl) at 25 °C.

Ligands	*Binding constant PAA / M^{-1}*	*Binding constant DNA / M^{-1}*	*Binding constant DNA+PAA / M^{-1}*	*Effect of PAA on affinity for DNA*
5.1	$(7.3 \pm 2.6) \times 10^4$ n = 0.1*	$(1.5 \pm 0.1) \times 10^4$ n = 3*a	$(3.7 \pm 0.4) \times 10^4$ n = 3*a	Increase
5.2	$(2.9 \pm 1.9) \times 10^5$ n = 0.7 ± 0.08	$(6.4 \pm 1.6) \times 10^4$ n = 3*a	$(2.0 \pm 0.5) \times 10^4$ n = 3*a	Decrease
5.4	No binding	$(3.4 \pm 0.7) \times 10^4$ n = 2.3 ± 0.25	$(4.2 \pm 1.1) \times 10^4$ n = 2.3 ± 0.3	No change
5.5	No binding	$(8.9 \pm 3.2) \times 10^4$ n = 3*	$(4.0 \pm 0.5) \times 10^4$ n = 3*	No change
5.7	$(2.7 \pm 0.6) \times 10^5$ n = 3*	$(7.7 \pm 1.5) \times 10^5$ n = 3*	$(8.2 \pm 1.3) \times 10^3$ n = 3*a	Decrease
5.8	$(6.1 \pm 2.7) \times 10^5$ n = 6.4 ± 1.2	$(4.4 \pm 0.5) \times 10^5$ n = 3*	$(1.4 \pm 0.2) \times 10^5$ n = 3*	Decrease
5.10	No binding	$(6.9 \pm 0.7) \times 10^3$ n = 3*	$(8.0 \pm 1.9) \times 10^3$ n = 3*	No change
5.11	No binding	$(1.6 \pm 0.2) \times 10^4$ n = 3*	$(1.9 \pm 0.2) \times 10^4$ n = 3*	No change
5.12	No binding	$(1.8 \pm 0.3) \times 10^5$ n = 3*	$(2.8 \pm 0.8) \times 10^5$ n = 3*	No change

a. apparent binding constant for the event following initial precipitation.
b. * restricted.

Table 5.4 describes the cationic ligands that can bind to DNA in the presence of PAA. Compounds **5.1, 5.2** and **5.7** interact with DNA in the presence of PAA in two events. The first event occurs when the concentration of ligand is high, and the concentration of DNA is still low. Under these conditions the ligand binds to both the highest affinity binding sites and to the negative sugar-phosphate backbone of DNA. As a result of those interactions precipitation will occur because of formation of a charge neutralised ligand-DNA complex. The second event occurs at high concentration of DNA. In this event, the ligand binds to the main binding sites, viz. in the minor groove or in intercalation sites of DNA.

Compounds **5.4, 5.5, 5.10, 5.11** and **5.12** do not show any change in affinity for DNA in the presence of PAA. This is in agreement with the observation that these compounds don't bind to PAA. Decreases in binding constant were observed for **5.2, 5.7** and **5.8**. That means the binding between these ligands and DNA in the presence of PAA is not in the absence of the polymer. For **5.2, 5.7** and **5.8**, this observation is as expected, considering they bind to PAA. For **5.1** an increase in the apparent binding constant was observed. This increase is probably the result of excess ligand at the beginning of the titration binding to PAA, rather than to secondary binding sites on the DNA. This means that the second event now corresponds to **5.1** moving from PAA to the primary binding site on DNA, rather than from precipitated complexes.

5.4 Potential use of block copolymers in directed assembly

The results of UV-visible titrations for oligo heteroaromatic compounds with POSA and PAA show that ligands **5.1, 5.2, 5.4, 5.5, 5.7, 5.8, 5.10, 5.11** and **5.12** bind to POSA and PAA (Table 4.5).

Table 5.5 Binding affinities and binding site sizes for binding of 5.1, 5.2, 5.4, 5.5, 5.7, 5.8, 5.10, 5.11 and 5.12 to POSA and PAA in buffer (25 mM MOPS, pH 7.0, 50 mM NaCl) at 25 °C.

Ligands	*Binding constant PAA* K / M^{-1}	*Binding constant POSA* K / M^{-1}
5.1	$(7.3 \pm 2.6) \times 10^4$ $n = 0.1^*$	$(6.8 \pm 1.1) \times 10^3$ $n = 3^*$a
5.2	$(2.9 \pm 1.9) \times 10^5$ $n = 0.7 \pm 0.08$	$(2.2 \pm 0.8) \times 10^3$ $n = 3^*$a
5.4	No binding	$(7.6 \pm 2.0) \times 10^3$ $n = 1^*$
5.5	No binding	$(2.0 \pm 1.7) \times 10^4$ $n = 0.26 \pm 0.08$
5.7	$(2.7 \pm 0.6) \times 10^5$ $n = 3^*$	$(1.4 \pm 0.85) \times 10^6$ $n = 3^*$
5.8	$(6.1 \pm 2.7) \times 10^5$ $n = 6.4 \pm 1.2.$	$(1.4 \pm 0.2) \times 10^4$ $n = 1^*$
5.10	No binding	$(3.2 \pm 0.7) \times 10^4$ $n = 6.1 \pm 0.7$
5.11	No binding	No binding
5.12	No binding	$(1.3 \pm 0.6) \times 10^5$ $n = 1^*$

a. apparent binding constant for the event following initial precipitation.
b. * restricted.

Cationic conjugated oligoheteraromatic **5.1, 5.2, 5.7** and **5.8** interact with POSA and PAA. However, the rest of the ligands bind to POSA only.

Compounds **5.1** and **5.2** bind to POSA and show two events, with a high ratio of ligands / POSA leading to a sharp decrease in absorbance as result of precipitation of ligand−POSA complexes. The next event with a low concentration of ligand leads to an increase in absorbance. In contrast, these compounds bind to PAA without precipitation.

The highest affinity is observed for **5.7** and **5.12** with a binding constant between $10^5 – 10^6$ M^{-1}. We may attribute this high affinity to the presence of more positive charges and aromatics rings which lead to an increase in electrostatic interactions and hydrophobic interaction between the ligands and POSA and PAA. The weakest binders are **5.1-5.2** with an apparent binding constant ~ 10^3 M^{-1}. The low affinities of **5.1-5.2** for POSA may be attributed to the presence of precipitation and subsequent dissolution of a POSA−ligand complex, leading to a decrease in the apparent affinity. The compounds **5.1-5.2** bind with PAA with high affinity.

It is interesting to speculate about what we could do with these molecules in terms of self assembly. Compounds **5.4, 5.5, 5.10** and **5.12** show selectivity in binding to POSA over PAA. Unfortunately, there are no compounds that are strongly selective for PAA over POSA in this data set. If this were the case, we could try to use a block copolymer to organise these molecules as illustrated in Figure 5.53.

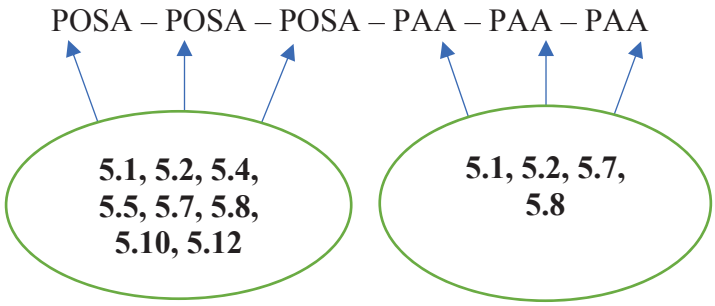

Figure 5.53: explains that molecules bind with POSA and others bind to PAA.

5.5 Conclusions

Chapter five provided the results of binding studies between different oligoheteroaromatic molecules and negative polymers POSA and PAA and the effect of POSA and PAA on DNA-binding properties. The binding constants $K_{binding}$ for ligands were between 10^3 M^{-1} and 10^6 M^{-1} with binding site sizes in a range of 0.1 to 6.0 monomeric units per molecule. Compounds **5.1, 5.2, 5.7** and **5.8** bind to POSA and PAA. In addition, ligands **5.4, 5.5, 5.10** and **5.12** bind with POSA only without any affinity for PAA.

The UV-visible results show that **5.1** and **5.7** bind to DNA in the presence of POSA and PAA with two events. Compound **5.8** binds to DNA in the presence of POSA with two events too. Compound **5.2** binds to DNA in the presence of PAA with two binding events. All ligands exhibit decreased affinity in the presence of POSA which could lead to false negatives. We also observed, compound **5.1** bind to DNA in the presence of POSA without any change in binding constant.

The decreasing affinity of compounds **5.2, 5.5, 5.**7 and **5.8** for DNA in the presence of PAA and POSA indicates that binding may lead to reduce the non-specific binding. Compounds **5.4, 5.5, 5.10, 5.11** and **5.12** do not show change in affinity for DNA. That means there is no effect of PAA on DNA biosensors involving these sensitisers.

5.6 Materials

5.6.1 Materials

Polystyrenesulfonic acid POSA was procured from Sigma-Aldrich and Acros as a solution. Polyacrylicacid with high molecular weight was purchased from Sigma-Aldrich. The buffer components were purchased from Melford Laboratories Ltd and Sigma-Aldrich. POSA and PAA concentrations were determined in term of monomeric units by molecular weight.

5.7 Solutions preparation

5.7.1 Polymers POSA and PAA preparation

All experiments were carried out in buffer (25 mM MOPS, 50 mM NaCl, pH 7.0, at 25 °C). POSA solutions were prepared by dilution ($M_1 \times V_1 = M_2 \times V_2$) in MOPS buffer of a 1 M stock solution of POSA. PAA with high molecular weight was dissolved in MOPS buffer. Concentrations of stock solutions were determined by weight.

5.8 Spectroscopy studies

2.0 ml of MOPS buffer was added in a 1.0 cm path length cuvette. Stock solutions of all molecules were prepared in MOPS buffer, sometimes involving 10 vol-% DMSO. All UV-visible titrations were carried out by adding aliquots of the stock solution of the macromolecules such as POSA, PAA and DNA into the 1.0 cm path length cuvette which contains ligand solution in MOPS, recording the absorption in the range of 200 - 800 nm after each addition. Absorptions were kept in the range of (0.0 - 1.0). Furthermore, to study the effect of POSA and PAA on DNA - binding, the same steps were carried out as before except first adding POSA and PAA after the ligand and then continuing to add DNA. The absorptions at selected wavelengths were plotted against macromolecules concentrations, and a multiple independent binding sites model was used to analyse the UV-visible spectra using the Origin 9.0 software.

Chapter Six

The interactions of π-conjugated ligands with surfactants and the effect of surfactant on DNA-binding

Abstract

We studied the interactions of π-conjugated molecules with different types of surfactants viz positive, negative and nonionic surfactants using UV-visible spectroscopy. All ligands contain a π-conjugated system and possess hydrophilic and hydrophobic side groups.[186-187] We show that cationic ligands bind to negatively charged sodium dodecyl sulphate (SDS) through electrostatic and hydrophobic binding. An anionic compound was found to interact strongly with positively charged cetyl trimethyl ammonium bromide (CTAB). Moreover, we used non-ionic surfactant polyoxyethylene glycol monolaurate of (Tween-20) to study the effect of surfactant on DNA binding properties of different molecules. We found some of our compounds, such as **6.1, 6.2, 6.4, 6.5, 6.7, 6.8** and **6.12**, bind to SDS while anionic molecules **6.4, 6.9** and **6.14** bind to CTAB. Compounds **6.12** and **6.15** demonstrated a decrease in affinity for DNA in the presence of Tween 20, suggesting that these potential sensitiser could bind to Tween 20 which may be a source of false negative results. Ligand **6.13** does not show any change in affinity for DNA in the presence of (Tween-20). This observation means that Tween 20 does not affect the sensitivity of our DNA biosensors. Electrostatic interactions between the oppositely charged groups are responsible for the interactions between surfactants and our potential sensitisers.

6.1 Introduction

6.1.1 surfactants

Surfactants are compounds which contain both hydrophobic tail groups and hydrophilic head groups.[188] In solution surfactants, such as sodium dodecyl sulphate(SDS) and cetyl trimethyl ammonium bromide (CTAB) can help to dissolve chemical compounds by dissociating aggregates. Moreover, surfactants are used to increase the solubility of reactants in aqueous solutions.[189]

The classification of surfactants depends on their polar head group. Ionic surfactants carry negative or positive charges. If the charges are negative, the surfactants are called anionic and if the charges are positive cationic. In addition, when a surfactant contains a head with two oppositely charged groups, it is named zwitterionic. Surfactants without a charge are called non-ionic. Sodium dodecyl sulphate (SDS) has the formula $CH_3(CH_2)_{11}SO_4Na$ and its structure is shown in Scheme 6.1. It is an anionic surfactant that can be used in cleaning and hygiene products.[190] CTAB (Scheme 6.1) with formula $(C_{16}H_{33})N(CH_3)_3Br$ is a cationic surfactant that can bind with negative ligands. Non-ionic surfactants include polyoxyethylene glycol monolaurate (Tween 20) which has formula $C_{58}H_{114}O_{26}$ (Scheme 6.1).

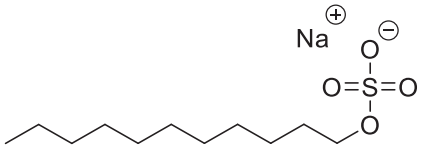

Sodium dodecyl sulfate (SDS)

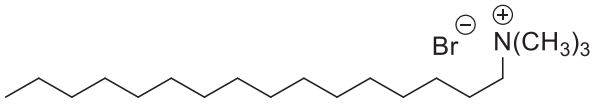

Cetyl trimethylammonium bromide (CTAB)

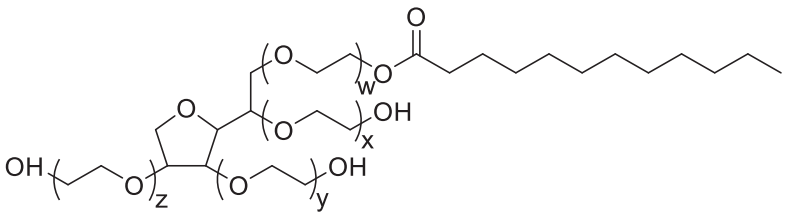

Polyoxyethylene glycol monolaurate solution (Tween-20)

Scheme 6.1

In aqueous solution, surfactants form aggregates. Surfactants can make different shapes of aggregates, for example, spherical micelles, rodlike micelles, wormlike micelles, bilayers and vesicles. These shapes of these aggregates depend on the equilibrium between the attraction of hydrophobic surfactant alkyl tails and the electrostatic repulsions of the head groups of the surfactants.[191-192]The relation between the aggregate and surfactant shape is described by the packing parameter.[193] The packing parameter (*P*) is given by equation 6.1. The shapes of aggregate depend on the value of P.

$$\mathbf{P} = \frac{\boldsymbol{V}}{\boldsymbol{a_0 l}} \qquad \text{……. 6.1}$$

V is the volume of the hydrocarbon part of the surfactant, *l* is the length of the extended all-trans alkyl tail, and a_0 the mean surface area of the head group.

Surfactants form micelles above the critical micelle concentration (CMC); when the surfactant molecules reach this critical concentration they will form micelles in which the hydrophobic tails (non-polar) bunch together inside the micelles whereas the polar headgroups (hydrophilic) are orientated to the bulk aqueous solution forming a polar shell.[194] Above the CMC, there is a dynamic equilibrium between surfactant molecules and micelles. The aggregation of polar surfactant and oppositely charged molecules will occur at low concentrations as result of the presence of these charges which leads to electrostatic interactions between them[195-196] as shown in Figure 6.1.

6.1.2 The interactions of surfactants with dyes

We studied in chapter six the interaction between cationic and anionic π-conjugated molecules with anionic and cationic surfactants such as sodium dodecyl sulphate (SDS) and cetyl trimethyl ammonium bromide (CTAB). Electrostatic interactions between the oppositely charged groups are responsible for the interactions between surfactants and our potential sensitisers.

Hydrophobic molecules, like our sensitisers, can bind to surfactants such as SDS and CTAB as shown in Figure 6.1. The presence of surfactant can, therefore, affect DNA-binding of potential sensitisers. In addition, it can be useful to wash biosensors using surfactants. Washing is essential because interactions with (bio)macromolecules can lead to some of the ligands sticking non-selectivily on the biosensor surface.

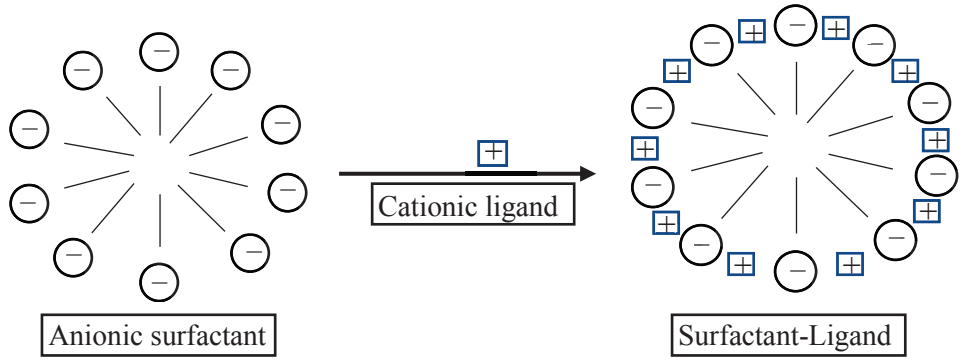

Figure 6.1: shows a complex of ligand and surfactant formed from the anionic surfactant and cationic ligand as observed by the interaction between them.

6.1.3 The potential effect of surfactants on biosensors

The presence of surfactants can affect the performance of biosensors. The interactions between sensitisers and surfactant and how these affect biosensor functioning can be studied using several techniques such as UV-visible spectroscopy, isothermal titration calorimetry (ITC) and circular dichroism spectroscopy. These methods allow the study of how different parameter is describing interactions of sensitisers with DNA change upon potential binding of these sensitisers to added macromolecules.

6.1.4 Aim

In this chapter, our objectives are to quantify the binding of compounds **6.1-6.14** (Scheme 1.5) to SDS, CTAB and study the effect of surfactant (Tween-20) on DNA binding properties of π-conjugated ligands. Tween-20 is a surfactant used in lateral flow assays.

6.2 Results and discussion

Part A: Interactions of DNA binders with the negatively charged surfactants sodium dodecyl sulphate

6.2.1 Compound 6.1 binding with SDS

We wanted to know whether **6.1** binds to SDS. The changes in absorption of **6.1** upon addition of SDS were measured in buffer (25 mM MOPS, pH 7.0 and 50 mM NaCl and 10 vol-% DMSO) at 25 °C (Figure 6.2). We used DMSO to prevent the precipitation that often occurs when SDS interacts with molecules of opposite charge.

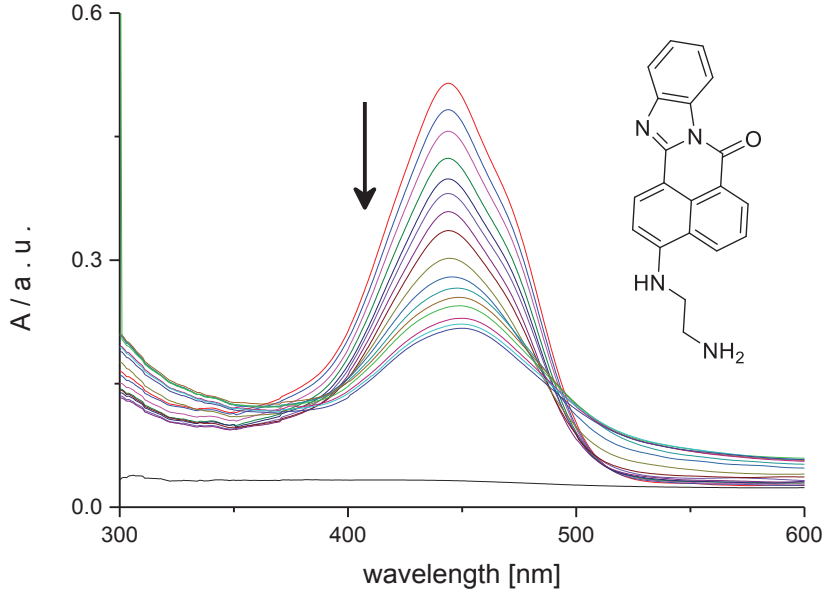

Figure 6.2: UV-visible spectra for 0.031 mM **6.1** upon addition of 0 – 0.28 mM SDS, at 25 °C in buffer (25 mM MOPS, pH 7.0, 50 mM NaCl and 10 vol-% DMSO).

Figure 6.2 shows a hypochromic shift, with a maximum change at 444 nm. This decrease in UV-visible absorption occurs as a result of the interaction of **6.1** with SDS. Figure 6.3 also shows that the absorbance in the range of 500-600 nm increases upon addition of SDS. This observation suggests precipitation of ligand-surfactant salts forms our aqueous solutions. Precipitation was also observed by naked eye. Precipitation has been reported before for combination of anionic surfactants and cationic ligand as well as for solutions of cationic surfactants and anionic ligand.[197]

Despite the precipitation, we quantify the apparent affinity of **6.1** for SDS by plotting the absorbance at 444 nm as a function of the concentration of SDS (Figure 6.3, Tables A55.124).

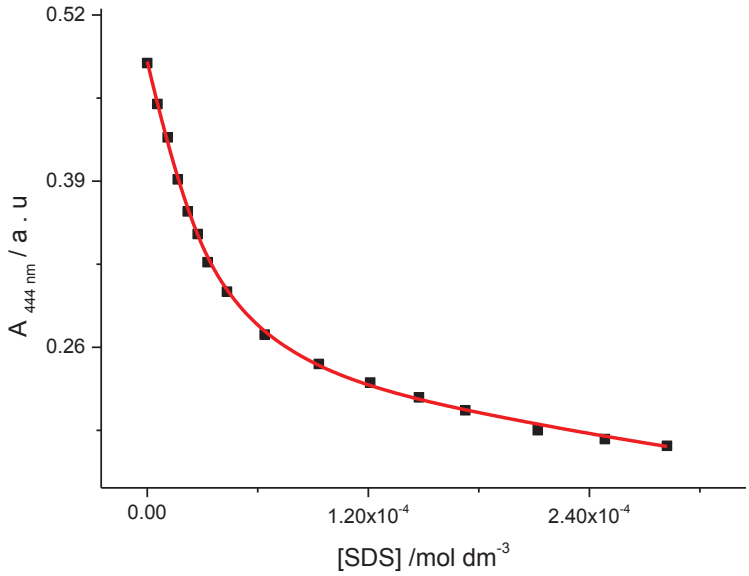

Figure 6.3: Absorbance at 444 nm for 0.031 mM **6.1** upon addition of 0 - 0.28 mM SDS, at 25 °C in buffer (25 mM MOPS, pH 7.0, 50 mM NaCl and 10 vol-% DMSO). The solid line represents the fit of a multiple independent sites model to the data.

The titration curve of Figure 6.3 was analysed by fitting a version of the multiple independent binding sites model, which also takes ligand dilution into account, to the data. This fit reproduces the data well and produces an apparent equilibrium constant K_{binding} of (8.4 ± 1.7) $\times 10^4$ M^{-1} and a stoichiometry of (1.02 ± 0.08) surfactant molecule per molecule of **6.1**. Electrostatic interactions between the oppositely charged groups are most likely responsible for the interaction of the anionic surfactant with **6.1**.

6.2.2 Compound 6.2 binding with SDS

We wanted to know whether **6.2** binds to SDS; the changes in absorption of **6.2** upon addition of SDS were measured in buffer (25 mM MOPS, pH 7.0 and 50 mM NaCl) at 25 °C (Figure 6.4).

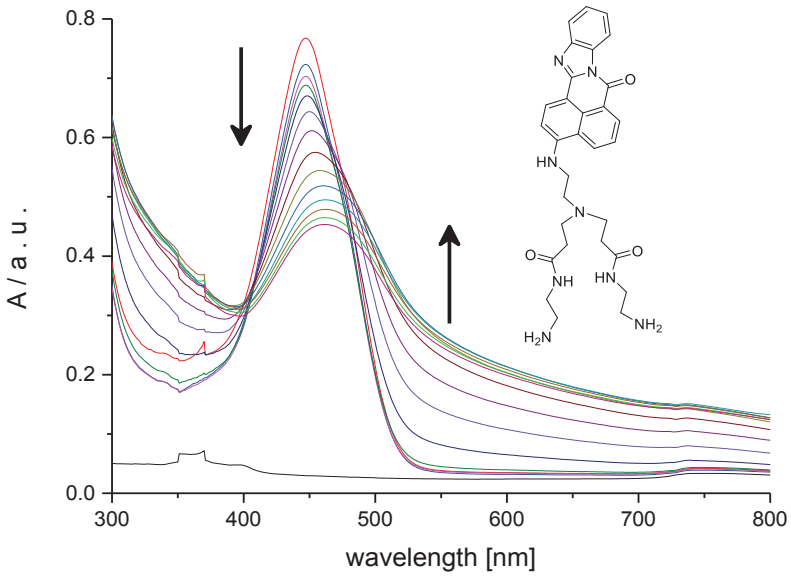

Figure 6.4: UV-visible spectra for 0.044 mM **6.2** upon addition of 0 – 0.32 mM SDS at 25 °C in buffer (25 mM MOPS, pH 7.0, 50 mM NaCl).

Figure 6.4 shows two events upon addition of SDS. The first event is a hypochromic shift with a maximum change at 447 nm. The second event shows a hyperchromic shift with a maximum change at 558 nm. In fact, Figure 6.4 shows that the absorbance in the range of 500-600 nm increases upon addition of SDS. This observation suggests precipitation of ligand -surfactant salt from our aqueous solution. Precipitation was also observed by naked eye.

Despite the precipitation, we quantify the affinity of **6.2** for SDS by plotting the absorbance at 447 and at 558 nm (representing scattering of light) as a function of the concentration of SDS (Figure 6.5, see Appendix, Tables A55.125).

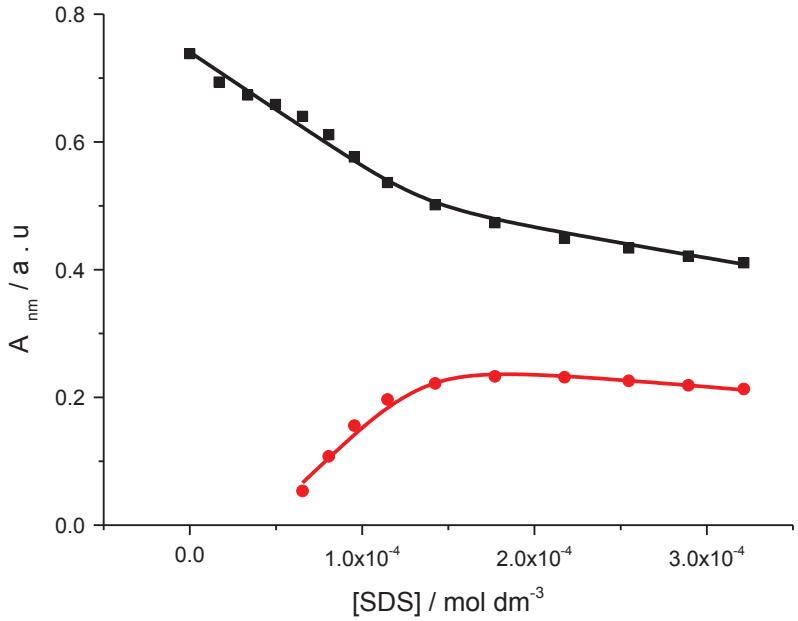

Figure 6.5: Absorbance at 447 nm and at 558 nm for 0.044 mM **6.2** upon addition of 0 - 0.32 mM SDS, at 25 °C in buffer (25 mM MOPS, pH 7.0, 50 mM NaCl). The solid lines represent a global fit of a multiple independent sites model to the data.

The titration curves of Figure 6.5 were analysed globally by fitting a type of the multiple independent binding sites model, which also takes ligand dilution into account, to the data. This fit reproduces the data well and gives an apparent equilibrium constant K_{binding} of $(2.2 \pm 2.1) \times 10^6\ \text{M}^{-1}$ and a stoichiometry of (3.4 ± 0.3) surfactant molecule per molecule of **6.2.** The obtained stoichiometry and binding constant seem reasonable and suggest strong binding between **6.2** and SDS due to electrostatic and hydrophobic interactions. The stoichiometry suggests that **6.2** is triply charged in the precipitated salt. This seems reasonable because **6.2** has three sites where protonation is likely to occur in aqueous solution.

6.2.3 Compound 6.4 binding with SDS

We wanted to know whether **6.4** binds to SDS. The changes in absorption of **6.4** upon addition of SDS were measured in buffer (25 mM MOPS, pH 7.0 and 50 mM NaCl) at 25 °C (Figure 6.6).

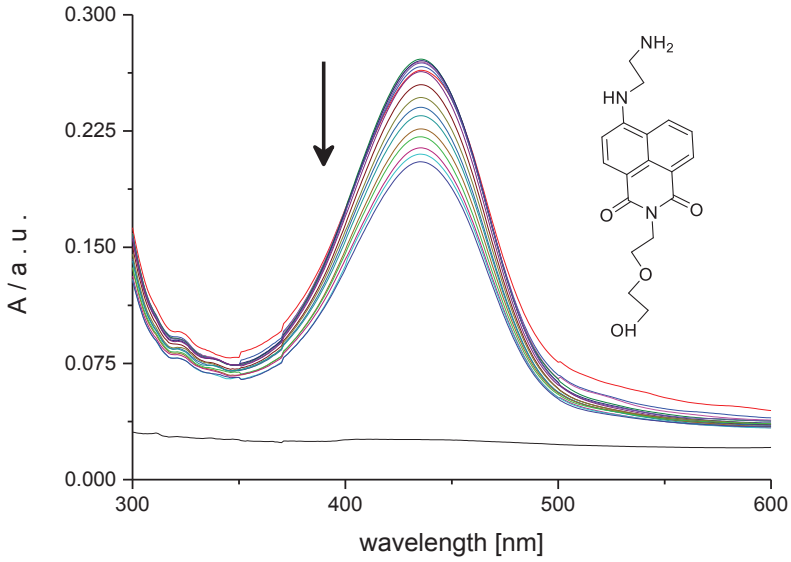

Figure 6.6: UV-visible spectra for 0.022 mM **6.4** upon addition of 0 – 0.40 mM SDS, at 25 °C in buffer (25 mM MOPS, pH 7.0, 50 mM NaCl).

Figure 6.6 shows a hypochromic shift (with a maximum change at 436 nm). This decrease in UV-visible absorption occurs because of the interaction of **6.4** with SDS. Figure 6.7 also shows that the absorbance in the range of 500 - 600 nm increases upon the first additions of SDS. This observation suggests precipitation of ligand -surfactant salt from our aqueous solution.

To quantify the affinity of **6.4** for SDS, the absorbance at 436 nm were plotted as a function of the concentration of SDS (Figure 6.7, see Appendix, Table A55.126).

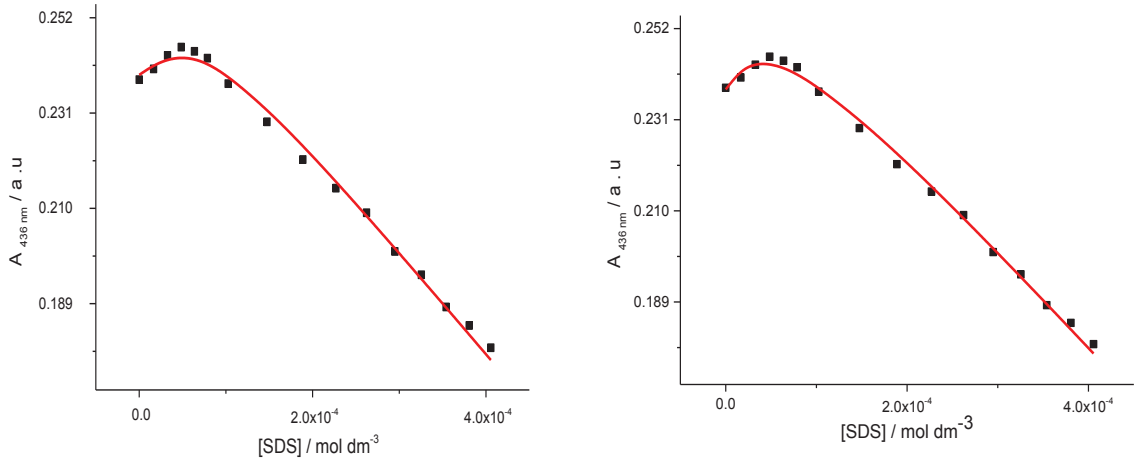

Figure 6.7: Absorbance at 436 nm for 0.022 mM **6.4** upon addition of 0 - 0.40 mM SDS, at 25 °C in buffer (25 mM MOPS, pH 7.0, 50 mM NaCl). The solid line represents the best fit to the data in terms of a multiple independent binding sites model.

The titration curve of Figure 6.7 was analysed by fitting the multiple independent binding sites model, which also takes ligand dilution into account, to the data. This fit reproduces the data well and gives an apparent equilibrium constant $K_{binding}$ of (2.1 ± 0.47) × 10^4 M^{-1} for a stoichiometry restricted at 1 to surfactant molecule per molecule of **6.4**.

6.2.4. Compound 6.5 binding with SDS

We need to know whether **6.5** binds to SDS; the changes in absorption of **6.5** upon addition of SDS were measured in buffer (25 mM MOPS, pH 7.0 and 50 mM NaCl and 10 vol-% DMSO) at 25 °C (Figure 6.8).

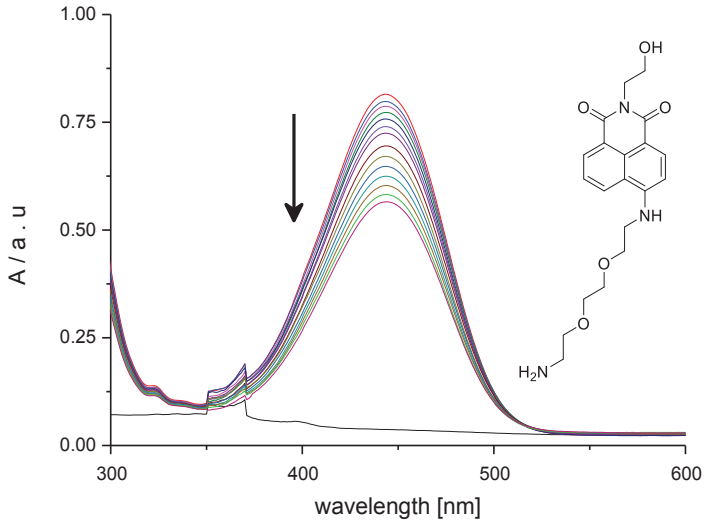

Figure 6.8: UV-visible spectra for 0.057 mM **6.5** upon addition of 0 - 0.35 mM SDS, at 25 °C in buffer (25 mM MOPS, pH 7.0, 50 mM NaCl, 10 vol-% DMSO).

Figure 6.8 shows a hypochromic shift in absorbance (at the λ_{max} of 444 nm) of **6.5** upon addition of SDS. We do not see a significant increase in absorbance between 550 and 600 nm. This change in UV-visible absorption may occur as a result of geometrical distortion of **6.5** when it interacts with SDS, but it may also be a local medium effect.

To quantify the affinity of **6.5** for SDS, the absorbance at 444 nm were plotted as a function of the concentration of SDS (Figure 6.9, see Appendix, Tables A55.127).

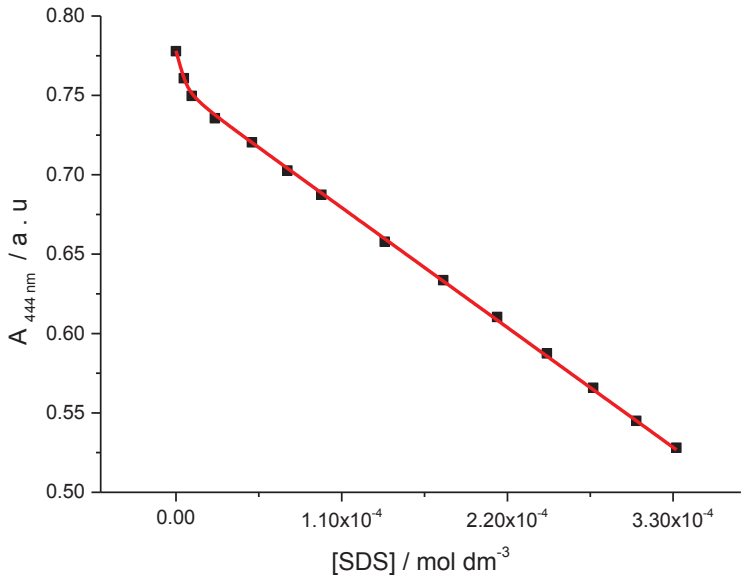

Figure 6.9: Absorbance at 444 nm for 0.071 mM **6.5** upon addition of 0 - 0.35 mM SDS, at 25 °C in buffer (25 mM MOPS, pH 7.0, 50 mM NaCl and 10 vol-% DMSO). The solid line represents the best fit to the data in terms of a multiple independent binding sites model.

The titration curve of Figure 6.9 was analysed by fitting a version of the multiple independent binding sites model, which also takes ligand dilution into account, to the data. This fit reproduces the data well and gives an equilibrium constant $K_{binding}$ of $(2.4 \pm 1.7) \times 10^5$ M^{-1} for a stoichiometry restricted to 0.1 surfactant molecule per molecule of **6.5**. We restricted the stoichiometry in order to obtain reasonable binding parameters. We attribute the lack of precipitation of **6.5** - SDS complex to the long hydrophilic side chain on **6.5** which keeps the complex in solution.

6.2.5 Compound 6.7 binding with SDS

We wanted to study the binding of **6.7** to SDS, the changes in absorption of **6.7** upon addition of SDS were measured in buffer (25 mM MOPS, pH 7.0 and 50 mM NaCl) at 25 °C (Figure 6.10).

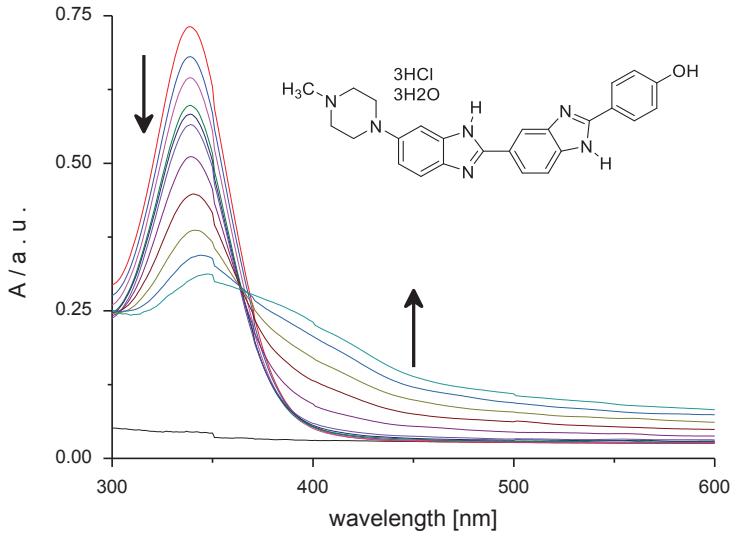

Figure 6.10: UV-visible spectra for 0.026 mM **6.7** upon addition of 0 - 0.15 mM SDS, at 25 °C in buffer (25 mM MOPS, pH 7.0, 50 mM NaCl).

Figure 6.10 shows a hypochromic shift at the λ_{max} of 339 nm and a hyperchromic shift at 415 nm for **6.7** upon addition of SDS. Figure 6.11 also shows that the absorbance in the range of 400 - 600 nm increases upon addition of SDS. This observation suggests precipitation of the ligand − surfactant salt from our aqueous solution. Precipitation was also observed by naked eye. The change in UV-visible absorption at 339 nm may occur as a result of geometrical distortion of **6.7** when it interacts with SDS, but it may also be a local medium effect.

To quantify the affinity of **6.7** for SDS, the absorbances at 339 and 415 nm were plotted as a function of the concentration of SDS (Figure 6.11, see Appendix, Tables A55.128).

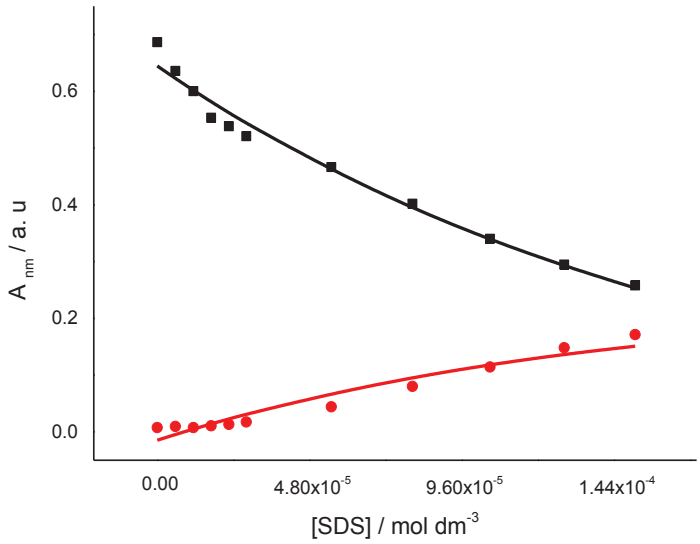

Figure 6.11: Absorbance at 339 nm and 415 nm for 0.026 mM **6.7** upon addition of 0 − 0.15 mM SDS, at 25 °C in buffer (25 mM MOPS, pH 7.0, 50 mM NaCl). The solid lines represent a global fit of a multiple independent binding sites model to the data.

The titration curves of Figure 6.11 were analysed globally by fitting a type of the multiple independent binding sites models, which also takes ligand dilution into account, to the data. This fit reproduces the data well and gives an apparent equilibrium constant $K_{binding}$ of $(1.5 \pm 1.4) \times 10^4$ M^{-1} for a stoichiometry restricted to 3.0 molecules of SDS per molecule of **6.7** molecules because of the potential of **6.7** to become triply pronated. The obtained binding parameters were reasonable.

6.2.6 Compound 6.8 binding with SDS

We wanted to know the binding of **6.8** to SDS, the changes in absorption of **6.8** upon addition of SDS were measured in buffer (25 mM MOPS, pH 7.0 and 50 mM NaCl and 10 vol-% DMSO) at 25 °C (Figure 6.12).

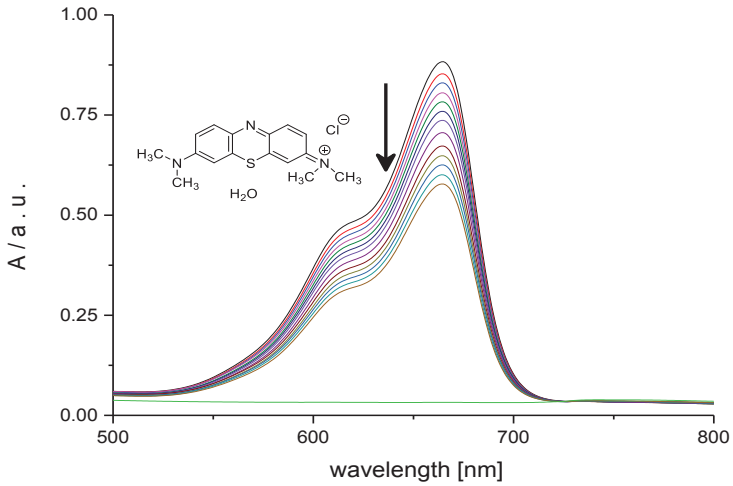

Figure 6.12: UV-visible spectra for 0.012 mM **6.8** upon addition of 0 - 0.36 mM SDS, at 25 °C in buffer (25 mM MOPS, pH 7.0, 50 mM NaCl and 10 vol-% DMSO).

Figure 6.12 shows a hypochromic shift in absorbance (at the λ_{max} of 665 nm) of **6.8** upon addition of SDS. This change in UV-visible absorption may occur because of geometrical distortion of **6.8** when it interacts with SDS, but it may also be a local medium effect.

To quantify the affinity of **6.8** for SDS, the absorbance at 665 nm were plotted as a function of the concentration of SDS (Figure 6.13, see Appendix, Tables A44.129).

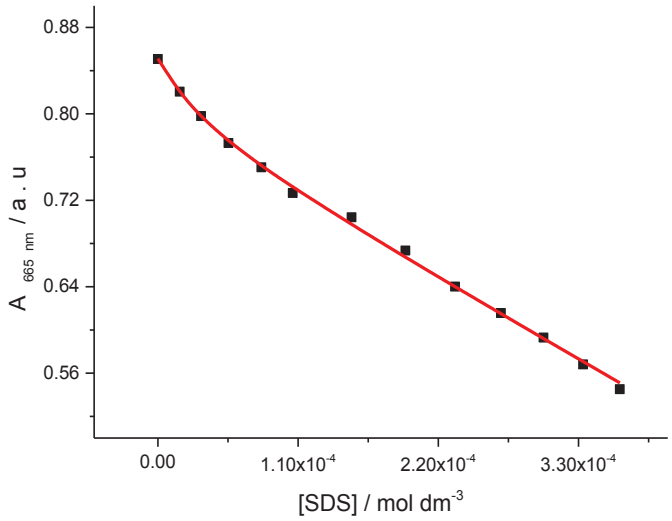

Figure 6.13: Absorbance at 665 nm for 0.012 mM **6.8** as a function of SDS, at 25 °C in buffer (25 mM MOPS, pH 7.0, 50 mM NaCl and 10 vol-% DMSO). The solid line represents the best fit to the data in terms of a multiple independent binding sites model.

Figure 6.13 shows a clear decrease in the absorbance for **6.8** upon the addition of SDS. The binding affinity $K_{binding}$ and stoichiometry were determined by fitting a multiple independent

binding sites model, which also takes ligand dilution into account to the data. The fit reproduces the data well and gives an equilibrium constant $K_{binding}$ of (3.6 ± 1.5) $\times 10^4$ M^{-1} for a stoichiometry restricted to one surfactant molecule per molecule of **6.8**. The obtained binding constant and stoichiometry seem reasonable.

6.2.7 Compound 6.12 binding with SDS

We wanted to study the binding of **6.12** to SDS. The changes in absorption of **6.12** upon addition of SDS were measured in buffer (25 mM MOPS, pH 7.0 and 50 mM NaCl and 10 vol-% DMSO) at 25 °C (Figure 6.14).

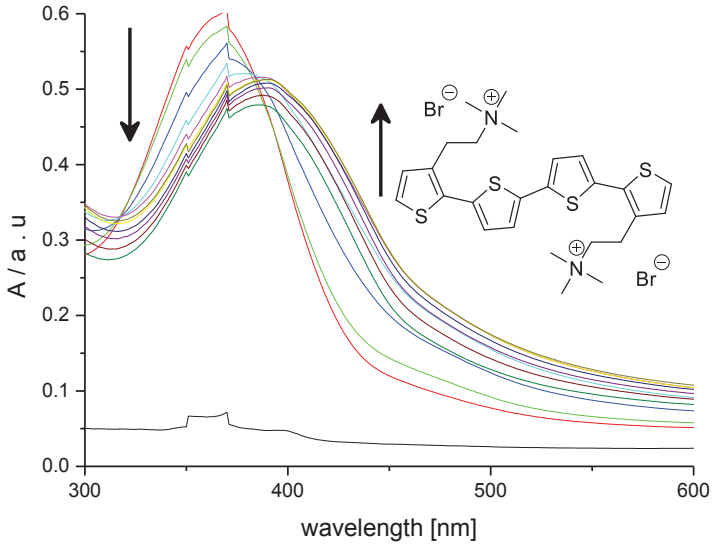

Figure 6.14: UV-visible spectra for 0.019 mM **6.12** upon addition of 0 - 0.22 mM SDS, at 25 °C in buffer (25 mM MOPS, pH 7.0, 50 mM NaCl and 10 vol-% DMSO).

Figure 6.14 shows two events upon addition of SDS. The first event is a hypochromic shift with a maximum change at 370 nm. The second event shows a hyperchromic shift with a maximum change at 404 nm, which appears to be part of the general increase in absorbance at high wavelengths we attribute this increase to scattering of light and thus to precipitation. This increase and decrease in UV-visible absorption may occur because of geometrical distortion of **6.12** when it interacts with SDS, but it may also be a local medium effect.

To quantify the apparent affinity of **6.12** for SDS, the absorbance at 370 and 404 nm were plotted as a function of the concentration of SDS (Figure 6.15, see Appendix, Tables A55.132).

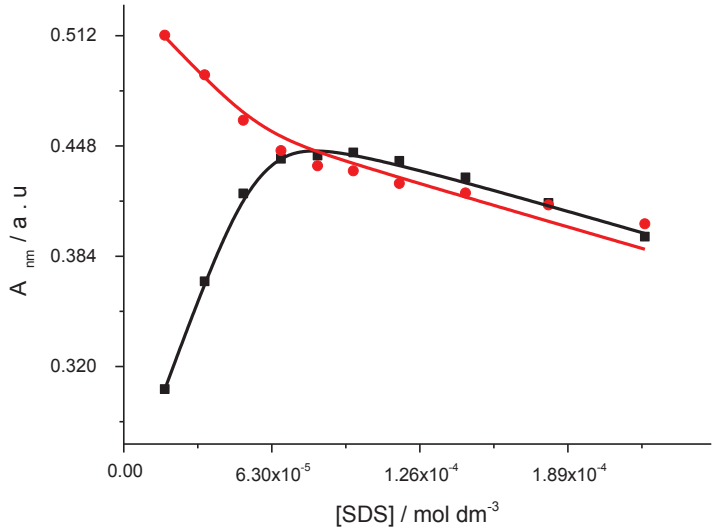

Figure 6.15: Absorbance at 370 nm and at 404 nm for 0.019 mM **6.12** upon addition of 0 − 0.22 mM SDS at 25 °C in buffer (25 mM MOPS, pH 7.0, 50 mM NaCl and 10 vol-% DMSO). The solid lines represent a global fit of a multiple independent sites model to the data.

The titration curves of Figure 6.15 were analysed globally by fitting a version of the multiple independent binding sites models, which also takes ligand dilution into account, to the data. This fit reproduces the data well and gives an apparent equilibrium constant $K_{binding}$ of (2.7 ± 2.2) $\times 10^6$ M^{-1} and a stoichiometry of (3.0 ± 0.2) surfactant molecule per molecule of **6.12.** The obtained value for affinity and stoichiometry seem reasonable, although a stoichiometry of two molecules of SDS per molecule of **6.12** was expected.

Further experiments showed that compound **6.10** and **6.11** did not show any binding with SDS (see appendix A46 for Compound **6.10** with SDS. Figure 46.1 and Figure A46.2, for data in tabular format, see Appendix, Tables A55.130); and (see A47 for Compound **6.11** with SDS. Figure 47.1 and Figure A47.2, for data in tabular format, see Appendix, Tables A55.131).

Summary

The results from UV-visible titrations for **6.1, 6.2, 6.4, 6.5, 6.7, 6.8** and **6.12** with SDS show that these ligands bind to SDS are summarised in Table 6.1.

Table 6.1 Binding affinities and binding stoichiometries for binding of 6.1, 6.2, 6.4, 6.5, 6.7, 6.8 and 6.12 to SDS in buffer (25 mM MOPS, pH 7.0, 50 mM NaCl) at 25 °C.

Ligands	*Binding constant for SDS* K / M^{-1}	*Stoichiometry* n
6.1	$(8.4 \pm 1.7) \times 10^4$	1.02 ± 0.03
6.2	$(2.2 \pm 2.1) \times 10^6$	$3.4 \pm 0.3.$
6.4	$(2.1 \pm 0.47) \times 10^4$	1^*
6.5	$(2.4 \pm 1.7) \times 10^5$	0.1^*
6.7	$(1.5 \pm 1.4) \times 10^4$	3^*
6.8	$(3.6 \pm 1.5) \times 10^4$	1^*
6.10	No binding	
6.11	No binding	
6.12	$(2.7 \pm 2.2) \times 10^6$	3.0 ± 0.2
* restricted		

Table 6.1 reveals that most of our cationic π-conjugated materials interact with sodium dodecyl sulphate. However, there are no interactions with **6.10** and **6.11** probably because of the negative charge on these compounds leads to repulsion with the negative charge of SDS. The highest binding constants of $10^6\ M^{-1}$ and $10^5\ M^{-1}$ are found for ligands that have more positive, charge, meaning strong interaction between molecules and surfactant.

Part B: Interactions of DNA binders with the positively charged of surfactant cetyltrimethyl-ammonium bromide

6.2.8 Compound 6.4 binding with CTAB

We wanted to know the binding of **6.4** to CTAB. The changes in absorption of **6.4** upon addition of CTAB were measured in buffer (25 mM MOPS, pH 7.0 and 50 mM NaCl) at 25 °C (Figure 6.16).

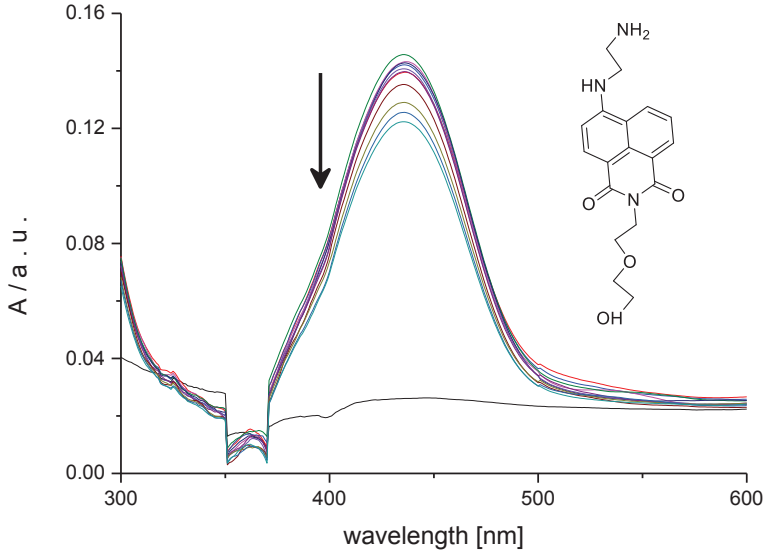

Figure 6.16: UV-visible spectra for 0.010 mM **6.4** upon addition of 0 – 0.42 mM CTAB, at 25 °C in buffer (25 mM MOPS, pH 7.0, 50 mM NaCl).

Figure 6.16 shows a small hyperchromic shift followed by a hypochromic shift in absorbance (at the λ_{max} of 435 nm) of **6.4** upon addition of CTAB. The increase in UV-visible absorption may occur as a result of geometrical distortion of **6.4** when it interacts with CTAB, but it may also be a local medium effect. The subsequent decrease is probably the result of dilution.

To quantify the affinity of **6.4** for CTAB by plotting the absorbance at 435 nm as a function of the concentration of CTAB (Figure 6.17, see Appendix, Tables A55.135).

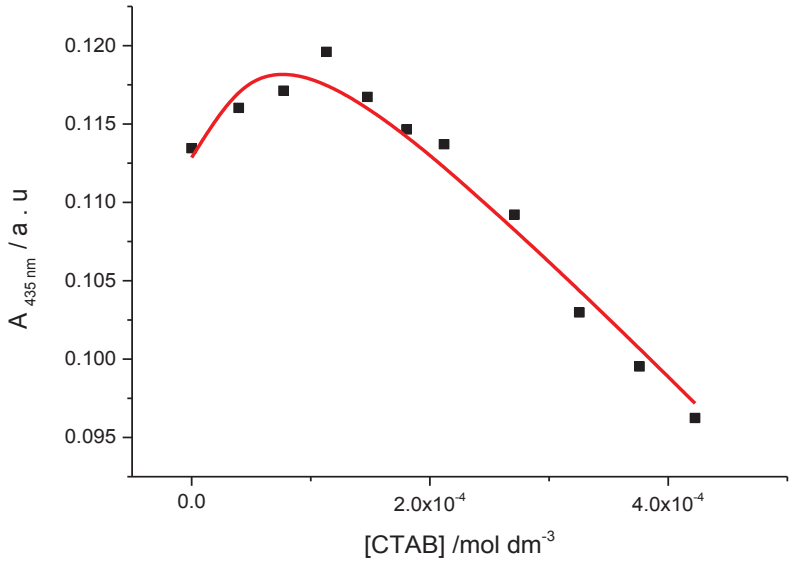

Figure 6.17: Absorbance at 435 nm for 0.010 mM **6.4** upon addition of 0 - 0.42 mM CTAB, at 25 °C in buffer (25 mM MOPS, pH 7.0, 50 mM NaCl). The solid line represents the best fit to the data in terms of a multiple independent binding sites model.

The titration curve in Figure 6.17 was analysed by fitting a version of the multiple independent binding sites model, which also takes ligand dilution into account, to the data. The fit gives an equilibrium constant $K_{binding}$ of $(1.4 \times 10^8 \pm 1.6 \times 10^9)$ M^{-1} for a stoichiometry (12.2 ± 1.1) surfactant molecules per **6.4**. The obtained binding parameters were unreasonable for both stoichiometry and binding constant. The fit reproduces the data well and gives an equilibrium constant $K_{binding}$ of $(1.7 \pm 0.7) \times 10^4$ M^{-1} for a stoichiometry restricted to 1 surfactant molecules per molecule of **6.4.** Electrostatic interactions between the oppositely charged groups are most likely responsible for the interaction of the cationic surfactant with **6.4**.

6.2.9 Compound 6.9 binding with CTAB

We wanted to investigate the binding of **6.9** to CTAB. The changes in absorption of **6.9** upon addition of CTAB were measured in buffer (25 mM MOPS, pH 7.0 and 50 mM NaCl) at 25 °C) (Figure 6.18).

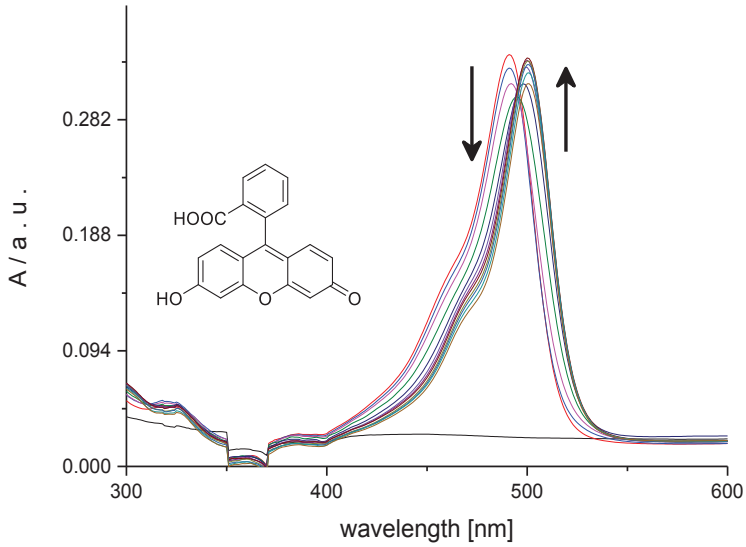

Figure 6.18: UV-visible spectra for 0.0061 mM **6.9** upon addition of 0 - 0.27 mM CTAB, at 25 °C in buffer (25 mM MOPS, pH 7.0, 50 mM NaCl).

Figure 6.18 shows two events. The first event involves a hypochromic shift with a maximum change at 500 nm. The second event shows a hyperchromic shift (with a maximum change at 500 nm). The decrease and increase in UV-visible absorption occur as a result of the interaction of **6.9** molecule with CTAB. The local medium effect would also be the result of the interaction, but it may also be a local medium effect.

To quantify the affinity of **6.9** for CTAB, we plotted the absorbances at 500 nm as a function of the concentration of CTAB (Figure 6.19, see Appendix, Tables A55.138).

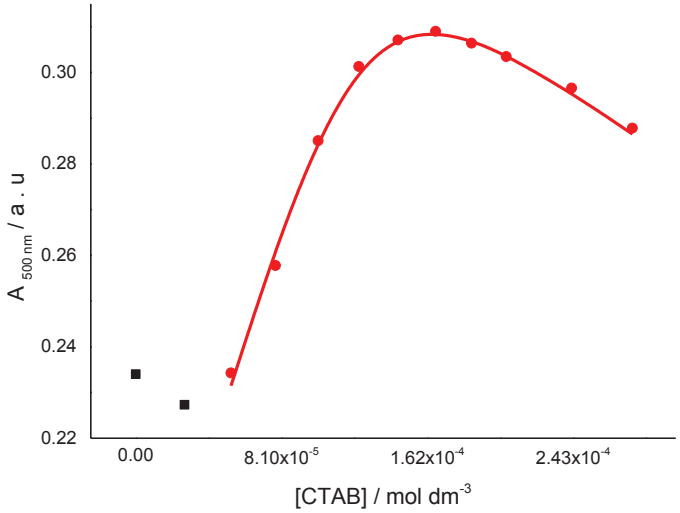

Figure 6.19: Absorbance at 500 nm for 0.067 mM **6.9** as a function of CTAB of 0 – 0.027 mM (■) and 0.052 - 0.27 mM (●) of CTAB, at 25 °C in buffer (25 mM MOPS, pH 7, 50 mM NaCl). The solid line represents a fit of a multiple independent sites model to the data in the 0.052 − 0.27 mM range (●).

Figure 6.19 shows two events. The first event corresponds to a decrease in the absorbance upon addition of 0 - 0.027 mM (■) CTAB. We attribute this decrease in absorbance to strong binding of **6.9** to CTAB, leading to precipitation as a result of charge neutralisation of the **6.9**-CTAB complex. This idea is in agreement with the fact $A_{500\,nm}$ reaches a minimum at a stoichiometry of two molecules of CTAB per molecule of **6.9**. The second event shows a clear increase in the absorbance of **6.9** upon addition 0.052 – 0.27 mM (●) of CTAB. The titration data in Figure 6.20 (with the first event not included) were analysed in terms of a multiple independent binding sites model, which also takes ligand dilution into account. The fit produces an apparent equilibrium constant $K_{binding}$ of (3.9 ± 1.2) × 10^6 M^{-1} for a stoichiometry of (23.9 ± 1.1) surfactants per molecule of **6.9**. We interpret this stoichiometry as the number of surfactant molecules required to present a micellar environment to the molecules of **6.9**.

6.2.10 Compound 6.14 binding with CTAB

We wanted to know whether **6.14** binds to CTAB. The changes in absorption of **6.14** upon addition of CTAB were measured in buffer (25 mM MOPS, pH 7.0 and 50 mM NaCl) at 25 °C (Figure 6.20).

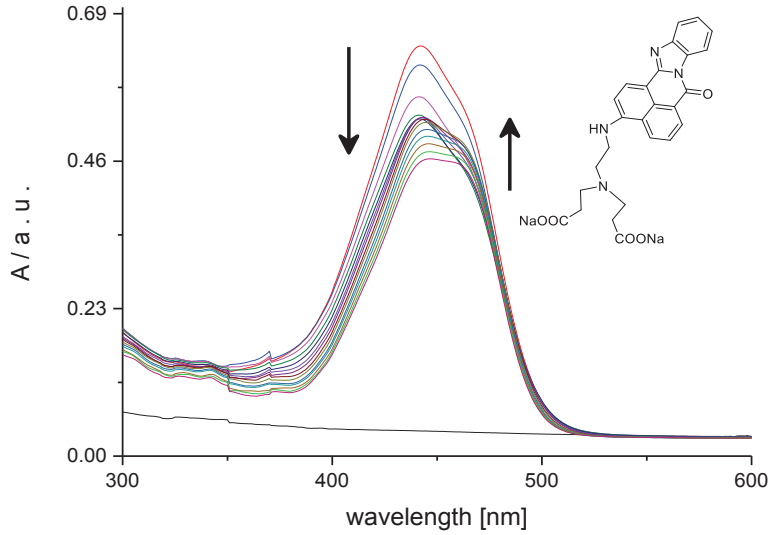

Figure 6.20: UV-visible spectra for 0.0067 mM **6.14** upon addition of 0 - 0.53 mM CTAB, at 25 °C in buffer (25 mM MOPS, pH 7.0, 50 mM NaCl).

Figure 6.20 shows two events. The first event involves a hypochromic shift with a maximum change at 457 nm. The second event shows a hyperchromic shift (with a maximum change at 457 nm). The increase and decrease in UV-visible absorption occur as a result of the interaction

of **6.14** molecule with CTAB. The local medium effect would also be the result of the interaction, but it may also be a local medium effect.

To quantify the affinity of **6.14** for CTAB, the absorbance at 457 nm were plotted as a function of the concentration of CTAB (Figure6.21, seeAppendix, Tables A55.142).

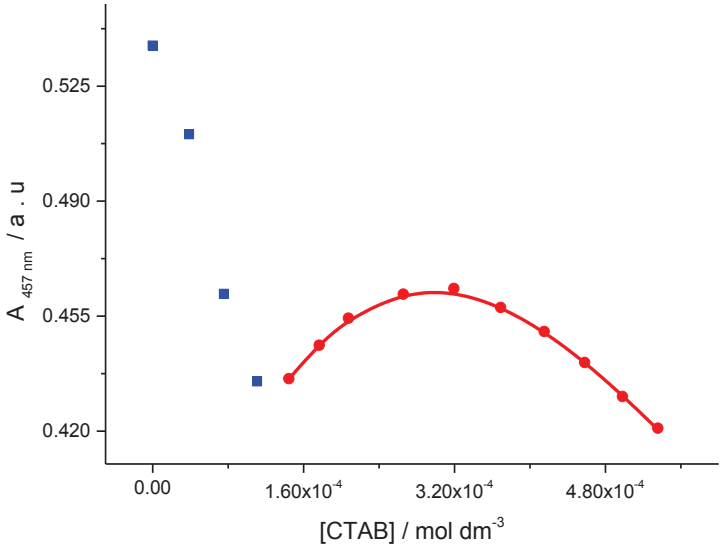

Figure 6.21: Absorbance at 457 nm for 0.067 mM **6.14** as a function of CTAB of 0 – 0.11 mM (■) and 0.14 - 0.53 mM (●) of CTAB, at 25 ºC in buffer (25 mM MOPS, pH 7, 50 mM NaCl). The solid line represents a fit of a multiple independent sites model to the data in the 0.14 - 0.53 mM range.

Figure 6.21 shows two events. The first event corresponds to a rapid decrease in the absorbance upon addition of 0 - 0.11 mM (■) CTAB. We attribute this decrease in absorbance to strong binding of **6.14** to CTAB, leading to precipitation as a result of charge neutralisation of the **6.14**-CTAB complex. This idea is in agreement with the fact $A_{457\ nm}$ reaches a minimum at a stoichiometry of two molecules of CTAB per molecule of **6.14.** The second event shows a clear increase in the absorbance of **6.14** upon addition 0.14 – 0.53 mM (●) of CTAB. The ligand **6.14** strongly interacts with CTAB, and the titration data in Figure 6.22 (with the first event not included) were analysed in terms of a multiple independent binding sites model, which also takes ligand dilution into account. The fit reproduces the data well and produces an apparent equilibrium constant $K_{binding}$ of (6.3 ±1.1) $\times 10^4$ M^{-1} for a stoichiometry of (4.5 ±0.3) molecules of CTAB per molecule of **6.14**. The obtained binding constant and stoichiometry seem reasonable. Titrations with CTAB were also carried out for **6.1, 6.2, 6.5, 6.8, 6.10, 6.11** and **6.12** did not show any binding with CTAB. (See appendixesA48-A54).

Summary

The results from UV-visible titrations for **6.1, 6.2, 6.4, 6.5, 6.7, 6.8, 6.9, 6.10, 6.11, 6.12** and **6.14** with CTAB are summarised in Table 6.1.

Table 6.1 Binding affinities and stoichiometry for binding of 6.1, 6.2, 6.4, 6.5, 6.7, 6.8, 6.9, 6.10, 6.11, 6.12 and 6.14 to CTAB in buffer (25 mM MOPS, pH 7.0, 50 mM NaCl) at 25 °C.

Ligands	***Binding constant for CTAB*** K / M^{-1}	**Stoichiometry** ***n***
6.1	No binding	
6.2	No binding	
6.4	$(1.7 \pm 0.7) \times 10^4$	1*
6.5	No binding	
6.7	No binding	
6.8	No binding	
6.9	$(9.7 \pm 4.1) \times 10^4$ a	3*
6.10	No binding	
6.11	No binding	
6.12	No binding	
6.14	$(6.3 \pm 1.1) \times 10^4$ a	4.5 ±0.3
a) apparent binding constant for the event following initial precipitation b) * restricted		

Table 6.1 shows that negatively charged π-conjugated aromatic molecules **6.9** and **6.14** bind to cetyl trimethyl ammonium bromide CTAB surprisingly, **6.4** also binds to CTAB. The affinity of negative molecules for cationic surfactant CTAB is moderately strong at 10^4 M^{-1} as result of electrostatic interaction and hydrophobic interaction. However, the rest of ligands don't show interacting with CTAB which could be because of the charges on the molecules.

Part c: The effect of nonionic surfactant on DNA binding

6.2.11 Compound 6.12 binding with DNA in the presence of 1 vol-% Tween-20.

We wanted to know whether the binding of **6.12** to DNA is affected the presence of Tween-20. The changes in absorption of **6.12** upon addition of DNA in the presence of 1 vol- % Tween-20 were measured in buffer (25 mM MOPS, pH 7.0, 50 mM NaCl, 1 vol- % Tween-20) at 25 °C (Figure 6.22). Tween-20 is surfactant used in lateral flow assays.

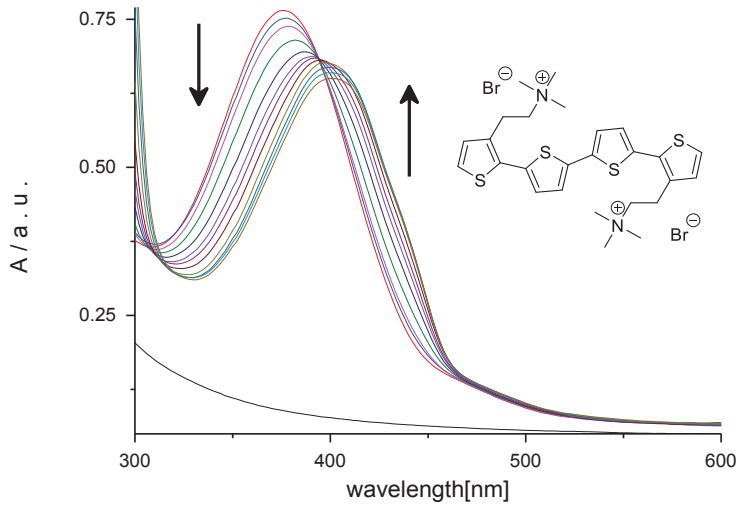

Figure 6.22: UV-visible spectra for 0.0242 mM **6.12** upon addition of 0 – 1.4 mM DNA in presence of 1 vol- % Tween, at 25 °C in buffer (25 mM MOPS, pH 7.0, 50 mM NaCl, 1 vol- % Tween-20).

Figure 6.22 shows a red shift, in absorbance of **6.12** upon addition of DNA in the presence of Tween-20. This change in UV-visible absorption probably occurs as a result of geometrical distortion of **6.12** when it interacts with DNA, but there may also be a local medium effect.

We quantified the affinity of **6.12** for DNA by plotting the absorbances at 368 and 430 nm as a function of the concentration of DNA in the presence of Tween-20 (Figure 6.23, for data in tabular format, see Appendix, Tables A55.143).

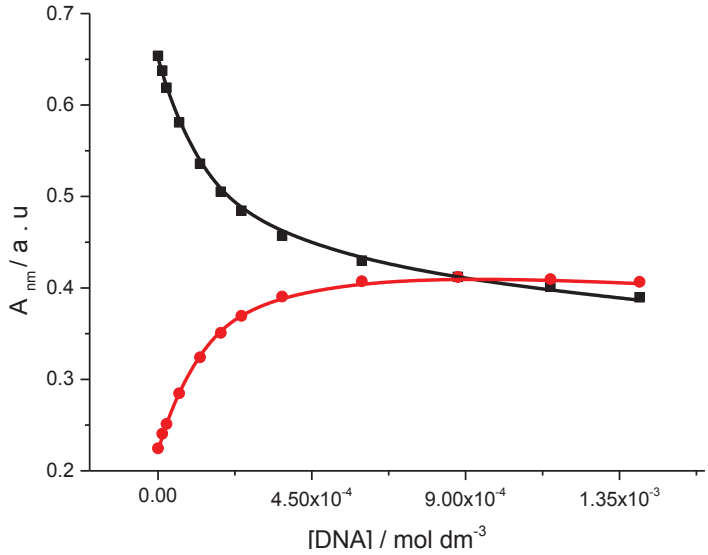

Figure 6.23: Absorbance at 368 nm (■) and 430 nm (●) for 0.0242 mM **6.12** as a function of DNA in the presence of 1 vol- %Tween-20, at 25 °C in buffer (25 mM MOPS, pH 7.0, 50 mM NaCl, 1 vol. % Tween-20). The solid lines represent a global fit of a multiple independent sites model to the data.

Figure 6.23 shows a clear decrease and increase in the absorbance for **6.12** upon addition of DNA in the presence of 1 vol- % Tween-20. The binding affinity $K_{binding}$ and for a binding sites size *n* were determined by globally fitting a multiple independent binding sites model, which also takes ligand dilution into account, to the data. A binding constant $K_{binding}$ of (3.7 ± 1.0) $\times 10^4$ M^{-1} for a binding site size (3.8 ± 0.67) base pairs was found. The obtained binding parameters were reasonable with a well-defined binding site size and binding constant. A $K_{binding}$ of (1.8 ± 0.38) $\times 10^5$ M^{-1} for a binding site size restricted to 3.0 base pairs was observed for **6.12** to DNA in absence 1 vol. % Tween-20. From the differences in the binding constant, it appears that Tween 20 does significantly compete with DNA for **6.12**, but it does not inhibit binding completely.

6.2.12 Compound 6.13 binding with DNA in the presence of 1 vol-% Tween-20.

We wanted to know whether the binding of **6.13** with DNA is affected the presence of Tween-20. The changes in absorption of **6.13** upon addition of DNA in the presence of Tween 20 were measured in buffer (25 mM MOPS, pH 7.0, 50 mM NaCl, 1 vol.% Tween-20) at 25 °C (Figure 6.24).

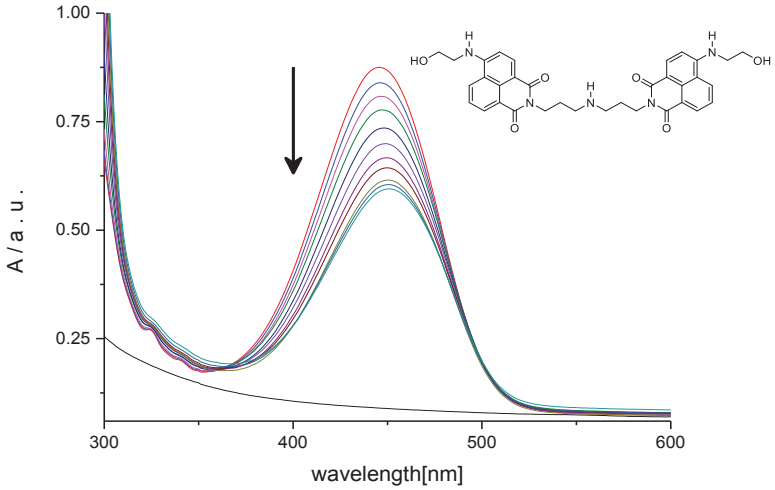

Figure 6.24: UV-visible spectra for 0.0363 mM **6.13** upon addition of 0 – 2.5 mM DNA in presence of Tween-20, at 25 °C in buffer (25 mM MOPS, pH 7.0, 50 mM NaCl, 1 vol. % Tween-20).

Figure 6.24 shows a hypochromic shift in absorbance (at the λ_{max} of 446 nm) of **6.13** upon addition of DNA in presence Tween-20. This change in UV-visible absorption may occur because of geometrical distortion of **6.13** when it interacts with DNA in the presence of Tween -20, but it may also be a local medium effect.

To quantify the affinity of **6.13** for DNA in the presence of Tween-20 by plotting the absorbances at 446 nm as a function of the concentration of DNA (Figure 6.25, see Appendix, Tables A55.144).

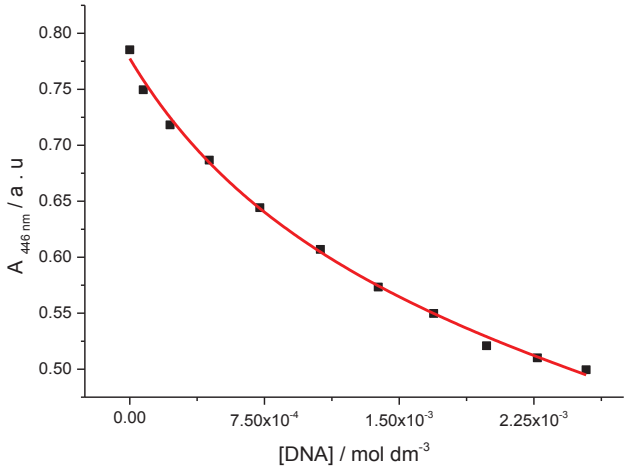

Figure 6.25: Absorbance at 446 nm for 0.0363 mM **6.13** as a function of DNA in the presence of Tween-20, at 25 °C in buffer (25 mM MOPS, pH 7.0, 50 mM NaCl, 1 vol. % Tween-20). The solid line represents the best fit to the data in terms of a multiple independent binding sites model.

Figure 6.25 shows a decrease in the absorbance for **6.13** upon addition of DNA in the presence of 1 vol- % Tween-20. The binding affinity $K_{binding}$ and binding sites size *n* were determined by fitting a multiple independent binding sites model, which also takes ligand dilution into account, to the data. A binding constant $K_{binding}$ of $(1.6\times10^{-3} \pm 0.1) \times10^{4}$ M^{-1} with a binding site size of $(1.8\times10^{-6} \pm 1.8\times10^{-4})$ base pairs was found. The obtained binding parameters were very small, and both stoichiometry and binding constant seem unreasonable. The data were therefore reanalysed with the stoichiometry restricted to 3.0 base pairs, giving an apparent equilibrium constant $K_{binding}$ of $(2.8 \pm 0.5) \times 10^{3}$ M^{-1}. A $K_{binding}$ of $(2.965 \pm 0.381) \times 10^{3}$ M^{-1} for a binding site size restricted to 3.0 base pairs was observed for **6.13** interacting with to DNA in the absence of Tween-20. From the similarity in the binding constant, it appears that Tween-20 does not significantly compete with DNA for **6.13**.

6.2.13 Compound 6.15 binding with DNA in the presence of 1 vol.% Tween-20.

We wanted to know whether the binding of **6.15** with DNA is affected the presence of Tween-20. The changes in absorption of **6.15** upon addition of DNA in the presence of Tween 20 were measured in buffer (25 mM MOPS, pH 7.0, 50 mM NaCl, 1 vol.% Tween-20) at 25 °C (Figure 6.26).

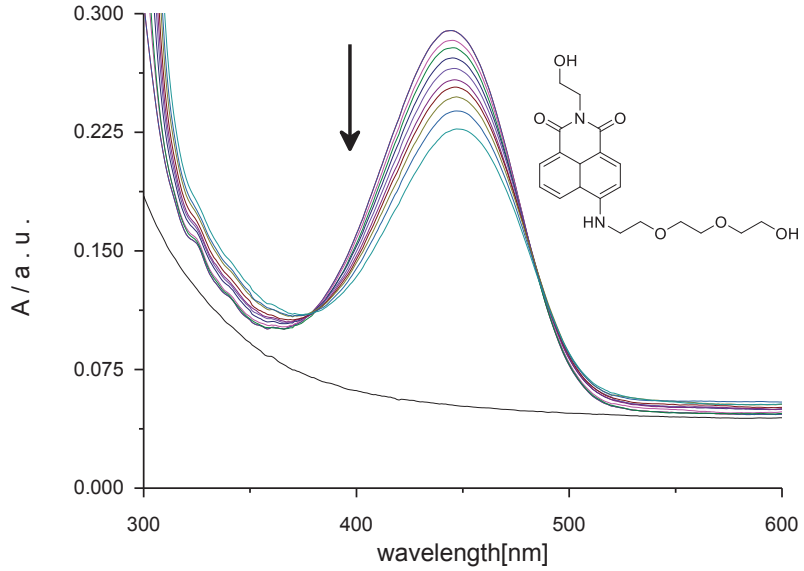

Figure 6.26: UV-visible spectra for 0.021 mM **6.15** upon addition of 0 – 2.05 mM DNA in presence of Tween-20, at 25 °C in buffer (25 mM MOPS, pH 7.0, 50 mM NaCl, 1 vol- % Tween-20).

Figure 6.26 shows a hypochromic shift in absorbance (at the λ_{max} of 445 nm) of **6.15** upon addition of DNA in presence Tween-20. This change in UV-visible absorption may occur because of geometrical distortion of **6.15** when it interacts with DNA in the presence of Tween -20, but it may also be a local medium effect.

To quantify the affinity of **6.15** for DNA by plotting the absorbances at 445 nm as a function of the concentration of DNA (Figure 6.27, see Appendix, Tables A55.145).

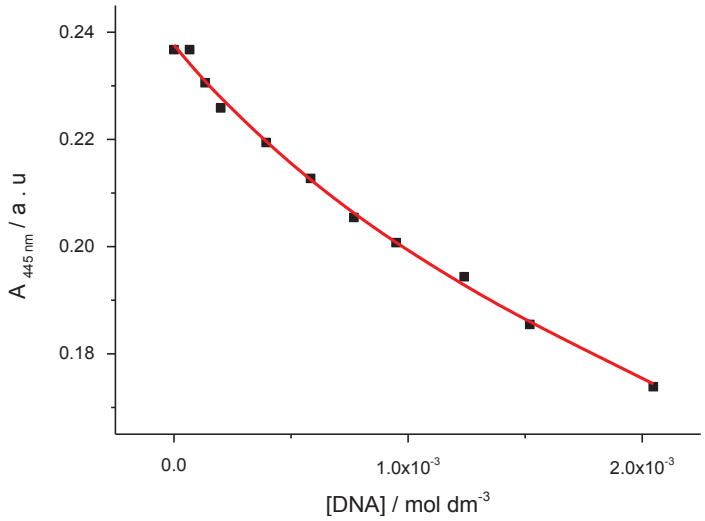

Figure 6.27: Absorbance at 445 nm for 0.021 mM **6.15** as a function of DNA in the presence of Tween-20, at 25 °C in buffer (25 mM MOPS, pH 7.0, 50 mM NaCl, 1 vol- % Tween-20). The solid line represents the best fit to the data in terms of a multiple independent binding sites model.

Figure 6.27 shows a decrease in the absorbance for **6.15** upon addition of DNA in the presence of 1 vol-% Tween-20. The binding affinity $K_{binding}$ and binding sites size *n* were determined by fitting a multiple independent binding sites model, which also takes ligand dilution into account, to the data. A binding constant $K_{binding}$ of $(2\times10^{-3} \pm 1.8) \times10^{5}$ M^{-1} with a binding site size of $(4\times10^{-1} \pm 318.8)$ base pairs was found. The obtained binding parameters were very small, and both stoichiometry and binding constant seem unreasonable. The data were therefore reanalysed with the stoichiometry restricted to 3.0 base pairs, giving an apparent equilibrium constant $K_{binding}$ of $(1.7 \pm 0.5) \times 10^{3}$ M^{-1}. A $K_{binding}$ of $(2.965 \pm 0.09) \times 10^{3}$ M^{-1} for a binding site size restricted to 3.0 base pairs was observed for **6.15** interacting with to DNA in the absence of Tween-20. From the difference in the binding constant, it appears that Tween-20 does significantly compete with DNA for **6.15**.

Summary

Table 6.3 Binding affinities and binding site sizes for binding of 6.12, 6.13 and 6.15 to DNA and the effect of 1 vol- % Tween-20 on DNA binding in buffer (25 mM MOPS, pH 7.0, 50 mM NaCl) at 25 °C.

Ligands	*Binding affinities DNA* K / M^{-1}	*Binding affinities for DNA with Tween-20* K / M^{-1}	*Effect of Tween-20 on affinity for DNA*
6.12	$(1.8 \pm 0.4) \times 10^5$ n = 3*	$(2.7 \pm 0.8)\ 10^4$ n = 3*	Decrease
6.13	$(2.9 \pm 0.3) \times 10^3$ n = 3*	$(2.8 \pm 0.5) \times 10^3$ n = 3*	No change
6.15	$(2.9 \pm 0.09) \times 10^3$ n = 3*	$(1.7 \pm 0.5) \times 10^3$ n = 3*	No change or small Decrease
a) * restricted			

Table 6.3 shows that some of the potential sensitisers bind to DNA in the presence of Tween-20. The affinity of **6.12** for DNA in the presence of Tween-20 is moderately strong ~ 10^4 M^{-1} compared to this affinity, **6.13** and **6.15** have low affinity ~ 10^3 M^{-1}. Compounds **6.12** and **6.15** seem to show a decrease in affinity in the presence of Tween-20 as a result of the interaction between the ligand and DNA, even though there is no charge in the surfactant Tween-20. From the difference in the binding constant, it appears that Tween-20 does significantly compete with DNA for **6.12** and **6.15**. The presence of this competition may be beneficial to avoid any non-specific interaction if we use **6.12** and **6.15** in a biosensor. There is no effect of surfactant on binding affinity between DNA and **6.13**.

6.3 Conclusion

According to the results presented in this chapter, cations **6.1, 6.2, 6.4, 6.5, 6.7, 6.8** and **6.12** bind with negative surfactant SDS by electrostatic and hydrophobic interaction. The anionic ligands (**6.9** and **6.14**) bind to CTAB by electrostatic interaction. Remarkably, **6.4** also appears to bind to CTAB. We found a decrease in affinity of **6.12** and **6.15** for DNA in the presence of Tween 20. In contrast, there is no effect of surfactant on binding between DNA to **6.13.**

6.4 Materials and Methods

6.4.1 Materials

SDS was procured from Acros and Sigma-Aldrich. CTAB was purchased from Sigma-Aldrich. The buffer components were purchased from Melford Laboratories Ltd and Sigma-Aldrich.

6.5 Solutions preparation

6.5.1 Surfactants, SDA, CTAB and Tween 20 preparation

All experiments were carried out in buffer (25 mM MOPS, 50 mM NaCl, pH 7.0, at 25 °C). SDS and CTAB were dissolved in MOPS buffer. To prepare the 1 vol- % Tween-20, we used 99 ml MOPS and 1 ml from polysorbate.

6.6 Spectroscopic studies

2.0 ml of MOPS buffer was added in a 1.0 cm path length cuvette. The stock solutions of all molecules in MOPS buffer, sometimes involving 10 vol-% DMSO were prepared as mentioned before (Section 6.2.1). All UV-visible titrations were carried out by adding aliquots of the macromolecules, such as SDS and CTAB, stock solutions into the 1.0 cm path length cuvette which contains the ligand solution in MOPS, recording the absorption in the range of 200 – 800 nm after each addition. Moreover, we used MOPS with 1 vol- % Tween-20 as a buffer to see the effect of surfactant on DNA binding. Absorptions were kept in the range of (0.0 - 1.0). The absorptions at selected wavelengths were plotted against macromolecule concentrations, and a multiple independent binding sites model was used to analyse the UV-visible data using the Origin 9.0 software.

Chapter Seven

Conclusions and future work

7.1 Conclusion

The aims of this thesis were to develop optoelectronically active DNA binders as sensitisers for sensors (Scheme 1.5) and to collect binding data that can be used in the use of biomacromolecules and optoelectronically active compounds in directed assembly. When sensitisers bind to DNA their spectroscopic and electronic properties may change, thus allowing applications such as biosensors. Binding of molecules with nucleic acids can also be used for the assembly of functional multicomponent structures containing active components templated by DNA.

In particular, this thesis explores the effect of natural biopolymers such as serum albumin (SA), hyaluronic acid (HA) and alginic acid (AA) and synthetic polymers such as sodium polystyrene sulfonic acid (POSA) and polyacrylic acid (PAA) on DNA-binding of potential sensitisers. In addition, we investigated the effect of surfactant on DNA-binding of potential sensitisers. The biophysical data is useful for improving sensitivity, selectivity and minimizing nonspecific binding to DNA biosensors.

From the results and discussion presented chapter 2 until 6, the overall conclusions are as follows. The majority of cationic oligoheteroaromatics explored reveal good binding with duplex DNA. Several of the ligands **3.1, 3.2, 3.3, 3.7** and **3.9** bind to SA in a moderately strong mode while ligands **3.1, 3.2, 3.8** and **3.10** were found to have a high affinity for transferrin TF. Ligands **3.1, 3.5, 3.7, 3.8, 3.10** and **3.11** do not show a change in the affinity for DNA in the presence of SA, but our work demonstrated a decrease in affinity of ligands **3.2, 3.4, 3.6** and **3.12** for DNA, suggesting that these potential sensitisers bind to serum albumin and this leads to a decreased apparent K_{binding}. This decrease could be a source of false negative results in our biosensors. Surprisingly an increase in the apparent affinity of **3.3** for DNA was also observed in the presence of SA, an effect attributed to sensitisers binding to serum albumin instead of to the DNA backbone and increasing apparent K_{binding} and this could cause false positives. TF also affected DNA binding; **3.2** showed a decrease in affinity for DNA in the presence of TF.

We found good binding of all compounds with AA but only **4.7** and **4.8** bind to HA. Most ligands bind to DNA in the presence of biopolymer without any change in a binding constant. Four molecules, viz. **4.1, 4.2, 4.7** and **4.8,** show changes in affinity for DNA in the presence of biopolymers.

Although the majority of cationic oligoheteroaromatics reveal good binding with DNA in the presence of POSA and PAA, there is a strong effect of POSA and PAA on DNA binding. All ligands expect **5.1**, exhibit decreased affinity in the presence of polymer POSA which could lead to false negatives if these compounds were used in a biosensor. Compounds **5.4, 5.10, 5.11** and **5.12** show no change in affinity for DNA in the presence of PAA.

Positive molecules, for example, **6.1, 6.2, 6.4, 6.5, 6.7, 6.8** and **6.12** bind with anionic surfactant SDS by electrostatic and hydrophobic interaction. Negative ligands bind to cationic CTAB. We also observed that Tween-20 decreases the affinity of sensitisers for DNA but doesn't fully suppress it.

7.2 Future work

The results from this thesis can help develop and improve the performance of biosensors. However there still are several areas which can be explored further to enable the optimisation of the biosensor.

1. The use of different types of potential DNA binders, in order to develop a structure-activity relationship and thus design new ligands to use as sensitisers in different types of genosensors.
2. Explore selectivity of oligoheteroaromatics for specific base pairs too, in the hope that this could lead to the application of this type of compound in more selective biosensors.
3. Different number of aromatic rings to make shorter aromatic systems as well as less cationic charge to avoid any difficulties resulting from poor solubility and precipitation.
4. Develop large molecules that can be used in electrochemical impedance spectroscopy EIS based biosensors.
5. Use different positive polymers and macromolecules to complement the work described here using negatively charged (bio)polymers.
6. We can use the potential of copolymers like POSA-PAA to see whether we can develop self−sorting systems.
7. Use different instruments like CD, ITC and fluorescence to study binding in more detail.

References

References

1. Gibson, D., Drug--DNA interactions and novel drug design. *The pharmacogenomics journal* **2002,** *2* (5), 275-277.
2. Porcheddu, A.; Giacomelli, G., Peptide Nucleic Acids (PNAs), A Chemical Overview. *Current Medicinal Chemistry* **2005,** *12* (22), 2561-2599.
3. Dervan, P. B., Molecular recognition of DNA by small molecules. *Bioorganic & Medicinal Chemistry* **2001,** *9* (9), 2215-2235.
4. Xie, Z.-R.; Hwang, M.-J., Ligand Binding Site Prediction Using Ligand Interacting and Binding Site-Enriched Protein Triangles. *Bioinformatics* **2012**.
5. Laurie, A. T. R.; Jackson, R. M., Q-SiteFinder: an energy-based method for the prediction of protein–ligand binding sites. *Bioinformatics* **2005,** *21* (9), 1908-1916.
6. Akiyama, Y.; Ma, Q.; Edgar, E.; Laikhter, A.; Hecht, S. M., Identification of strong DNA binding motifs for bleomycin. *Journal of the American Chemical Society* **2008,** *130* (30), 9650-9651.
7. Campbell, N. H.; Smith, D. L.; Reszka, A. P.; Neidle, S.; O'Hagan, D., Fluorine in medicinal chemistry: β-fluorination of peripheral pyrrolidines attached to acridine ligands affects their interactions with G-quadruplex DNA. *Organic & biomolecular chemistry* **2011,** *9* (5), 1328-1331.
8. Lyles, M. B.; Cameron, I. L., Interactions of the DNA intercalator acridine orange, with itself, with caffeine, and with double stranded DNA. *Biophysical chemistry* **2002,** *96* (1), 53-76.
9. Shi, Y.; Guo, C.; Sun, Y.; Liu, Z.; Xu, F.; Zhang, Y.; Wen, Z.; Li, Z., Interaction between DNA and microcystin-LR studied by spectra analysis and atomic force microscopy. *Biomacromolecules* **2011,** *12* (3), 797-803.
10. Elder, R. M.; Emrick, T.; Jayaraman, A., Understanding the effect of polylysine architecture on DNA binding using molecular dynamics simulations. *Biomacromolecules* **2011,** *12* (11), 3870-3879.
11. Najari, A.; Ho, H. A.; Gravel, J.-F.; Nobert, P.; Boudreau, D.; Leclerc, M., Reagentless ultrasensitive specific DNA array detection based on responsive polymeric biochips. *Analytical chemistry* **2006,** *78* (22), 7896-7899.
12. Gottesfeld, J. M.; Neely, L.; Trauger, J. W.; Baird, E. E.; Dervan, P. B., Regulation of gene expression by small molecules. *Nature* **1997,** *387* (6629), 202.
13. Kongsuphol, P.; Ng, H. H.; Pursey, J. P.; Arya, S. K.; Wong, C. C.; Stulz, E.; Park, M. K., EIS-based biosensor for ultra-sensitive detection of TNF-alpha from non-diluted human serum. *Biosensors & Bioelectronics* **2014,** *61*, 274-279.
14. Daniels, J. S.; Pourmand, N., Label-free impedance biosensors: Opportunities and challenges. *Electroanalysis* **2007,** *19* (12), 1239-1257.
15. Morange, M., The Central Dogma of molecular biology. *Resonance* **2009,** *14* (3), 236-247.
16. Winters, T., Gene targeted agents: new opportunities for rational drug development. *Current opinion in molecular therapeutics* **2000,** *2* (6), 670-681.
17. Bloomfield, V.; Crothers, D.; Tinoco, J.; Hearst, J.; Wemmer, D.; Killman, P.; Turner, D., Bases, nucleosides, and nucleotides. *Nucleic Acids: Structures, Properties, and Functions (University Science Books, Sausalito, CA, 2000)* **2000**, 13-43.
18. Watson, J. D.; Crick, F. H., A structure for deoxyribose nucleic acid. *Nature* **1953,** *171* (4356), 737-738.
19. Watson, J. D.; Crick, F., *A structure for deoxyribose nucleic acid*. [Macmillan]: [London], 1953.

20. Saenger, W., Forces stabilizing associations between bases: hydrogen bonding and base stacking. In *Principles of Nucleic Acid Structure*, Springer: 1984; pp 116-158.
21. Watson, J. D.; Crick, F. H., Molecular structure of nucleic acids. *Nature* **1953,** *171* (4356), 737-738.
22. Yakovchuk, P.; Protozanova, E.; Frank-Kamenetskii, M. D., Base-stacking and base-pairing contributions into thermal stability of the DNA double helix. *Nucleic acids research* **2006,** *34* (2), 564-574.
23. Blackburn, G. M., *Nucleic acids in chemistry and biology*. Royal Society of Chemistry: 2006.
24. Bloomfield, V.; Crothers, D.; Tinoco, J., Bases, nucleosides, and nucleotides. *Nucleic Acids: Structures, Properties, and Functions (University Science Books, Sausalito, CA, 2000)* **2000**, 13-43.
25. Ussery, D. W., DNA Structure: A-, B-and Z-DNA Helix Families. *eLS* **2002**.
26. Wang, A.; Quigley, G. J.; Kolpak, F. J.; Crawford, J. L.; Van Boom, J. H.; van der Marel, G.; Rich, A., Molecular structure of a left-handed double helical DNA fragment at atomic resolution. *Nature* **1979,** *282* (5740), 680-686.
27. Cozzone, A. J., Proteins: Fundamental Chemical Properties. In *eLS*, John Wiley & Sons, Ltd: 2001.
28. Wedemeyer, W. J.; Scheraga, H. A., Protein Folding: Overview of Pathways. In *eLS*, John Wiley & Sons, Ltd: 2001.
29. Landry, Y.; Gies, J. P., Drugs and their molecular targets: an updated overview. *Fundamental & clinical pharmacology* **2008,** *22* (1), 1-18.
30. Latchman, D. S., How can we use our growing understanding of gene transcription to discover effective new medicines? *Current opinion in biotechnology* **1997,** *8* (6), 713-717.
31. Lander, E. S.; Linton, L. M.; Birren, B.; Nusbaum, C.; Zody, M. C.; Baldwin, J.; Devon, K.; Dewar, K.; Doyle, M.; FitzHugh, W., Initial sequencing and analysis of the human genome. *Nature* **2001,** *409* (6822), 860-921.
32. Hossain, M.; Khan, A. Y.; Kumar, G. S., Interaction of the anticancer plant alkaloid sanguinarine with bovine serum albumin. *PLoS One* **2011,** *6* (4), e18333.
33. Carter, D. C.; Ho, J. X., Structure of serum albumin. In *Advances in Protein Chemistry; Lipoproteins, apolipoproteins, and lipases*, Schumaker, V. N., Ed. 1994; Vol. 45, pp 153-203.
34. Barbero, N.; Barni, E.; Barolo, C.; Quagliotto, P.; Viscardi, G.; Napione, L.; Pavan, S.; Bussolino, F., A study of the interaction between fluorescein sodium salt and bovine serum albumin by steady-state fluorescence. *Dyes and Pigments* **2009,** *80* (3), 307-313.
35. Carter, D. C.; Chang, B.; Ho, J. X.; Keeling, K.; Krishnasami, Z., Preliminary crystallographic studies of four crystal forms of serum albumin. *The FEBS Journal* **1994,** *226* (3), 1049-1052.
36. Chen, C.; Ma, M.; Zhang, J.; Wang, L.; Xiang, B., Spectroscopic investigation of the interaction of bovine serum albumin with a novel cardiac agent V-09. *Spectroscopy-an International Journal* **2008,** *22* (1), 43-50.
37. He, X. M.; Carter, D. C., ATOMIC-STRUCTURE AND CHEMISTRY OF HUMAN SERUM-ALBUMIN. *Nature* **1992,** *358* (6383), 209-215.
38. Cistola, D. P.; Small, D. M., Fatty acid distribution in systems modeling the normal and diabetic human circulation. A 13C nuclear magnetic resonance study. *The Journal of clinical investigation* **1991,** *87* (4), 1431-1441.
39. Chung, M. C.-M., Structure and function of transferrin. *Biochemical Education* **1984,** *12* (4), 146-154.
40. Cheng, Y.; Zak, O.; Aisen, P.; Harrison, S. C.; Walz, T., Structure of the Human Transferrin Receptor-Transferrin Complex. *Cell* **2004,** *116* (4), 565-576.
41. Zhang, J.; Sun, Y.; Xu, B.; Zhang, H.; Gao, Y.; Zhang, H.; Song, D., A novel surface plasmon resonance biosensor based on graphene oxide decorated with gold nanorod–antibody

conjugates for determination of transferrin. *Biosensors and Bioelectronics* **2013,** *45* (Supplement C), 230-236.
42. Eckenroth, B. E.; Steere, A. N.; Chasteen, N. D.; Everse, S. J.; Mason, A. B., How the binding of human transferrin primes the transferrin receptor potentiating iron release at endosomal pH. *Proceedings of the National Academy of Sciences* **2011,** *108* (32), 13089-13094.
43. Nadagouda, M. N.; Varma, R. S., Synthesis of thermally stable carboxymethyl cellulose/metal biodegradable nanocomposites for potential biological applications. *Biomacromolecules* **2007,** *8* (9), 2762-2767.
44. Moroianu, C.; Samoilescu, G., ANALELE UNIVERSITĂŢII "EFTIMIE MURGU" REŞIŢA ANUL XV, NR. 1, 2008, ISSN 1453-7397.
45. Hamley, I. W.; Hamley, I. W., *The physics of block copolymers*. Oxford University Press New York: 1998; Vol. 19.
46. Lynd, N. A.; Hillmyer, M. A., Influence of polydispersity on the self-assembly of diblock copolymers. *Macromolecules* **2005,** *38* (21), 8803-8810.
47. Hillmyer, M. A.; Bates, F. S., Synthesis and characterization of model polyalkane− poly (ethylene oxide) block copolymers. *Macromolecules* **1996,** *29* (22), 6994-7002.
48. Lim Soo, P.; Eisenberg, A., Preparation of block copolymer vesicles in solution. *Journal of Polymer Science Part B: Polymer Physics* **2004,** *42* (6), 923-938.
49. Yu, G.-e.; Eisenberg, A., Multiple morphologies formed from an amphiphilic ABC triblock copolymer in solution. *Macromolecules* **1998,** *31* (16), 5546-5549.
50. Kita-Tokarczyk, K.; Grumelard, J.; Haefele, T.; Meier, W., Block copolymer vesicles—using concepts from polymer chemistry to mimic biomembranes. *Polymer* **2005,** *46* (11), 3540-3563.
51. Shirakawa, H., The discovery of polyacetylene film: the dawning of an era of conducting polymers (Nobel lecture). *Angewandte Chemie International Edition* **2001,** *40* (14), 2574-2580.
52. García, G.; Timón, V.; Hernández-Laguna, A.; Navarro, A.; Fernández-Gómez, M., Influence of the alkyl and alkoxy side chains on the electronic structure and charge-transport properties of polythiophene derivatives. *Physical Chemistry Chemical Physics* **2011,** *13* (21), 10091-10099.
53. Jaiswal, M.; Menon, R., Polymer electronic materials: a review of charge transport. *Polymer international* **2006,** *55* (12), 1371-1384.
54. Shirakawa, H.; Louis, E. J.; MacDiarmid, A. G.; Chiang, C. K.; Heeger, A. J., Synthesis of electrically conducting organic polymers: halogen derivatives of polyacetylene,(CH) x. *Journal of the Chemical Society, Chemical Communications* **1977,** (16), 578-580.
55. Reddinger, J. L.; Reynolds, J. R., Molecular engineering of π-conjugated polymers. In *Radical Polymerisation Polyelectrolytes*, Springer: 1999; pp 57-122.
56. Ho, H.-A.; Najari, A.; Leclerc, M., Optical detection of DNA and proteins with cationic polythiophenes. *Accounts of chemical research* **2008,** *41* (2), 168-178.
57. Nilsson, K. P. R.; Inganäs, O., Chip and solution detection of DNA hybridization using a luminescent zwitterionic polythiophene derivative. *Nature materials* **2003,** *2* (6), 419-424.
58. Mishra, A.; Ma, C.-Q.; Bauerle, P., Functional oligothiophenes: molecular design for multidimensional nanoarchitectures and their applications. *Chemical reviews* **2009,** *109* (3), 1141-1276.
59. Murphy, A. R.; Fréchet, J. M., Organic semiconducting oligomers for use in thin film transistors. *Chemical reviews* **2007,** *107* (4), 1066-1096.
60. Wilson, W. D.; Tanious, F. A.; Ding, D.; Kumar, A.; Boykin, D. W.; Colson, P.; Houssier, C.; Bailly, C., Nucleic acid interactions of unfused aromatic cations: evaluation of proposed minor-groove, major-groove, and intercalation binding modes. *Journal of the American Chemical Society* **1998,** *120* (40), 10310-10321.

61. Garnier, F.; Korri-Youssoufi, H.; Srivastava, P.; Mandrand, B.; Delair, T., Toward intelligent polymers: DNA sensors based on oligonucleotide-functionalized polypyrroles. *Synthetic Metals* **1999,** *100* (1), 89-94.
62. McQuade, D. T.; Pullen, A. E.; Swager, T. M., Conjugated polymer-based chemical sensors. *Chemical Reviews* **2000,** *100* (7), 2537-2574.
63. Drummond, T. G.; Hill, M. G.; Barton, J. K., Electrochemical DNA sensors. *Nature biotechnology* **2003,** *21* (10), 1192-1199.
64. Dey, D.; Goswami, T., Optical biosensors: a revolution towards quantum nanoscale electronics device fabrication. *BioMed Research International* **2011,** *2011*.
65. Grieshaber, D.; MacKenzie, R.; Voeroes, J.; Reimhult, E., Electrochemical biosensors-sensor principles and architectures. *Sensors* **2008,** *8* (3), 1400-1458.
66. Scheller, F.; Hintsche, R.; Pfeiffer, D.; Schubert, F.; Riedel, K.; Kindervater, R., Biosensors: fundamentals, applications and trends. *Sensors and Actuators B: Chemical* **1991,** *4* (1-2), 197-206.
67. Marazuela, M.; Moreno-Bondi, M., Fiber-optic biosensors-an overview. *Analytical and bioanalytical chemistry* **2002,** *372* (5), 664-682.
68. Wang, J., Survey and summary: from DNA biosensors to gene chips. *Nucleic acids research* **2000,** *28* (16), 3011-3016.
69. Regan, E. M.; Hallett, A. J.; Wong, L. C.; Saeed, I. Q.; Langdon-Jones, E. E.; Buurma, N. J.; Pope, S. J.; Estrela, P., A novel cobalt complex for enhancing amperometric and impedimetric DNA detection. *Electrochimica Acta* **2014,** *128*, 10-15.
70. Clark, L. C.; Lyons, C., Electrode systems for continuous monitoring in cardiovascular surgery. *Annals of the New York Academy of sciences* **1962,** *102* (1), 29-45.
71. Yoo, E.-H.; Lee, S.-Y., Glucose biosensors: an overview of use in clinical practice. *Sensors* **2010,** *10* (5), 4558-4576.
72. Keusgen, M., Biosensors: new approaches in drug discovery. *Naturwissenschaften* **2002,** *89* (10), 433-444.
73. Kongsuphol, P.; Ng, H. H.; Pursey, J. P.; Arya, S. K.; Wong, C. C.; Stulz, E.; Park, M. K., EIS-based biosensor for ultra-sensitive detection of TNF-α from non-diluted human serum. *Biosensors and Bioelectronics* **2014,** *61*, 274-279.
74. Pearson, J.; Gill, A.; Vadgama, P., Analytical aspects of biosensors. *Annals of clinical biochemistry* **2000,** *37* (2), 119-145.
75. Taton, T. A.; Mirkin, C. A.; Letsinger, R. L., Scanometric DNA array detection with nanoparticle probes. *Science* **2000,** *289* (5485), 1757-1760.
76. Ho, H. A.; Boissinot, M.; Bergeron, M. G.; Corbeil, G.; Doré, K.; Boudreau, D.; Leclerc, M., Colorimetric and fluorometric detection of nucleic acids using cationic polythiophene derivatives. *Angewandte Chemie* **2002,** *114* (9), 1618-1621.
77. Åslund, A.; Nilsson, K. P. R.; Konradsson, P., Fluorescent oligo and poly-thiophenes and their utilization for recording biological events of diverse origin—when organic chemistry meets biology. *Journal of chemical biology* **2009,** *2* (4), 161-175.
78. Cammann, K., Bio-sensors based on ion-selective electrodes. *Fresenius' Journal of Analytical Chemistry* **1977,** *287* (1), 1-9.
79. Bakker, E.; Telting-Diaz, M., Electrochemical sensors. *Analytical chemistry* **2002,** *74* (12), 2781-2800.
80. Alligrant, T. M.; Nettleton, E. G.; Crooks, R. M., Electrochemical detection of individual DNA hybridization events. *Lab on a Chip* **2013,** *13* (3), 349-354.
81. Cai, Z.; Song, Y.; Wu, Y.; Zhu, Z.; Yang, C. J.; Chen, X., An electrochemical sensor based on label-free functional allosteric molecular beacons for detection target DNA/miRNA. *Biosensors and Bioelectronics* **2013,** *41*, 783-788.

82. Balintová, J.; Špaček, J.; Pohl, R.; Brázdová, M.; Havran, L.; Fojta, M.; Hocek, M., Azidophenyl as a click-transformable redox label of DNA suitable for electrochemical detection of DNA–protein interactions. *Chemical Science* **2015,** *6* (1), 575-587.
83. Korri-Youssoufi, H.; Garnier, F.; Srivastava, P.; Godillot, P.; Yassar, A., Toward bioelectronics: specific DNA recognition based on an oligonucleotide-functionalized polypyrrole. *Journal of the American Chemical Society* **1997,** *119* (31), 7388-7389.
84. Mohanty, S. P., Biosensors: A survey report. *University of South Florida, USA* **2001**.
85. Li, G.; Koßmehl, G.; Welzel, H. P.; Engelmann, G.; Hunnius, W. D.; Plieth, W.; Zhu, H., Reactive groups on polymer coated electrodes, 7. New electrogenerated electroactive polythiophenes with different protected carboxyl groups. *Macromolecular Chemistry and Physics* **1998,** *199* (4), 525-533.
86. Lee, T.-Y.; Shim, Y.-B., Direct DNA hybridization detection based on the oligonucleotide-functionalized conductive polymer. *Analytical chemistry* **2001,** *73* (22), 5629-5632.
87. Rinken, T., State of the Art in Biosensors—General Aspects. InTech: 2013.
88. Salgado, A. M.; Silva, L. M.; Coelho, M. A. Z., Development of Potentiometric Urea Biosensor Based on Canavalia ensiformis Urease. In *Biosensors-Emerging Materials and Applications*, InTech: 2011.
89. Kasemo, B., Biological surface science. *Surface science* **2002,** *500* (1), 656-677.
90. Putzbach, W.; Ronkainen, N. J., Immobilization techniques in the fabrication of nanomaterial-based electrochemical biosensors: A review. *Sensors* **2013,** *13* (4), 4811-4840.
91. Wilson, W. D.; Gough, A. N.; Doyle, J. J.; Davidson, M. W., Coralyne. Intercalation with DNA as a possible mechanism of antileukemic action. *Journal of medicinal chemistry* **1976,** *19* (10), 1261-1263.
92. Schmidt, C.; Möller, J.; Hesslau, U.; Bauer, M.; Gabbert, T.; Kremer, B., University clinics in the competitive hospital market. *Der Anaesthesist* **2005,** *54* (7), 694-702.
93. Lerman, L., Structural considerations in the interaction of DNA and acridines. *Journal of molecular biology* **1961,** *3* (1), 18IN13-30IN14.
94. Shui, X.; Sines, C. C.; McFail-Isom, L.; VanDerveer, D.; Williams, L. D., Structure of the Potassium Form of CGCGAATTCGCG: DNA Deformation by Electrostatic Collapse around Inorganic Cations†. *Biochemistry* **1998,** *37* (48), 16877-16887.
95. Dickerson, R. E.; Kopka, M. L.; Pjura, P., A random-walk model for helix bending in B-DNA. *Proceedings of the National Academy of Sciences* **1983,** *80* (23), 7099-7103.
96. Barlow, D. J.; Thornton, J., Ion-pairs in proteins. *Journal of molecular biology* **1983,** *168* (4), 867-885.
97. Chaires, J. B.; Dattagupta, N.; Crothers, D. M., Studies on interaction of anthracycline antibiotics and deoxyribonucleic acid: equilibrium binding studies on the interaction of daunomycin with deoxyribonucleic acid. *Biochemistry* **1982,** *21* (17), 3933-3940.
98. Neto, B. A.; Lapis, A. A., Recent developments in the chemistry of deoxyribonucleic acid (DNA) intercalators: principles, design, synthesis, applications and trends. *Molecules* **2009,** *14* (5), 1725-1746.
99. Zimmer, C.; Wähnert, U., Nonintercalating DNA-binding ligands: specificity of the interaction and their use as tools in biophysical, biochemical and biological investigations of the genetic material. *Progress in biophysics and molecular biology* **1986,** *47* (1), 31-112.
100. Cholody, W. M.; Kosakowska-Cholody, T.; Hollingshead, M. G.; Hariprakasha, H. K.; Michejda, C. J., A new synthetic agent with potent but selective cytotoxic activity against cancer. *Journal of medicinal chemistry* **2005,** *48* (13), 4474-4481.
101. Boresch, S.; Karplus, M., The meaning of component analysis: decomposition of the free energy in terms of specific interactions. Elsevier: 1995.
102. Strekowski, L.; Wilson, B., Noncovalent interactions with DNA: an overview. *Mutation Research/Fundamental and Molecular Mechanisms of Mutagenesis* **2007,** *623* (1), 3-13.

103. Rao, S. N.; Kollman, P. A., Molecular mechanical simulations on double intercalation of 9-amino acridine into d (CGCGCGC) X d (GCGCGCG): analysis of the physical basis for the neighbor-exclusion principle. *Proceedings of the National Academy of Sciences* **1987,** *84* (16), 5735-5739.
104. Denny, W., DNA-intercalating ligands as anti-cancer drugs: prospects for future design. *Anti-cancer drug design* **1989,** *4* (4), 241-263.
105. Dickerson, R. E., Crystal structure analysis of a complete turn of B-DNA. *Nature* **1980,** *287*, 755-758.
106. Vázquez, M. E.; Caamaño, A. M.; Mascarenas, J., From transcription factors to designed sequence-specific DNA-binding peptides. *Chemical Society Reviews* **2003,** *32* (6), 338-349.
107. Palchaudhuri, R.; Hergenrother, P. J., DNA as a target for anticancer compounds: methods to determine the mode of binding and the mechanism of action. *Current opinion in biotechnology* **2007,** *18* (6), 497-503.
108. Chaires, J. B., Energetics of drug–DNA interactions. *Biopolymers* **1997,** *44* (3), 201-215.
109. Bischoff, G.; Hoffmann, S., DNA-binding of drugs used in medicinal therapies. *Current medicinal chemistry* **2002,** *9* (3), 321-348.
110. Halley, J.; Winkler, D. A., Consistent concepts of self-organization and self-assembly. *Complexity* **2008,** *14* (2), 10-17.
111. Chen, Z.; Lohr, A.; Saha-Möller, C. R.; Würthner, F., Self-assembled π-stacks of functional dyes in solution: structural and thermodynamic features. *Chemical Society Reviews* **2009,** *38* (2), 564-584.
112. Abbel, R.; Grenier, C.; Pouderoijen, M. J.; Stouwdam, J. W.; Leclere, P. E.; Sijbesma, R. P.; Meijer, E.; Schenning, A. P., White-light emitting hydrogen-bonded supramolecular copolymers based on π-conjugated oligomers. *Journal of the American Chemical Society* **2008,** *131* (2), 833-843.
113. Meyer, E. A.; Castellano, R. K.; Diederich, F., Interactions with aromatic rings in chemical and biological recognition. *Angewandte Chemie International Edition* **2003,** *42* (11), 1210-1250.
114. Hoeben, F. J.; Jonkheijm, P.; Meijer, E.; Schenning, A. P., About supramolecular assemblies of π-conjugated systems. *Chemical Reviews* **2005,** *105* (4), 1491-1546.
115. Schmid, F. X., Biological Macromolecules: UV-visible Spectrophotometry. *eLS* **2001**.
116. Upstone, S. L., Ultraviolet/Visible Light Absorption Spectrophotometry in Clinical Chemistry. In *Encyclopedia of Analytical Chemistry*, John Wiley & Sons, Ltd: 2006.
117. Moore, J. W.; Pearson, R. G., *Kinetics and Mechanism*. Wiley: New York, N.Y., 1981.
118. Pavia, D.; Lampman, G.; Kriz, G., Ultraviolet Spectroscopy. Introduction to Spectroscopy. *Harcourt College Publishers, Edition* **2001,** *3* (2001), 353-358.
119. Buurma, N. J.; Haq, I., Calorimetric and spectroscopic studies of Hoechst 33258: self-association and binding to non-cognate DNA. *Journal of molecular biology* **2008,** *381* (3), 607-621.
120. Mark, A. E.; van Gunsteren, W. F., Decomposition of the Free Energy of a System in Terms of Specific Interactions: Implications for Theoretical and Experimental Studies. *Journal of Molecular Biology* **1994,** *240* (2), 167-176.
121. Dill, K. A., Additivity Principles in Biochemistry. *Journal of Biological Chemistry* **1997,** *272* (2), 701-704.
122. Buurma, N. J.; Haq, I., Advances in the analysis of isothermal titration calorimetry data for ligand–DNA interactions. *Methods* **2007,** *42* (2), 162-172.
123. Freyer, M. W.; Lewis, E. A., Isothermal titration calorimetry: experimental design, data analysis, and probing macromolecule/ligand binding and kinetic interactions. *Methods in cell biology* **2008,** *84*, 79-113.

124. Jelesarov, I.; Bosshard, H. R., Isothermal titration calorimetry and differential scanning calorimetry as complementary tools to investigate the energetics of biomolecular recognition. *Journal of Molecular Recognition* **1999,** *12* (1), 3-18.
125. Nordén, B.; Rodger, A.; Dafforn, T., *Linear dichroism and circular dichroism*. The Royal Society of Chemistry: 2010.
126. Norden, B.; Kubista, M.; Kurucsev, T., Linear dichroism spectroscopy of nucleic acids. *Quarterly Reviews of Biophysics* **1992,** *25* (1), 51-170.
127. Eriksson, M.; Nordén, B., Linear and circular dichroism of drug-nucleic acid complexes. *Methods in enzymology* **2001,** *340*, 68-98.
128. Garbett, N. C.; Ragazzon, P. A.; Chaires, J. B., Circular dichroism to determine binding mode and affinity of ligand–DNA interactions. *NATURE PROTOCOLS - ELECTRONIC EDITION-* **2007,** *2* (12), 3166-3172.
129. Garbett, N. C.; Ragazzon, P. A.; Chaires, J. B., Circular dichroism to determine binding mode and affinity of ligand-DNA interactions. *Nature Protocols* **2007,** *2* (12), 3166.
130. El-Betany, A. M.; Vachova, L.; Bezzu, C. G.; Pope, S. J.; McKeown, N. B., The synthesis and study of fluorescent PAMAM-based dendritic molecules. *Tetrahedron* **2013,** *69* (39), 8439-8445.
131. Mandal, T.; Kumar, M. V. S.; Maiti, P. K., DNA assisted self-assembly of PAMAM dendrimers. *The Journal of Physical Chemistry B* **2014,** *118* (40), 11805-11815.
132. Choi, Y.; Mecke, A.; Orr, B. G.; Banaszak Holl, M. M.; Baker, J. R., DNA-directed synthesis of generation 7 and 5 PAMAM dendrimer nanoclusters. *Nano Letters* **2004,** *4* (3), 391-397.
133. Wu, L. P.; Ficker, M.; Christensen, J. B.; Trohopoulos, P. N.; Moghimi, S. M., Dendrimers in Medicine: Therapeutic Concepts and Pharmaceutical Challenges. *Bioconjugate chemistry* **2015,** *26* (7), 1198-211.
134. Boas, U.; Christensen, J. B.; Heegaard, P. M. H., *Dendrimers in medicine and biotechnology : new molecular tools*. RSC Pub.: Cambridge, 2006.
135. Banerjee, S.; Kitchen, J. A.; Gunnlaugsson, T.; Kelly, J. M., The effect of the 4-amino functionality on the photophysical and DNA binding properties of alkyl-pyridinium derived 1,8-naphthalimides. *Org. Biomol. Chem. Organic & Biomolecular Chemistry* **2013,** *11* (34), 5642.
136. Veale, E. B.; Gunnlaugsson, T., Synthesis, Photophysical, and DNA Binding Studies of Fluorescent Trögers Base Derived 4-Amino-1,8-naphthalimide Supramolecular Clefts. *J. Org. Chem. The Journal of Organic Chemistry* **2010,** *75* (16), 5513-5525.
137. Veale, E. B.; Frlmannsson, D. O.; Gunnlaugsson, T.; Lawler, M., 4-Amino-1,8-naphthalimide-based tröger's bases as high affinity DNA targeting fluorescent supramolecular scaffolds. *Org. Lett. Organic Letters* **2009,** *11* (18), 4040-4043.
138. Saeed, I. Q., Optoelectronically active sensitisers for
the selective detection of nucleic acid
biomarkers. **December 2016**.
139. Portugal, J.; Waring, M. J., Assignment of DNA binding sites for 4′,6-diamidine-2-phenylindole and bisbenzimide (Hoechst 33258). A comparative footprinting study. *Biochimica et Biophysica Acta (BBA) - Gene Structure and Expression* **1988,** *949* (2), 158-168.
140. Searle, M. S.; Embrey, K. J., Sequence-specific interaction of Hoescht 33258 with the minor grooVe of an adenine-tract DNA duplex studied in solution by 1 H NMR spectroscopy. *Nucleic Acids Research* **1990,** *18* (13), 3753-3762.
141. Moon, J. H.; Kim, S. K.; Sehlstedt, U.; Rodger, A.; Nordén, B., DNA structural features responsible for sequence-dependent binding geometries of Hoechst 33258. *Biopolymers* **1996,** *38* (5), 593-606.
142. Chen, T., In situ detection of mycoplasma contamination in cell cultures by fluorescent Hoechst 33258 stain. *Experimental cell research* **1977,** *104* (2), 255-262.

143. Holmquist, G., Hoechst 33258 fluorescent staining of Drosophila chromosomes. *Chromosoma* **1975,** *49* (4), 333-356.
144. Pjura, P. E.; Grzeskowiak, K.; Dickerson, R. E., Binding of Hoechst 33258 to the minor groove of B-DNA. *Journal of Molecular Biology* **1987,** *197* (2), 257-271.
145. Harshman, K. D.; Dervan, P. B., Molecular recognition of B-DNA by Hoechst 33258+. *Nucleic acids research* **1985,** *13* (13), 4825-4835.
146. Vega, M. C.; GARCÍA SÁEZ, I.; Aymami, J.; Eritja, R.; MAREL, G. A.; BOOM, J. H.; Rich, A.; Coll, M., Three-dimensional crystal structure of the A-tract DNA dodecamer d (CGCAAATTTGCG) complexed with the minor-groove-binding drug Hoechst 33258. *The FEBS Journal* **1994,** *222* (3), 721-726.
147. Ojha, H.; Murari, B. M.; Anand, S.; Hassan, M. I.; Ahmad, F.; Chaudhury, N. K., Interaction of DNA minor groove binder Hoechst 33258 with bovine serum albumin. *Chemical and Pharmaceutical Bulletin* **2009,** *57* (5), 481-486.
148. Bailly, C.; Colson, P.; Hénichart, J.-P.; Houssier, C., The different binding modes of Hoechst 33258 to DNA studied by electirc linear dichroism. *Nucleic Acids Research* **1993,** *21* (16), 3705-3709.
149. Gravatt, G. L.; Baguley, B. C.; Wilson, W. R.; Denny, W. A., DNA-directed alkylating agents. 6. Synthesis and antitumor activity of DNA minor groove-targeted aniline mustard analogs of pibenzimol (Hoechst 33258). *Journal of medicinal chemistry* **1994,** *37* (25), 4338-4345.
150. Ebrahimi, S.; Bibby, M.; Fox, K.; Douglas, K., Synthesis, DNA binding, footprinting and in vitro antitumour studies of a meta-hydroxy analogue of Hoechst 33258. *Anti-cancer drug design* **1995,** *10* (6), 463-479.
151. Hossain, M.; Kumar, G. S., DNA intercalation of methylene blue and quinacrine: new insights into base and sequence specificity from structural and thermodynamic studies with polynucleotides. *Molecular BioSystems* **2009,** *5* (11), 1311-1322.
152. Tuite, E.; Norden, B., Sequence-specific interactions of methylene blue with polynucleotides and DNA: a spectroscopic study. *Journal of the American Chemical Society* **1994,** *116* (17), 7548-7556.
153. Rohs, R.; Sklenar, H., Methylene blue binding to DNA with alternating AT base sequence: minor groove binding is favored over intercalation. *Journal of Biomolecular Structure and Dynamics* **2004,** *21* (5), 699-711.
154. Sjöback, R.; Nygren, J.; Kubista, M., Absorption and fluorescence properties of fluorescein. *Spectrochimica Acta Part A: Molecular and Biomolecular Spectroscopy* **1995,** *51* (6), L7-L21.
155. Smith, L. M.; Sanders, J. Z.; Kaiser, R. J.; Hughes, P.; Dodd, C.; Connell, C. R.; Heiner, C.; Kent, S. B.; Hood, L. E., Fluorescence detection in automated DNA sequence analysis. *Nature* **1986,** *321* (6071), 674-679.
156. Cheng, Y.-F.; Dovichi, N. J., Subattomole amino acid analysis by capillary zone electrophoresis and laser-induced fluorescence. *Science* **1988,** *242* (4878), 562.
157. Zanker, V.; Peter, W., Die prototropen formen des fluoresceins. *European Journal of Inorganic Chemistry* **1958,** *91* (3), 572-580.
158. Lindqvist, L., *A flash photolysis study of fluorescein*. Almqvist & Wiksell: 1960; Vol. 16.
159. Noga, E.; Udomkusonsri, P., Fluorescein: a rapid, sensitive, nonlethal method for detecting skin ulceration in fish. *Veterinary pathology* **2002,** *39* (6), 726-731.
160. Perry, C. A., Information technology and the curriculum: A status report. *Educause Quarterly* **2004,** *27* (4), 28-37.
161. Canete, M.; Villanueva, A.; Juarranz, A.; Stockert, J., A study of interaction of thioflavine T with DNA: evidence for intercalation. *Cellular and molecular biology* **1987,** *33* (2), 191-199.

162. KELIÉNYI, G., On the histochemistry of azo group-free thiazole dyes. *Journal of Histochemistry & Cytochemistry* **1967,** *15* (3), 172-180.
163. Khin-Maung-U, M.-K.; Nyunt-Nyunt-Wai, A.-K., Clinical trial of berberine in acute watery diarrhoea. *British medical journal (Clinical research ed.)* **1985,** *291* (6509), 1601.
164. Jantová, S.; Košt'álová, D., Effect of berberine on proliferation, cell cycle and apoptosis in HeLa and L1210 cells. *Journal of pharmacy and pharmacology* **2003,** *55* (8), 1143-1149.
165. Asai, M.; Iwata, N.; Yoshikawa, A.; Aizaki, Y.; Ishiura, S.; Saido, T. C.; Maruyama, K., Berberine alters the processing of Alzheimer's amyloid precursor protein to decrease Aβ secretion. *Biochemical and biophysical research communications* **2007,** *352* (2), 498-502.
166. Lau, C. W.; Yao, X. Q.; Chen, Z. Y.; Ko, W. H.; Huang, Y., Cardiovascular actions of berberine. *Cardiovascular Therapeutics* **2001,** *19* (3), 234-244.
167. Kundu, N.; Roy, A.; Banik, D.; Sarkar, N., Unveiling the Mode of Interaction of Berberine Alkaloid in Different Supramolecular Confined Environments: Interplay of Surface Charge between Nano-Confined Charged Layer and DNA. *The Journal of Physical Chemistry B* **2016,** *120* (6), 1106-1120.
168. Capobianco, M. L.; Barbarella, G.; Manetto, A., Oligothiophenes as fluorescent markers for biological applications. *Molecules* **2012,** *17* (1), 910-933.
169. Gonçalves, V. C.; Balogh, D. T., Optical chemical sensors using polythiophene derivatives as active layer for detection of volatile organic compounds. *Sensors and Actuators B: Chemical* **2012,** *162* (1), 307-312.
170. Nilsson, K. P. R.; Rydberg, J.; Baltzer, L.; Inganäs, O., Self-assembly of synthetic peptides control conformation and optical properties of a zwitterionic polythiophene derivative. *Proceedings of the National Academy of Sciences of the United States of America* **2003,** *100* (18), 10170-10174.
171. Regan, E. M.; Hallett, A. J.; Wong, L. C. C.; Saeed, I. Q.; Langdon-Jones, E. E.; Buurma, N. J.; Pope, S. J. A.; Estrela, P., A novel cobalt complex for enhancing amperometric and impedimetric DNA detection. *Electrochimica Acta* **2014,** *128*, 10-15.
172. Saeed, I. Q. Optoelectronically active sensitisers for the selective detection of nucleic acid biomarkers. Cardiff University, 2016.
173. Stokke, T.; Steen, H. B., Multiple binding modes for Hoechst 33258 to DNA. *Journal of Histochemistry & Cytochemistry* **1985,** *33* (4), 333-338.
174. Biancardi, A.; Biver, T.; Burgalassi, A.; Mattonai, M.; Secco, F.; Venturini, M., Mechanistic aspects of thioflavin-T self-aggregation and DNA binding: evidence for dimer attack on DNA grooves. *Physical chemistry chemical physics : PCCP* **2014,** *16* (37), 20061-72.
175. Biancardi, A.; Biver, T.; Mennucci, B., Fluorescent dyes in the context of DNA-binding: The case of Thioflavin T. *Int J Quantum Chem International Journal of Quantum Chemistry* **2017,** *117* (8).
176. G. Gumenyuk, V.; Bashmakova, N.; Kutovyy, S.; Yashchuk, V.; Zaika, L., *Binding Parameters of Alkaloids Berberine and Sanguinarine with DNA*. 2012; Vol. 56.
177. Ren, J.; Chaires, J. B., Sequence and structural selectivity of nucleic acid binding ligands. *Biochemistry* **1999,** *38* (49), 16067-16075.
178. D'Elia, N. L.; Gravina, N.; Ruso, J. M.; Marco-Brown, J. L.; Sieben, J. M.; Messina, P. V., Albumin-mediated deposition of bone-like apatite onto nano-sized surfaces: Effect of surface reactivity and interfacial hydration. *Journal of Colloid and Interface Science* **2017,** *494*, 345-354.
179. Saari, H.; Konttinen, Y. T.; Friman, C.; Sorsa, T., Differential effects of reactive oxygen species on native synovial fluid and purified human umbilical cord hyaluronate. *Inflammation* **1993,** *17* (4), 403-415.

180. Meyer, K.; Hobby, G. L.; Chaffee, E.; Dawson, M. H., Relationship between "Spreading Factor" and Hyaluronidase.∗. *Proceedings of the Society for Experimental Biology and Medicine* **1940,** *44* (1), 294-296.
181. Dorin, I. M., *Thiophene-based DNA binders for sensing, nano-bioelectronics, and therapeutic purposes*. Cardiff University (United Kingdom): 2010.
182. Manesh, K.; Santhosh, P.; Gopalan, A.; Lee, K., Electrocatalytic oxidation of NADH at gold nanoparticles loaded poly (3, 4-ethylenedioxythiophene)–poly (styrene sulfonic acid) film modified electrode and integration of alcohol dehydrogenase for alcohol sensing. *Talanta* **2008,** *75* (5), 1307-1314.
183. Ghosh, S.; Inganäs, O., Conducting polymer hydrogels as 3D electrodes: applications for supercapacitors. *Advanced Materials* **1999,** *11* (14), 1214-1218.
184. De Dardel, F.; Arden, T. V., Ion exchangers. *Ullmann's encyclopedia of industrial chemistry* **2008**.
185. Escara, J. F.; Hutton, J. R., Thermal stability and renaturation of DNA in dimethyl sulfoxide solutions: acceleration of the renaturation rate. *Biopolymers* **1980,** *19* (7), 1315-1327.
186. Wolf, P. A.; Havekotte, M. J., Microemulsions of oil in water and alcohol. Google Patents: 1989.
187. Holmberg, K.; Jönsson, B.; Kronberg, B.; Lindman, B., Microemulsions. *Surfactants and Polymers in Aqueous Solution, Second Edition* **2002**, 139-155.
188. Kosswig, K., Surfactants. In *Ullmann's Encyclopedia of Industrial Chemistry*, Wiley-VCH Verlag GmbH & Co. KGaA: 2000.
189. Buurma, N. J., Aggregation and reactivity in aqueous solutions of cationic surfactants and aromatic anions across concentration scales. *Current Opinion in Colloid & Interface Science* **2017,** *32* (Supplement C), 69-75.
190. Smulders, E.; Von Rybinski, W.; Sung, E.; Rähse, W.; Steber, J.; Wiebel, F.; Nordskog, A., *Laundry detergents*. Wiley Online Library: 2007.
191. Tanford, C., *The Hydrophobic Effect: Formation of Micelles and Biological Membranes 2d Ed*. J. Wiley.: 1980.
192. Israelachvili, J. N.; Mitchell, D. J.; Ninham, B. W., Theory of self-assembly of hydrocarbon amphiphiles into micelles and bilayers. *Journal of the Chemical Society, Faraday Transactions 2: Molecular and Chemical Physics* **1976,** *72*, 1525-1568.
193. Israelachvili, J. N., Refinement of the fluid-mosaic model of membrane structure. *Biochimica et Biophysica Acta (BBA)-Biomembranes* **1977,** *469* (2), 221-225.
194. Carale, T. R.; Pham, Q. T.; Blankschtein, D., Salt effects on intramicellar interactions and micellization of nonionic surfactants in aqueous solutions. *Langmuir* **1994,** *10* (1), 109-121.
195. Wang, G.-J.; Engberts, J. B., Induction of aggregate formation of cationic polysoaps and surfactants by low concentrations of additives in aqueous solution. *Langmuir* **1994,** *10* (8), 2583-2587.
196. Buwalda, R. T.; Jonker, J. M.; Engberts, J. B., Aggregation of azo dyes with cationic amphiphiles at low concentrations in aqueous solution. *Langmuir* **1999,** *15* (4), 1083-1089.
197. Mukerjee, P.; Mysels, K. J., A Re-evaluation of the Spectral Change Method of Determining Critical Micelle Concentration1. *Journal of the American Chemical Society* **1955,** *77* (11), 2937-2943.